Failure of Rubber Components under Fatigue

Samuel Asare

School of Engineering and Materials Science

Queen Mary University of London

A thesis submitted in partial fulfilment of the requirements of the Degree of Doctor of Philosophy

July 2013

Abstract

Rubber components under cyclic loading conditions often are considered to have failed as a result of the stiffness changing to an amount that makes the part no longer useful. This thesis considers three distinctive but related aspect of the fatigue failure exhibited by rubber components. The first considers the reduction in stiffness that can result from a phenomenon known as cyclic stress relaxation. The second considers fatigue crack growth encountered resulting in potentially catastrophic failure. The final issue relates to the complex topography of the resulting fatigue fracture surfaces.

Previous work has shown that the amount of relaxation observed from cycle to cycle is significantly greater than that expected from static relaxation tests alone. In this thesis the reduction in the stress attained on the second and successive loading cycles as compared with the stress attained on the first cycle in a stress strain cyclic test of fixed strain amplitude has been measured for elastomer test pieces and engineering components. Adopting the approach of Davies et al. (1996) the peak force, under cyclic testing to a specific maximum displacement, plotted against the number of cycles on logarithmic scales produces a straight line graph, whose slope correlates to the rate of cyclic stress relaxation per decade. Plotting the rate of stress relaxation per decade against the maximum average strain energy density attained in the cycle reduces the data measured in different deformation modes for both simple test pieces and components to a single curve. This approach allows the cyclic stress relaxation in a real component under any deformation to be predicted from simple laboratory tests (Asare et al., 2009).

Earlier work (Busfield et al., 2005) has shown that a fracture mechanics approach can predict fatigue failure in rubber or elastomer components using a finite element analysis technique that calculates the strain energy release rate for cracks introduced into bonded rubber components. This thesis extends this previous work to examine real fatigue measurements made at both room temperature and 70±1ºC in both tension and shear using cylindrical rubber to metal bonded components. Dynamic testing of these components generated fatigue failures not only in the bulk of the component but also at the rubber to metal bond interface. The fatigue crack growth characteristics were measured independently using a pure shear test piece. Using this independent crack growth data and an accurate estimate for the initial flaw size allowed

the fatigue life to be calculated. The fracture mechanics approach predicted the crack growth rates accurately at both room temperature and 70±1ºC (Asare et al., 2011).

Fatigue crack growth often results in rough fatigue crack surfaces. The rough fatigue crack surface is, in part, thought to result from anisotropy being developed at the front of a crack tip. This anisotropy in strength whereby the material is less strong in the direction that the material is stretched might allow the fatigue crack to grow in an unanticipated direction. It might also allow the crack front to split. Therefore the final part of this thesis examines how, once split, the strain energy release rate associated with growth of each split fatigue crack develops as the cracks extend in a pure shear crack growth test specimen. The aim being to understand how the extent of out of plane crack growth that results might allow a better understanding of the generation of particular crack tip roughness profiles. Using a method of extending one split crack at a time, whilst keeping a second split crack at a constant length, it has been possible to evaluate the initial strain energy release rates of split cracks of different configurations in a pure shear specimen. It was observed that, for a split crack in a pure shear specimen, the initial strain energy release rate available for crack growth depends on the precise location of the split crack. It is also clear that the tearing energy is shared evenly when the crack tip is split into two paths of equal length, but as one crack accelerates ahead it quickly increases in tearing energy and leaves the slower crack behind. It is thought that this phenomenon is responsible for a lot of the roughness observed on the resulting fracture surfaces.

Contents

Figures

Tables

Acknowledgement

I would like to express my sincere gratitude to my supervisors, Dr. James Busfield and Professor Alan Thomas, for their guidance, tremendous help, and encouragement throughout the course of this research work.

I would like to express my gratitude to the Department of Materials, Queen Mary, University of London, for my fees scholarship which enabled me to pursue my research studies. I am also grateful to Trelleborg AVS for the supply of materials for this research work. I am thankful to my colleagues in the rubber group and all others who contributed in one way or another to make my research studies a success.

Finally, I am deeply thankful to my family and friends for their continuous support and encouragement throughout my studies.

Abbreviations

ACM	Polyacrylate rubber
AEM	Ethylene-acrylic rubber
ASTM	American society for testing and materials
BR	Butadiene rubber
CM	Chlorinated polyethylene
CR	Polychloroprene
CSM	Chorosulfonated polyethylene
CV	Conventional systems
ECO	Epichlorohydrin rubber
EPR, EPDM	Ethylene-propylene rubber
EV	Efficient systems
FEA	Finite element analysis
FKM	Fluorocarbon rubbers
HAF	High abrasion furnace
HNBR	Hydrogenated nitrile rubber
IIR	Butyl rubber
IR	Synthetic rubber
MBTS	Benzothiazyl Disulfide
MQ	Silicone rubber
NBR	Acrylonitrile-butadiene rubber
NR	Natural rubber
phr	Parts by mass per hundred elastomer
SBR	Styrene-butadiene rubber
S_E	Surface free energy per unit area
SEF	Strain energy function
SMR	Standard Malaysian Rubber
S-N	Stress versus fatigue life relation
T	Polysulfide rubber
TMTM	Tetramethylthiuram Monosulfide
WLF	Williams, Landel and Ferry (1955)

Symbols

λ_1, λ_2, λ_3 = Principal extension ratios

A = Area of a single fracture surface

A_t = Crack growth constant

B = Bulk modulus

C = Arbitrary constant

c = Crack length

C_1 and C_2 = Mooney constants

C_1' and C_2' = WLF constants

C_0 = Edge crack length at T_0

d = Diameter of the modelled crack tip

d = Effective tip diameter

d_b = Diameter of the strained crack tip

dc/dn = Crack growth per cycle

e = Engineering strain

E = Young's modulus

F = Force

G = Shear Modulus

h = Thickness of the specimen

$\boldsymbol{k}$ = Boltzmann constant

k_z = Rate constant due to Ozone

l = Length

l_0 = Un-gripped height of a pure shear specimen

m_c = Number average molecular weight of segments of molecules between successive cross-links

N = Count of chains per unit volume

N = Moles of cross-links per unit volume

n = Number of moles of chains per unit volume

N_f = Number of cycles to failure

N_m = Measured number of cycles

N_p = Predicted number of cycles

$P(r)$ = Probability density function

Q = Heat

r = End-to-end distance

$\boldsymbol{R}$ = Gas constant

r_t = Radius of the semi circle

S = Entropy

t = Sheet thickness

T = Tearing energy

ϑ = Temperature

t = time

T_c = Critical strain energy release rate

T_g = Glass transition temperature

T_M = Temperature at which the test is conducted

T_0 = Threshold strain energy release rate

U = Internal energy

V = Volume of rubber

V_S = Molar volume of the swelling solvent

W = Elastic stored energy per unit volume

w = Pure shear specimen width

W_α = Elastic stored energy per unit volume of the rubber at the crack tip

w_0 = Total width of the test piece

W_b = Work to break per unit volume of rubber

W_t = A suitable average of W_α

x = A strip of material at the cracked part of the test piece that is not energy free

α = Angular distance

γ = Shear strain

θ = Angle

λ = Extension ratio

ρ = Density

σ = Engineering stress

$\sigma_1, \sigma_2, \sigma_3$ = Principal stresses

υ = Poison ratio

Φ = Volume fraction of polymer in the swollen gel

χ = Polymer-solvent interaction parameter

Ψ, χ = Steady state crack growth constants

CHAPTER ONE

1.0 General Introduction

In recent years, industrial competition has led elastomer component manufacturers to validate their products analytically prior to manufacture to ensure more robust design and to try to reduce product lead times. The prediction of the fatigue life of elastomer components, such as tyres, suspension components and engine and gearbox mounts, has become a necessary research subject (Busfield et al., 2005). An essential prerequisite, therefore, for the finite element simulation of mechanical fatigue is an accurate knowledge of the material behaviour.

Elastomers exhibit a highly non-linear material behaviour characterised by three main phenomena: a non-linear elastic behaviour under static load; a rate dependent or viscoelastic behaviour with hysteresis under cyclic loading and the Payne effect (Payne, 1962), which involves a substantial decrease in the storage modulus of a particle reinforced elastomer with an increase in the amplitude of mechanical oscillations. Another important phenomenon is cyclic stress relaxation which is observed in elastomer materials. The cyclic stress relaxation involves a reduction in the stress attained on the second and successive loading cycles as compared with the stress attained on the first cycle in a stress strain cyclic test of fixed strain amplitude. Cyclic stress relaxation itself is a manifestation of one specific type of fatigue behaviour of elastomeric materials used in engineering applications. A detailed qualitative and quantitative understanding of cyclic stress relaxation, therefore, is a necessary step towards a scientific evaluation of the fatigue life of a rubber product.

In this work, the cyclic stress relaxation behaviour of a cylindrical rubber to metal bonded component and test pieces made from carbon black filled natural rubber material were measured experimentally. The cylindrical rubber to metal bonded component was displaced to different fixed maximum displacements in tension and shear deformation modes whilst, the test pieces were deformed to different fixed maximum displacements in pure shear deformation mode. The objectives of these tests were first to confirm the linear logarithmic dependence of the force at maximum displacement on the logarithm of the number of cycles for successive cycles observed by Davies et al. for a wide range of filled elastomer compound test pieces deformed in tension (Davies, De, and Thomas, 1996). Secondly, and more importantly, to develop

an approach to correlate the rate of cyclic stress relaxation measured in elastomer components to that measured in test pieces using an appropriate physical quantity – found to be the maximum average strain energy density in this work. This aspect of the work has been published in Asare et al., (2009). The method developed in the cyclic stress relaxation work was subsequently incorporated into the finite element analysis based approach to fatigue life prediction – to account for cyclic stress relaxation quantitatively (Asare et al., 2011).

Extensive work has been done in the past on the prediction of fatigue life of elastomer components. Busfield et al. (2005) presented a fracture mechanics approach, which uses finite element analysis techniques, to calculate strain energy release rates for cracks located in three-dimensional components, in combination with experimental measurements of cyclic crack growth rates of specific strain energy release rates, to predict the cyclic crack growth rate and the eventual fatigue failure of an elastomeric engineering component in three modes of deformation, namely: tension, simple shear and combined shear and tensile (45º angle) deformations. They used a gearbox mount with a narrowly shaped middle section which raises the strain energy density in this section under deformation and therefore failure initiation in the middle section of the elastomer component. Their work was limited to room temperature conditions and also prediction of the crack growth in the component after inserting an initial razor cut into the middle section of the elastomer component. The cyclic stress relaxation associated with fatigue crack growth was also poorly accounted for by pre-stressing the test piece for stress strain characterisation to an arbitrary strain for 1000 cycles.

The research described here extends this previous work to examine real fatigue measurements made at both room temperature and 70±1ºC in both tension and shear using the cylindrical rubber to metal bonded component used in the cyclic stress relaxation studies. The objective being to validate the fracture mechanics approach to fatigue life prediction at above room temperature conditions. The cylindrical rubber to metal bonded component generated fatigue failures not only in the bulk of the component but also at the rubber to metal bond interface. In calculating the strain energy release rates necessary for fatigue life prediction using the finite element analysis (FEA) based fracture mechanics approach, the cyclic stress relaxation associated with fatigue crack growth in the elastomer component is often poorly accounted for by pre-stressing the test piece for stress strain characterisation to an arbitrary strain for 1000 cycles. An original method is proposed in this work to

quantitatively account for the component cyclic stress relaxation, associated with the fatigue crack growth, in the FEA strain energy release rate calculations, by characterising the stress strain behaviour of the component material test piece after repeated stressing for 1000 cycles, at a maximum average strain energy density comparable to that obtained in the component when loaded. The material fatigue crack growth characteristics were measured independently using a pure shear crack growth test specimen. This independent crack growth data and an accurate estimate for the initial flaw size, around the rubber-metal bond edge of the cylindrical component, allowed the fatigue life to be calculated. The fracture mechanics approach predicted the crack growth rates well at both room temperature and 70±1ºC. This aspect of adopting fracture mechanics at elevated environmental service temperatures being entirely novel.

Fatigue crack growth often results in rough fatigue crack surfaces. The rough fatigue crack surface is, in part, thought to result from strain induced strength anisotropy in front of the advancing fatigue crack which can then cause the crack to split during crack growth. Part of this thesis examines strain energy release rates associated with growth of split fatigue cracks, in a pure shear specimen, in an attempt to investigate how fatigue crack bifurcation alters fatigue crack surface roughness. Using a method of extending one split crack at a time, whilst keeping a second split crack at a constant length, it has been possible to evaluate the initial strain energy release rate for a split crack at different locations in a pure shear specimen. It was observed that, for a split crack in a pure shear specimen, the initial strain energy release rates available for crack growth depend on the location of the split crack in relation to the central horizontal plane of the specimen. This work also shows that, split cracks closer to the central plane of the pure shear specimen possess higher strain energy release rates for growth than split cracks displaced further from the central plane. This trend becomes more pronounced at higher global strains. It is concluded in this work that the observed roughness of fatigue crack surfaces, to a large extent, may be the result of a cyclic process involving a fatigue crack tip splitting, the twin growth of both split cracks with the one that has a higher energy release rate eventually accelerating and leaving behind the lower energy release rate component.

In Chapter two a literature review of elastomer materials including their uses and properties is presented. The stress-strain behaviour of elastomer materials, cyclic stress relaxation and the concept of elastomer fracture mechanics are discussed. This

review examines both the experiments done by earlier workers and the theories that have been developed to explain the behaviour.

In Chapter three the material and experimental methods used to test the cylindrical rubber to metal bonded component and test pieces in this work are presented in detail. The finite element analysis technique for strain energy release rate calculations is also explained.

Chapter four presents the results and discussion of the cyclic stress relaxation behaviour of the cylindrical rubber to metal bonded component and test pieces. The effects of maximum loading displacement and mode of deformation of the component on the cyclic stress relaxation rate are discussed. Finally an original approach based upon the average strain energy density in the component is proposed to correlate the cyclic stress relaxation rate found in the test pieces with the rate measured in the engineering components.

In chapter five, the results and discussion of fatigue life prediction of the cylindrical rubber to metal bonded component are presented. It is demonstrated that a fracture mechanics based approach can predict the fatigue life of elastomer engineering components both at room temperature and for the first time at 70±1ºC.

Chapter six presents the results and discussion of FEA calculated strain energy release rates of growing split cracks in a pure shear specimen. Chapter seven summarises the conclusions and future work for the entire thesis.

CHAPTER TWO

2.0 Literature Review

2.1 Definition of a rubber and an elastomer

An elastomer is a macromolecular material which returns rapidly approximately to its initial dimensions and shape after substantial deformation by a weak stress and the release of the stress. A rubber is an elastomer which can be, or already is, modified to a state in which it is essentially insoluble (but can swell) in a solvent and which in its modified state cannot be easily remoulded to a permanent shape by the application of heat and moderate pressure (BS3558-1).

2.2 Properties and uses of elastomers

In general elastomers exhibit the following combination of physical properties; a low tensile modulus (0.5 – 10 MPa), high extensibility, good strength, low permeability and good electrical insulation properties (Morton, 1987). Elastomers are used in tyres, in sealing applications, as protection against abrasion and vibration, as electrical insulation, in corrosion protection, in conveyor belting applications, and in hoses and tubes. Three physical requirements are needed to be fulfilled for a material to exhibit rubber-like behaviour:

1) The molecular chains have to be flexible and the molecular weight has to be large with, for the most part, very weak interactions between the molecular chains.
2) The chains should be fairly regular on a molecular level. These chains need to be connected to each other in a loose network by chemical bonds, usually via a short segment called a cross-link. A molecular weight of about 10 000 between junction points is a typical value for vulcanised natural rubber (Brydson, 1988; Sperling, 1986).
3) The glass transition temperature of the material must be below the temperature of application of the material (Sperling, 2001).

2.3 Types of elastomers

Elastomers can be classified into general-purpose elastomers and specialty elastomers. This classification is mainly based on suitability of the elastomer for a given application. Though general purpose elastomers are widely used, in some applications they can become unsuitable. This may be due to insufficient properties such as solvent resistance, aging resistance, and/or temperature resistance. As an alternative, several special purpose elastomers (specialty elastomers) have been developed to meet these needs. General-purpose elastomers include styrene-butadiene rubber (SBR), butadiene rubber (BR), and polyisoprene – both natural rubber (NR) and synthetic rubber (IR). Specialty elastomers include polychloroprene (CR), acrylonitrile-butadiene rubber (NBR), hydrogenated nitrile rubber (HNBR), Butyl rubber (IIR), ethylene-propylene rubber (EPR, EPDM), silicone rubber (MQ), polysulfide rubber (T), chlorosulfonated polyethylene (CSM), polyacrylate rubber (ACM), fluorocarbon rubbers (FKM), chlorinated polyethylene (CM), epichlorohydrin rubber (ECO) and ethylene-acrylic rubber (AEM) (Gent, 1992).

2.3.1 Natural rubber (NR)

Natural rubber (NR) is a polymer prepared either by the smoked sheet or the hevea crumb process from field latex (Allen and Bloomfield, 1963). The rubber consists mainly of linear cis-1,4-polyisoprene with a number average molar mass of about 10^5 –10^6 and has a glass transition temperature T_g, of approximately –70°C. It has the same empirical formula as trans-1,4-polyisoprene called Gutta-percha, $(C_5H_8)_n$ having one carbon-carbon double bond for each C_5H_8 unit, the difference being solely in the spatial arrangement of the carbon-carbon bond adjacent to the double bond (Treloar, 1975). A diagram illustrating the structure of the repeat units for NR and Gutta-percha is given in figure 2.1. These differences give markedly different physical properties for the two materials, with NR being rubbery at room temperature while Gutta-percha being a crystalline solid. NR crystallises at low temperature (maximum rate at – 26°C) and upon straining. This is a consequence of a high degree of stereo regularity, permitting a regular molecular alignment upon stretching. The ability to strain crystallise imparts outstanding strength and gives vulcanisates with high crack growth resistance at very large gross deformations. Unfortunately, NR also has a high

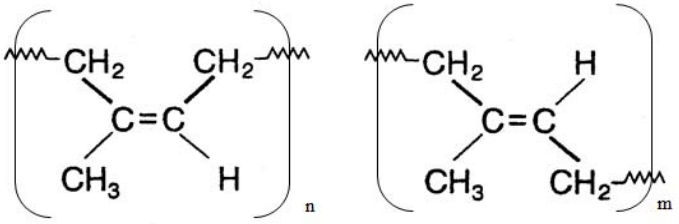

Figure 2.1 (a) cis-polyisoprene (NR) (b) trans-polyisoprene (gutta percha)

chemical reactivity with the ambient environment, in particular with oxygen and even higher reactivity with ozone (Morton, 1987; Cunneen and Higgins, 1963; Treloar, 1975).

2.3.2 **Polyisoprene (synthetic) rubber (IR)**

Isoprene rubber (IR) is a synthetic rubber equivalent to NR with almost the same chemical structure, 94-98% of cis-1,4-polyisoprene and 6-2% of trans-3,4-polyisoprene (Blow, 1971). IR is produced both anionically and by Ziegler-Natta polymerisation. NR and IR are both recognised as exhibiting strain induced crystallisation. Under large strains these rubbers have extremely high strengths and fatigue resistance with IR compounds having a lower modulus than similarly formulated NR compositions due to a reduction in the strain-induced crystallisation especially at the highest rates of deformation.

2.3.3 **Styrene-butadiene rubber (SBR)**

Styrene-butadiene rubber (SBR) is the most widely used synthetic rubber with the largest global production volume. SBR is a random copolymer of styrene and butadiene made by free radical emulsion polymerisation or anionically in solution. The most commonly used SBR consists of 23.5% styrene and 76.5% butadiene, with a glass transition temperature, T_g, of approximately –53°C (Barlow, 1988). A diagram illustrating the structure of the repeat units of SBR is given in figure 2.2.

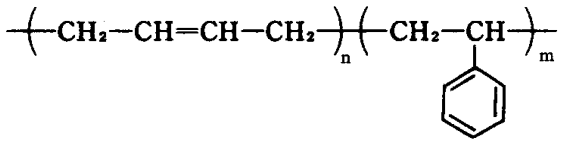

Figure 2.2 Chemical structure of styrene-butadiene rubber (SBR)

SBR is known as an essentially non strain-crystallising rubber, as under a large strain, only limited if any crystallisation can take place. This feature results in significant differences between the mechanical properties of NR (a strain crystallising rubber) and SBR. SBR has lower tensile strength and tear resistance and it is necessary to reinforce all SBR compounds for use in engineering applications with fillers such as carbon black to impart more useful properties. It is also quite a common practice to blend SBR with other rubbers to improve some of its basic properties.

2.3.4 **Polybutadiene rubber (BR)**

BR is a homopolymer of butadiene (C_4H_6) and can be made either by solution or emulsion polymerisation. It is a non-polar rubber like NR and SBR, with a very low T_g approximately –100°C. The 1,4-polybutadiene is an approximately equal mix of cis and trans. Because of the regularity of its structure BR has a tendency to crystallise that depends on the amount of cis and trans present (Blow, 1971). A diagram illustrating the structure of repeat units is given in figure 2.3. BR is a resilient rubber which is commonly used in combination with NR and SBR in long life rubber tyre treads.

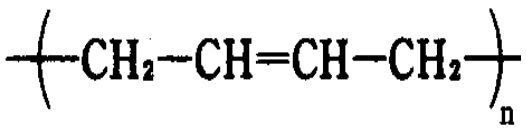

Figure 2.3 Chemical structure of polybutadiene rubber (BR)

2.4 Compounding of a rubber compound

None of the elastomers mentioned in section 2.3 have useful properties until they have been properly formulated. Rubber compounding is a process of blending the rubber with vulcanising agents and other substances to produce a homogeneous mix. Ingredients used in a rubber compound may be classified in the approximate order of importance as follows (Blow, 1971; Morton, 1987):

1. Vulcanising agents; these are chemicals which can initiate the chemical cross-linking of the rubber molecules leading to the formation of a three-dimensional macromolecular network. The most common cross linking agents are based around a sulphur curing system.
2. Accelerators; these are substances which can increase the rate of sulphur combination with rubber. They are capable of promoting more efficient use of sulphur; that is more cross-links, for a given amount of sulphur. They are also used to reduce the vulcanisation time.
3. Activators; these are also used to increase the vulcanisation rate. They activate the accelerators, which become more efficient. The most common system being zinc oxide and stearic acid in combination to create soluble zinc ions that activate the intermediate reactions involved in cross-link formation.
4. Fillers; these are added to reinforce or modify physical properties, impart certain processing properties, or potentially in lower specification products to reduce cost. Carbon black and silica are popular types of fillers which are used to increase the stiffness and strength of the elastomers.
5. Processing aids; these are materials used to modify rubber during mixing or processing steps. Processing oils are often used when fillers are mixed with rubber. These are hydrocarbon oils and their presence reduces the frictional energy during mixing.
6. Protective agents; these are added to protect the rubber from degradation. The types of protective agent used depend on the use of the finished product. Waxes are incorporated to protect the rubber against ozone attack while chemicals such as 1,2-dihydro-2,2,4-trimethyl-6-phenyl quinoline are used to protect against other forms of oxidative degradation.
7. Additional ingredients can be used for specific purposes but are not normally required in the majority of rubber compounds. Examples are retarders (the

opposite of accelerators), colouring pigments, blowing aids, deodorants and fire retardants.

Mixing of the compounding ingredients with rubber is usually carried out on a two-roll mill or in an internal mixer (Morton, 1987).

2.5 Vulcanisation

A raw rubber often known as an elastomer or occasionally as a gum rubber is a soft-flexible material. It shows viscoelastic properties since the molecules interact with their neighbours due to forces of attraction and physical entanglements. Without cross-links, the elastomer only exhibits limited elastic properties. Rubber is tacky when hot and slowly crystallises to a rather hard and tough material when stored at low temperature (for NR this is below 15°C) (Wood and Bekkedahl, 1946). In the unvulcanised state, raw rubber only has rather limited uses but it can be transformed into a more useful highly elastic state through a process called vulcanisation. Vulcanisation is the chemical treatment of a natural or synthetic rubber by the addition of a vulcanising agent such as sulphur, peroxides (or metal oxides) followed by curing at elevated temperature and/or pressure into a stable, elastic and resilient material. Vulcanisation of rubber creates cross-links, which form chemical bonds between the long network chains of the rubber matrix. A diagram illustrating the structure of gum rubber before and after vulcanisation is given in figure 2.4 (Barlow, 1988; Chapman and Porter, 1988). Measurements of vulcanisation characteristics using an oscillating disc rheometer (ODR) or moving-die rheometer (MDR) is common practice in the rubber industry to help determine the kinetics of the cross-linking process. An oscillating rotor is surrounded by a test compound, which is enclosed in a heated chamber. The torque required to oscillate the rotor is monitored as a function of time at the temperature chosen for vulcanisation. Figure 2.5 shows a typical torque-time curve along with characteristic terms to describe the different behaviours. The scorch time, t_{s1} is the time at which the torque is 0.1 Nm above minimum torque. It gives an indication of the safe period before the mix becomes impossible to process further due to the formation of cross-links (Morrell, 1987).

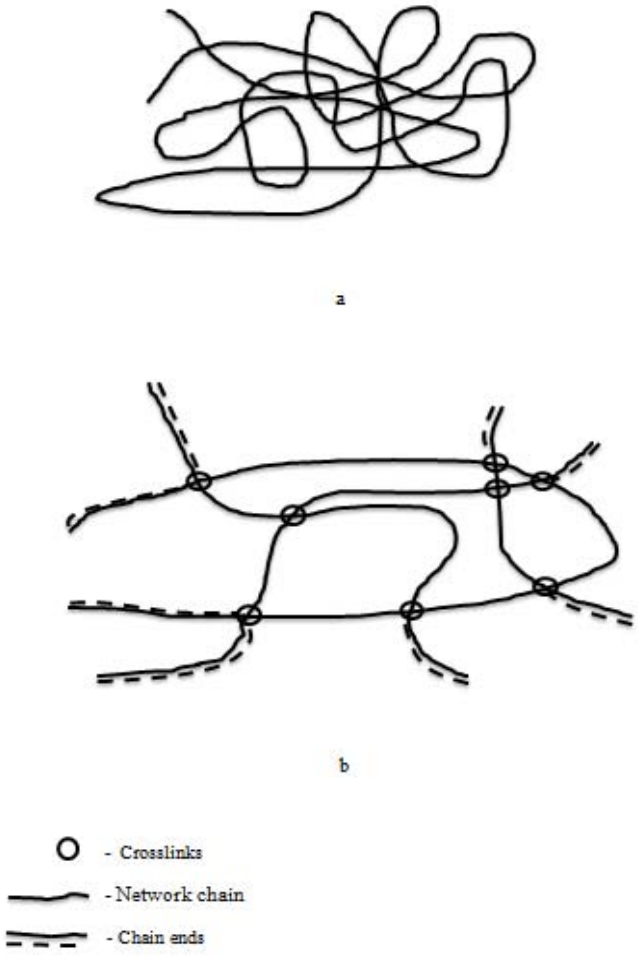

Figure 2.4 Rubber structure: (a) before vulcanisation and (b) after vulcanisation.

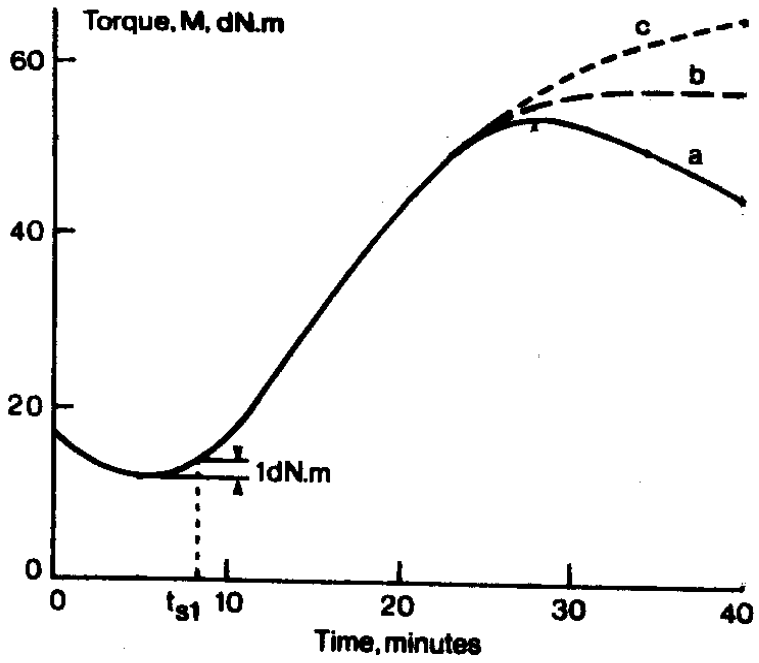

Figure 2.5 Illustration of the three different curemeter responses (Hamed, 1992).

At the start of the test, there is a sudden increase in torque. Then, as the elastomer is heated, its viscosity decreases, resulting in a net decrease in torque. Eventually, the compound begins to vulcanise and transform into an elastic solid (known as an elastomer), and the torque rises. Molecular chain scission may also occur; however, an increasing torque indicates that an increase in cross-links is dominant. If the torque reaches a plateau (curve b), this indicates a completion of curing and the formation of a stable network. If chain scission and/or cross-link breakage become dominant during prolonged heating, the torque passes through a maximum and then decreases (curve a), a phenomenon termed reversion. Some NR compounds, particularly at high curing temperatures, exhibit reversion. On the other hand, some compounds show a slowly increasing torque at long cure times often called creeping cure (curve c). This behaviour often occurs in compounds that initially form many polysulphidic linkages. With extended cure times, these linkages may break down and re-form into linkages of lower sulphur rank, thereby increasing the total number of cross-links (Hamed, 1992).

2.5.1 **The vulcanising systems**

In general, the type and number of cross-links formed between the network chains affect both the physical and chemical properties of the material. The number of cross-links depends on the amount and the type of vulcanising agent added. The time allowed for curing/vulcanisation also produces different types of cross-links and imparts different properties to the rubber vulcanisates. However, only the three kinds of cross-link systems that are of commercial importance are discussed in the following sections.

2.5.2 **Accelerated sulphur vulcanisation**

Accelerated sulphur vulcanisation was discovered in the 19th Century in separate works carried out by Goodyear and Hancock and is still the most widely used cross-linking method. A vulcanising system comprises a mixture of additives required to vulcanise or "cure" a rubber. The three main classes of chemicals used for curing in this vulcanising system are vulcanising agents, accelerators and activators. Accelerated sulphur vulcanisation systems may give mono-, di-, tri- or higher polysulphidic cross-links and the types of cross-links obtained are determined by the amount and type of vulcanisation systems used (the ratio of mass of sulphur to accelerator) (Porter, 1969). They also contain main chain modifications such as cyclic sulphides, pendent accelerator group, and extra network materials which are primarily vulcanisation residues. A diagrammatic representation of the network structure of a sulphur vulcanisate is shown in figure 2.6. The accelerated sulphur vulcanisation systems can be classified into three types:

1. Conventional systems (CV); containing high sulphur to accelerator ratios.
2. Efficient systems (EV); containing high accelerator to sulphur ratios.
3. Semi efficient systems (Semi-EV); that is, intermediate between 1 and 2.

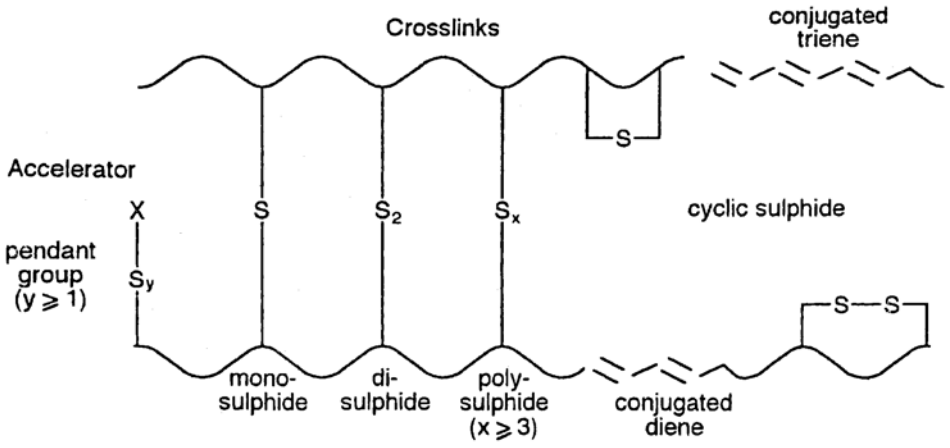

Figure 2.6 A diagrammatic representation of the network structure of a sulphur vulcanisate (Chapman and Porter, 1988).

2.5.3 **Conventional sulphur systems**

Conventional vulcanising systems (CV systems) have a high ratio of sulphur (2–3.5 phr by mass) to accelerator (0.5–1.0 phr by mass). These systems contain more polysulphidic cross-links (70–80%) than the disulphidic cross-links (20–30%) with a relatively high degree of polymer chain modification. These systems give vulcanisates which have excellent initial properties like strength, resilience and resistance to fatigue and abrasion and are satisfactory for many applications. However, they show poor heat and oxidation resistance because the polysulphidic cross-links are thermally unstable and can be readily oxidised (Porter, 1968).

2.5.4 **Efficient sulphur systems**

Efficient vulcanising systems (EV systems) have a low ratio of sulphur (0.3–1.0 phr by mass) to accelerator (2.0–6.0 phr by mass). They give mainly monosulphidic cross-links and less polymer chain modification. EV systems show good heat stability and oxidation resistance, but have a poorer resistance to fatigue because of the presence of the monosulphidic cross-links (Chapman and Porter, 1988; Skinner and Watson, 1967).

2.5.5 **Semi-efficient sulphur systems**

Semi efficient vulcanising systems are intermediate between CV systems and EV systems, with similar levels of accelerator (1.0–2.5 phr by mass) and sulphur (1.0–2.0 phr by mass) (Porter, 1973). This results in approximately equal amounts of monosulphidic and polysulphidic chains to be present in the rubber network. They offer a compromise between a good resistance to thermal ageing and a good fatigue life performance.

2.5.6 **Peroxide vulcanisation**

Peroxides are another curing system for rubbers. Unlike sulphur curing, double bonds are not required along the polymer chain for peroxide vulcanisation. Saturated rubbers like ethylene propylene rubber and silicone rubber cannot be cross-linked by sulphur and accelerators, and organic peroxides are often used for their vulcanisation. When peroxides decompose, free radicals are formed on the polymer chains, and these chains then combine to form carbon-to-carbon bonds (C-C) which serve as cross-links. A diagram illustrating the cross-link system in peroxide vulcanisation is given in figure 2.7.

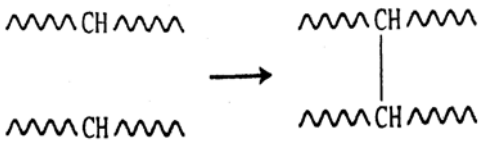

Figure 2.7 Chemical structure of carbon to carbon cross-link in a peroxide cured network.

Peroxide vulcanisates have the best heat resistance when suitable antioxidants are also included due to the good stability of C-C cross-links (Bristow, 1970). However, cure rates are slow and their formation can require higher temperatures. Long cure times are needed to ensure the complete decomposition of the peroxide so that resistance to

oxidative ageing is retained. Peroxide vulcanisates have a worse resistance to low temperature crystallisation and inferior strength properties compared with sulphur vulcanised rubber (Barlow, 1988; Baker, 1988).

2.6 **Rubber-like elasticity**

Elastomers exhibit a unique property of being capable of being stretched to several hundred percents of their original length when loaded and recovering upon removal of the load. For most engineering elastomers, extension within the range of 200% to 1000% is typical. The engineering stress-strain relationship becomes non-linear at deformations that are this large and much lower. As a result a single parameter (Young's modulus) to describe the modulus of the elastomer is inappropriate. However, as is the case with most solids at small strains, the force extension relationship is considered to be approximately linear and a small strain elastic modulus is often used in engineering practice.

2.6.1 **Rubber-like elasticity (at small strains)**

Elastomers can be considered to be elastic and isotropic in their undeformed state and can, therefore, be characterised by only two fundamental elastic constants. The first deals with the materials resistance to compression under a hydrostatic pressure. It is termed the bulk modulus B and defined as the ratio of the applied pressure to the volumetric strain. The second term is the shear modulus G, which is defined as the ratio of the applied shear stress τ required to produce a shear strain γ. The other frequently used small strain elastic constants, the tensile modulus E and Poisson's ratio ν, are related to the bulk modulus and the shear modulus as shown below,

$$G = \frac{E}{2(1+\nu)} \qquad \text{(Eq.2-1)}$$

$$B = \frac{E}{3(1-2\nu)} \qquad \text{(Eq.2-2)}$$

Elastomers being a unique class of engineering materials have very low shear and tensile moduli (in the region of 0.5–10 MPa) while the bulk modulus is typically very large (at about 1.5–2.0 GPa). As a result the value of Poisson's ratio is close to 0.5 (typically, 0.4995) (Sperling, 2001) and the tensile modulus E is almost exactly equal to $3G$. For many engineering applications elastomers can be considered as being

incompressible and the elastic behaviour at small strains (<10% strain) can be defined by just a single elastic constant *G* (Gent, 1992).

2.6.2 **Rubber-like elasticity (at large strains)**

There are two main approaches that attempt to describe the large strain behaviour of elastomers. These are either molecular models based around the configuration entropy of the rubber network (the simplest of which is known as the simple statistical theory) and various other phenomenological approaches (Sperling, 2001).

1) Molecular approach

   The molecular approach is based on the random morphology of the rubber chain molecular network in three-dimensions and the response of this network to the application or removal of a force.

2) Phenomenological approach

   The phenomenological approach can be based on classical mechanics, and just attempts to model the behaviour in a suitable mathematical way without assuming any specific arrangement of the polymer molecules.

Both approaches can result in the derivation of a stored or strain energy function (SEF). This is a measure of the amount of recoverable elastic energy W, stored in a unit volume of the material having been subjected to a specific state of strain.

2.6.3 **Thermodynamics of elastomer deformation**

Two phenomena are observed in elastomers, which indicate that elastic behaviour and the thermodynamic behaviour are related.

1. When an elastomer is stretched rapidly, it warms up. Conversely, when a stretched specimen is allowed to contract, it cools down.
2. Under conditions of constant load, the stretched length decreases on heating and increases on cooling.

The two effects are known as the thermo-elastic properties or Gough-Joule effects (Treloar, 1975). It is possible to explain these two phenomena by considering the deformation of the rubber in thermodynamic terms. The first law of thermodynamics gives the definition for a change in the internal energy, dU:

$$\mathrm{d}U = \mathrm{d}Q + \mathrm{d}W \qquad \text{(Eq.2-3)}$$

where dQ is the heat absorbed by the system and dW is the work done by external force. This equation states that the increase in dU in any change taking place in a system equals the sum of the energy added to the system by the heat process, dQ, and the work performed on it dW.

The second law of thermodynamics defines the entropy change dS in any reversible process as:

$$\mathrm{d}S = \frac{\mathrm{d}Q}{\vartheta} \qquad \text{(Eq.2-4)}$$

where ϑ is the temperature and dS is the change in the entropy of the system.

For a reversible process, combining both laws of thermodynamics gives;

$$\mathrm{d}U = \vartheta \mathrm{d}S + \mathrm{d}W \qquad \text{(Eq.2-5)}$$

For elastic solids, the work done by the applied stress is important. If tensile force is F and l is the initial length of the elastic specimen in the direction of the force, the work done in creating an elongation dl is:

$$\mathrm{d}W = F\mathrm{d}l \qquad \text{(Eq.2-6)}$$

The force, F in the tension mode can be expressed from equation 2-6 in the form of

$$F = \left(\frac{\partial U}{\partial l}\right)_{\vartheta} - \vartheta\left(\frac{\partial S}{\partial l}\right)_{\vartheta} \qquad \text{(Eq.2-7)}$$

The first term refers to the change in internal energy with extension and the second term to the change in entropy with extension. From thermodynamic considerations it can be shown that:

$$\left(\frac{\partial F}{\partial \vartheta}\right)_{1} = -\left(\frac{\partial S}{\partial l}\right)_{\vartheta} \qquad \text{(Eq.2-8)}$$

This gives the entropy change per unit extension, $\left(\frac{\partial S}{\partial l}\right)_{\vartheta}$, in terms of the temperature coefficient of tension at constant length $\left(\frac{\partial F}{\partial \vartheta}\right)_{1}$, which can be measured. When an elastomer is stretched the randomly coiled molecules are straightened and this decreases the disorder and hence also decreases the entropy of the network. Therefore, the entropy of elongation at constant temperature must be negative. Therefore,

$$F = \left(\frac{\partial U}{\partial l}\right)_{\vartheta} + \vartheta\left(\frac{\partial F}{\partial \vartheta}\right)_{1} \qquad \text{(Eq.2-9)}$$

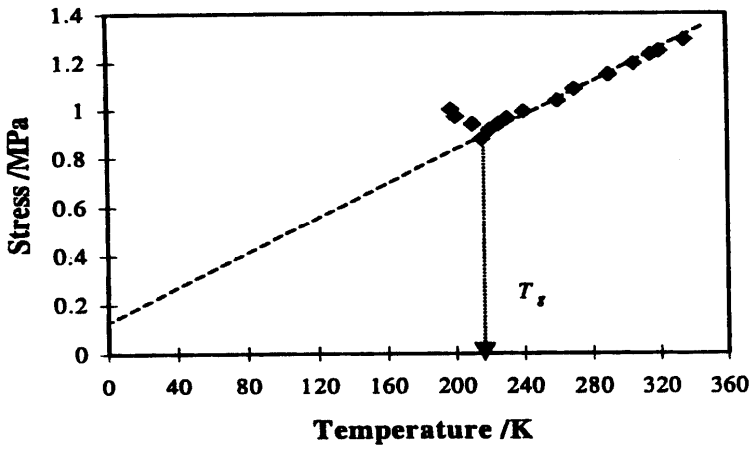

Figure 2.8 Stress at constant extension as a function of absolute temperature, at an extension of 350% (Meyer and Ferri, 1935)

This equation allows the internal energy term and entropy term to be evaluated. Meyer and Ferri (1935) investigated the relation between the force, at an applied strain of 350%, against the temperature. Their results are shown in figure 2.8 and indicate that the relationship between stress and temperature in the rubbery region, when the temperature is higher than the glass transition temperature, is linear and can be extrapolated to approximately zero tension at absolute zero temperature. This relationship implies that the change in the entropy with an extension is temperature independent. The approximately zero intercept indicates that there is virtually no change in the internal energy associated with the extension. The small discrepancy might be explained by complications caused by the effects of thermal expansion. From the thermodynamic theory, it is seen that the deformation of the rubber network involves a reversible transformation of work into heat. This thermodynamic concept is a basic foundation for the statistical development of the kinetic theory of rubber elasticity.

2.6.4 **The statistical theory of elasticity**

The statistical treatment requires the calculation of the entropy of the whole assembly of chains as a function of the macroscopic state of strain in the sample and the derivation of the free energy or work of deformation. The work done in deforming the rubber elastically is considered to arise from the decrease in entropy when the molecules are forced by deformation to take up a less probable configuration. The development of the theory for a cross-linked rubber has been carried out by a number of workers; Kuhn (1936), Wall (1942), James and Guth (1943) and Treloar (1943).

The assumptions of the theory are:

1. The network contains N chains per unit volume each containing q identical, freely jointed links of length l. A chain is defined as a segment of molecules between successive cross-links.
2. The rubber deforms in a manner which causes the configurational entropy of the chains to alter, but which results in no change in internal energy.
3. The distribution of possible end to end distance, r, follows a Gaussian distribution in the unstrained state described by a probability density function:

$$\mathrm{P}(r)\mathrm{d}r = \left(\frac{b^3}{\pi^{3/2}}\right) 4\pi r^2 \exp(-b^2 r^2)\mathrm{d}r \qquad \text{(Eq.2-10)}$$

where $b^2 = \dfrac{3}{2ql^2}$. It follows that the root-mean-square distance is given by $\sqrt{\bar{r}^2} = l\sqrt{q}$ and it is implicit in assuming a Gaussian distribution that $r << ql$; in other words the end to end distance of the chains is much less than their fully extended length.

4. The volume remains unchanged on deformation. (That is the material is incompressible).
5. The cross-links move in deformation as if embedded in an elastic continuum so that the components of length in each chain change in the same ratio as in the bulk rubber. This is known as the assumption of affine deformation.
6. The entropy of the individual chains is given by:

$$S = C - \frac{3\mathbf{k}r^2}{2ql^2} \qquad \text{(Eq.2-11)}$$

where C is arbitrary constant and **k** is the Boltzmann constant. The entropy of the network is the sum of the entropies of the individual chains.

Using equation 2-11 to calculate the entropy change associated with deforming a chain and summed over the assembly of N chains yields:

$$\Delta S = -\frac{1}{2} N\mathbf{k}(\lambda_1^2 + \lambda_2^2 + \lambda_3^2 - 3) \qquad \text{(Eq.2-12)}$$

where ΔS is the change in entropy of the network per unit volume under a deformation in which λ_1, λ_2 and λ_3 are the three principal extension ratios (the ratios of the stretched to unstretched length) along three mutually perpendicular axes. Thus a unit cube would be deformed into a cuboid of edge lengths λ_1, λ_2 and λ_3. The basic assumption of the kinetic theory is that all states of deformation have the same internal energy $(\Delta U = 0)$ and the same non-configurational entropy. Hence, for an isothermal reversible process the work W done by the applied forces becomes:

$$W = \Delta U - \vartheta \Delta S = -\vartheta \Delta S \qquad \text{(Eq.2-13)}$$

The work of deformation per unit volume is then:

$$W = \frac{1}{2} N\mathbf{k}\vartheta(\lambda_1^2 + \lambda_2^2 + \lambda_3^2 - 3) \qquad \text{(Eq.2-14)}$$

W represents the work of deformation or elastically stored energy per unit volume and is also called the strain energy function. It is convenient to write:

$$G = N\mathbf{k}\vartheta = nR\vartheta = \frac{\rho \mathbf{R}\vartheta}{m_c} \qquad \text{(Eq.2-15)}$$

where n is the number of moles of chains per unit volume, ρ is the density of rubber, **R** is the gas constant, ϑ is the temperature and m_c is the number average molecular weight of segments of molecules between successive cross-links. Equation 2-14 becomes:

$$W = \frac{1}{2} G(\lambda_1^2 + \lambda_2^2 + \lambda_3^2 - 3) \qquad \text{(Eq.2-16)}$$

Thus, the strain energy function represented by equation 2-16 involves only one physical constant, G, which may be determined from the degree of cross-linking in the rubber. If the assumption of constant volume is applied then;

$$\lambda_1 \lambda_2 \lambda_3 = 1 \qquad \text{(Eq.2-17)}$$

in simple tensile extension which can be defined in terms of a single extension ratio λ. The two equal contractions in the transverse directions can be derived from the incompressibility condition as:

$$\lambda_1 = \lambda, \quad \lambda_2 = \lambda_3 = \frac{1}{\sqrt{\lambda}} \qquad \text{(Eq.2-18)}$$

and equation 2-16 becomes:

$$W = \frac{1}{2} G(\lambda^2 + \frac{2}{\lambda} - 3) \qquad \text{(Eq.2-19)}$$

The force per unit undeformed cross sectional area or engineering stress σ required to deform the network is given by (Treloar, 1975):

$$\sigma = \frac{\mathrm{d}W}{\mathrm{d}\lambda} = G(\lambda - \frac{1}{\lambda^2}) \qquad \text{(Eq.2-20)}$$

For an incompressible material the state of deformation is unaffected by the imposition of the hydrostatic stress. The differences between any two principal stresses in any homogeneous deformation may be determined absolutely. These are given by:

$$\sigma_1 - \sigma_2 = G\left(\lambda_1^2 - \lambda_2^2\right)$$

$$\sigma_2 - \sigma_3 = G\left(\lambda_2^2 - \lambda_2^2\right)$$

$$\sigma_3 - \sigma_1 = G\left(\lambda_3^2 - \lambda_1^2\right) \qquad \text{(Eq.2-21)}$$

The stress-strain behaviour for particular modes of deformation may be determined from equation 2-21 by the substitution of the appropriate relationships for the stresses and the extension ratios. Experimental examination of the stress-strain relationships in figure 2.9 (tensile stress versus strain plotted with the relation predicted in tension using equation 2-20) however, reveals significant deviations between the theoretical and experimental results. In simple extension there are two distinct deviations (Treloar, 1944). This theory is subject to all the limitations imposed by the assumption of the Gaussian chain behaviour and in addition to the assumption of affine deformation. The theory worked quite well over a limited range of extension ratios ranging from about 1.0 to 1.3. Above this range, deviations from the theory were apparent, especially in uniaxial extensions where, at extension ratios between 1.3 and 5.5, the theory predicted a modulus that was higher. At extensions greater than 5.5, the measured stress-strain behaviour for an actual elastomer showed a marked upturn which this simple statistical theory failed to predict. The deviation at higher strains (>400%) is caused by the effects of a finite chain extensibility which is not considered (Wall, 1942; James and Guth, 1943). In strain crystallising elastomers, strain-induced crystallisation effects, which also increase the materials stiffness, dominate at high strains.

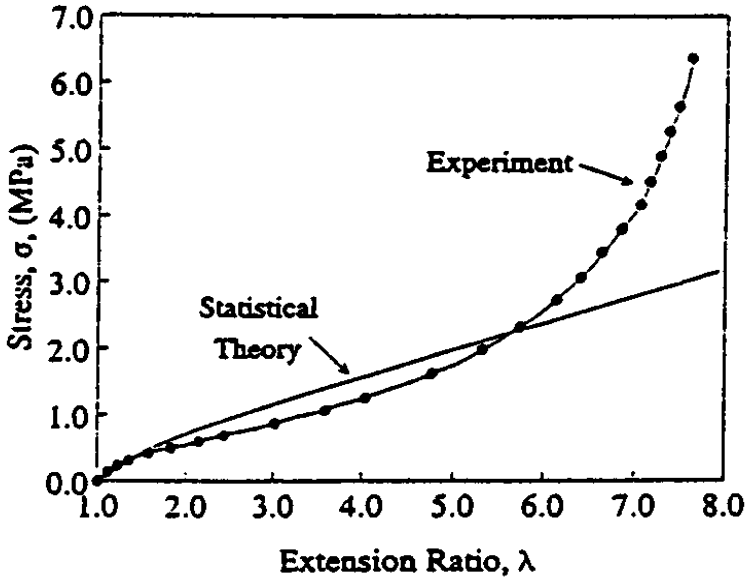

Figure 2.9 Comparison of statistical theory with experimental data for unfilled elastomers by Treloar (1975).

2.6.5 **Phenomenological theories**

Phenomenological approaches are based upon a mathematical description of the stress-strain behaviour and not on molecular or structural concepts of the material, assuming an isotropic material in the unstrained state. These theories represent the large strain behaviour of both unfilled elastomers and filled elastomers. This, rather general, treatment of the stress-strain relations of rubber-like solids started with Mooney (1940) before the derivation of the statistical theory, and was further developed by Rivlin (1956). Other forms of the stored energy function have been developed by many workers since then, a detailed review of Rivlin's theory and the work of others, including the Yeoh stored energy function which was used in all the finite element analysis work in this thesis, can be found in Busfield (2000). The Yeoh stored energy function was chosen to model the material behaviour in this work because of its accuracy in modelling the stiffness behaviour of filled elastomers at large strains. The Yeoh stored energy function is also able to accurately predict the stress strain behaviour of filled elastomers in different deformation modes using experimental data measured in one simple deformation mode such as uni-axial extension. The Yeoh model differs

from other higher order models in that it depends on the first strain invariant only. Its accuracy at fitting stress strain data at low strains is limited and therefore caution needs to be excercised when applying this model at low strains (Gent, 1992). In the following section, the theory of Mooney is reviewed.

2.6.6 **The theory of Mooney**

One of the earliest and most widely applied of the phenomenological theories is that due to Mooney (1940). Mooney was concerned with the problem of developing a general theory for large elastic deformations. Making use of the assumptions that a rubber is incompressible and isotropic in the unstrained state, and that Hooke's Law is obeyed in simple shear, Mooney derived by purely mathematical arguments based on the considerations of symmetry, the following stored energy function,

$$W = C_1\left(\lambda_1^2 + \lambda_2^2 + \lambda_3^2 - 3\right) + C_2\left(\frac{1}{\lambda_1^2} + \frac{1}{\lambda_2^2} + \frac{1}{\lambda_3^2} - 3\right) \qquad \text{(Eq.2-22)}$$

which contains two elastic constants, C_1 and C_2. The first term in equation 2-22 corresponds to the form derived from the statistical theory with $2C_1 = N\mathbf{k}\vartheta$. The statistical theory is therefore a particular case of the Mooney function corresponding to $C_2 = 0$.

For a simple extension or uniaxial compression, where $\lambda_2 = \lambda_3 = \frac{1}{\sqrt{\lambda}}$ equation 2-22 becomes,

$$W = C_1\left(\lambda_1^2 + \frac{2}{\lambda_1} - 3\right) + C_2\left(\frac{1}{\lambda_1^2} + 2\lambda_1 - 3\right) \qquad \text{(Eq.2-23)}$$

and the nominal stress is given by

$$\sigma = \frac{\mathrm{d}W}{\mathrm{d}\lambda} = 2\left(\lambda_1 - \frac{1}{\lambda_1^2}\right)\left(C_1 + \frac{C_2}{\lambda_1}\right) \qquad \text{(Eq.2-24)}$$

The term C_1 was found to be dependent on the cross-link density and was consequently related to the elastic constant of the statistical theory (Gumbrell et al, 1953). The origin of the C_2 term is still not clear, but it can be regarded as a measure of the departure of the observed stress-strain relationship from the form suggested by the statistical theory. Numerous experiments have been carried out which give support to the applicability of the Mooney equation in simple extension for natural rubber and other polymers (Grumbell et al., 1953; Mooney, 1940). However, the data of Rivlin and Saunders

(1951) for equibiaxial extension (which is kinematically equivalent to uniaxial compression) showed a marked deviation from the Mooney relationship. Figure 2.10 shows the relationship between the extension and compression. In the extension region ($1/\lambda<1$) the Mooney line corresponds to a value of $C_2/C_1\approx0.8$, but in compression ($1/\lambda>1$), C_2 was found to be about zero. Thus, when considering the extension and compression data together, it is clear that the Mooney equation is no improvement over the statistical theory. Taken as a whole, the Mooney equation does not seem to give a closer fit to the experimental data than the statistical theory. The interpretation of experimental data using the Mooney equation must be treated with caution since the Mooney form of the stored energy function cannot be adequately used to describe the mechanical properties of rubber for all possible types of strain, particularly those in compression predicted using properties measured in tension.

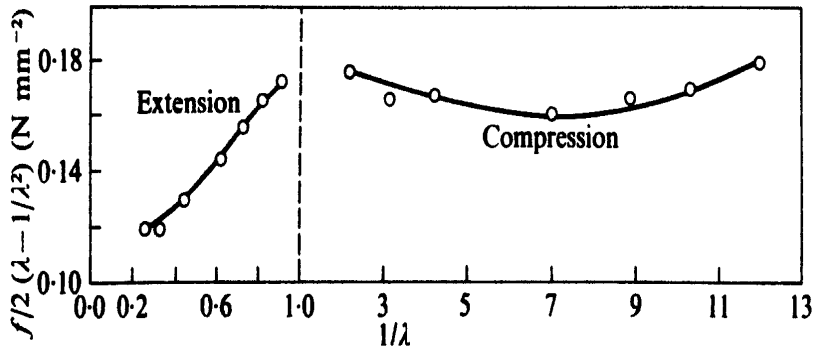

Figure 2.10 Mooney plot for data of simple extension and uniaxial compression (Treloar, 1975).

2.6.7 **Imperfect elasticity**

The preceding section of rubber-like elasticity was concerned mainly with the ideal behaviour of elastomers, which were assumed to follow reversible relations between load and displacement. In practice, deviations from such ideal behaviour are to be expected. An ideal elastic solid obeys Hooke's law: stress is proportional to strain. An ideal viscous liquid obeys Newton's law: stress is proportional to rate of change of strain with time. Many materials and elastomers in particular, have properties that are intermediate between these two cases. The response of these materials, which act neither as ideal elastic solids nor as ideal liquids, is known as viscoelastic behaviour. While viscous properties might be desired in elastomers for shock damping applications, many industrial problems arise as a consequence of excessive viscous response. Such common phenomena as stress relaxation, creep, compression set (and unrecovered deformations, in general), energy losses during a deformation cycle ("hysteresis"), limited rebound, heat generation, temperature rise during flexing and cyclic stress relaxation are all manifestations of the inelastic properties of elastomers.

2.6.8 **Stress relaxation, creep, set recovery and hysteresis**

Stress relaxation is a time-dependent reduction in stress under constant deformation. It is usually defined as the loss in stress expressed as a percentage of the initial stress. Thus,

$$\text{Stress loss } (t) = \frac{\sigma_o - \sigma_t}{\sigma_o} \times 100\% \qquad \text{(Eq.2-25)}$$

where σ_0 is the initial stress and σ_t is the stress at time t. The rate of stress relaxation is then the stress relaxation divided by some function of time.

Creep is the increase in strain with time at a specified load and is usually expressed as a percentage of the initial deflection. Thus,

$$\text{Creep } (t) = \frac{l_t - l_i}{l_i} \times 100\% \qquad \text{(Eq.2-26)}$$

where l_t is the length of rubber specimen at time t and l_i is the initial extended length of the specimens. The initial deflection must be measured at a defined initial time t_o, which should be about 10 times longer than the time taken to apply the deformation. Set is a specific deformation, which remains when a material is released from the force imposed on it. Thus, set measures the ability of the elastomer to recover its original

dimensions. When the deformation is tensile, it is referred to as tension set. Hence, tension set is defined as:

$$\text{Set}\,(t) = \frac{l_x - l_o}{l_i - l_o} \times 100\% \qquad \text{(Eq.2-27)}$$

where l_x is the recovered length, l_o is the initial length and l_i is the extended length (Gent, 1992). Energy lost during loading and unloading cycles in a cyclic test is termed hysteresis. Here the energy dissipated during a loading cycle is considered as the area between the loading and the unloading cycle. Examples are shown in Figure 2.11 taken from Lindley (1974b). For an unfilled elastomer, the magnitude of the energy loss at extension ratios below 3 is quite small. Payne and Whittaker (1972) showed that at higher extension ratios in excess of 4 with strain crystallising elastomers, such as natural rubber, the amount of hysteresis was dramatically increased due to the formation and the dissolution of strain induced crystals during the loading cycle. This hysteresis, expressed as the fraction of the energy input lost, increases as the fraction of particulate filler is increased. Payne (1962) and Deeprasertkul (2000) attributed this to the breakdown and reformations of the agglomerates of the carbon black particles that can themselves dissipate energy.

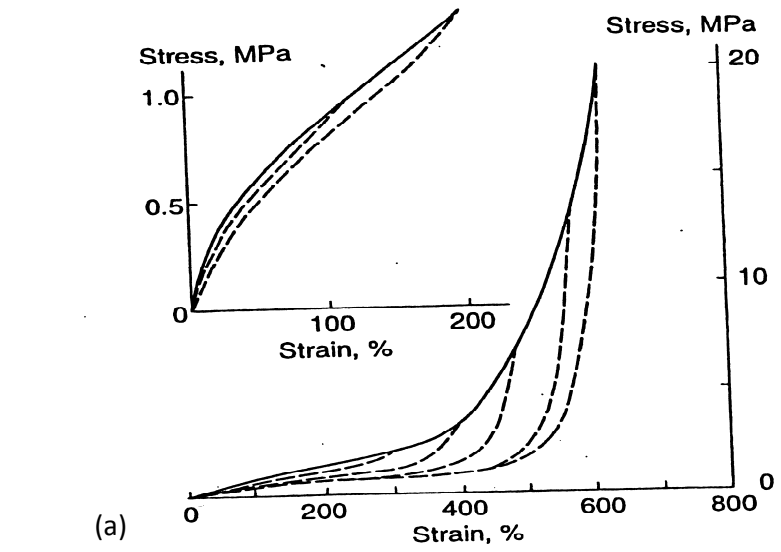

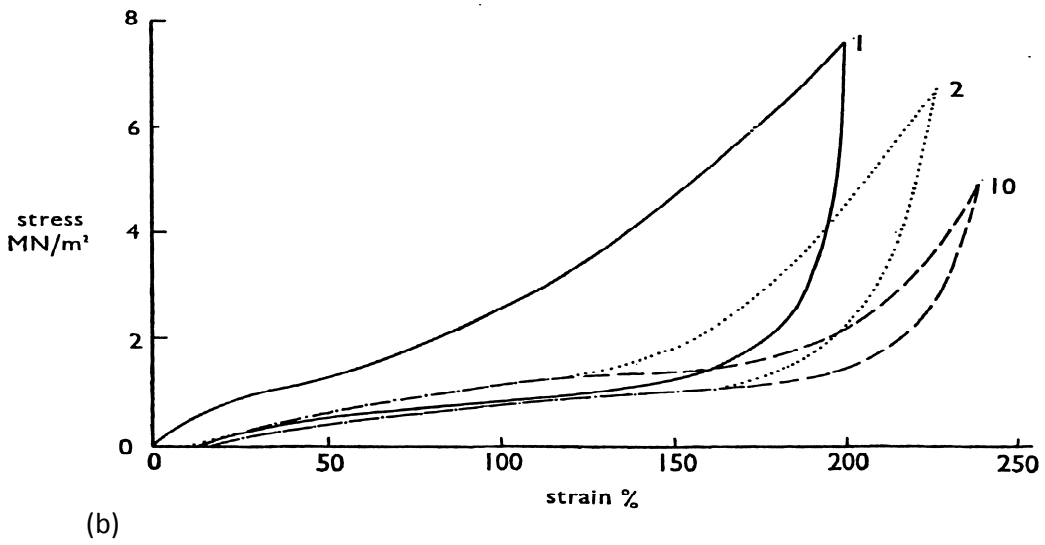

Figure 2.11 Hysteresis loops for natural rubber taken from Lindley (1974b). (a) The first cycle loops for unfilled natural rubber extended to various strains and (b) first, second and tenth cycle loops for a natural rubber that contains 50 phr of carbon black.

2.6.9 **Cyclic stress relaxation**

Many engineering components undergo repeated stressing. Under repeated stressing it is well known that rubber materials exhibit cyclic stress relaxation. Under specific conditions for many components, this results in fatigue failure such as that described by Busfield et al. (2005), Papadopoulos et al. (2008) and Busfield et al. (2002). Cyclic stress relaxation involves a reduction in the stress attained on the second and successive loading cycles as compared with the stress attained on the first cycle in a stress strain cyclic test of fixed strain amplitude. This cyclic stress relaxation behaviour is sometimes mistakenly referred to as the Mullins (1948) effect. This is inappropriate, as the classical Mullins effect describes behaviour where if the maximum strain experienced previously by the rubber is exceeded, the stress strain curve returns to the value measured in the virgin cycle. The relaxation phenomenon has been studied for simple extension by Derham and Thomas (1977), McKenna and Zappas (1981), Davies et al. (1996) and Pond and Thomas (1979), but not for other deformation modes. It was found that the fractional relaxation or creep rate was strongly dependent on the maximum stress as well as the composition of the compound. In particular the filler content and the ability to strain crystallise appears to be important in enhancing the relaxation rate. Rubber in engineering applications experiences many modes of deformation. One of the key aims of this thesis is therefore to examine how cyclic stress relaxation might be predicted in more than one mode of deformation. In chapter 4, results of cyclic stress relaxation measurements on test pieces and cylindrical bonded elastomer components will be presented and discussed.

2.7 **Fracture mechanics**

A fracture mechanics approach that was based upon an energy balance approach was originally developed by Griffith in 1920 for brittle materials. Griffith observed that the stress needed to fracture bulk glass was much less compared with the theoretical stress needed for breaking atomic bonds in the glass. Griffith conducted experiments on glass fibres which showed an increase in the fracture stress of the glass fibre samples as the diameter decreased. Griffith attributed the observed reduction in strength of the bulk glass compared with its theoretical strength and the increase in the fracture stress of the glass fibre with a decrease in its diameter to the presence of microscopic flaws (cracks) in the bulk of the glass material. In an effort to quantitatively assess the

influence of these flaws on the strength of the material Griffith assumed that, a crack in a strained sheet of glass will grow if the elastic stored energy released due to the crack growth was greater than the free energy required to create a new surface. He thus established a fracture criterion expressed in differential form as shown in equation 2-28.

$$2S_{\mathrm{E}} = -\frac{1}{t}\left(\frac{\partial U}{\partial c}\right)_{l} \qquad \text{(Eq.2-28)}$$

where S_{E} is the surface free energy per unit area, U is the total elastic energy stored in the sheet, c is the crack length, t is the sheet thickness and the subscript l indicates that the differentiation is carried out at constant overall extension so that the externally applied forces do no work. The adoption of the elasticity solution for the stress distribution in a loaded sheet containing an elliptical hole, made it possible for Griffith to calculate the differential for a crack in an infinite sheet. The results generated in his experiments containing flaws of a given size were in agreement with measurements of the surface energy of molten glass using the expression in Equation 2-28 above.

2.7.1 **Fracture mechanics of rubber**

The problem of crack growth in elastomers was originally studied by Rivlin and Thomas (1953). They extended the Griffith criterion for the growth of a crack in a brittle material to the case of vulcanised rubber. Griffith's approach can be applied to elastomers since it is not limited to small strains and linear elastic responses. However, the decrease in elastic strain energy in elastomers is not used only to increase surface free energy of the cracked body, but it is also partly transformed to other forms of energy, like irreversible deformations of the bulk of the material and dissipative processes at the crack tip. These dissipative processes at the crack tip occur in a relatively small volume of the material compared with the overall dimensions of the body. The three factors that determine the magnitude of the dissipation are: the viscoelastic properties of the elastomer, the strain in the crack tip region and the rate at which the crack is growing. Therefore, the energy required to drive a crack at a particular rate is a material characteristic and is defined as strain energy release rate which is also sometimes known as the tearing energy, T (Rivlin and Thomas, 1953).

$$T = -\frac{dU}{dA} \qquad \text{(Eq.2-29)}$$

where A is the area of a single fracture surface.

The detail of the crack tip is a very important aspect of the fracture process as stated earlier. In the work of Thomas (1955) he showed that a relationship exists between the strain energy release rate and the strain distribution around the tip of a crack of a defined radius in a test piece. Considering an incision of the form of two parallel sided slits terminated by a semicircle in a test piece, he proposed:

$$-\Delta U = \int_{-\frac{\pi}{2}}^{+\frac{\pi}{2}} W_\alpha \Delta c h r_t \cos\alpha \mathrm{d}\alpha \qquad \text{(Eq.2-30)}$$

where W_α is the elastic stored energy per unit volume of the rubber at the crack tip at an angular distance α from the pole, h is the thickness of the specimen and r_t is the radius of the semi-circle (figure 2.12).

Using equation 2-30 he showed that:

$$T = -\frac{1}{h}\left(\frac{\mathrm{d}U}{\mathrm{d}c}\right)_l = r_t \int_{-\frac{\pi}{2}}^{+\frac{\pi}{2}} W_\alpha \cos\alpha \mathrm{d}\alpha = W_t 2r_t = W_t d \qquad \text{(Eq.2-31)}$$

where W_t is a suitable average of W_α and d is the diameter of the model crack tip. Calculations of the strain energy release rate using the relation proposed, considering the over-all forces or strains applied to the test piece (Rivlin and Thomas, 1953), and that determined considering the strain distribution around the crack tip (Thomas, 1955) compared excellently. Thomas (1955) further showed that when test pieces were extended to tensile rupture, W_t in Equation 2-31 becomes the work to break per unit volume of rubber, W_b, and Equation 2-31 takes the form,

$$T = W_b d_b \text{ or } W_b = \frac{T}{d_b} \qquad \text{(Eq.2-32)}$$

where d_b is the diameter of the strained crack tip that results in a tensile rupture.

He verified this relationship experimentally by measuring the strain energy release rate of test pieces having modelled tip diameters in the range of 1mm to 3mm and found T/d_b to be fairly constant and approximately equal to the work to break (W_b) in tensile tests.

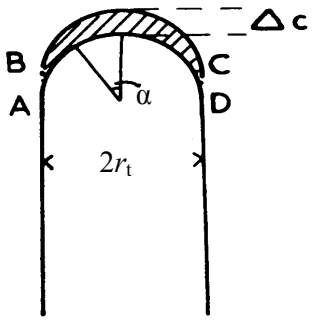

Figure 2.12 Schematic diagram for the shape of a crack tip used in equation Eq.2-30 (Thomas, 1955).

Following the work of Thomas (1955), extensive research has been carried out by other workers on the crack tip such as the work of Gent and Henry (1967). Andrews (1961, 1963) showed by applying a microscopic technique that, a combination of hysteresis and large displacements results in blunting of the crack tip in highly deformable materials. Andrews provided better understanding of the crack tip strain distribution and thus confirmed Thomas' (1955) conclusions. Rice (1968) developed a mathematical method which related the local crack tip conditions to the strain energy release rate known as the J-integral. The integral expresses an energy balance in a volume of material surrounding a crack tip. Rice showed that the value of the integral is independent of the choice of integration path. Hence, the path can be chosen close to the crack tip to give a measure of local crack tip conditions. The integration path may also be chosen to follow the boundaries of the specimen. Mars and Fatemi (2002) reported that under this condition the integral turns out to be equivalent to the strain energy release rate. It can be inferred, therefore, that the strain energy release rate is a measure of the intensity of local crack tip fields for a given material and crack tip geometry.

2.7.2 **Analytical expressions for the strain energy release rate, *T*, for some test piece geometries**

For rubber, we cannot assume that strains, and therefore stresses, are infinitesimal hence analytical calculation of T for a particular case may be very difficult. Rivlin and Thomas (1953), however, presented several different test pieces for which analytical expressions for T may be derived.

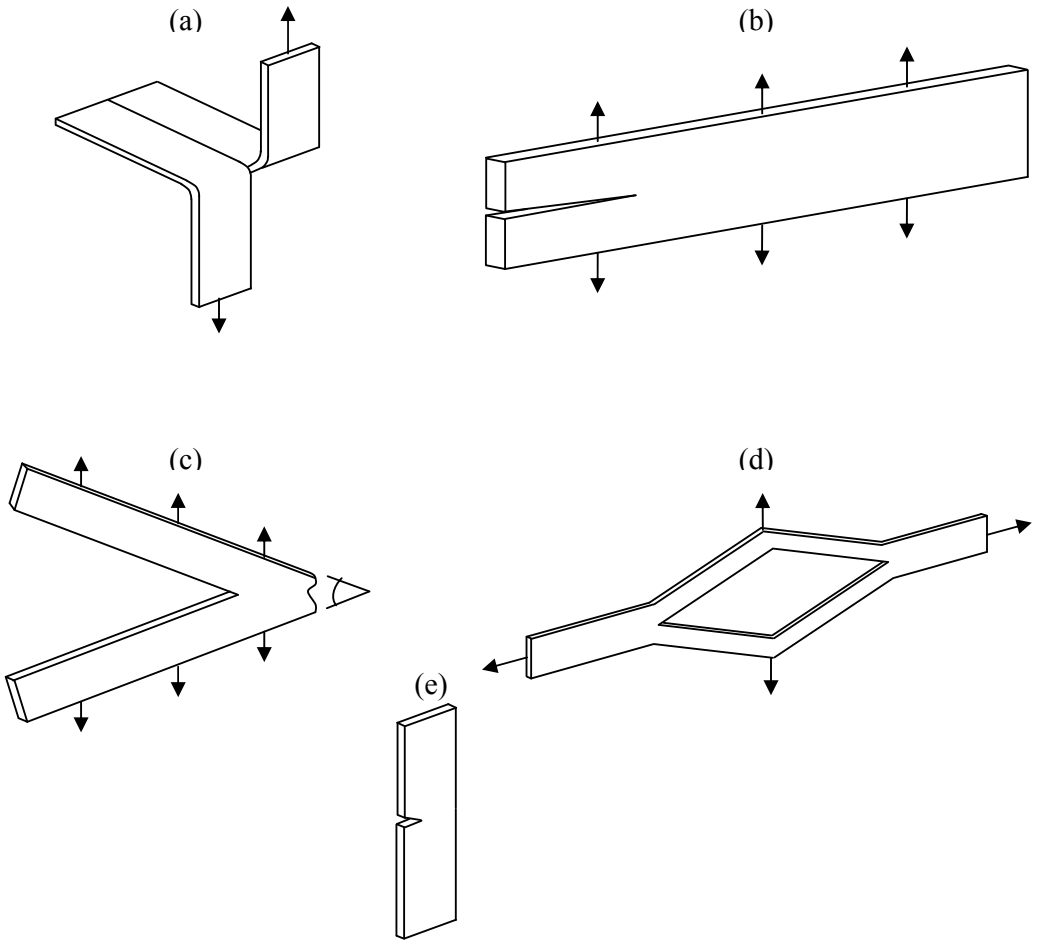

Figure 2.13 Types of tear test-pieces (a) trouser (b) pure shear (c) angled (d) split and (e) edge crack (Busfield, 2000).

Rivlin and Thomas (1953), Greensmith and Thomas (1955), Thomas (1960) and Lake et al. (1969) used differently shaped test pieces of the same material to test the hypothesis that the energy required to grow a crack at a given rate is geometrically independent and hence a material characteristic alone. Diagrams of the test piece geometries they used are shown in figure 2.13. The resulting relationships for calculating T for the different geometries are given below:

1. The trouser test crack growth measurement:

$$T = \frac{2F\lambda}{h} - w_0 W \qquad \text{(Eq.2-33)}$$

where F is the applied tearing force, λ is the extension ratio in the legs, h is the specimen thickness in the unstrained state, w_0 is the total width of the test piece and W is the elastic stored energy density in the legs of the test piece that are in simple extension.

2. The pure shear crack growth test:

This is preferred for crack growth studies because the crack grows at a constant rate for a specified applied strain. This enables the strain energy release rate to be determined as the complications caused by the stress concentration effects at the crack tip are eliminated. The strain energy release rate is given by,

$$T = Wl_0 \qquad \text{(Eq.2-34)}$$

where W is the elastic stored energy density in the region of the test piece which is subjected to the pure shear state and l_0 is the unstrained distance between the two parallel clamps.

3. The angle crack growth test:

$$T = \frac{2F}{t}\sin\left(\frac{\theta}{2}\right) \qquad \text{(Eq.2-35)}$$

where F and t are again the applied force and the test piece thickness and θ is the angle between the separating legs.

4. The split crack growth test:

$$T = \{[\ F_A\,\lambda_A \sin\theta + F_B\,(\lambda_A \cos\theta - \lambda_B)]/t\} - w_0\,(W_A - W_B) \qquad \text{(Eq.2-36)}$$

where F_A and F_B are the forces applied to the respective pairs of legs, λ_A, λ_B and W_A, W_B the corresponding extension ratios and stored energy densities respectively in the legs. 2θ corresponds to the angle of the opening ($\tan\theta = F_A / F_B$) and w_0 and t are the width and thickness of the test piece.

5. The edge crack in a tensile crack growth test piece:

In this case the strain energy release rate is given by

$$T = 2kWc \qquad \text{(Eq.2-37)}$$

where W is the elastic stored energy density in the bulk of the material at large strains, c is the crack length, and k is a changing strain dependent term, given as,

$$k \approx \frac{\pi}{\sqrt{\lambda}} \qquad \text{(Eq.2-38)}$$

where λ is the extension ratio (Lake, 1970).

2.7.3 **Microscopic flaws**

The work of Griffith in 1920 indicated the existence of intrinsic flaws in materials. Work by Mars and Fatami (2003) suggested that the fatigue phenomenon in elastomers consists of two stages: the crack nucleation stage and subsequently the crack growth stage. This view of the fatigue phenomenon assumes that no inherent flaws pre-exist in the elastomer material contrary to the observations made by Griffith in his work. Tsunoda (2001) in his work noted that fatigue crack initiation may arise from accidental scratches and nicks on the moulded or cut surface of the elastomer material. Further to that, Gent and Tompkins (1969) suggested that even if such scratches and nicks are carefully avoided by moulding the rubber material against polished glass surface, the breaking strength of the rubber is not increased dramatically. This implies that other sources of flaws such as dirt, dust particles, local inhomogeneities in cross-link density and filler particle distributions may be present in the material. An approach for estimating the size of intrinsic flaws in a material is by using equation 2-37 and taking T to be T_0 and c to be c_0. Here, T_0 is the threshold strain energy release rate and c_0, the edge crack length at T_0, the intrinsic flaw size. The threshold strain energy release rate may be described as the special energy release rate when the crack tip energy losses are minimised. Lake and Thomas (1967) carried out cyclic crack growth tests where they defined the minimum tearing limit at which cyclic crack growth will occur. They suggested that below T_0 crack growth was solely attributed to chemical attack by ozone. It is interesting to note that, the average size of intrinsic flaws has been found by this approach to be independent of the material compound formulation and of the order of 25 to 50μm. The work of Abraham (2002) and Kingston and Muhr (2012) suggest that there are flaws in commercial rubber components that have lengths in excess of 200μm. Abraham (2002) showed that the large scatter normally occurring in

a set of fatigue tests on rubber compounds could be eliminated by introducing regular flaws of 200μm throughout the test samples. It is useful to recall, however, that the rubber material type and formulation has effect on the strength of the elastomer. It appears that, there is no clear distinction between the crack nucleation and subsequent growth states as suggested by Fatami (2003). What then appears to be important is the rate at which an existing flaw of a given size grows for a specific set of loading conditions.

2.7.4 **The cyclic fatigue crack growth phenomenon**

In the work of Rivlin and Thomas (1953) they established that the energy required to grow a crack in a material at a given rate is a material characteristic. It is also generally observed that the extent of crack growth during a loading cycle is determined by the maximum strain energy release rate achieved in the loading cycle and that, the extent of crack growth is not affected very much by the manner in which the maximum strain energy release rate was achieved even for relatively viscous materials (Gent et al., 1964). The relationship between crack growth rate per cycle and the strain energy release rate may be represented mathematically in the form:

$$\frac{\mathrm{d}c}{\mathrm{d}n} = f(T) \qquad \text{(Eq.2-39)}$$

The crack growth rate per cycle and the strain energy release rate relationship is known as the crack growth characteristic of the material because it is independent of the test piece geometry. Lake (1983) presented typical curves of the crack growth characteristic for NR and SBR materials measured under relaxing conditions. Figure 2.14 (Lake, 1983) shows three distinct regions of crack growth characteristics. In region I the strain energy release rate, T, is less than the threshold strain energy release rate T_0 and hence no mechanical crack growth occurs (Tsunoda, 2001). Below T_0, crack growth is caused by ozone degradation and the crack growth characteristic may be expressed as:

$$\frac{\mathrm{d}c}{\mathrm{d}n} = k_z[O_3] = R_z \qquad \text{(Eq.2-40)}$$

where k_z is the rate constant due to ozone, $[O_3]$ is the ozone concentration and R_z is the crack growth rate. The chemical reaction between ozone and carbon-carbon double bonds, which are present in the backbone of natural and various olefin rubbers, is very rapid, resulting in molecular scission. Ozone attacks rubbers above a critical tensile

stress equivalent to a strain energy release rate of about 0.1 J/m^2 for unprotected NR and SBR compounds.

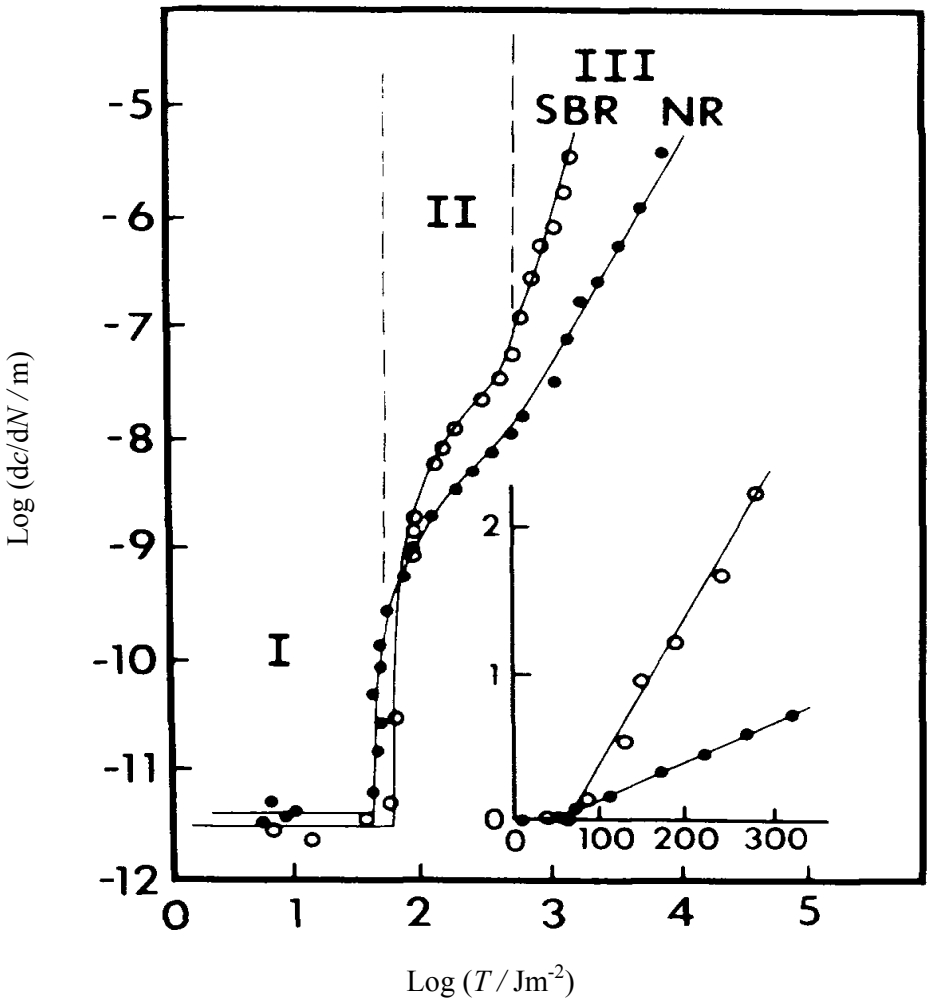

Figure 2.14 Crack growth per cycle, d*c*/d*n*, as a function of strain energy release rate, *T*, for unfilled NR (●) and SBR (o). The inset shows the region near the threshold strain energy release rate for mechanical fatigue, T_0, plotted on a linear scale (Lake (1983)).

Above this critical energy level, the rate of crack growth is proportional to ozone concentration (O_3) and independent of the strain energy release rate as expressed by equation 2-40. In region II, the crack growth is dependent on both ozone attack and mechanical factors in a somewhat linear and additive fashion. This may be expressed mathematically as:

$$\frac{\mathrm{d}c}{\mathrm{d}n} = R_z + A_t\left(T - T_0\right) \qquad \text{(Eq.2-41)}$$

where A_t is a crack growth constant for region II. In region III, the power law dependency between crack growth rate and T has been found for many rubbers as well as for non-rubbery materials. Thus;

$$\frac{dc}{dn} = \chi T^{\psi} \qquad \text{(Eq.2-42)}$$

where χ and ψ are constants, characteristic of region III. For natural rubber ψ is about 2, and for SBR, ψ is about 4. In general, ψ lies between 2 and 6 for most elastomers, depending mainly on the rubber and to a lesser extent on secondary factors such as compounding ingredients. At the highest values of strain energy release rate, dc/dn approaches the velocity of the elastic waves in rubber, about 50ms^{-1}. Thus;

$$T = T_c \qquad \text{(Eq.2-43)}$$

where T_c is the critical strain energy release rate, where catastrophic tearing takes place.

2.7.5 **The characteristics of steady state cyclic crack growth**

Lake and Thomas (1967) showed that the surface energy for elastomers amount to about 2 Jm^{-2}. The work of Greensmith et al. (1960), shown in figure 2.15, confirmed that unfilled SBR which does not undergo strain crystallisation at large strains, that a specific value of T is required to propagate a crack at a specific rate. Typical values of T for crack growth have been shown to lie in the region of 0.5 – 10 kJm^{-2} which is considerably greater than the surface energy of elastomers. This confirms that other irreversible changes occur as the crack is extended. The magnitude of the strain energy release rate depends significantly on the irreversible energy losses that take place as the crack is extended. These energy loss processes are dependent on temperature and so is the crack growth versus strain energy release rate relationship. The relationship between crack growth rate, temperature, and strain energy release rate is presented in figure 2.16 for unfilled SBR, NR and FT black filled SBR. Figure 2.16(a) which represents a plot for an unfilled SBR shows that strain energy release rate increases with increasing crack growth rate and decreasing temperature. Mullins (1959) pointed out that this dependence highlights the influence of visco-elastic energy dissipation processes. However, for the strain crystallising rubber NR, Figure 2.16(b), the effect of temperature on the rate of tear is much lower.

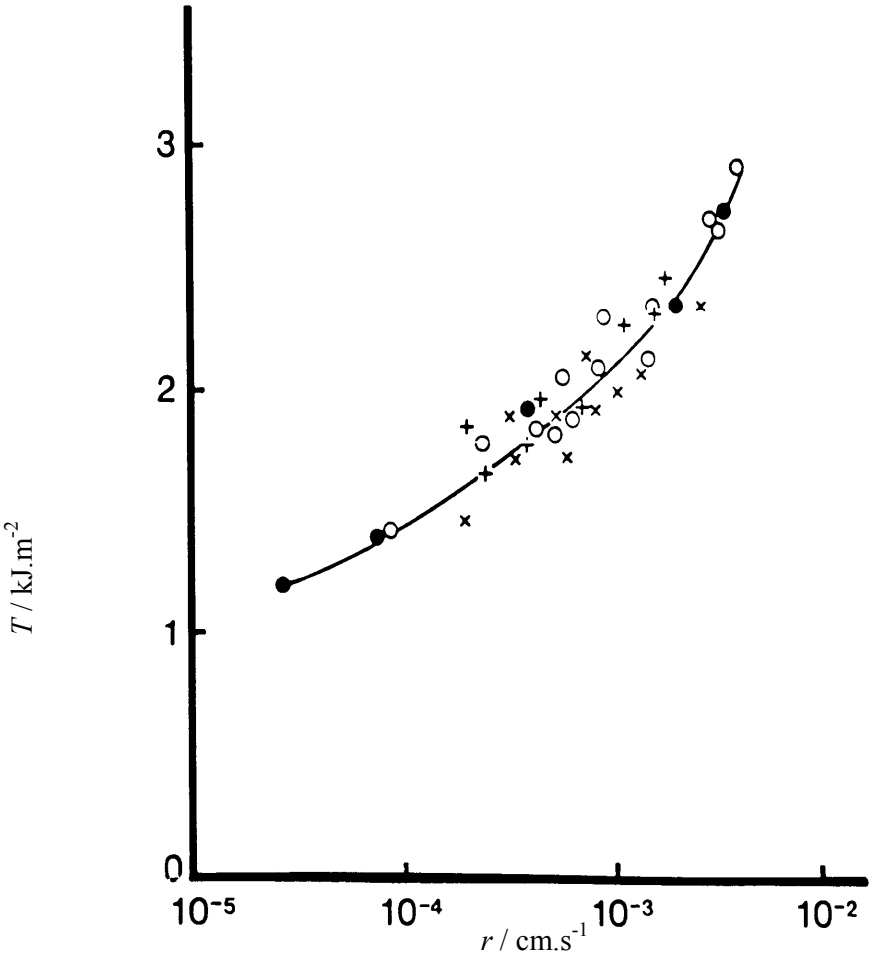

Figure 2.15 The strain energy release rate, *T* versus crack growth rate (*r*) for an unfilled SBR using the various test piece geometries shown in Figure 2.13. × - trousers; + - pure shear; ○ - angled and ● - split (Greensmith et al., 1960).

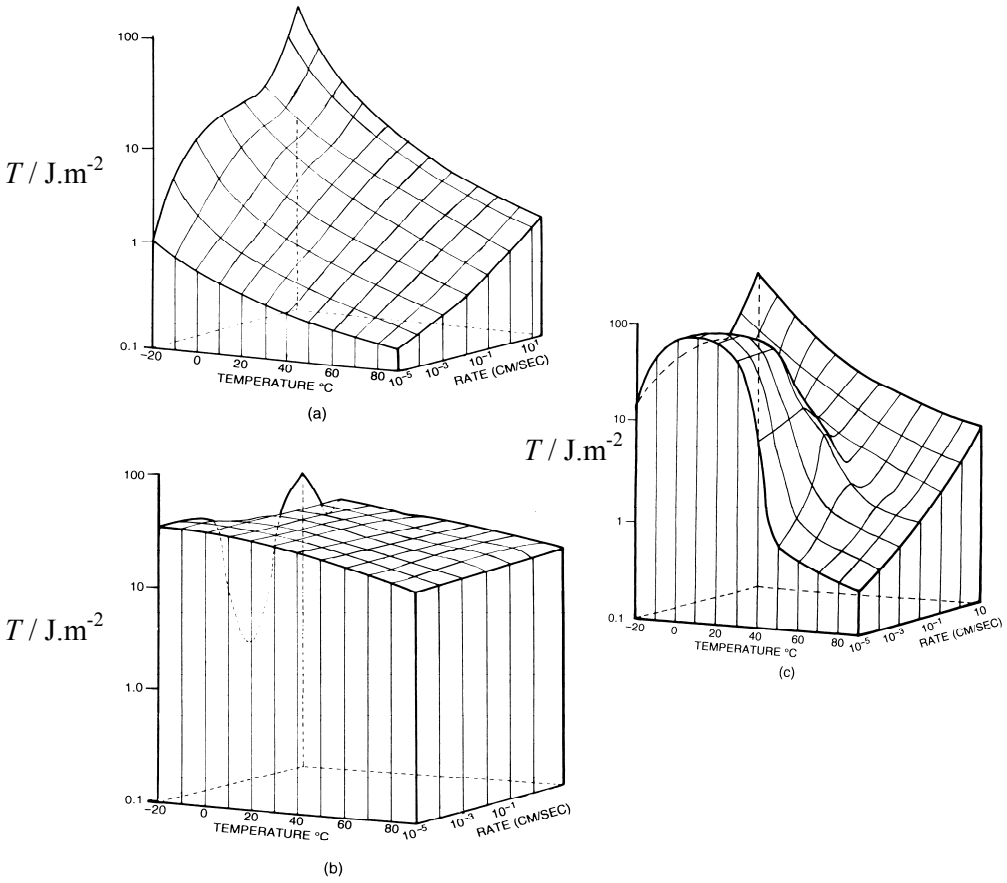

Figure 2.16 The effect of crack growth rate and temperature on strain energy release rate, *T* for (a) unfilled SBR, (b) unfilled NR and (c) FT black filled SBR. (Greensmith and Thomas, 1955).

In this case, strain crystallisation has the dominant influence on the crack growth behaviour and, according to Tsunoda (2001), the high strain energy release rate observed in NR, over a wide range of crack growth rates and temperatures, could be attributed to the high energy losses associated with the heat of strain crystallisation. The plot for carbon black filled SBR represented in Figure 2.16(c) demonstrates a plateau at low crack growth rates and at low temperatures. This plateau shows that a wide range of tear rates can exist for a specific strain energy release rate which results in the formation of knotty crack growth. Beyond this region, knotty crack growth does not occur and as a result the carbon black loading is responsible for a minimal increase in strain energy release rate compared with that of unfilled SBR. This leads to the conclusion that initiation of knotty crack growth depends on both crack growth rate and temperature. Tsunoda (2001) observed that even in the presence of carbon black, the crack growth behaviour is governed mainly by visco-elastic effects. In the presence of carbon black the strain energy release rate can, over certain ranges, decrease with increasing crack growth rate due to the onset of some degree of strength anisotropy. This phenomenon is also called crack tip blunting or knotty-tearing and is thought to be caused by strain-induced crystallisation or the presence of carbon black. "Knotty" tearing consists of a discontinuous stick-slip process, in which the tear develops laterally or even circularly under increasing force until a new tear breaks ahead and the tear force drops sharply. The tear pattern then repeats itself. Figure 2.17 (c) presents an example together with three other types of tear with their respective force and tear patterns. Steady tearing results in macroscopic surface roughness: small deviations from the tear path produce stick-slip tear and longer deviations give knotty-tearing. Apart from crystallisation mechanical energy loss due to hysteresis is also related to the visco-elastic properties of the material. The degree of dissipation is determined by the internal viscosity of the material which is a function of temperature. Williams et al. (1955) developed an equation which rationalises the temperature dependence of viscosity for glass-forming liquids. The equation is known as the WLF equation and is given as,

$$\log(a_t) = \frac{-C_1^{'}(T_M - T_S)}{C_2^{'} + T_M - T_S} \qquad \text{(Eq.2-44)}$$

where $T_S = T_g + 50^oC$, and T_M is the temperature at which the test is conducted. $C_1^{'}$ and $C_2^{'}$ are the WLF constants which have been found to vary from polymer to polymer (Sperling, 2001). Andrews (1964) used a WLF type relation to correlate rupture data at

various temperatures for non-crystallising elastomers. He observed that there is a close correlation between the strain energy release rate and the internal viscosity. Tsunoda (2001) carried out work on an unfilled SBR. In Figure 2.18 (Tsunoda, 2001) as expected the strain energy release rate, T available to drive a crack at a given rate decreased with increasing temperature as the visco-elastic losses decreased. The data were then shifted using Equation 2-44, taking $C_1^{'}$ = 8.86 and $C_2^{'}$ = 101.6 for unfilled SBR, to form the WLF relationship (Figure 2.19) (Tsunoda, 2001). The fact that the results from different temperatures superimposed in the fast crack growth rate range is also expected since the large visco-elastic losses at these rates were likely to dominate the crack growth process. The data in the slow crack growth range does not superimpose as well. This is where rough fracture surfaces developed suggesting that here the effective tip diameter, d also varied with temperature. Tsunoda (2001) remarked that fracture surfaces at a given rate become rougher with increasing temperature. This could be attributed to cavitation occurring more readily due to increased temperature. With increasing temperature the extent of cavitation increased as the elastic modulus decreased and hence d increased, resulting in rougher fracture surfaces. The strain energy release rate and hence the crack growth behaviour of an unfilled rubber depends on the nature of the backbone of the polymer molecule, the molar mass and the concentration and nature of cross-links. Depending on the vulcanisation process employed (Tsunoda, 2001), widely different strengths for the same polymer backbone can be produced, even when compared at similar degrees of cross-linking. Brown et al. (1987) investigated the effect of vulcanising systems on the strain energy release rate for mono-sulphide, poly-sulphide and peroxide cross-linked systems. The results are presented in Figure 2.20. From the plot, where the shear modulus is indicative of the cross-link density, the strain energy release rate required for a crack to grow at $10\mu ms^{-1}$ decreases with increasing shear modulus in all three vulcanising systems. The observed ranking of the strength was poly-sulphide cross-links had the greatest strength followed by mono-sulphide cross-links with the peroxide system producing the weakest cross-linked network. The decreasing order of strength follows an increase in the bond strength of the cross-link. Mullins (1959) concluded in his work that mechanically weak cross-links presumably re-distributed local stresses in the network by breaking and reforming during deformation. It is assumed that the poly-sulphidic cross-links break before the main polymer backbone chain under the high

stresses around the crack tip resulting in higher strength for the poly-sulphidic cross-links than for C-C cross-links.

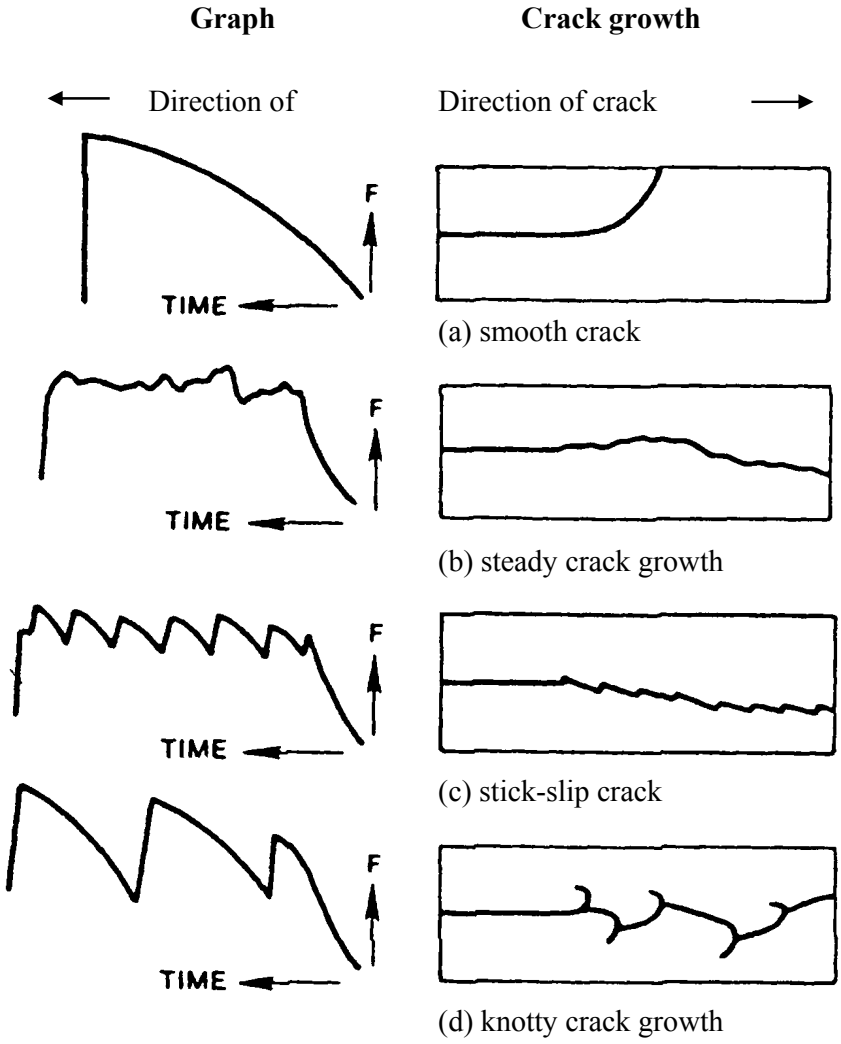

Figure 2.17 Schematic diagrams illustrating force–time relationships and crack paths for different types of crack growth (Papadopoulos, 2006).

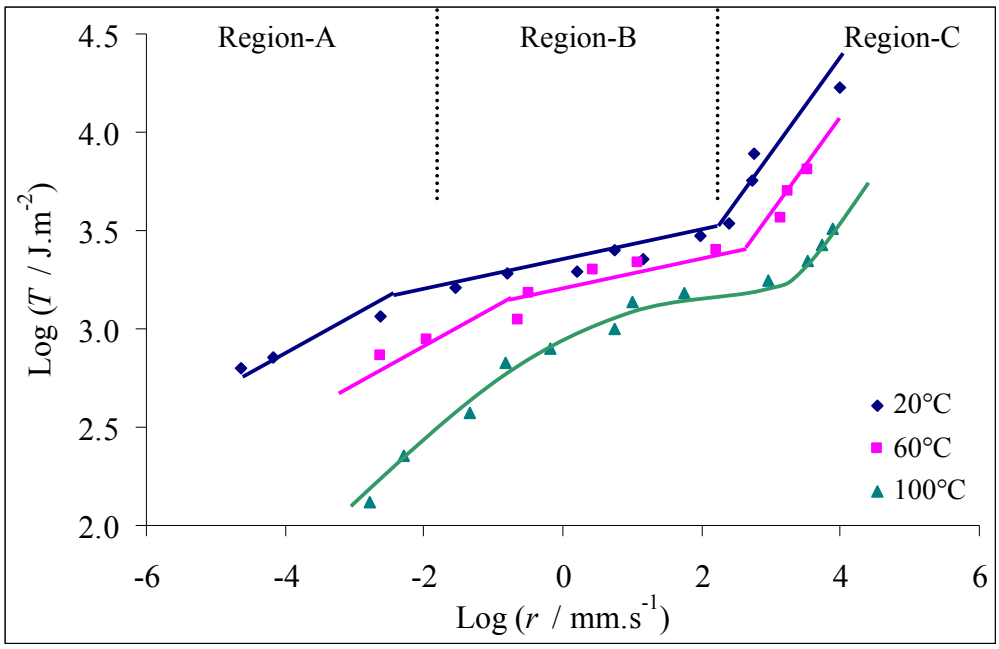

Figure 2.18 The effect of temperature on the *T*/*r* relationship for unfilled SBR (Tsunoda, 2001).

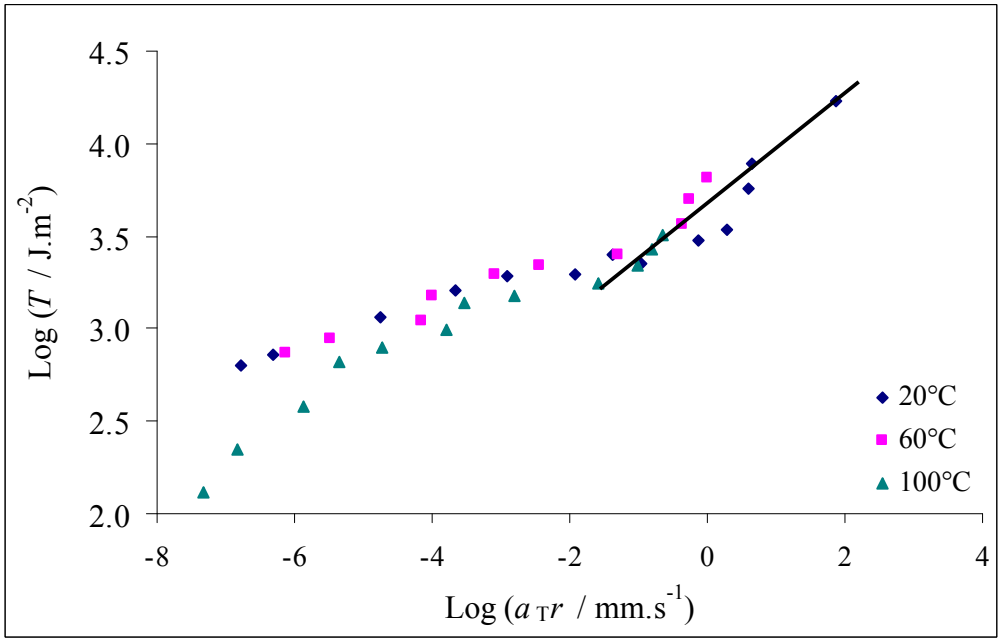

Figure 2.19 Superposition of the data given in Figure 2.18 using the WLF shift factor a_T (Tsunoda, 2001).

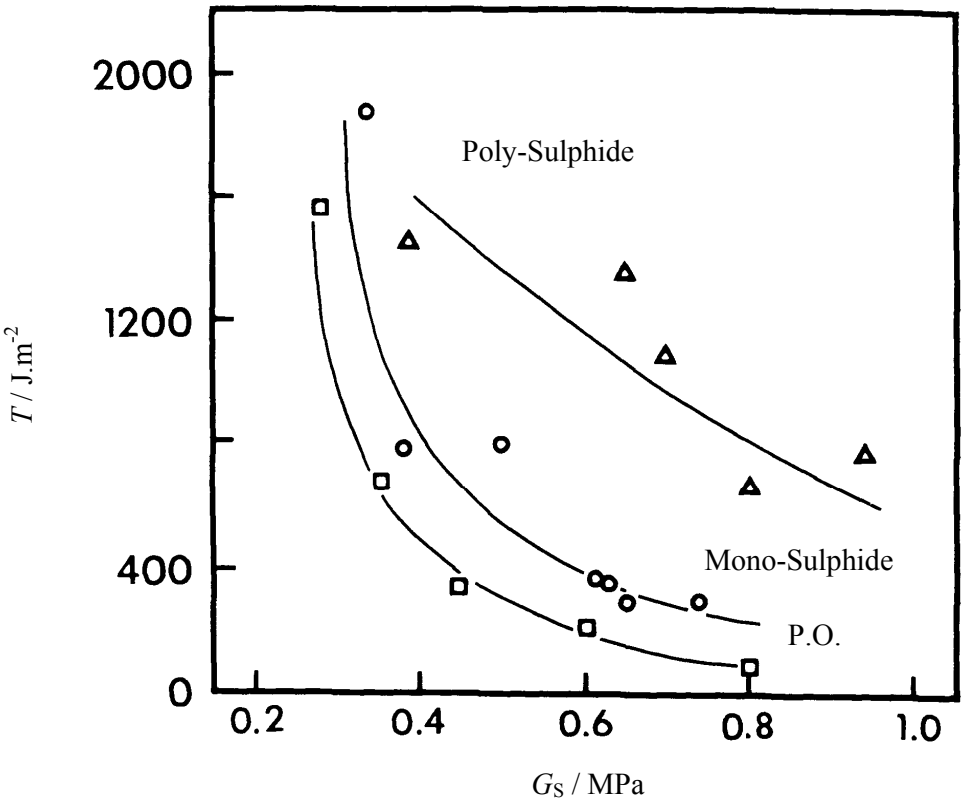

Figure 2.20 Effect of the vulcanising system and cross-link density on the crack growth behaviour for unfilled NR at a crack growth rate of 10μms^{-1} (Brown, Porter and Thomas, 1987).

2.7.6 **Effect of test variables on fatigue crack growth**

A number of factors are known to affect cyclic fatigue crack growth tests: the maximum and minimum loading limits (also expressed as the R-ratio), the test frequency and the test temperature. The R-ratio is defined as the ratio of the minimum test displacement to the maximum test displacement in a displacement controlled cyclic test or the ratio of the minimum load to the maximum load in a load controlled cyclic test. When the R-ratio is equal to zero, the loading condition is said to be fully relaxing whereas when the R-ratio is not equal to zero the loading condition is said to be non-fully relaxing. Lake and Lindley (1964) observed in the case of NR materials a decrease in the crack growth per cycle under non-fully relaxing loading conditions.

Figure 2.21 shows the difference in crack growth rate per cycle when the minimum strain energy release rate in a loading cycle is about 6% of the maximum, the threshold strain energy release rate is effectively increased and the crack growth per cycle at higher strain energy release rates is reduced by a factor of 10. Strain crystallisation in the highly strained region around the crack tip is thought to be responsible for this behaviour. According to Thomas (1974) the crystals melt as the strain decreases to zero. As a result increments of crack growth occur on subsequent extension before strain crystallisation takes place. SBR materials are non-crystallising and the phenomenon is not present. In the experimental work of this thesis only NR materials were examined. In order to avoid the complications arising from non-fully relaxing loading conditions, all crack growth experiments were carried out under fully relaxing conditions for both test pieces and elastomer components. Another difference between non-crystallising and strain crystallising elastomers is their response to the frequency of cyclic testing.

In the case of non-crystallising materials such as SBR, the total crack growth is a result of two components; the time dependent and a dynamic crack growth component. Ellul (1992) reported on the significant effect of frequency on non-crystallising rubbers which reflects the time dependent component of the cyclic crack growth, which is superimposed onto the dynamic crack growth component. This time dependent component dominates the behaviour at low frequencies and reflects the steady tearing that can arise in these non-crystallising rubbers. For strain crystallising elastomers the crack growth does not occur in a time dependent manner and cracks can only propagate above a given critical applied strain energy release rate. Consequently, the time dependent component is much less important and the cyclic frequency has only a very small effect on the crack growth per cycle. However, if the frequency is high, especially for bulky components, excessive heat can be generated and the predominant cause of failure is now no longer mechanical cyclic crack growth but rather as a result of elevated temperature degradation. The effects of temperature are significant on non-crystallising elastomers.

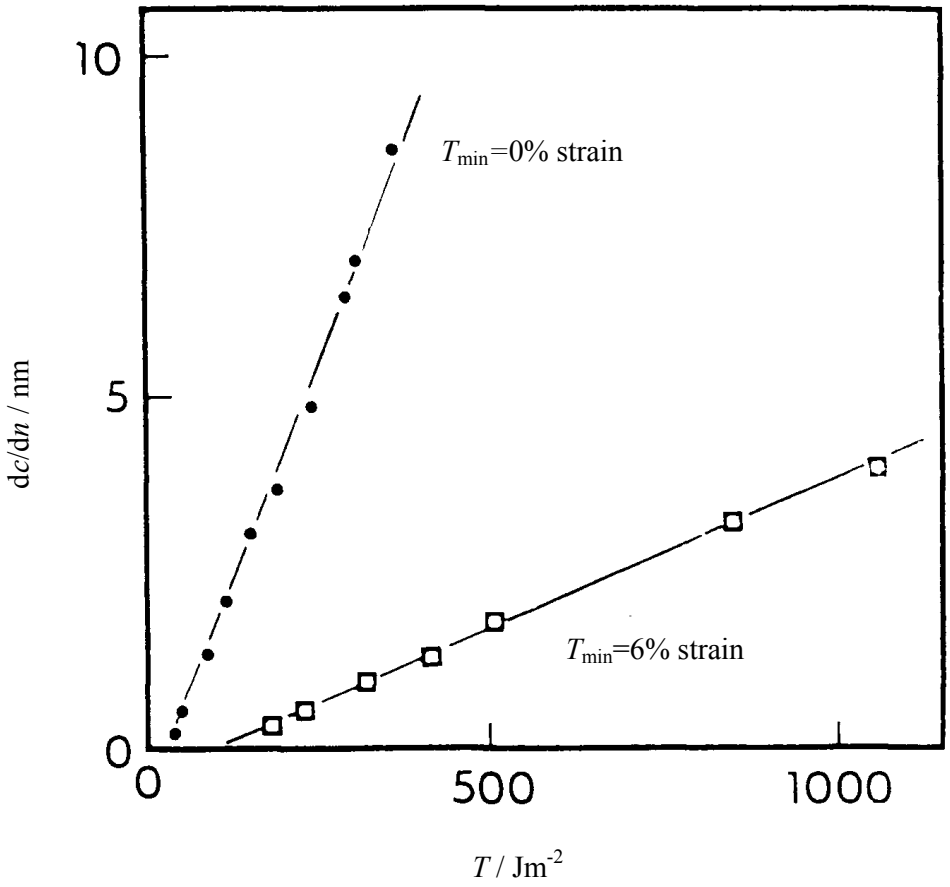

Figure 2.21 The crack growth per cycle, dc/dn, as a function of maximum strain energy release rate, T, for different minimum tearing energies, T_{min}. T_{min} = 0% and T_{min} = 6% of the maximum (Lake and Lindley, 1964).

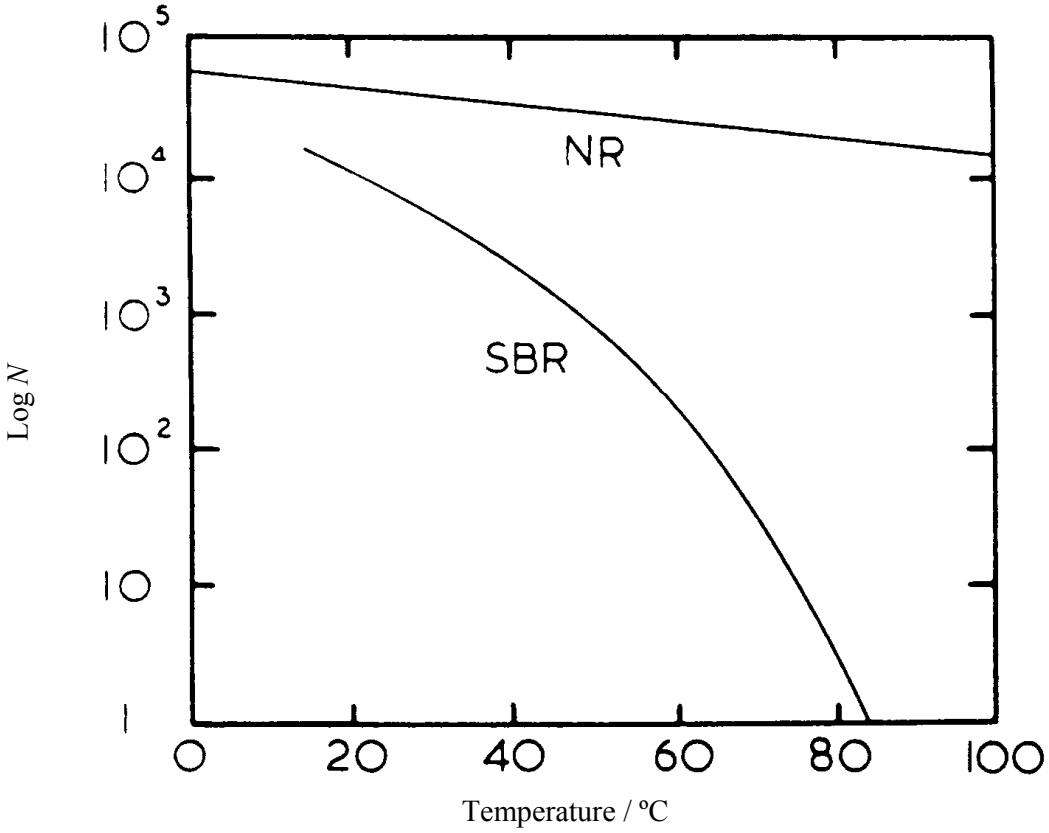

Figure 2.22 Cyclic life, *N* as a function of temperature for unfilled NR and SBR determined using tensile test specimens (Lake and Lindley, 1964).

Figure 2.22 shows the difference in the fatigue life with increase in temperature between NR and SBR unfilled materials. The decrease in the fatigue life of SBR is 10^4-fold compared with a 4-fold decrease for the unfilled NR when the temperature is raised from 0°C to 100°C. In the case of carbon black filled materials, a general increase in the crack growth rate with increasing temperature is observed in both NR and synthetic rubbers.

2.7.7 **Fatigue life prediction**

Traditionally, the fatigue characteristics of materials, including rubbers, were determined by a "Wöhler" curve, also known as *S*-*N* curve (*S* denotes the applied dynamic stress σ for a stress controlled test or, alternatively, strain ε for a strain controlled test, and *N* is the number of cycles to failure). Normally, the dynamic stress range (or strain range) is plotted against the number of cycles to failure on a logarithmic scale (Gent, 1992). With elastomer materials, the results obtained from this approach would be specific to the particular specimen geometry and loading conditions which may not be representative of the typical service conditions for a given engineering component. Therefore, it is not possible to derive specific materials data in order to calculate the failure of any component geometry. In addition, long testing times would be required to obtain the *S*-*N* data for a wide range of geometries and the scatter in the measured results can be large. Jerrams et al. (2012) have shown that the scatter in fatigue life predicted by the *S*-*N* (Wöhler) curve approach can be greatly reduced by using the equi-biaxial bubble inflation test method. On real design and development projects, it is frequently observed that the *S*-*N* prediction and measured fatigue lives can be out by factors in excess of three orders of magnitude. The inability of the S-*N* method to reliably predict the fatigue life of rubber engineering components has led to development of an alternative approach.

Busfield et al. (2005) presented a fracture mechanics approach, which uses finite element analysis techniques to calculate strain energy release rates for cracks located in three-dimensional components, in combination with experimental measurements of cyclic crack growth rates of specific strain energy release rate, to predict the cyclic crack growth propagation rate and the eventual fatigue failure of an elastomeric engineering component. Lake (G. J. Lake, 1995) reviewed the fracture mechanics approach adopted in the work of Busfield et al. (2005). According to Busfield (2000) it is likely that as a crack increases in size, geometric effects in the

region of the crack will alter the magnitude of the strain energy release rate, T. Therefore, an analytical or finite element based technique could be employed to establish a relationship between the changes in strain energy release rate T with the change in crack size c in the form shown in equation 2-45 below:

$$T = F(c) \qquad \text{(Eq.2-45)}$$

By combining Equations 2-42 and 2-45 it is possible to derive a single functional relationship between the cyclic crack growth rate and the size of a crack,

$$\frac{\mathrm{d}c}{\mathrm{d}n} = \varphi(c) \qquad \text{(Eq.2-46)}$$

Rearranging the above equation and integrating allows a prediction of the number of cycles to failure, N_f to be established thus:

$$\int_{c_0}^{c} \frac{\mathrm{d}c}{\varphi(c)} = \int \mathrm{d}n = N_f \qquad \text{(Eq.2-47)}$$

Employing a fracture mechanics based approach, Busfield et al (2005) successfully predicted the number of cycles to grow a crack, located in a bonded gearbox mount, to within a factor of 2 accuracy in three modes of deformation namely: tension, simple shear and combined shear and tensile (45º angle) deformations. Their work was limited to room temperature conditions and also a prediction of the crack growth in the component after inserting an initial razor cut into the middle section of the elastomer component. This thesis discusses an extension of their work by using the fracture mechanics approach to predict the fatigue life of a bonded cylindrical elastomer component at room temperature and for the first time at 70±1ºC in tension and shear deformation modes. The cylindrical geometry of the components studied in this work resulted in fatigue failure not only in the bulk but also at the rubber to metal bond interface. In chapter five, fatigue life prediction results for the bonded cylindrical elastomer components studied are presented and discussed.

2.7.8 **Fatigue crack surfaces**

The study of fatigue crack surfaces has been the subject of scientific research for many decades. In many cases fatigue crack surfaces are observed to be rough. The roughness associated with fatigue crack surfaces is prominent when one compares the surface morphology of a sharp razor cut to that obtained after the crack has grown to steady state rate in an elastomer material. Papadopoulos (2008) reviews this phenomenon in a work which investigates rate transitions in fatigue crack growth in

elastomers. The rough fatigue crack surface is, in part, thought to be the result of the fatigue crack splitting during fatigue crack growth. Thomas (1958) in an explanation of the transition from sharp razor cut crack tip to a rough steady state crack tip suggested the rough crack tip to consist of multiple sharp crack tips. The study of fracture surfaces in elastomer materials is usually qualitative because no single technique can readily describe all the features present or can accurately describe the fracture surface structure. Fukahori and Andrews (1978) studied 2D fracture surface microscopic images by counting the number of steps crossing a reference line and weighted these according to their apparent depth. They differentiated the degrees of roughness by assuming that the broader the step lines, the deeper the steps, with the deeper steps casting a greater shadow. The technique gives an indication of the roughness at various parts of the fracture surfaces but; it would be challenging to differentiate small variations in depth. They observed fracture surface roughness in rubber at various values of strain energy release rate (tearing energy) under steady tearing and noted that there is a direct relation between the rate of propagation and the nature of the crack tip. They reported a general observation that increased crack growth rate due to an increase in the strain energy release rate results in smoother elastomer fracture surfaces. Gent and Pulford (1984) used a similar method to measure the distance between steps of the surface texture of 2D images. They attributed the variation in roughness to the joining of secondary cracks originating from flaws and filler particles. Furthermore, they observed that for the more tear resistant materials, the height of the steps was greater. Quantitative analysis of fracture surface roughness is not a simple task since there is no widely accepted parameter. Although there is general agreement that fatigue crack surfaces become rough with crack growth and that the extent of roughness is linked to the strain energy release rate associated with the crack growth, there is no general agreement as yet on the mechanisms responsible for the creation of the rough fracture surfaces. Gent et al. (2003) investigated why cracks turn sideways by considering a rubber sheet with a small edge crack subjected to a far-field simple extension. They calculated the strain energy release rate for crack growth in both the forwards and the sideways directions. They observed that when the imposed extension is large, the strain energy release rate at which a small sideways crack will initiate is found to be about 60% of that for forwards crack growth for their specific material. In this thesis, finite element analysis results of strain energy release rate associated with growth of split fatigue cracks compared with, the strain energy release rate of a single straight crack

through the horizontal centre-line of a filled Natural Rubber pure shear specimen is presented. The objective of this study being to investigate the effect of fatigue crack bifurcation on the generation of fatigue crack surface roughness by examining the behaviour of the characteristic strain energy release rates associated with growth of split fatigue cracks. Chapter six of this thesis discusses the results of the crack bifurcation studies.

2.8 **Finite element analysis (FEA)**

The finite element method is a numerical analysis technique for obtaining approximate solutions to a wide variety of engineering problems. Although originally developed to study stresses in complex engineering structures, it has since been extended and applied to a broad field of engineering disciplines. Because of its diversity and flexibility as an analysis tool, it is has received much attention in industry and academia.

2.8.1 **The FEA concept**

Engineers are often called upon to solve problems in which either the geometry or some other feature is irregular or "arbitrary". Without much effort, the necessary governing equations and boundary conditions for these problems are established but one sees immediately that no simple analytical solution to the equations of state can be established. Analytical solutions to problems of this type seldom exist. One possibility is to make simplifying assumptions – to ignore the difficulties and reduce the problem to one that can be handled. Sometimes this procedure works; but, more often than not, it leads to serious inaccuracies or wrong answers. With the increased computer power available today it has become possible to retain the complexities of the problem and to still find an approximate numerical solution. In a continuum problem of any dimension, the field variable (whether it is pressure, temperature, displacement, stress, or some other quantity) possesses infinite values because it is a function of each generic point in the body or solution region. As a result, the problem is one with an infinite number of unknowns. The finite element method regards the solution region as built up of many small, interconnected sub-regions or elements. Since these elements can be put together in a variety of ways, they can be used to represent exceedingly complex shapes. The finite element discretisation procedures reduce the problem to one of a finite number of unknowns by dividing the solution region into elements and by expressing the

unknown field variables in terms of assumed approximating functions within each element. The approximating functions (sometimes called interpolation functions) are defined in terms of the values of the field variables at specific points called nodes or nodal points. Nodes usually sit on the element boundaries where typically neighbouring elements are connected. The nodal values of the field variable and the interpolation functions for the elements completely define the behaviour of the field variable within the elements. For the finite element representation of a problem the nodal values of the field variable become the unknowns. Once the unknowns are found, the interpolation functions define the field variable throughout the assembly of the elements. A feature of the finite element method is its ability to formulate solutions for individual elements before putting them together to represent the entire problem. For example if one is treating a problem in stress analysis, the force-displacement or stiffness characteristics of each individual element can be found and the characteristics of the individual elements are assembled to find the stiffness of the whole structure. In essence, a complex problem is reduced to a series of greatly simplified problems (Huebner et al., 2001).

Another advantage of the finite element method is the variety of ways in which one can formulate the properties of individual elements. There are basically three different ways. The first approach to obtaining element properties is called the direct approach because its origin is traceable to the direct stiffness method of structural analysis. The direct approach can be used for relatively simple problems. Element properties obtained by the direct approach can also be determined by the variational approach. Whereas the direct approach can be used to formulate element properties for only the simplest element shapes, the variational approach can be employed for both simple and sophisticated element shapes. A third and even more versatile approach to deriving element properties has its basis in mathematics and is known as the weighted residuals approach. The weighted residuals approach begins with the governing equations of the problem and proceeds without relying on a variational statement. This approach is advantageous because it affords a means to extend the finite element method to problems where no functional is available. The method of weighted residuals is widely used to derive element properties for nonstructural applications such as heat transfer and fluid mechanics (Huebner et al., 2001).

Regardless of the approach used to find the element properties, the solution of a continuum problem by the finite element method always follows an orderly step-by-

step process. A general summary of how the finite element method works is listed below (Huebner et al., 2001):

1. Discretise the Continuum – The first step is to divide the continuum or solution region into elements. A variety of element shapes (Figure 2.23) may be used, and different element shapes may be employed in the same solution region. For instance, when analysing an elastic structure that has different types of components such as plates and beams, it is not only desirable but also necessary to use different elements in the same solution.

2. Select interpolation functions – The next step is to assign nodes to each element and then choose the interpolation function to represent the variation of the field variable over the element. The field variable may be a scalar, a vector, or a higher-order tensor. Often, polynomials are selected as interpolation functions for the field variable because they are easy to integrate and differentiate. The degree of the polynomial chosen depends on the number of nodes assigned to the element, the nature and number of unknowns at each node, and certain continuity requirements imposed at the nodes and along the element boundaries. The magnitude of the field variable as well as the magnitude of its derivative may be the unknowns at the nodes.

3. Find the element properties – Once the finite element model has been established (that is, once the element and their interpolation functions have been selected), we are ready to determine the matrix equations expressing the properties of the individual elements. For this task, one of the three approaches mentioned earlier: the direct approach, the variational approach, or the weighted residuals approach may be used.

4. Assemble the element properties to obtain the system equations – To find the properties of the overall system modelled by the network of elements all the element properties must be "assembled". In other words, we combine the matrix equations expressing the behaviour of the elements and form the matrix equations expressing the behaviour of the entire system. The matrix equations for the system have the same form as the equations for an individual element except that they contain many more terms because they include all nodes. The basis for the assembly procedure stems from the fact that at a node, where elements are interconnected, the value of the field variable is the same for each element sharing that node.

5. Impose the boundary conditions – Before the system equations are ready for solution they must be modified to account for the boundary conditions of the problem. At this stage we impose known nodal values of the dependent variables or nodal loads.

6. Solve the system equations – The assembly process gives a set of simultaneous equations that must be solved to obtain the unknown nodal values of the problem. If the problem describes steady or equilibrium behaviour, then a set of linear or nonlinear algebraic equations are solved. If the problem is unsteady the nodal unknowns are a function of time, and a set of linear or nonlinear ordinary differential equations are solved.

7. Make additional computations if desired – Many times the solution of the system equations can be used to calculate other important parameters. For instance, in a structural problem the nodal unknowns are displacement components from which element strains and stresses may be calculated. Similarly, in a heat-conduction problem the nodal unknowns are temperatures, and from these heat fluxes may be calculated.

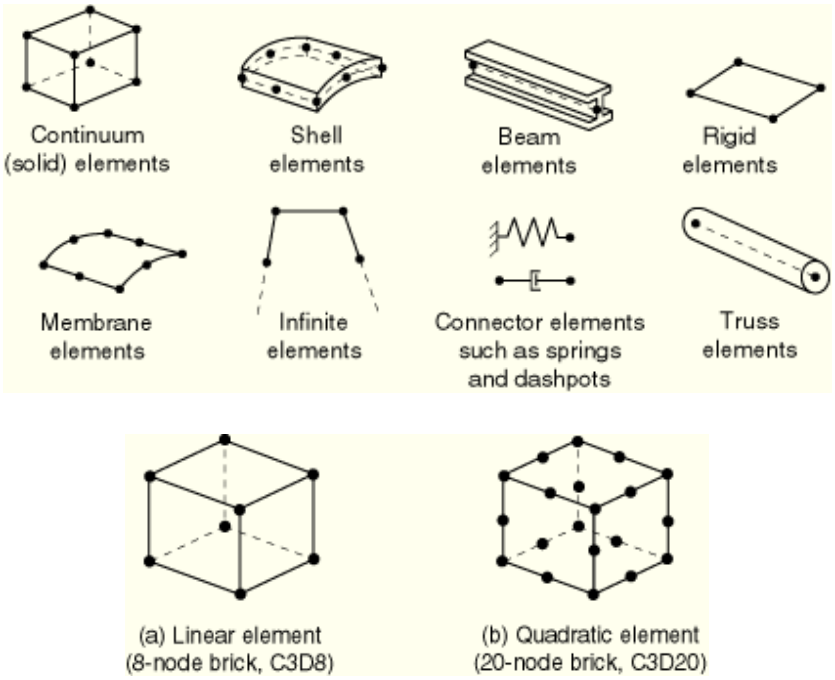

Figure 2.23 Different types of element shapes (Abaqus Manual, 1998).

2.8.2 **Typical procedures for developing a finite element model using an FEA programme**

Busfield (2000) detailed five separate stages involved in developing a typical finite element model as given below:

1. Determination of the most suitable type of analytical model to accurately represent the component behaviour. Factors that require consideration are: sources of the geometrical shape of a design, its expected structural behaviour when subjected to loads, typical applied loads and material properties.
2. Mesh generation. The model is broken up into finite elements to form a mesh of elements and nodes. In some cases, in rubber FEA, the mesh deforms at large strains to an extent whereby certain elements assume unacceptable shapes, and aspect ratios. When this occurs, 'rezoning' is required. This process takes the stress state from the deformed mesh and maps the solution onto a new mesh created by the user that has the same overall geometric shape with smaller element distortions. In this way, the analysis can be resumed.
3. Definition of the boundary conditions and the material properties of all the elements. An input deck is then assembled, which describes the geometric problem in a tabulated form.
4. This input deck can then be submitted to a dedicated equation solver working on a powerful computer. This will calculate a numerical solution for the mesh being considered with the appropriate boundary conditions and material properties.
5. Analysis of the results to determine whether the numerical solution is satisfactory. The analysis is followed by the post-processing phase, where an examination is done on such quantities as nodal displacements, stress contours, failure criteria, distribution of contact forces, strain energy contours and so on. A successful rubber analysis requires: a non-linear FEA code preferably with the necessary materials test data input and good pre- and post-processing software which is closely coupled to the solver to generate the model and allow a careful interrogation of the analysis results.

As stated in stage 3 above, an input deck is required to describe the problem under consideration. The data required is given below:

Header - Statement to define the problem, the title section, and the format of the output files.

Geometry - Define the positions, in co-ordinate space of the nodes and the spatial arrangement of the material about the nodes using elements.
Material Definition - Ascribe the type of model as 1D-2D-3D and the type of material. For elastomers this is most usually achieved by using a Hyperelastic material definition, which describes the mechanical behaviour of an elastomer using a strain energy function.
Boundary Conditions - Define the global displacements, symmetry constraints and the relationships prescribed by Multi-Point Constraints (MPCs) where nodes can be tied together.
Step Definition - Define the type of analysis and the actual loading conditions.

2.8.3 **Types of FEA models**

Engineering structures can be complex in their shape and state of loading hence creating a full 3D finite element analysis model can be both time consuming and difficult to solve. A 3D solid with insignificant dimension in one direction which is loaded in the plane of the body may be modelled as a plane stress finite element model (2D) to simplify the problem. Similarly a 3D solid which is infinitely long with a geometry and loading conditions that do not vary in its longitudinal direction may be modelled as a plane strain finite element model (2D) to simplify the problem. When faced with a problem which cannot be reduced to a 2D model to enable ease of analysis, recourse is often made to various symmetry approximations to simplify the model geometry namely: Axial symmetry, planar symmetry, cyclic symmetry and repetitive symmetry. It is important however, that the loading and constraints conditions are applied to the model in such a way that they truly reflect the symmetry of the problem (Fagan, 1992).

2.8.4 **Axial symmetry**

This type of symmetry takes into account a constant variable distribution in the circumferential direction. This type of a problem is similar to those of plane strain, since the distributions and loading experienced in axial symmetry problems are limited to two directions which are the radial and axial directions (Figure 2.24(a)).

2.8.5 **Planar symmetry**

An appropriate example of this is a flat plate with a hole loaded uniformly. Modelling a quarter of the flat plate is adequate. It is critical to apply the correct constraint conditions throughout the model; that is the horizontal displacements must equal zero along the vertical line of symmetry and the vertical displacements must equal zero along the horizontal line of symmetry (Figure 2.24(b)).

2.8.6 **Finite element analysis of elastomers**

FEA of elastomers became a reality for the elastomer component design engineer in the early 1980s with commercial finite element programmes such as MARC®. Since that time, additional FEA programs such as ANSYS® and ABAQUS® have incorporated analysing elastomer-like materials (Gent, 1992). In this work, the commercial software Abaqus CAE (version 6.6-1) was used to create all the FEA models and the analysis and results output were made by Abaqus solver and Abaqus viewer (version 6.6-1) respectively. The filled natural rubber material was modelled as hyperelastic using the Yeoh stored energy function (SEF) (Busfield, 2000) for all the FEA modelling and analysis done in this work.

Busfield (2000) discusses several constitutive theories for modelling large elastic deformations of rubber based on the strain energy density function. Examples of such theories include: the Neo-Hookean SEF, the Mooney SEF, the Rivlin SEF, the Ogden SEF and the Yeoh SEF. The Yeoh SEF was chosen to model the material behaviour in this work because of its accuracy in modelling the stiffness behaviour of filled elastomers at large strains. The Yeoh SEF is also able to accurately predict the stress strain behaviour of filled elastomers in different deformation modes using experimental data measured in one simple deformation mode such as uni-axial extension. In a finite element analysis it is possible to employ a range of different types of elements to describe the component geometry. The basic shapes available in the finite element method vary from a single point of no dimensions to a full volume or three-dimensional shape. Rectangular two-dimensional and brick three-dimensional elements were used throughout this work. Since elastomer materials are incompressible (Poisson's ratio ≈ 0.5) it becomes necessary with Abaqus to use reformulated (hybrid) elements. These elements interpolate the hydrostatic pressure (or the volume change) separately. Without this the analysis becomes over constrained and the model would

again be locked into its original shape irrespective of the applied forces. Two of the most common element formulations applicable to continuum problems are the normal and reduced integration elements. A fewer number of integration points are required with the reduced integration elements affording less computing time. On the other hand, the normal integration element involves calculations at several locations distributed in each element which leads to longer computing time. The choice between the two, in a typical elastomer component finite element analysis problem, may depend on factors such as the strain level expected in the elastomer component being modelled and the degree of accuracy to which the relevant field variable is to be calculated.

2.8.7 **Modelling cyclic fatigue crack growth**

The fracture mechanics approach to fatigue life prediction involves the calculation of the strain energy release rate associated with the growth of a crack (this could be a pre-existing flaw in an elastomer component). What makes the strain energy release rate a suitable parameter for modelling crack growth is the relationship between the strain energy release rate and dissipative processes that occur at the crack tip. Busfield et al. (1999) evaluated three different methods for calculating the strain energy release rate namely: the energy balance, the J-integral and the crack tip closure approaches:

The J-Integral: This is based on the work of Rice (1968) and it has been implemented in the Abaqus FEA software. The advantage of this approach is that it requires only a single analysis model to calculate the strain energy release rate.

The crack tip closure: This technique measures the forces required to close up the nodes on a crack tip and integrates the force by the distance the nodes move when unstrained. The work done is evaluated by the integral $\int F.\mathrm{d}e$, where e is the distance to close up the nodes and F is a measure of the nodal force.

The energy balance approach: With this approach the difference in the magnitude of the internal stored energy (dU) is calculated between two models held at a fixed displacement when the crack tip area A is extended by a small area (dA). The strain energy release rate is equal to dU/dA. This technique is also known as the node release or the virtual crack extension technique. The change in total energy calculated when a small crack is extended a small amount is little, therefore it is essential that the models are identical remote from the crack otherwise the errors inherent in the finite

element technique will mask the changes to the model as the crack is extended (Busfield, 2000).

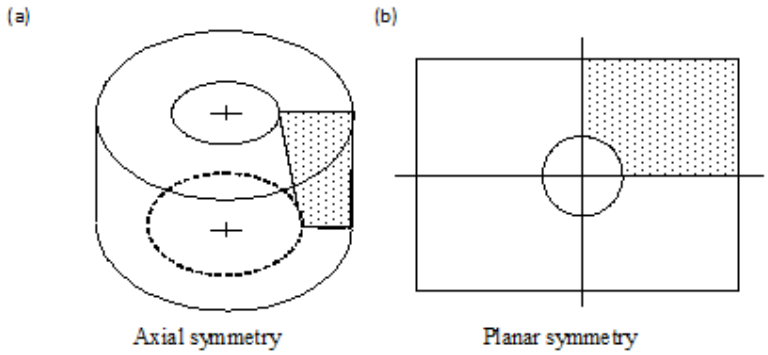

Figure 2.24 A schematic to demonstrate axial symmetry and planar symmetry commonly adopted to simplify the finite element modelling of a component (Busfield, 2000)

2.9 Motivation for this study

As can be seen in earlier discussions, cyclic stress relaxation, a manifestation of fatigue which is often mistakenly referred to as Mullins effect and neglected in fatigue life predictions, has been studied for simple extension but not for other deformation modes. The cyclic stress relaxation rate is found to be different in different modes of deformation, yet there is no single parameter which explains the observed difference in relaxation rates in the different modes of deformation. Therefore, in this work, cyclic stress relaxation will be measure in test pieces and components and for different deformation modes. An attempt will be made to correlate the observed amounts of cyclic stress relaxation in different modes of deformation using a single parameter. The understanding gained from this approach will be used to quantitatively account for the cyclic stress relaxation phenomenon in the fracture mechanics approach to fatigue life prediction of elastomer components.

As can be seen in the work of Busfield et al., (2005) described earlier, the fracture mechanics approach to fatigue life prediction of elastomer components gives good results at room temperature conditions after inserting an initial cut into the elastomer component. The applicability of the fracture mechanics approach to fatigue life prediction at elevated temperatures, however, is not known. As a result a programme of studies will be carried out to validate the fracture mechanics approach to

fatigue life prediction at elevated temperatures and without an initial razor cut in the elastomer component.

Fatigue crack growth often results in rough fatigue crack surfaces. The rough fatigue crack surface is, in part, thought to result from a strain induced strength anisotropy in front of the advancing fatigue crack which can cause the crack to split during crack growth. The characteristics of the strain energy release rates associated with the growth of split fatigue cracks is not well studied. Part of this thesis will examine strain energy release rates associated with growth of split fatigue cracks, in a pure shear specimen, in an attempt to understand the effect of fatigue crack bifurcation and its relation to fatigue crack surface roughness.

CHAPTER THREE

3.0 Materials, Experimental and FEA Methods

3.1 Introduction

In this chapter the elastomer material, experimental and finite element methods used in the study of cyclic stress relaxation, fatigue life prediction using the fracture mechanics approach and fatigue crack surface roughness are described in detail. The equipment and the test procedures, as well as the conditions that are used to obtain the scientific data that are discussed in chapters 4, 5 and 6 are also explained.

In the first part of this research, the cyclic stress relaxation of the filled NR material and the bonded cylindrical components used in this work was measured. This was achieved by loading test pieces of the material and components supplied by Trelleborg AVS cyclically to a fixed displacement whilst measuring the force at the maximum displacement for each cycle. A detailed description of the experimental procedure used is presented in section 3.4. In the second part of this work, fatigue crack growth in elastomer test pieces and components were measured experimentally. The finite element method was employed to calculate the strain energy release rates associated with crack growth in elastomer components. The methods used to characterise the elastomer material together with the finite element procedures, and crack growth measurements, are also presented in this chapter. The third aspect of this work examines the effect of fatigue crack bifurcation (crack tip splitting) on the observed roughness of the fatigue crack surfaces. This was achieved by using FEA to calculate the strain energy release rates associated with growth of split fatigue cracks in a pure shear test piece. In this chapter, the method used to calculate the strain energy release rates of split fatigue cracks is also explained.

3.2 Materials

The material used in this work were commercially formulated 65 phr HAF 330 carbon black filled natural rubber (NR) compound supplied by Trelleborg AVS. The hardness of the material, determined using ASTM D2240 test method was 62 IRHD. The formulation of the compound is presented in Table 3.1.

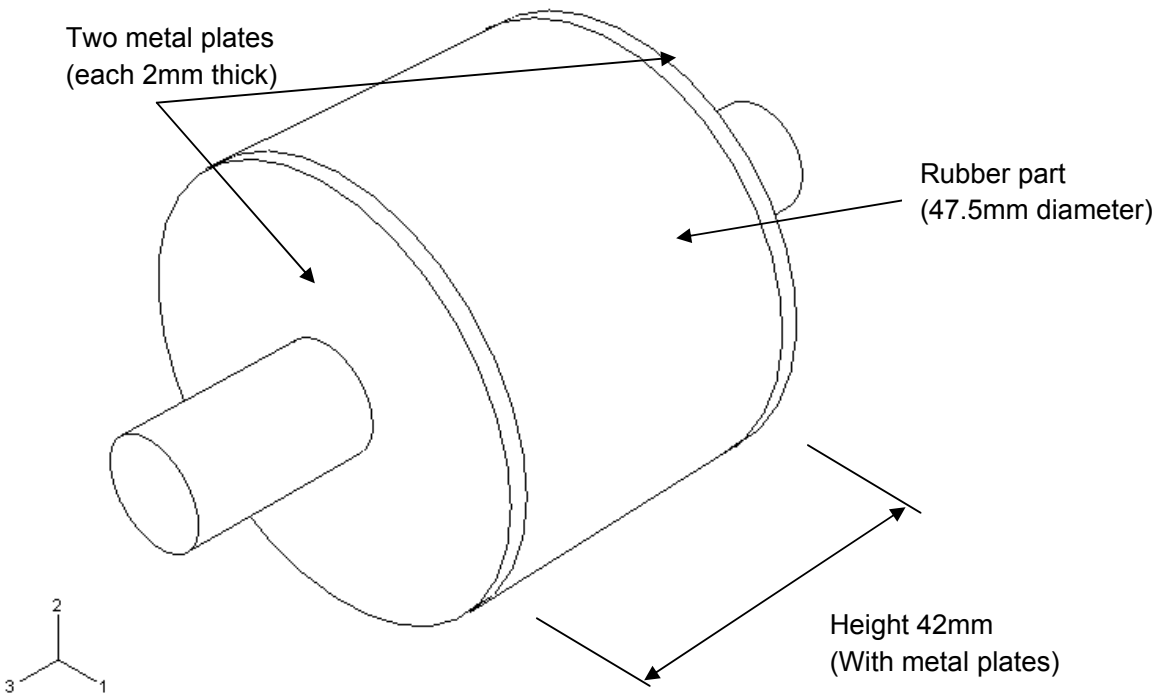

Figure 3.1 Picture and a schematic of a typical bonded cylindrical suspension component

The rubber materials were supplied as rubber sheets of approximately 2mm thickness, from which pure shear samples of 175mm width (***w***), 25mm height ($\boldsymbol{l_0} \approx$ 14mm) and approximately 2mm thickness (***t***), were prepared as well as dumbbell test pieces using an ASTM D412 type C dumbbell die. In addition, simple bonded cylindrical suspension mounts were injection moulded using the same compound. Figure 3.1 shows a picture and a schematic of a typical bonded cylindrical suspension component used in this study. It has dimensions of 42mm in height (including bonded metal plates) and a diameter of approximately 47.5mm. The two metal end-plates were each 2mm in thickness. Figure 3.2 shows a schematic of a pure shear specimen.

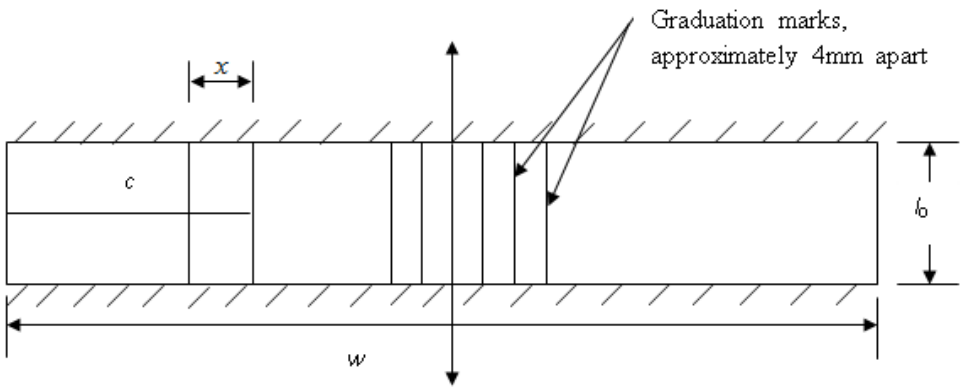

Figure 3.2 A schematic of a pure shear specimen

Table 3.1 Formulation for the materials used in this study

Ingredients	Type	phr
Rubber	SMR10CV	100
Carbon Black	N330(HAF)	65
Stearic Acid		2
Zinc Oxide		5
Accelerator	TMTM-75	0.7
Accelerator	MBTS-80	1.5
Sulphur		1.5

3.3 Material characterisation

3.3.1 Material stress strain characterisation

The mechanical stress strain behaviour of the filled NR material used in this research was characterised experimentally at both room temperature (23±2°C) and 70±1°C. In order to do this, dumbbell specimens were prepared from the rubber sheets supplied by Trelleborg AVS using an ASTM D412 type C dumbbell die. The equipment used to carry out the measurements at room temperature (23±2°C) was an Instron 5567 universal test machine equipped with 1 kN load cell, to measure the force, and an optical extensometer to measure the displacement (strain) of the two white marks inserted on the front face of the test pieces. The following procedure was followed to measure the stress strain behaviour of the test pieces:

1. Calibrate the load cell and the optical extensometer fitted to the Instron 5567 universal test machine.
2. With the dumbbell specimen un-gripped, insert two white marks on the reduced width section of the specimen equidistant from the centre and perpendicular to the longitudinal axis using a marker pen.
3. Measure the distance between the two white marks inserted on the dumbbell specimen using a Vernier calliper and recorded the distance. Measure the width of the

dumbbell specimen at three different points along the reduced width section using a Vernier calliper and recorded the values.

4. Both ends of the dumbbell specimen were gripped and mounted into the assembly on the Instron 5567 test machine.

5. Carefully set up the sample in position and use the optical extensometer to measure again the distance between the two white marks to confirm the initial distance before testing.

6. Reset the load cell on the Instron 5567 test machine to zero.

7. Run the tensile test using a test speed of 50mm/min.

8. Record the tensile force data from the load cell and the distance between the two white marks measured using the optical extensometer to determine the room temperature stress strain behaviour of the material.

To determine the stress strain behaviour at 70±1°C the experiment was repeated using an Instron 8801 servo-hydraulic test machine and an environment chamber to provide the required temperature equipped with a 1 kN load cell, to measure the force, and thermocouples to measure the temperature of the air in the oven. With the sample in the environment chamber it was not possible to measure the strain using the optical follower, so the strain was recorded manually for the elevated temperature testing at 70±1°C. The test piece was stretched incrementally by uniform small displacements. After allowing the load to equilibrate the load cell output (force) was recorded. The displacement between the two white marks on the surface of the test piece was manually measured using a travelling microscope. In all stress strain measurements at 70±1°C the dumbbell sample was carefully mounted into the oven which was already heated to 70±1°C and allowed approximately an hour for the sample to thermally equilibrate with the surrounding air temperature. For all the stress strain characterisation work (both room temperature and at 70±1°C), measurements were made on virgin dumbbell samples as well as dumbbell samples softened by cyclic loading by 999 pre-cycles. The softening of the dumbbell specimens was done using the Instron 8801 servo-hydraulic test machine operated at a frequency of 1 Hz to an approximate maximum pre-strain of 90%. The virgin stress strain behaviour was used for stiffness and crack initiation region studies whereas the 1000^{th} cycle stress strain behaviour was used to calculate strain energy release rates associated with crack growth in the elastomer materials and components.

3.3.2 **Bonded cylindrical component force deflection measurement**

The force deflection behaviour of the bonded cylindrical component was measured at room temperature (23±2°C) and at 70±1ºC (in an oven) using Instron 8801 servo-hydraulic test machine operating under a static load condition and at a strain rate of 50mm/min. The virgin force deflection behaviour and the 1000^{th} cycle force deflection behaviour (after softening the component for 999 cycles at a strain energy density or displacement equivalent to that found when a dumbbell specimen is stretched at 90% strain in tension) were both measured at room temperature and 70±1ºC for the bonded cylindrical component.

3.3.3 **Equilibrium swelling tests**

Equilibrium swelling tests were carried out using n-decane as the swelling agent to determine the cross-link density of the elastomer sheet materials and that of the bonded cylindrical component material. Samples were cut from both the elastomer sheet material and the bonded cylindrical component material and weighed using a mass balance. The test samples were placed in bottles and n-decane was added to the samples in the bottles, until all the samples were fully immersed in n-decane, and the bottles were covered. The test samples were carefully removed from the n-decane and weighed from time to time to observe the changes in mass. The tests were stopped when no further change in mass was observed between subsequent readings of the mass of the samples. The cross link density of the elastomer materials was determined using the Flory Rehner equation given below:

$$N = -\frac{1}{2V_S}\frac{In(1-\phi)+\phi+\chi\phi^2}{\phi^{1/3}-\phi/2} \qquad \text{(Eq.3-1)}$$

Where:

N = moles of cross links per unit volume

V_S = molar volume of the swelling solvent

Φ = volume fraction of polymer in the swollen gel

χ = polymer-solvent interaction parameter

3.4 **Measurement of cyclic stress relaxation**

An Instron 8872 Servo-hydraulic test machine was used to measure the cyclic stress relaxation behaviour of both the pure shear test pieces and the bonded cylindrical

components. Cyclic constant maximum displacement tests with sinusoidal wave form at 1 Hz frequency under fully relaxing conditions were carried out on all samples up to 3000 cycles. The pure shear samples were deformed over a range of maximum strains from 20% - 150%. The bonded cylindrical components were deformed in tension, shear and compression by the following amounts, expressed as a percentage of the original rubber section height, 26% - 92%, 26% - 158% and 16% - 63% respectively. All measurements were carried out at 23±2°C. The maximum (peak) force attained at maximum displacement was monitored and recorded throughout each test with 1kN and 25kN load cells for test pieces and bonded cylindrical components respectively. Figures 3.3, 3.4 and 3.5 below show the set up used to measure the cyclic stress relaxation of the pure shear test pieces and the bonded cylindrical components.

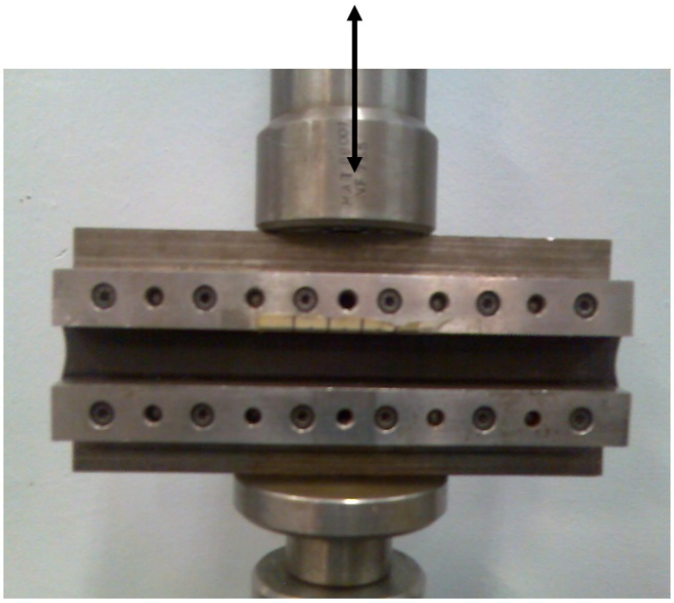

Figure 3.3 Set up for pure shear cyclic stress relaxation measurement

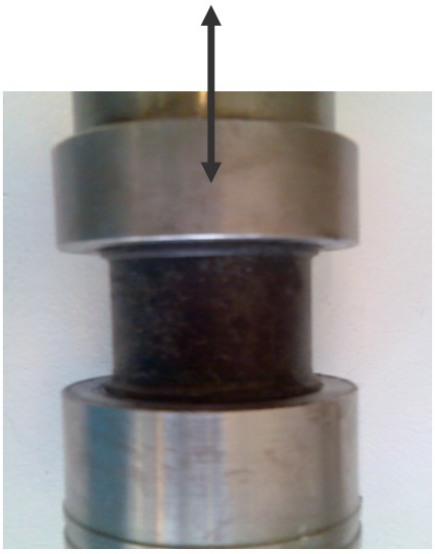

Figure 3.4 Set up for bonded cylindrical component cyclic stress relaxation measurement in tension and compression modes of deformation

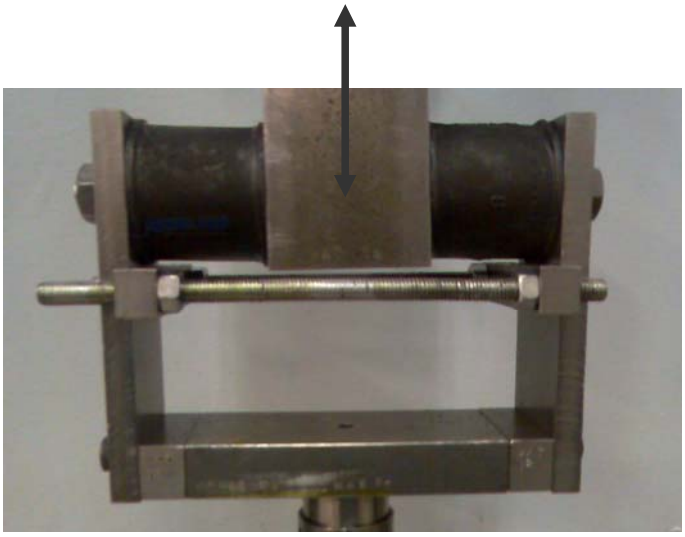

Figure 3.5 Set up for bonded cylindrical component cyclic stress relaxation measurement in simple shear mode of deformation

The objective of the cyclic stress relaxation tests was to measure the cyclic stress relaxation rates of material test pieces and engineering components in different modes of deformation and to establish a correlation between them. Using the maximum force versus number of cycles data, a log-log plot was made for both the pure shear cyclic stress relaxation and the bonded cylindrical component's cyclic stress relaxation data. The slopes of the straight lines obtained from the log-log plots are a measure of the cyclic stress relaxation rate per decade for the respective pure shear samples and the bonded cylindrical components at defined test amplitudes. Chapter four presents the results and discusses the cyclic stress relaxation measurements.

3.4.1 **Average strain energy density determination**

Figure 3.6 shows typical force deflection behaviour of an engineering component. The area under the force deflection curve gives the stored elastic energy (U) in the component. In this work, the stored elastic energy was calculated for the different maximum (constant) test amplitudes at which cyclic stress relaxation measurements were made. The second cycle force deflection curve for each constant amplitude cyclic stress relaxation test was used for the stored elastic energy calculations. The second cycle curve was used due to the difficulty of capturing completely using the servo-hydraulic test machine the entirety of the first loading cycle. This results in a loss of the first ¼ of the first cycle force deflection behaviour leaving only ¾ of the first cycle force deflection curve measured. To determine the volume of the rubber part of the cylindrical engineering component, the cross sectional area was calculated (knowing the component diameter) and multiplied by the height of the rubber part of the component. The volume of the pure shear samples was calculated by multiplying the dimensions (height, width and thickness) of the test piece. Dividing the stored elastic energy by the volume of the rubber part, equation 3-2, gives the average strain energy density (J/m^3).

$$W = \frac{U}{V} \qquad \text{(Eq.3-2)}$$

where

U is the stored energy in J

V is volume of rubber in m^3

W is the average strain energy density in J/m^3

In chapter four a correlation of the cyclic stress relaxation rates of pure shear test

pieces and the bonded cylindrical engineering component, measured in different modes of deformation, in terms of average strain energy density is presented and discussed.

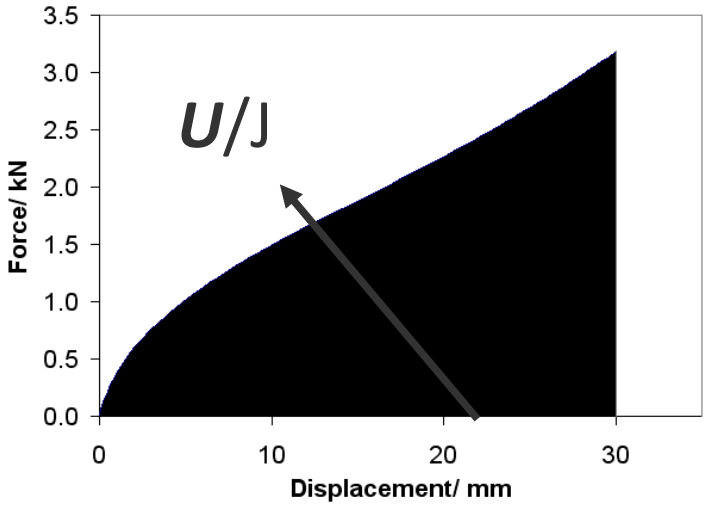

Figure 3.6 Typical force deflection behaviour of an engineering component; the area under the curve is the stored elastic energy in the component at that specific displacement

3.5 Experimental fatigue crack growth measurements

3.5.1 Pure shear crack growth characterisation

To characterise the elastomer material's pure shear crack growth behaviour, pure shear crack growth samples were prepared from the sheets of elastomer materials supplied by Trelleborg AVS (figure 3.2). An initial razor cut of 30mm length was inserted at one side of the specimens approximately equidistant between the grips. The remaining sections of the pure shear test pieces along which the crack would grow were identified by inserting vertical marks using a white marker pen at intervals of approximately 4mm. As can be seen in figure 3.7, a pure shear specimen under load has four main regions of deformation state thus, region "A", region "B", region "C" and region "D". Region "A" is undeformed. Region "B" around the crack tip has a complex stress field. Region "C" is in pure shear mode of deformation. Region "D" is close to the free edge so its behaviour is complex (Rivlin and Thomas, 1953). Inserting an initial razor cut of 30mm ensures that edge effects are avoided in the crack growth measurement and that the crack grows effectively reducing the region of the test piece in pure shear. The pure shear test pieces were gripped and tested using an Instron 8872

servo-hydraulic test machine equipped with a 25kN load cell. The wave form of the test was sinusoidal with a frequency of 1Hz. For all the crack growth measurements, care was taken to ensure that the initial relative high crack growth rate due to the sharp razor crack tip (Thomas, 1958) was eliminated from the measurement by allowing the initial razor crack to grow approximately 10mm before starting to record the crack growth versus number of cycles data. Allowing the crack to grow about 10mm before beginning the crack growth data measurement ensures that the crack tip transforms from the initial sharp and smooth razor cut tip to a more typical steady state crack growth tip. All the crack growth measurements were carried out under fully relaxing conditions. Crack lengths were measured at corresponding number of cycles for tests at different amplitudes by visually counting the number of graduation marks crossed by the growing crack along the pure shear specimen. Plots of crack length against number of cycles were then made to calculate the crack growth rate (dc/dn) for specific amplitudes. The 65 phr filled NR material was characterised at both room temperature (23±2°C) and at 70±1ºC in an oven.

It has been shown (Busfield et al., 1997) that for a pure shear test piece (figure 3.2) with unstrained height (l_0), thickness (t), width (w), and a crack of size (c) the strain energy release rate (T) can be calculated from equation 3-2 below:

$$T = \frac{U}{t(w - c + x)} \qquad \text{(Eq.3-3)}$$

where x is a strip of material in the cracked part of the test piece that is not energy free. x has been experimentally found to be about 28% of l_0 (De, 1994). U is the stored energy for a given test amplitude. Using equation 3-3, the strain energy release rates for the different pure shear test amplitudes were calculated for both the room temperature pure shear crack growth test amplitudes and that measured at 70±1ºC. A plot of log dc/dn against log T was made to determine the pure shear line of the material at both room temperature and 70±1ºC. The results of the crack growth behaviour measurements are presented in chapter five of this thesis.

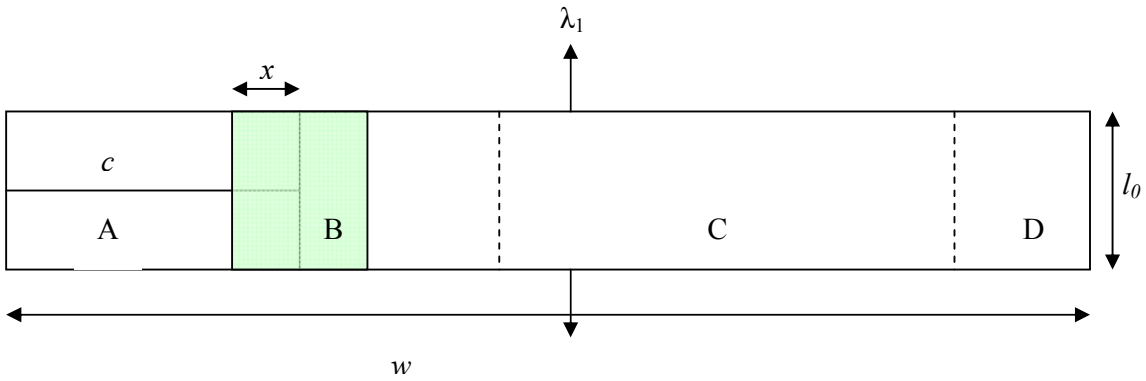

Figure 3.7 A schematic of various regions according to the state of deformation in a pure shear sample. All the dimensions are referred to the undeformed state. The entire shaded area is region B.

3.5.2 Bonded cylindrical component fatigue crack growth measurement

The bonded cylindrical component was tested at different amplitudes and at a frequency of 1Hz at room temperature and 70±1ºC to determine the experimental number of cycles required to grow cracks to a measurable size. Sinusoidal wave form was used in all the tests. No initial razor cuts were inserted into the component and the experiment was conducted under fully relaxing conditions. It was observed in the experiment that cracks initiated at the rubber-metal bond edge of the bonded cylindrical component. The size of the crack was measured by stopping the test and using a depth probe (the protruding metallic rod from the end of a Vernier calliper) into the crack. Fatigue tests were conducted in tension and in shear modes of deformation. Experimental results of number of cycles and corresponding crack length for the bonded cylindrical elastomer components are presented and discussed in chapter five.

3.6 Finite element analysis

3.6.1 Introduction

The finite element analysis technique was used to predict the stiffness of the bonded cylindrical component, predict failure initiation sites on the bonded cylindrical component and to calculate the strain energy release rate associated with cracks located in the bonded cylindrical component and pure shear test pieces. The energy balance

technique was used to calculate the strain energy release rate associated with crack growth in the elastomer test pieces and components. With this approach, the difference in the magnitude of the total internal strain energy dU is calculated between two models held at a fixed displacement where the crack tip area A is extended by a small area dA. The strain energy release rate is given by equation 3-4. This technique is also known as the node release or the virtual crack extension technique. Developing a finite element model generally involves the definition of the necessary component or test piece geometry, the definition of an appropriate material model, the application of boundary conditions and loading, the meshing of the model and then compiling the information so that it can be submitted to calculate the solution. In this research work, the commercial software Abaqus CAE (version 6.6-1) was used to create all the FEA models and the analysis and results output were carried out using Abaqus solver (version 6.6-1) and Abaqus viewer (version 6.6-1). A number of models were created to predict the component's stiffness and to model the fatigue crack growth phenomenon in the bonded cylindrical component under different modes of fatigue loading. Models were also created to calculate the strain energy release rates associated with the growth of split fatigue cracks. The following sections describe in detail the FEA models created in this work.

$$T = -\frac{dU}{dA} \qquad \text{(Eq.3-4)}$$

where

T is the strain energy release rate (commonly called tearing energy in the rubber literature),

A is the area of a single fracture surface, and

U is a measure of the internal stored energy.

3.6.2 **FEA model of the bonded cylindrical component to predict stiffness**

The bonded cylindrical component was first modelled to evaluate its stiffness. The component geometry was modelled in 3D using Abaqus CAE with the rubber part having a diameter of 47.5 mm and a height of 38 mm. The elastomer material of the component was modelled as hyperelastic material using the Yeoh stored energy function. Experimental stress strain behaviour determined using a dumbbell test piece was used to derive the three coefficients required for the Yeoh stored energy function in Abaqus in order to calculate the deformation state and the reaction forces. The model

was meshed with an 8-node linear brick, hybrid, constant pressure elements C3D8H. The top surface nodes of the component were constrained in the x and y-translational directions and allowed to translate in the z-direction. All the top surface rotational degrees of freedom were constrained. All translational and rotational degrees of freedom of the bottom surface were constrained. An output request of a summation of all the reaction forces of the top surface nodes was made and used together with the top surface translation in the z-direction to predict the force displacement behaviour of the component. Figure 3.8 below shows the undeformed and deformed FEA models of the bonded cylindrical elastomer component in tension. Figure 3.9 shows the undeformed and deformed models of the bonded cylindrical component in shear.

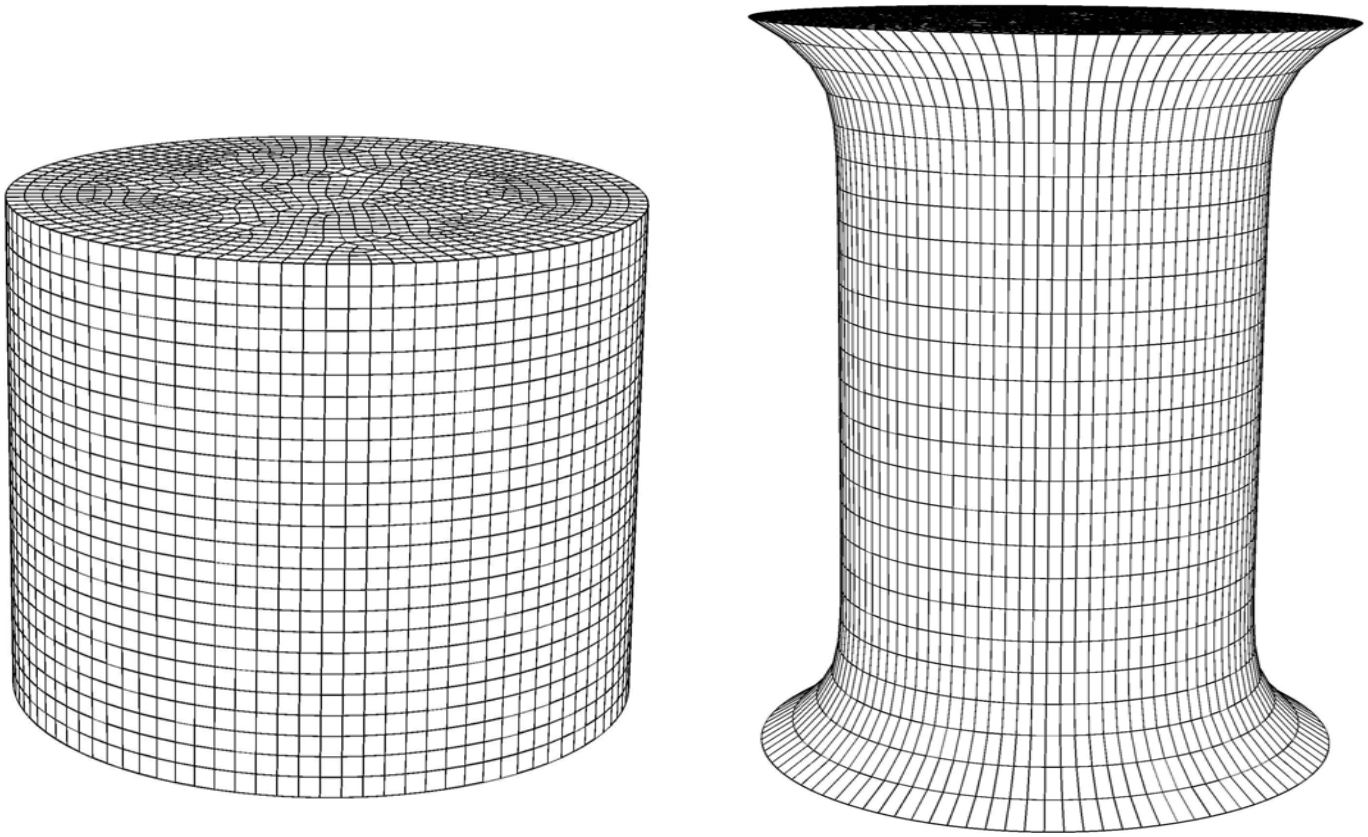

(a) **(b)**

Figure 3.8 A meshed undeformed cylindrical component (a) and a meshed cylindrical component deformed in tension (b)

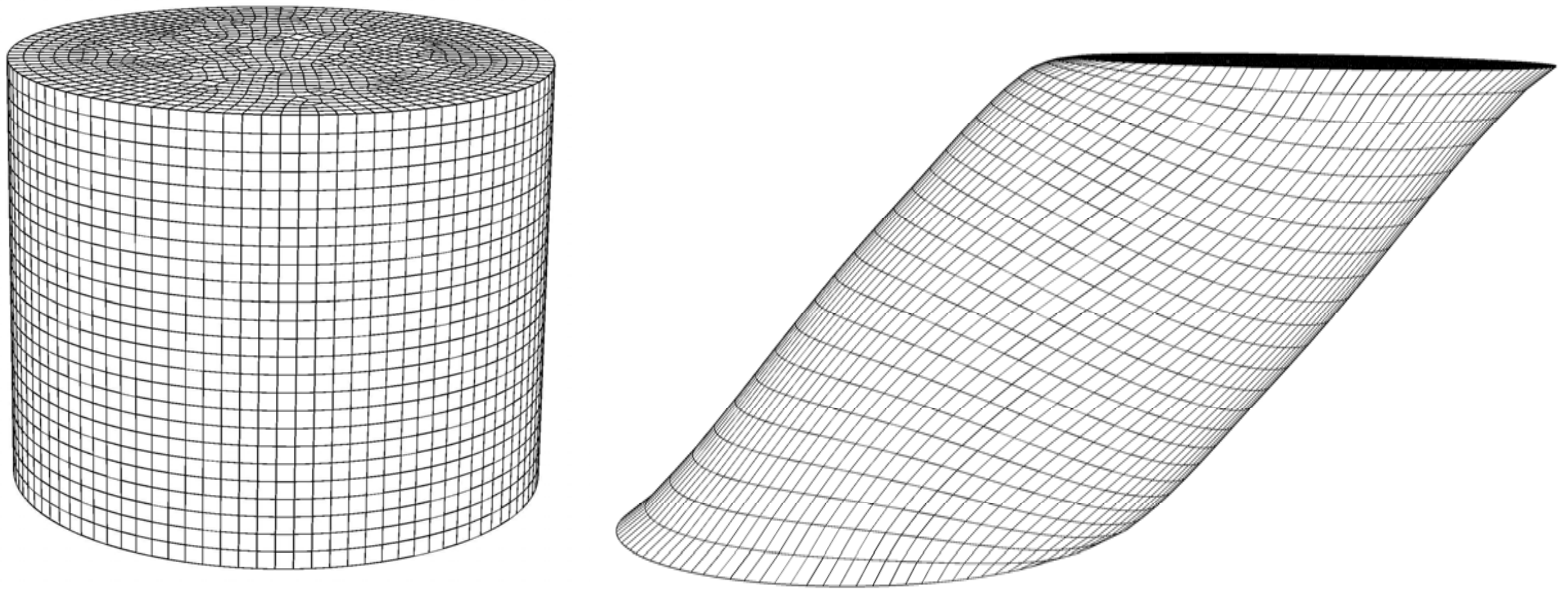

(a) (b)

Figure 3.9 A meshed undeformed cylindrical component (a) and a meshed cylindrical component deformed in simple shear (b)

3.6.3 **Modelling crack growth in a tensile deformation mode**

Considering the cylindrical geometry of the bonded elastomer component and the nature of the distribution of strain energy in tension, crack initiation and growth was predicted to start at the rubber-metal bond edge as this is the region of highest strain energy density. The initial assumption was for the crack to grow from the edge along the rubber-metal bond interface into the component at both bonded ends. In an effort to model this, an axisymmetric model was created using Abaqus CAE and meshed with a 4-node bilinear axisymmetric quadrilateral, hybrid, constant pressure elements (CAX4H). This model describes a crack growth profile where the crack grows circumferentially, starting from the rubber metal-bond edge, into the rubber-metal bond interface at both bonded ends of the component. In figure 3.10 an undeformed axisymmetric model, a deformed axisymmetric model without a crack and a deformed axisymmetric model with a crack are shown. The axisymmetric model exploits the symmetric nature of the geometry of the bonded component and the loading. It reduces a complex three dimensional problem to a much simpler two dimensional problem. In figure 3.10 nodes along the central y-axis have their x and z-translational as well as their rotational degrees of freedom constrained. Similarly nodes along the symmetry imposed x-axis have their y and z-translational and rotational degrees of freedom constrained. The crack growth along the rubber-metal bond interface was modelled by deforming the model to the displacement of interest and then releasing the nodes along the edge of the model. For simplicity, the metal plates at the ends of the bonded component were not modelled. In order to determine strain energy release rates for cracks of the size of initial flaws around the rubber-metal bond edge, the model was meshed with size 0.2 mm for the first 1 mm of crack growth. Results of the stored energy versus crack length as well as strain energy release rate and crack length for this model are presented and discussed in chapter five.

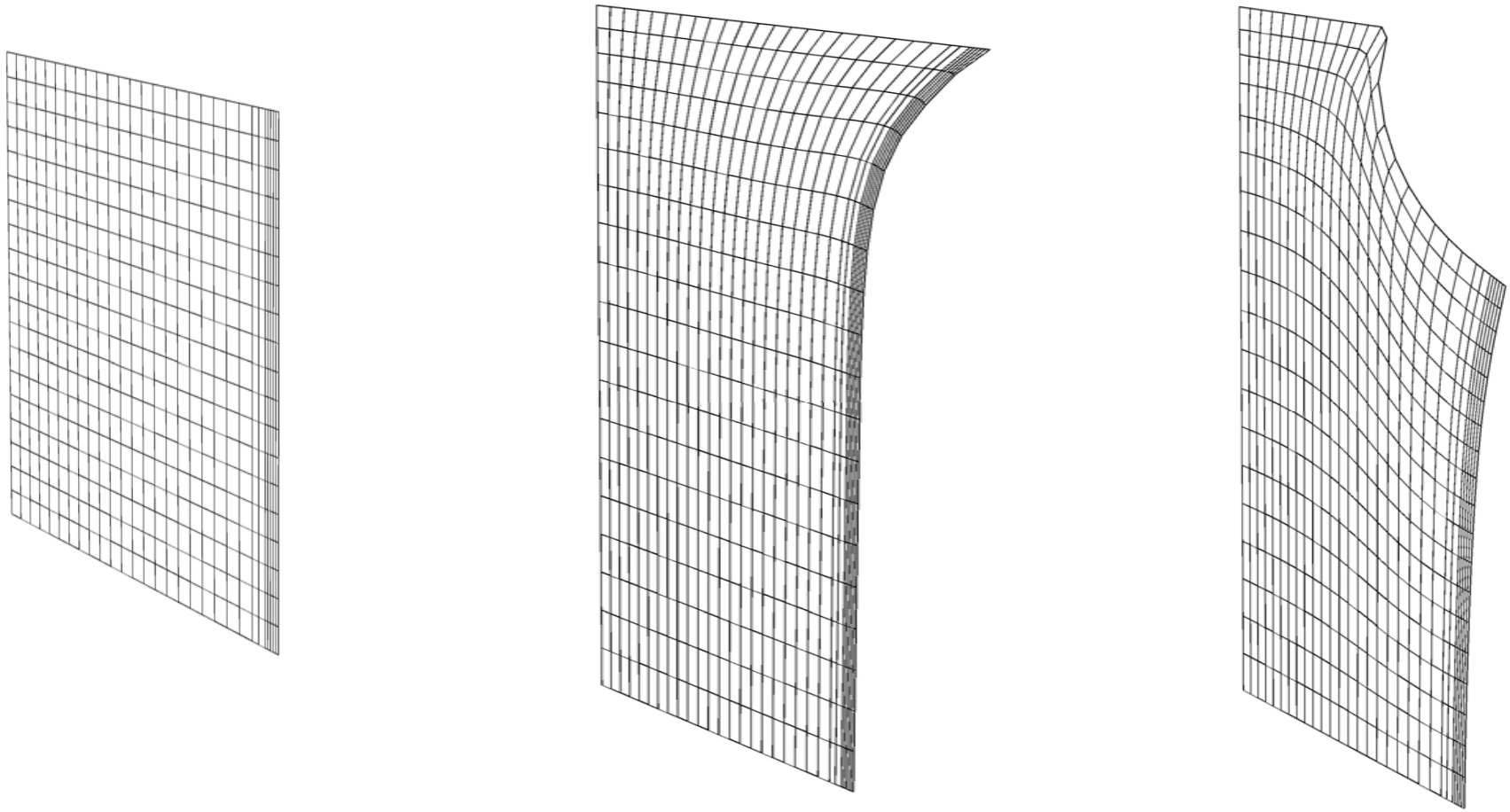

(a) (b) (c)

Figure 3.10 An undeformed axisymmetric mesh (a), a tension deformed axisymmetric mesh (b) and a tension deformed axisymmetric mesh with a crack (c)

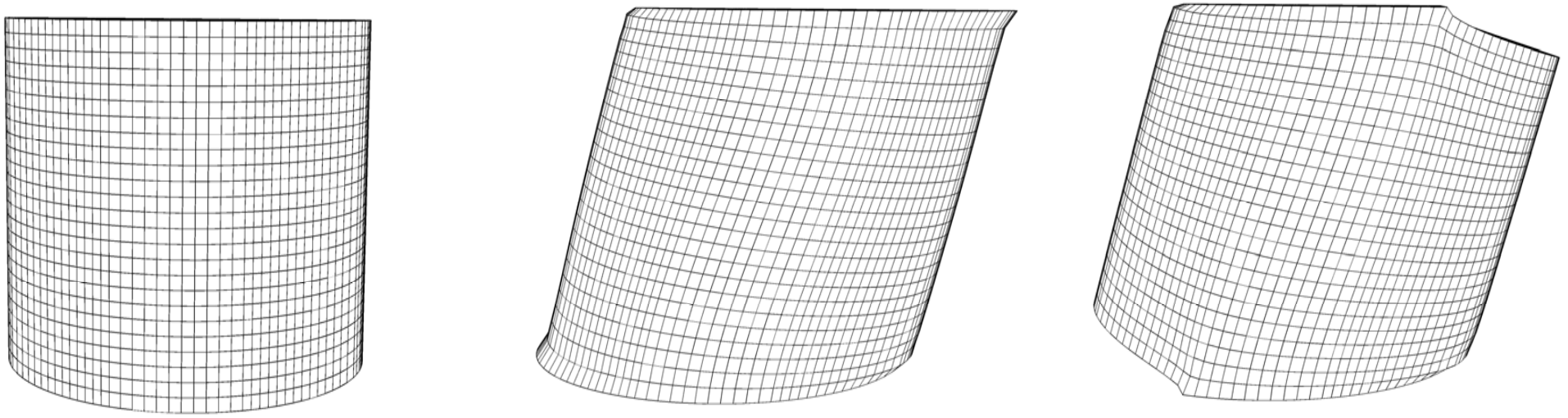

(a) (b) (c)

Figure 3.11 An undeformed half symmetry mesh (a), a simple shear deformed half symmetry mesh (b) and a simple shear deformed half symmetry mesh containing two large cracks (c)

3.6.4 **Modelling crack growth in shear deformation mode**

Crack growth in a simple shear deformation mode was predicted to initiate at the rubber-metal bond edge and propagate along the rubber-metal bond interface due to the nature of the strain energy density distribution in the component under deformation. To model the component's fatigue crack growth in shear a half symmetry three-dimensional model was used exploiting the symmetry found in the cylindrical component and the crack growth profile. Figure 3.11 shows an undeformed half symmetry model, a simple shear deformed half symmetry model without a crack and a simple shear deformed half symmetry model with cracks. The half symmetry model was developed in 3D with Abaqus CAE and meshed with an 8-node linear brick, hybrid, constant pressure elements C3D8H. The elastomer material was again modelled using the Yeoh stored energy function using coefficients derived from the experimental stress strain data measured on the dumbbell test pieces. This again allowed the calculation of the total stored energy variation associated with the crack growth and hence allowed the derivation of the strain energy release rate. To account for small changes in the strain energy due to growth of defects (flaws) at the rubber–metal bond edge, the model was meshed with a mesh size of 0.2 mm for the first 1 mm of crack growth. The virtual crack extension technique was used to calculate the strain energy release rate associated with crack growth along the rubber-metal bond interface.

3.6.5 **Modelling crack bifurcation in a pure shear test piece**

In figure 3.12, a schematic of the finite element analysis models developed for the crack bifurcation studies is shown. All the crack bifurcation models were developed as 2D plane stress models and meshed with a 4-node bilinear plane stress quadrilateral, reduced integration, hour-glass control elements (CPS4R). All the models were seeded with a global element seed size of 0.5 mm. The filled natural rubber material was modelled as an incompressible hyperelastic material using the Yeoh material model in Abaqus CAE (version 6.6-1) using the experimental 1000^{th} cycle stress strain data. In all the finite element analysis a full pure shear test piece was modelled. The models developed follow the schematic of figure 3.12, where a single crack (c) splits into two cracks c_1 and c_2 with both cracks parallel to the horizontal centre-line of the pure shear test piece and at a vertical distance of x and y, for c_1 and c_2 respectively, from it. Several different instances of the schematic in figure 3.12 were analysed in this work.

In each, the vertical distance of split crack c_1 above the horizontal plane (x mm) was kept constant at 4 mm. The vertical distance of split crack c_2 (y mm), however, was varied in each case and had values of 0.5 mm, 1 mm, 2 mm, 3 mm and 4 mm respectively. For each model instance of the schematic in figure 3.12, with the model at a fixed displacement, the length of one crack (say the length of c_2) was held constant whilst the other crack (c_1) was incrementally extended and the overall stored energy of the model as well as the crack surface area calculated at each incremental extension. This process was repeated for both split cracks (thus c_1 and c_2) in each of the different models. In all the models, split cracks c_1 and c_2 had initial lengths of 1 mm prior to extending one split crack whilst keeping the other constant. For each specified displacement, a plot of stored energy in the model against one of the corresponding crack surface areas at each incremental crack extension was then made. Following the virtual crack extension technique, for a fixed displacement of the model, the strain energy release rate of the advancing crack at a given crack length can be determined as the negative of the gradient of the total stored energy in the model against the crack surface area curve around the crack length of interest. Gradients at specific crack lengths along the stored energy against crack surface area curves, therefore, give the strain energy release rate crack length relationships for all the different split crack profiles. To distinguish between the strain energy release rate data of split cracks c_1 and c_2 in their respective model instances, the following labelling convention was adopted; thus, in a model instance where the initial length of split crack c_1 was kept constant and the crack had at a vertical distance x = 4 mm from the horizontal centre-line of the pure shear specimen and, the length of split crack c_2 was incrementally extended and the crack had a vertical distance y = 0.5 mm, the label for the strain energy release rate data is presented as "c_1=4mm c_2=0.5mm c_2 extended". In the results and discussion section in chapter six, graphs of strain energy release rate data for the split cracks are presented and labelled following this convention. The strain energy release rate data for a single crack in a pure shear specimen is simply labelled as "single crack tearing energy" in this work. It is important to mention that, the strain energy release rate of a single crack through the horizontal centre-line of a pure shear specimen is a constant.

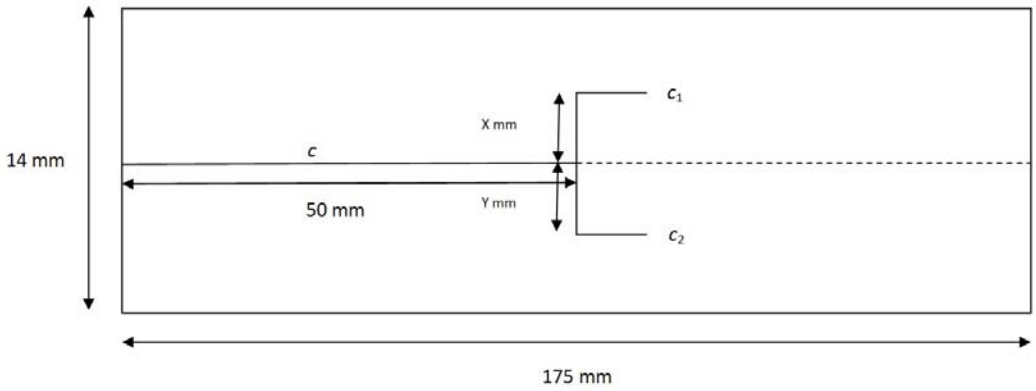

Figure 3.12 A schematic of a pure shear specimen with a crack (*c*) splitting into two cracks c_1 and c_2: Both c_1 and c_2 are parallel to the horizontal centre-line of the specimen

CHAPTER FOUR

4.0 Cyclic Stress Relaxation

4.1 Introduction

Dynamically loaded engineering components undergo repeated stressing. Under specific conditions for many rubber components this results in fatigue failure (Busfield et al, 2005). Laboratory tests of vulcanised rubber also suggest that they may experience stress relaxation or creep which is substantially greater than might have been expected from static measurements (Davies et al., 1996; Pond and Thomas, 1979). This cyclic stress relaxation behaviour is sometimes mistakenly referred to as the Mullins (1948) effect. This is inappropriate, as the classical Mullins effect describes behaviour where if the maximum strain experienced previously by the rubber is exceeded, the stress strain curve returns to the value measured in the virgin cycle. The relaxation phenomenon has been studied for simple extension by Derham and Thomas (1977), McKenna and Zappas (1981), Davies et al (1996) and Pond and Thomas (1979) but not for other deformation modes. It was found that the fractional relaxation or creep rate was strongly dependent on the maximum stress as well as the composition of the compound. In particular the filler content and the ability to strain crystallise appear to be important in enhancing the relaxation rate. A possible reason for this is that under large stresses the chemical bonds, particularly in the cross-links, can fracture with the crystallites acting as stress raisers. A close correlation was found between the amount of creep and the molecular scission estimated from the measurements of set and changes in the equilibrium swelling by Pond and Thomas (1979).

In engineering applications, the rubber experiences many modes of deformation and this chapter presents experimental results of cyclic stress relaxation measured in other modes of deformation. The chapter also discusses how the various relaxation rates from different deformation modes can be inter-related and how relaxation rates may be estimated for components of complex shape using data measured from test pieces.

4.2 **Results and Discussion**

In chapter three, the material and methods used to measure the cyclic stress relaxation results presented here were discussed in detail. Stress relaxation measurements were made using 65 phr carbon black filled natural rubber material prepared as both a flat sheet cut into pure shear test pieces and bonded cylindrical engineering components. In figure 4.1 below, typical cyclic stress relaxation behaviour of bonded cylindrical engineering components deformed in simple shear to positive 60mm maximum displacement from zero displacement level is shown.

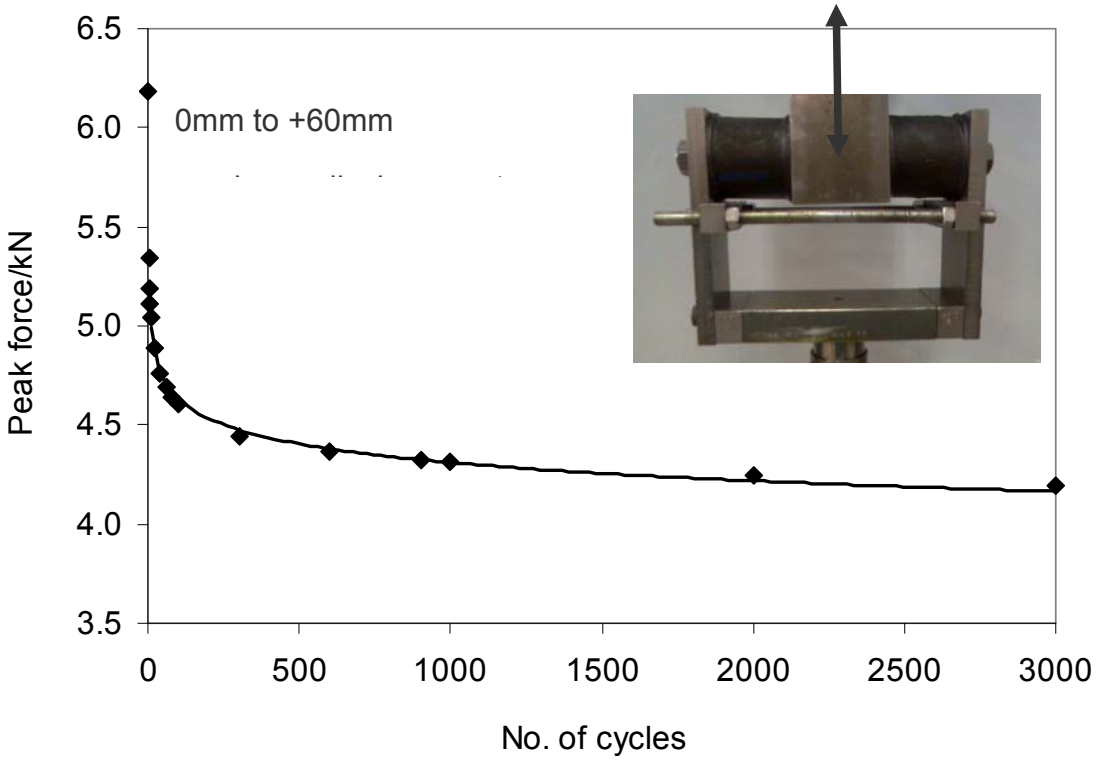

Figure 4.1 The maximum force versus number of cycles data for two bonded suspension mounts deformed in cyclic simple shear from 0mm to +60mm displacements.

The relaxation behaviour is typically non-linear as has been observed by earlier workers (Davies et al., 1996). The decrease in stress from cycle to cycle is rapid during the initial stages of the relaxation with subsequent stress decreases becoming relatively less. Clearly the relaxation continues over the entire range of the data and this is

contrary to earlier remarks in the general literature that cyclic stress relaxation occurs over about 10 cycles or so. The relaxation behaviour in figure 4.1 was also observed for the rubber test pieces and also when the components were tested in other modes of deformation including simple tension and compression.

The mechanism of relaxation has been discussed in earlier papers by Pond and Thomas (1979), Derham and Thomas (1977) and Davies et al (1996). It appears to involve strain induced crystallisation and the rupture of chemical bonds, especially those in the sulphur-sulphur cross-links. These sulphur-sulphur cross-links are mechanically weaker than primary carbon-carbon bonds or even carbon cross-links. This weakness is believed to promote greater strength as they effectively introduce a yielding mechanism (Thomas, 1974). Thus rubber compounds that are designed for maximum strength often show greater cyclic stress relaxation. This picture is complicated by the presence of filler, which appears to increase the stress relaxation rate, making a contribution even in a non-crystallising rubber such as styrene butadiene rubber (Pond and Thomas, 1979). The presence of the filler causes strain amplification (Mullins and Tobin, 1965) which will both stiffen the materials and will also most likely make these effects of cyclic stress relaxation more significant even at relatively modest strains.

Davies et al. (1996) showed that the cyclic stress relaxation behaviour observed in figure 4.1 may be plotted using logarithmic axes. The slope of the resulting plot is a measure of the rate of cyclic stress relaxation per decade. Figure 4.2 presents results of cyclic stress relaxation measurements made on the pure shear samples for a range of different maximum strains. Apart from the initial points taken from the first few cycles, the data reduces to simple straight lines. The causes of the less than perfect fit for the first point results from the first maximum displacement being attained before a whole loading and unloading cycle has been completed as discussed by Davies et al (1996). Figure 4.3 shows how the slopes of the lines fitted to data in figure 4.2 change with the maximum strain in the test cycle. The cyclic stress relaxation rate shows an approximately five fold increase as the deformation is increased from 20% to 150% of the original test piece height.

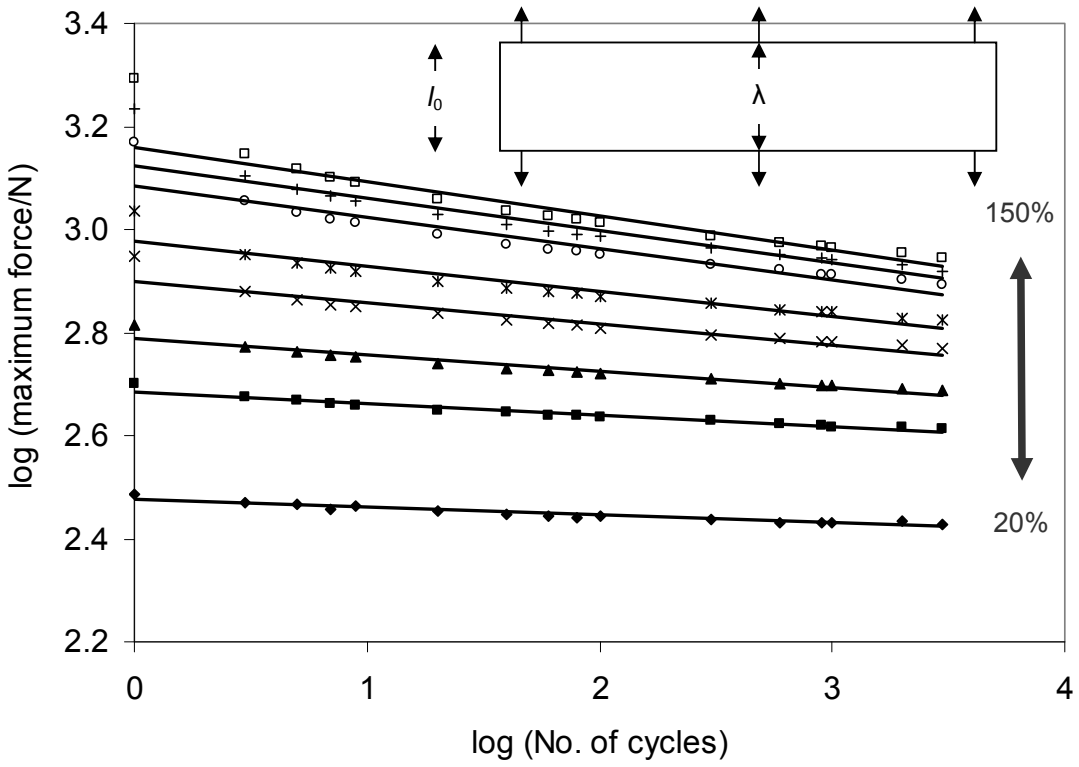

Figure 4.2 Plot of log (maximum force) against log (number of cycles) for pure shear samples tested at 20%, 40%, 60%, 80%, 100%, 120%, 140% and 150% maximum engineering strain.

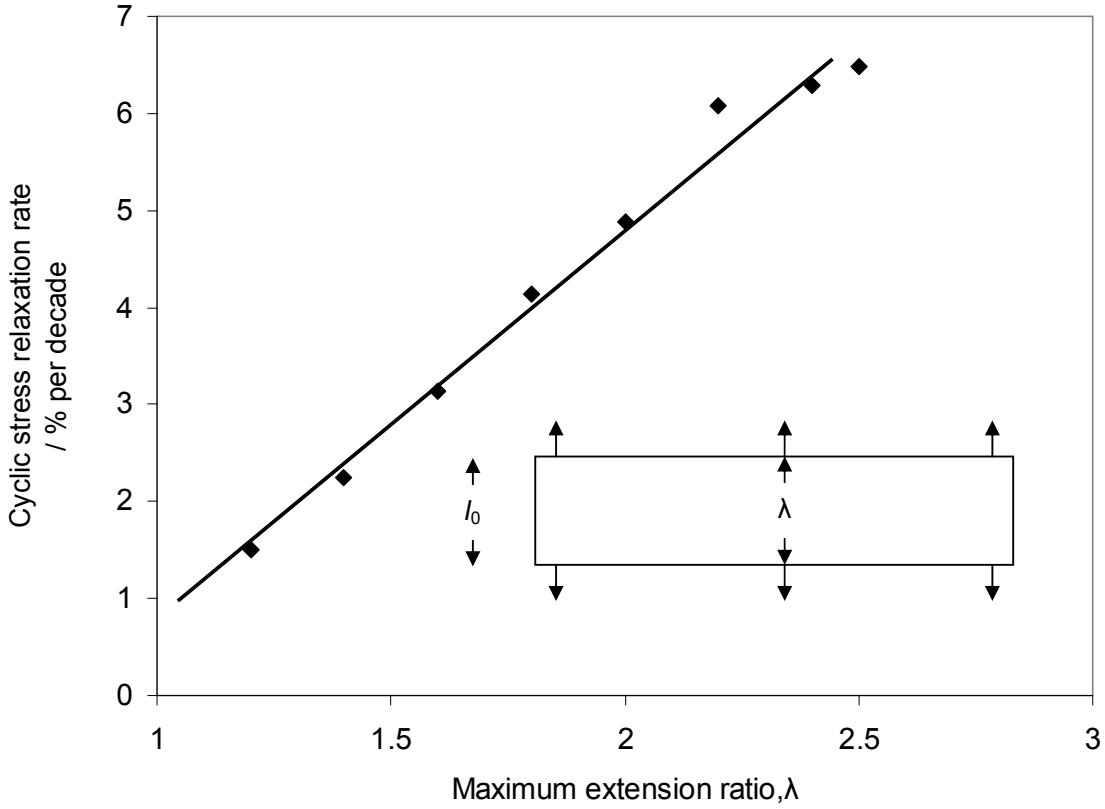

Figure 4.3 Cyclic stress relaxation rate against extension ratio for the pure shear test pieces

The cyclic stress relaxation measurements made on the bonded cylindrical engineering components in tensile, shear and compressive deformation directions are presented in figures 4.4, 4.5 and 4.6 respectively. In figure 4.7 a plot of the slopes of the lines fitted to data in figures 4.2, 4.4, 4.5 and 4.6 are plotted together in terms of maximum extension ratio (deformation). For the bonded component, the maximum deformation was expressed as a percentage of the component's original rubber section height. In each respective deformation mode it is apparent that the rate of cyclic stress relaxation increases with the extent of the deformation in figure 4.7. It is immediately obvious in figure 4.7 that the rate of cyclic stress relaxation is very different when compared in terms of the respective maximum cyclic deformation for the different deformation modes. One approach to the unification of these results is as follows. When a filled rubber is deformed, the elastic energy will be stressed in the rubber phase only and will thus reflect the deformation of the rubber chains between the cross links. It is thought

that the stress in a chain will be the factor which induces fracture in the chemical bonds (in either the main chain or the cross-link) or possibly slippage of the rubber molecules over the surface of the filler. These being the two factors most commonly proposed to explain cyclic stress relaxation. If so then the maximum average energy density proposed by Muhr et al (1988) and adopted by Busfield and Thomas (1999) to model indentation hardness may be an appropriate parameter with which to attempt correlation between the various different deformation modes. The deformations applied to the bonded suspension mount are not perfectly homogeneous, the extension and compression modes in particular having non uniform strains. Thus the maximum average strain energy density, simply derived by dividing the work done on the sample up to working strain by the volume of rubber, was adopted as the parameter to describe the cyclic stress relaxation rate. The outcome of presenting the results in this way is shown in figure 4.8. This shows that this approach works well and that even for an inhomogeneous strain state found in the component the average strain energy density is a useful measure.

This approach gives promise that it may be applied to more complex geometries and loading regimes encountered in engineering applications, so that the cyclic stress relaxation for a component may be estimated from laboratory measurements to determine the behaviour of the material itself.

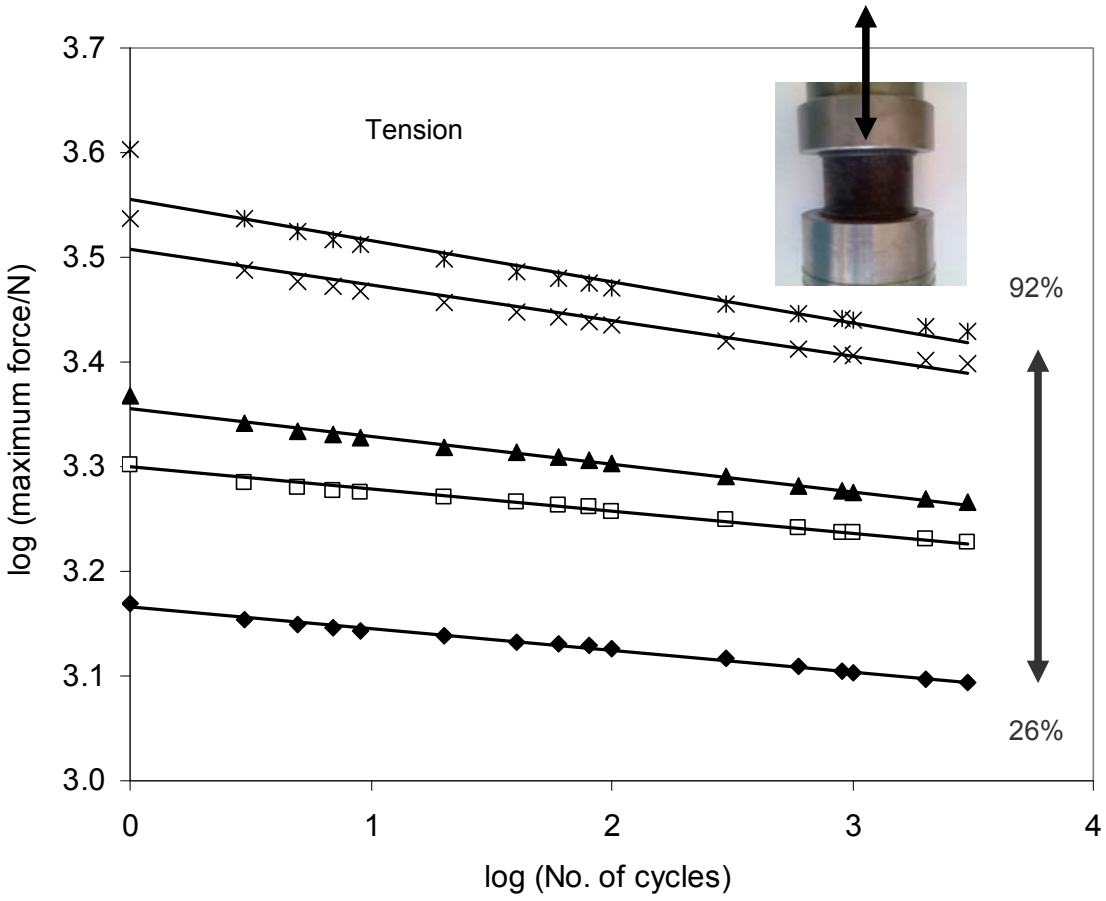

Figure 4.4 Plot of log peak force (maximum force) against log (number of cycles) for the bonded suspension mount at 26%, 40%, 53%, 79% and 92% maximum displacement expressed as a percentage of the rubber cylinder height in tension.

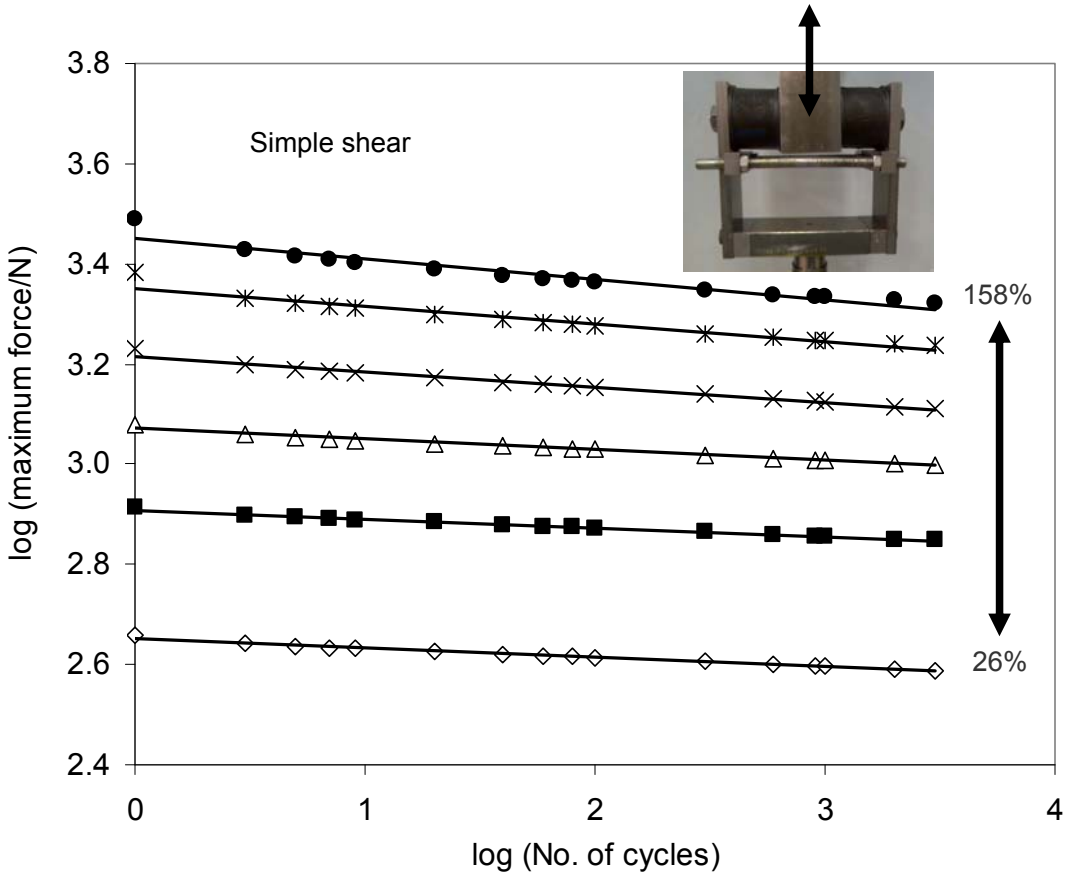

Figure 4.5 Plot of log peak force (maximum force) against log (number of cycles) for the bonded suspension mount at 26%, 53%, 79%, 105%, 132% and 158% maximum shear displacement expressed as a percentage of the rubber cylinder height.

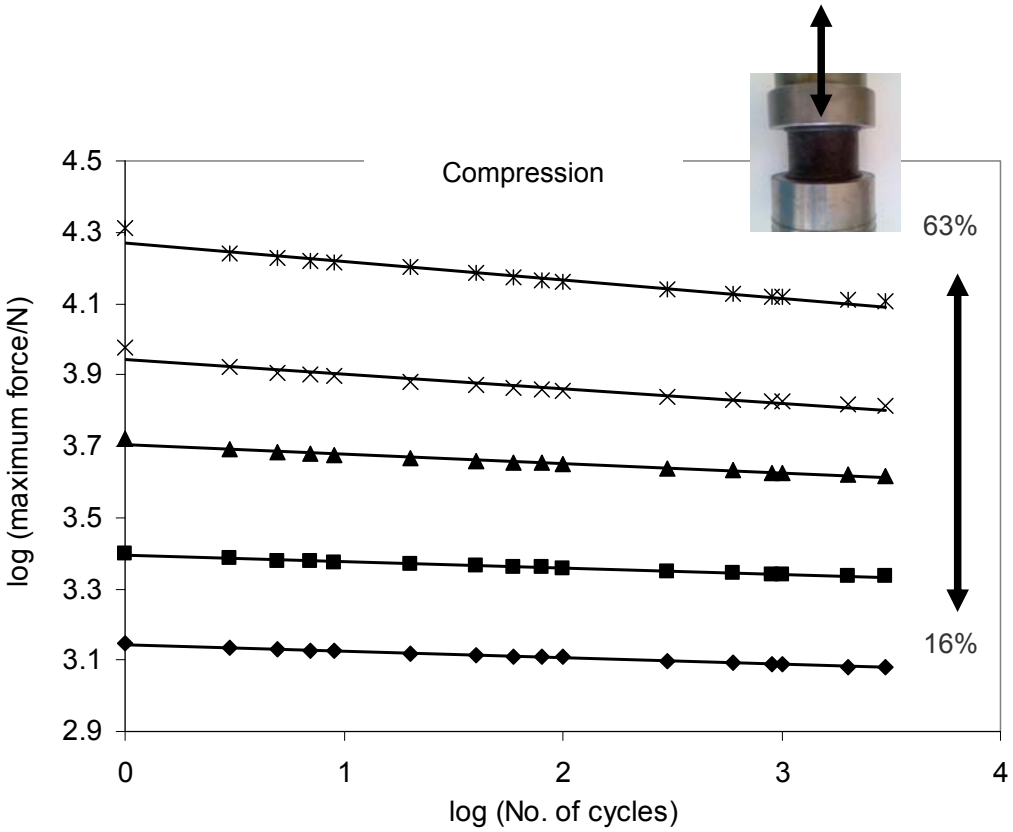

Figure 4.6 Plot of log peak force (maximum force) against log (number of cycles) for the bonded suspension mount at 16%, 26%, 42%, 53% and 63% maximum compression, expressed as a percentage of the cylinder rubber section height.

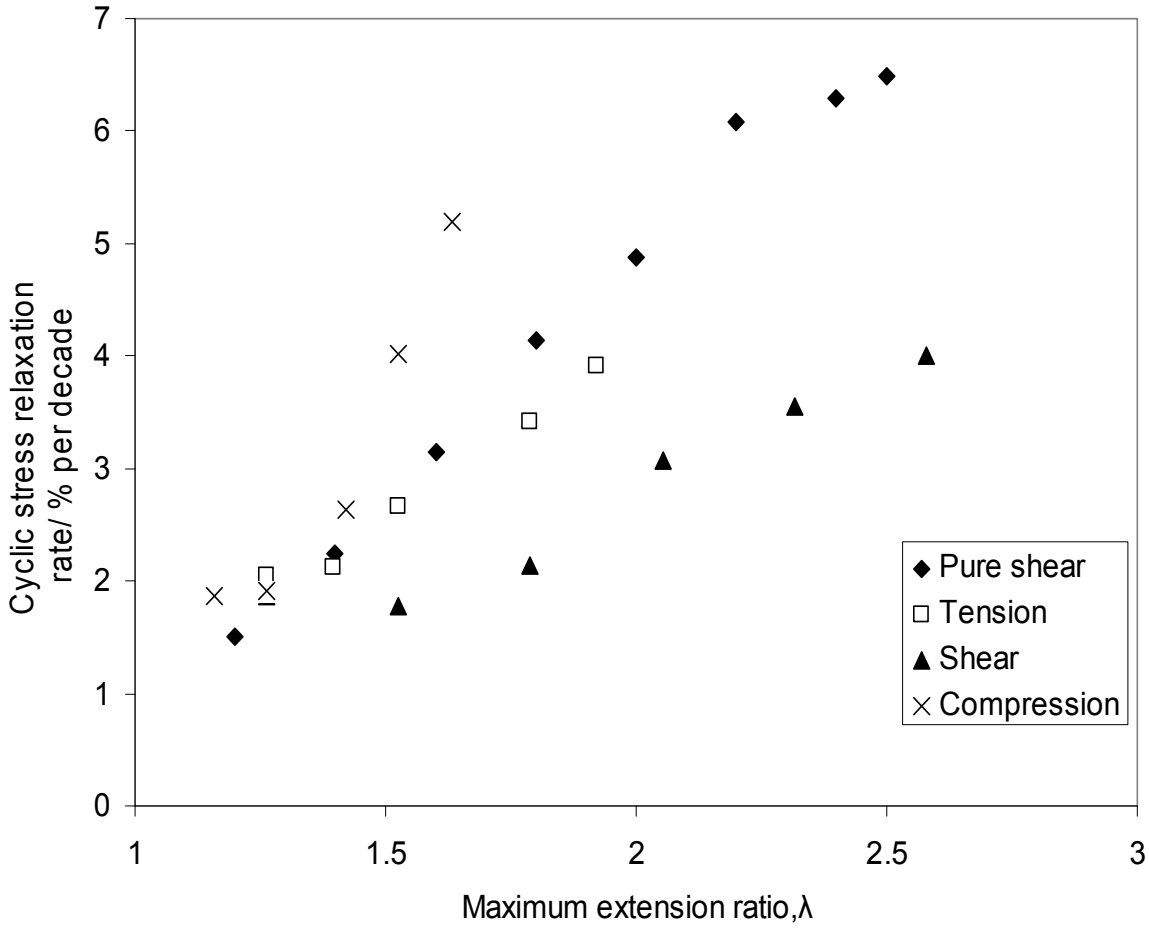

Figure 4.7 Cyclic stress relaxation rate plotted against the maximum engineering strain for the pure shear test pieces and maximum displacement divided by the rubber cylinder height for the suspension mount under different deformations

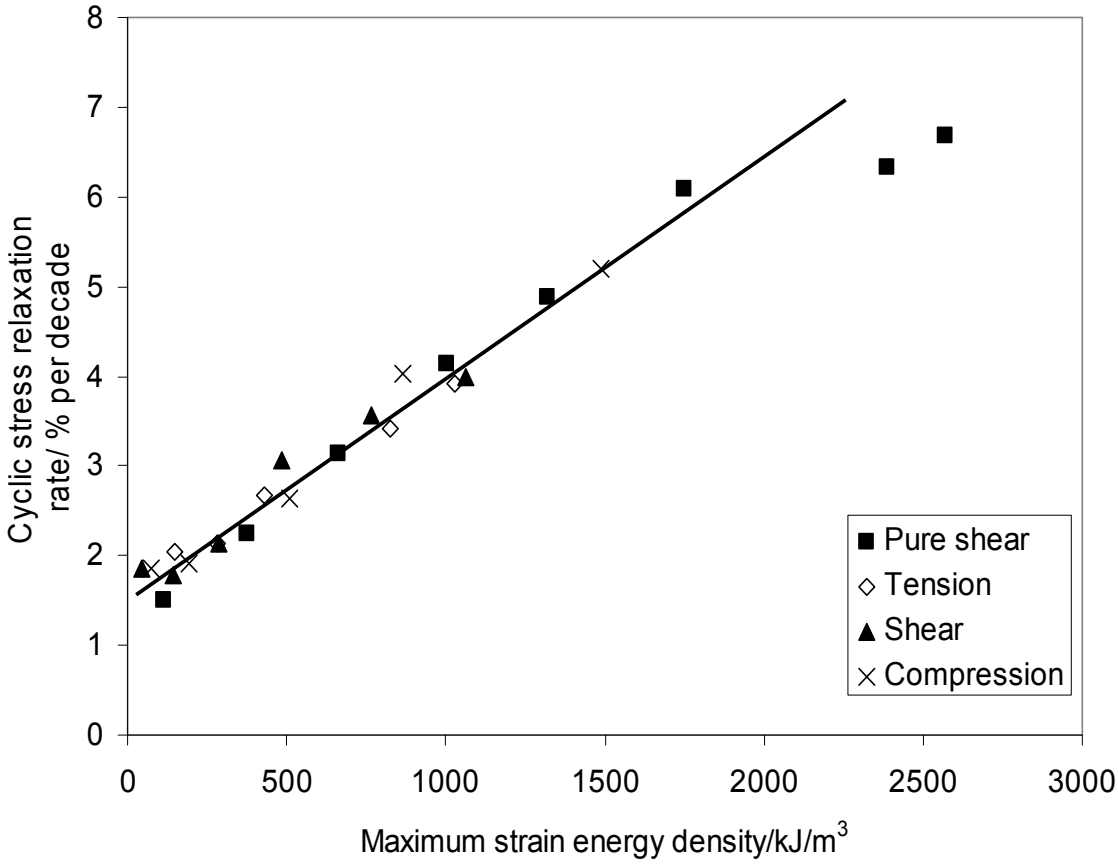

Figure 4.8 Cyclic stress relaxation rate plotted against the maximum average strain energy density for the pure shear test pieces and the suspension mount under different deformations

4.3 **Conclusion**

Cyclic stress relaxation has been studied for bonded cylindrical engineering components and test pieces. The results of the studies confirm that the cyclic stress relaxation rate increases with displacement amplitude (strain) for all directions of deformation in test pieces and components. Plotting the cyclic stress relaxation rate in terms of average strain energy density, reduces both test piece and component data to a single straight line. This suggests a general dependence of the cyclic stress relaxation rate only relies on the average maximum strain energy density experienced in a loading cycle. The average strain energy density concept presents an approach for determining the amount of cyclic stress relaxation of an elastomer component from a measure of the material's cyclic stress relaxation behaviour.

CHAPTER FIVE

5.0 Fatigue Life Prediction

5.1 Introduction

Elastomer components fail at cyclic strain amplitudes much lower than their catastrophic tear strength due to cumulative cyclic fatigue crack growth. Fatigue cracks usually initiate in regions of high strain energy density in components. In general, the rate of crack growth is determined by the geometry of the component and the nature and magnitude of the deformation imposed. The empirical approach of stress versus the number of cycles to failure (*S*–*N*) (W. D. Callister, 1994), which is traditionally used to determine the fatigue life of components, has also been adopted by the elastomer component industry. An alternative approach to predicting the fatigue life of carbon black filled elastomer test pieces makes use of fracture mechanics. Lake (1995) reviewed the fracture mechanics approach adopted in the present study. Here, the energy required to drive the crack at a given rate is defined as the strain energy release rate which is also referred to as the tearing energy *T*.

$$T = -\frac{dU}{dA} \qquad \text{(Eq.5-1)}$$

where A is the area of a single fracture surface of the crack and U is a measure of the internal energy stored in the component. The magnitude of T is mostly determined by the viscous work that has to be done in the crack tip region. Rivlin and Thomas (1953) showed that the relationship between crack growth rate and the strain energy release rate is a material property, which is independent of the mode of loading and specimen geometry. Similarly, it has been shown by Lindley and Thomas (1962) that a characteristic crack growth rate per cycle relationship exists for an elastomer that is dependent only on the maximum strain energy release rate attained during the loading cycle. Busfield and Ng (2005) reported that the actual strain energy release rate against applied loading relationships has been difficult to calculate accurately for anything other than the simplest components, hence for more complex component types, researchers have resorted to approximate relationships for the strain energy release rate. For instance, Lindley and Stevenson (1982) used an approximate fracture mechanics approach to predict the fatigue behaviour of engineering mounts loaded in compression

where, estimates of fatigue lives were made that were of the correct order of magnitude. This technique for predicting fatigue failure has been dramatically extended by the arrival of large deformation finite element analysis. It is now possible to calculate the strain energy release rate for specific loading configurations for cracks in components of any geometry. Gent and Wang (1993) adopted this type of FEA approach to study the crack growth behaviour of bonded elastomer suspension components subjected to large shear. This technique was successfully used to predict the strain energy release rate and hence the mode of failure for these types of components. Busfield et al. (2005) extended the FEA based fracture mechanics approach by calculating the relationships between strain energy release rate and crack size for a gearbox mount at different amplitudes of cyclic fatigue loading and combined with material crack growth rate versus strain energy release rate relationships to predict crack growth rate in the gearbox mount under different modes of loading. In their work, Busfield et al. (2005) made predictions of crack growth rate and therefore fatigue life for room temperature conditions. In practice elastomer engineering components usually operate above the ambient temperature as a result of hysteresis. This thesis extends the work of Busfield et al. (2005) to examine real fatigue measurements made at both room temperature and for the first time 70±1ºC. Effort was made in this work to calculate the strain energy release rate of small cracks of the order of the size of existing defects (flaws) observed, after careful visual inspection, at the rubber-metal bond edge of the cylindrical component.

In chapter three of this thesis, the material, experimental and FEA methods used to collect data for the fatigue life prediction of the bonded cylindrical elastomer component is explained. Dumbbell specimens, pure shear specimens and bonded cylindrical elastomer components were prepared from a 65 phr carbon black filled NR material. The dumbbell specimens were used for uni-axial stress strain characterisation whereas the pure shear specimens were used for fatigue crack growth characterisation. The bonded cylindrical components were used in experiments to validate the predicted number of fatigue cycles required to grow a crack in the component to a measurable size.

5.2 **Results and discussions**

In this chapter, material characterisation results, results of FEA calculations of strain energy release rate versus crack length relationships, fatigue life prediction and experimentally measured number of fatigue cycles to grow a crack in the bonded cylindrical component are presented and discussed.

5.2.1 **Material stress strain behaviour**

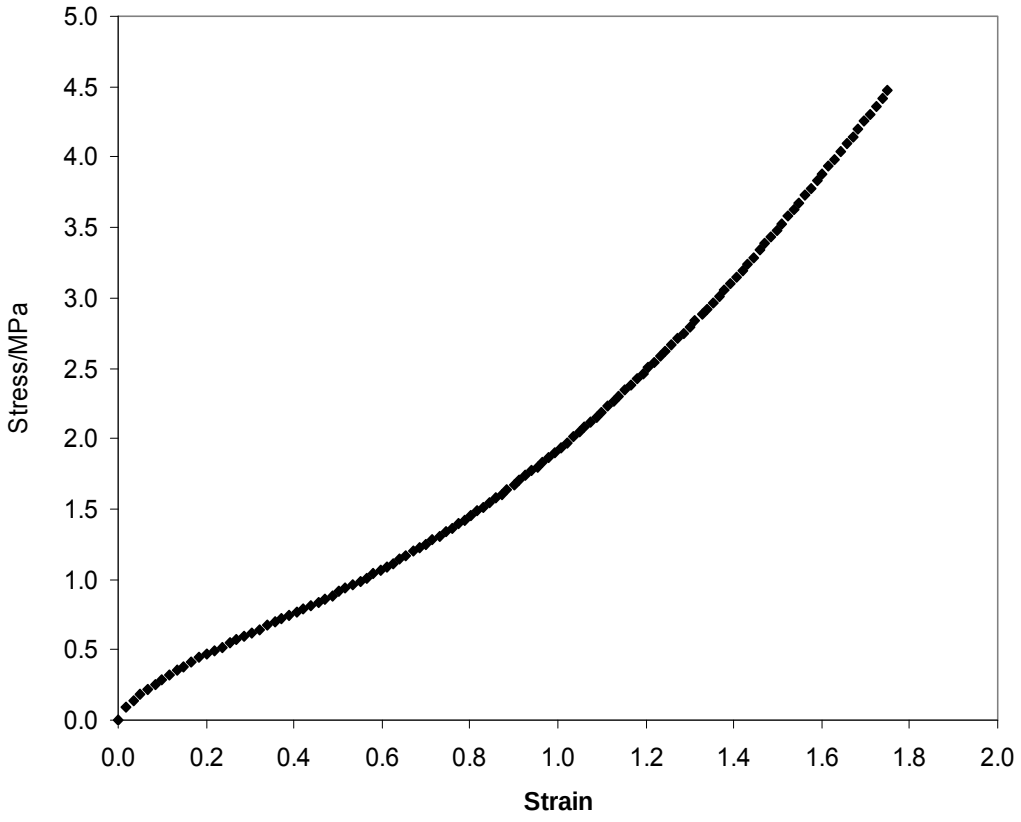

Figure 5.1 Virgin stress strain behaviour of the elastomer material (NR, 65 phr) at room temperature obtained from a dumbbell test piece

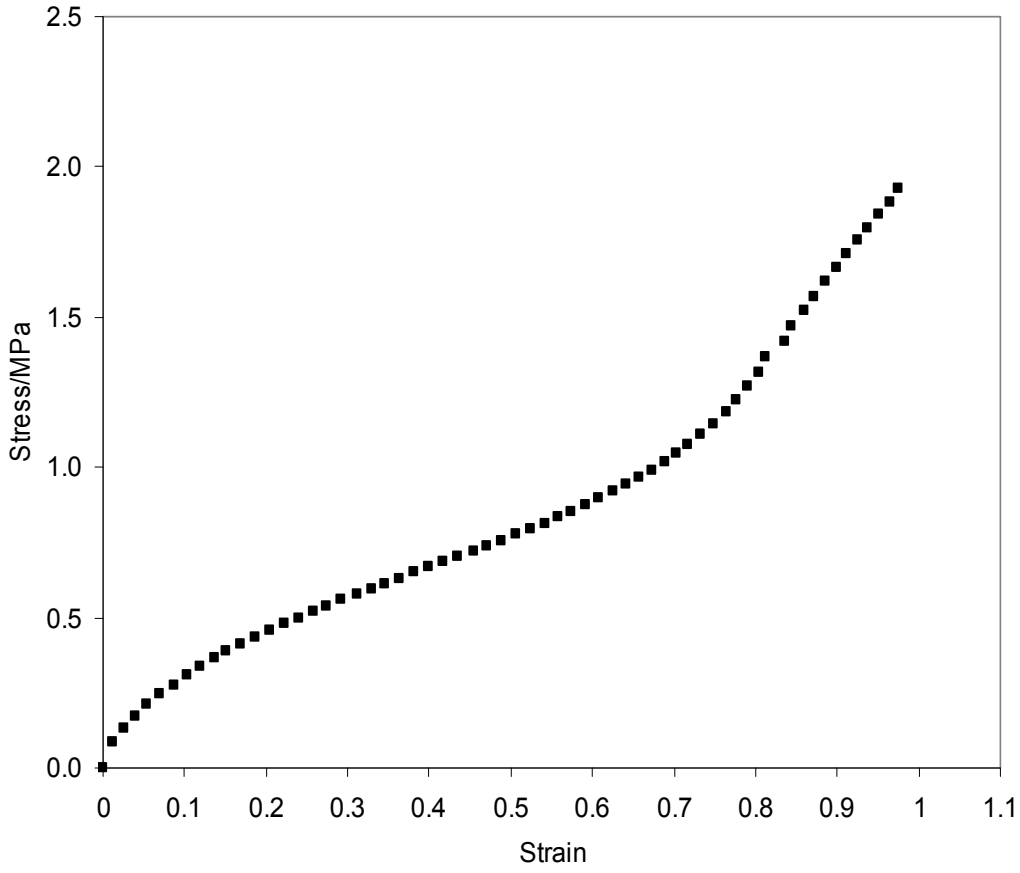

Figure 5.2 1000th cycle stress strain behaviour of the elastomer material (NR, 65 phr) measured at room temperature from a dumbbell test piece after softening at 90% strain for 999 cycles

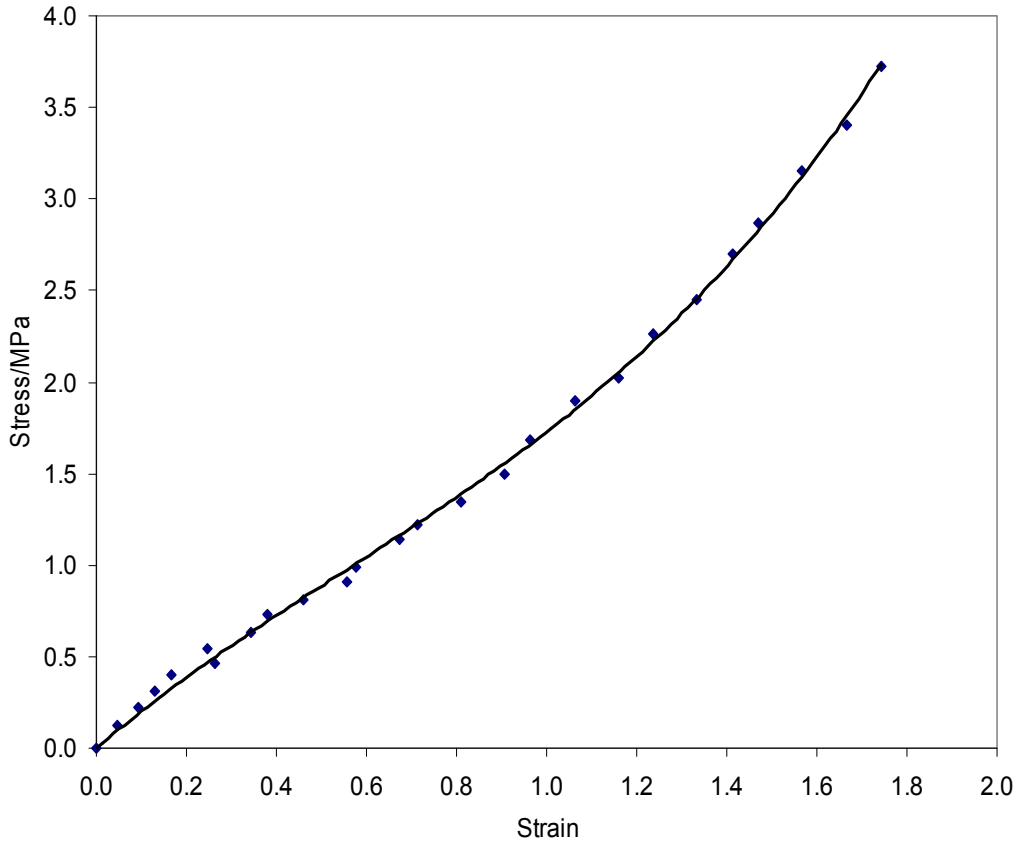

Figure 5.3 Virgin stress strain behaviour of the elastomer material (NR, 65 phr) at 70 ºC obtained from a dumbbell test piece

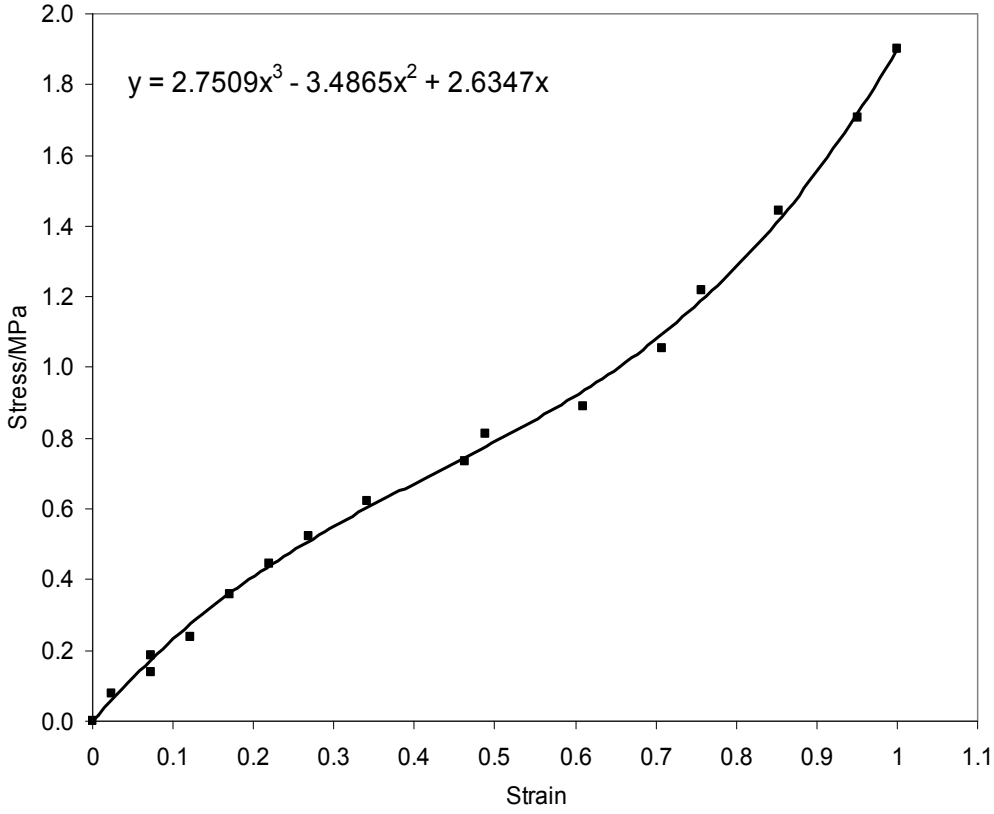

Figure 5.4 1000th cycle stress strain behaviour of the elastomer material (NR, 65 phr) measured at 70 ºC from a dumbbell test piece after softening at 90% strain for 999 cycles

All the stress strain curves presented above are typical of a filled elastomer material and were required in order to use a finite element approach to determine the strain energy distribution in the bonded cylindrical component under load. The carbon black filled natural rubber material's mechanical behaviour was initially modelled using the virgin stress strain curves of figures 5.1 and 5.3 to observe the regions of high strain energy density. Figures 3.8 and 3.9 in chapter three show typical meshed finite element analysis models of the bonded cylindrical component. Under both tensile and shear deformation directions, the regions of highest strain energy density were observed to be around the rubber-metal bond edge of the bonded cylindrical component. In general fatigue crack growth initiates in components where the strain energy density or stress concentration is the greatest (Busfield et al., 2005). The models

of the bonded component under strain allow the strain energy distribution in tension and shear deformation modes to be determined and so, it was possible to predict the regions where fatigue crack growth and subsequent failure may initiate at both room temperature and 70±1ºC.

In order to calculate the relationship between strain energy release rate and crack length in the cylindrical component, both 2D and 3D models (Chapter 3, figures 3.10 and 3.11) of crack growth at the rubber-metal bond interface were made. To calculate the fracture behaviour, the material stress strain behaviour from the 1000^{th} cycle stress strain curves shown in figures 5.2 and 5.4 was used. In figure 5.4, the experimentally measured 1000^{th} cycle stress strain curve was fitted using a polynomial to characterise the experimental data using a Yeoh type stored energy function. This provided the necessary number of stress strain points at 70±1ºC needed in the Abaqus FEA software to ensure accurate stress strain interpolation by the FEA software. Using the 1000^{th} cycle stress strain curves ensured that the initial cyclic stress relaxation, described in Chapter 4 (Asare et al., 2010) and which is associated with fatigue crack growth was in part accounted for and that the stored energies were not significantly over estimated by the FEA models. The results of the stored energy crack length relationships at both room temperature and 70±1ºC for different modes of deformation are presented and discussed in section 5.5 below.

5.2.2 **Equilibrium swelling test results**

Figure 5.5 shows the equilibrium swelling in n-decane of a sample taken from a component (Component) compared with samples cut from three different rubber sheets (S1, S6 and S7). The sheet materials cured from nominally identical materials swell to a greater extent in n-decane than materials taken from the component. This indicates that the degree of cross linking in the component material was slightly greater than that in the sheet material. Using the Flory-Rehner equation (Eq.3-1), a cross link density of 1.452×10^{-4} mol/cm^3 was calculated, from the average absorbed decane measured on three different sheets, for the sheet material and 1.609×10^{-4} mol/cm^3 for the bonded cylindrical component material. The average cross link density of the bonded cylindrical component material was found to be about 10% higher than that of the sheet material, possibly arising as the sheets were compression moulded whereas the components were injection moulded.

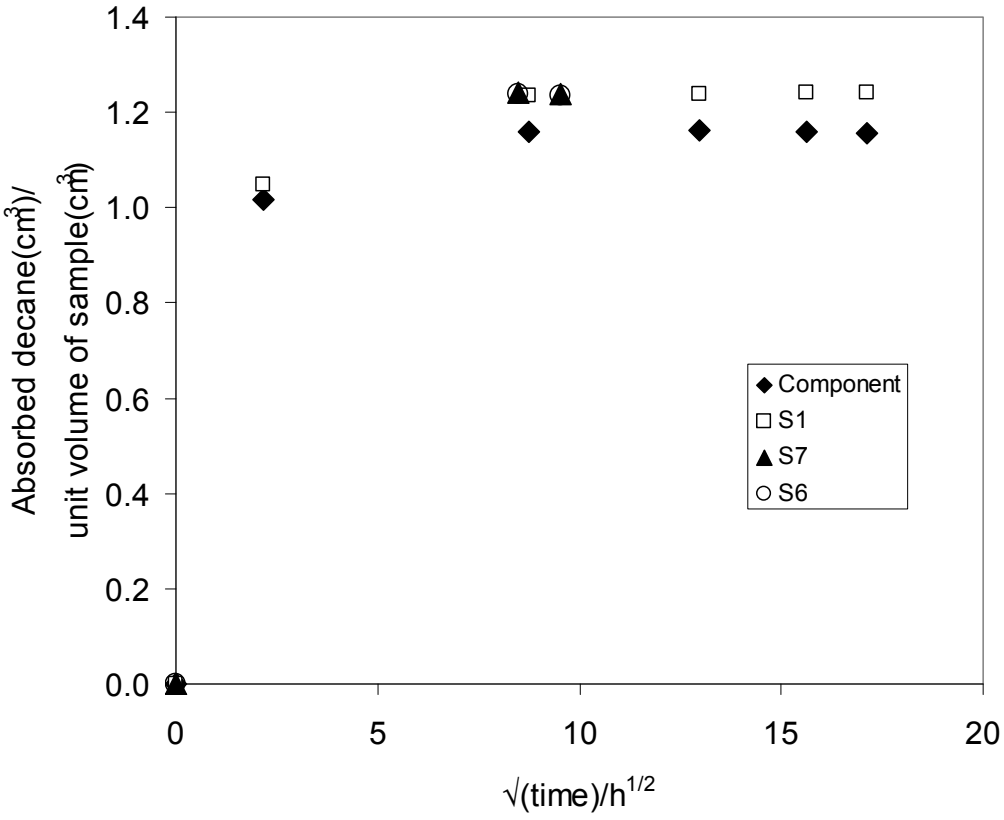

Figure 5.5 Plot of absorbed n-decane per unit volume of sample for bonded cylindrical component sample, sheet samples S1, S6 and S7

5.2.3 **Material pure shear crack growth characterisation**

Figures 5.6 (a to h) and 5.7 (a to g) present the results of many different pure shear crack growth characterisations done at both room temperature and at 70±1ºC. The plot of crack length against number of cycles for each test amplitude produces quite reliable linear plots with limited scatter, where the slope equals the rate of cyclic crack growth at that amplitude. The room temperature pure shear characterisation was carried out at strain energy release rates of 10 kJ/m^2, 13 kJ/m^2, 17 kJ/m^2, 20 kJ/m^2, 24 kJ/m^2, 26 kJ/m^2, 29 kJ/m^2 and 35 kJ/m^2. The 70±1ºC pure shear characterisation was carried out at strain energy release rates of 4 kJ/m^2, 7 kJ/m^2, 10 kJ/m^2, 13 kJ/m^2, 15 kJ/m^2, 18 kJ/m^2 and 21 kJ/m^2. It has been shown that for a pure shear crack growth test piece (Chapter 3, figure 3.2) with an unstrained height of l_0, thickness t, width w, and a crack of size c the strain energy release rate, T is given as Eq.3-3. The strain energy release rate for the different pure shear crack growth test amplitudes was thus calculated for

both the room temperature tests and for those at 70±1ºC. A plot of crack growth rate per cycle d*c*/d*n* against the strain energy release rate, *T* is plotted using logarithmic scales in figure 5.8 for both test temperatures. The data shown in figure 5.8 was fitted to the power law relationship given by equation 5-2 below:

$$\frac{dc}{dn} = XT^{\psi} \qquad \text{(Eq.5-2)}$$

Ψ is typically around a value of 2 for natural rubber compounds. A value of 1.8 for room temperature and 2.4 for 70±1ºC as is shown in figure 5.8 for the present material (NR, 65 phr), is in good agreement with equation 5-2 and results obtained for natural rubber materials by earlier workers. Figure 5.8 shows clearly that the material becomes weaker at elevated temperatures. This confirms that a rise in the temperature will make the material weaker and therefore the fatigue life of elastomer materials and components lower (Gent, 1992). This arises as the increase in temperature moves the rubber further from the glass transition temperature and hence makes it less viscoelastic. This reduction in damping behaviour makes it easier for cracks to propagate. Since many elastomer engineering components operate at elevated service temperatures, it is important to extend the fracture mechanics approach to fatigue life prediction at elevated temperatures to determine the practical applicability of the approach.

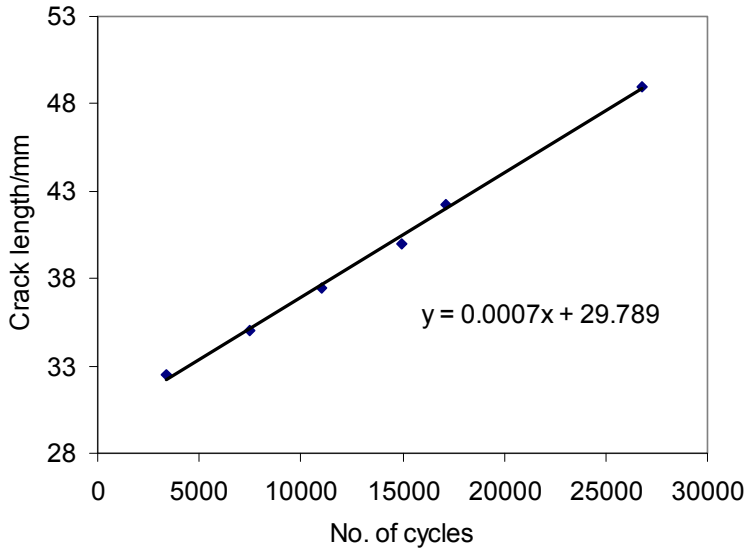

Figure 5.6(a) A plot of Crack length against No. of cycles for 5mm sinusoidal displacement amplitude at room temperature

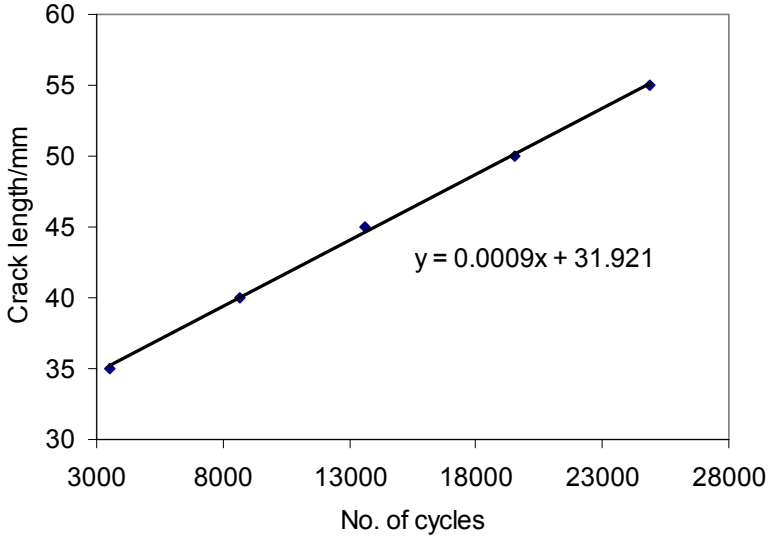

Figure 5.6(b) A plot of Crack length against No. of cycles for 6mm sinusoidal displacement amplitude at room temperature

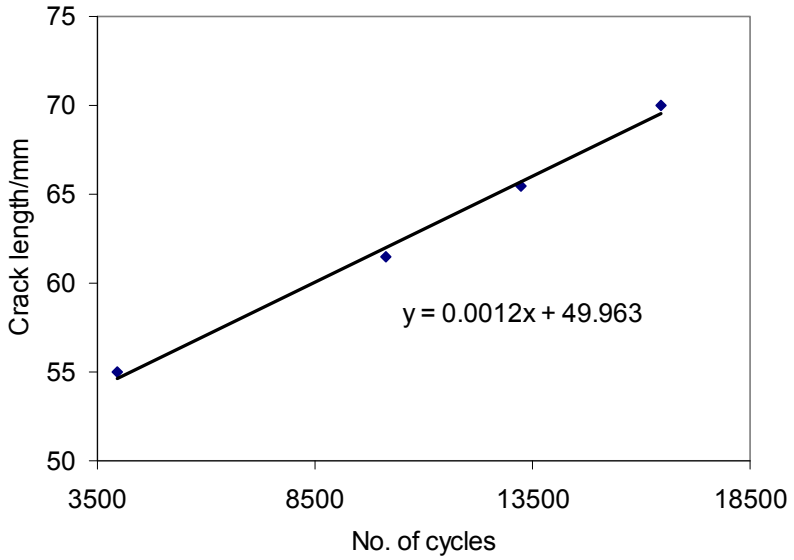

Figure 5.6(c) A plot of Crack length against No. of cycles for 7mm sinusoidal displacement amplitude at room temperature

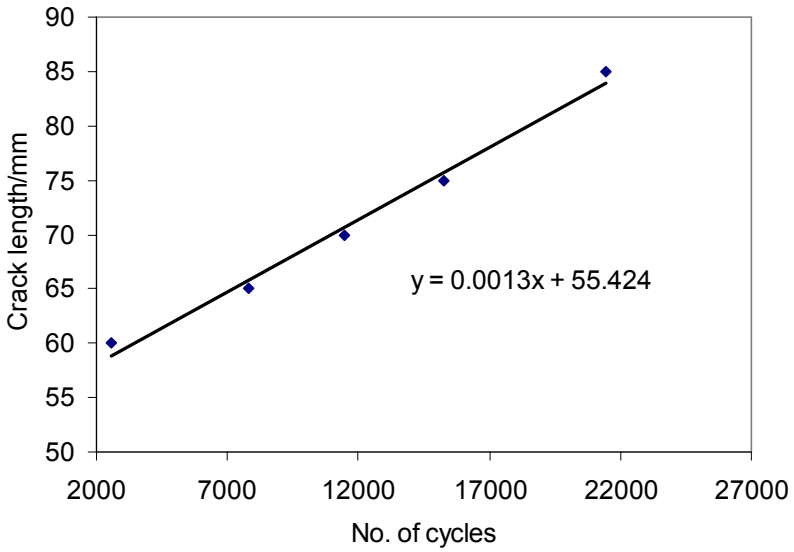

Figure 5.6(d) A plot of Crack length against No. of cycles for 8mm sinusoidal displacement amplitude at room temperature

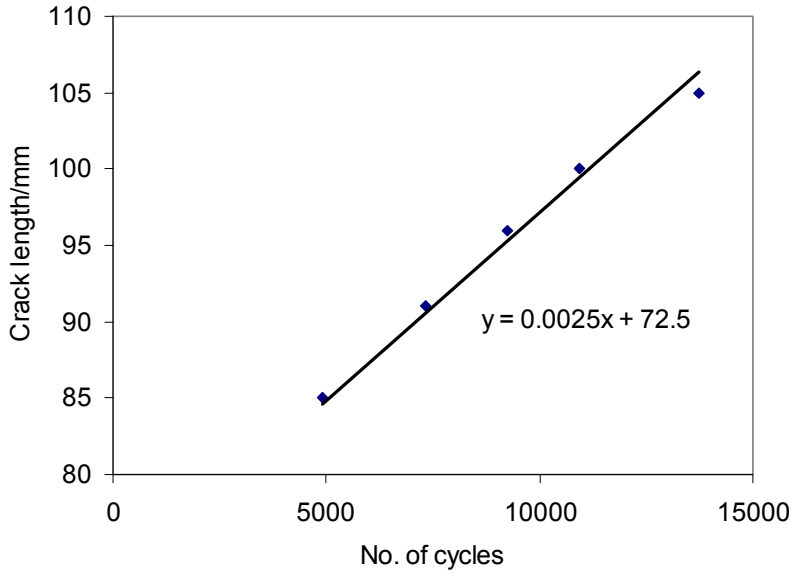

Figure 5.6(e) A plot of Crack length against No. of cycles for 9mm sinusoidal displacement amplitude at room temperature

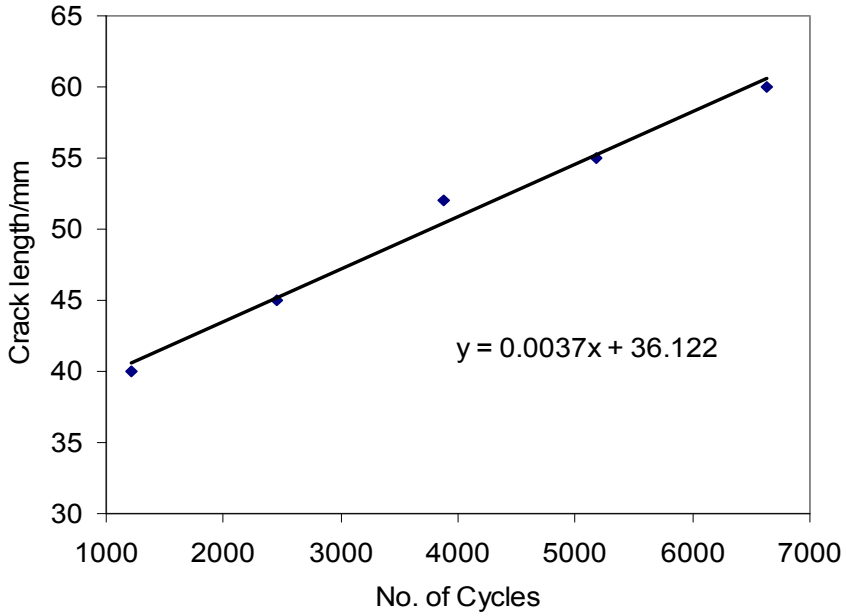

Figure 5.6(f) A plot of Crack length against No. of cycles for 10mm sinusoidal displacement amplitude at room temperature

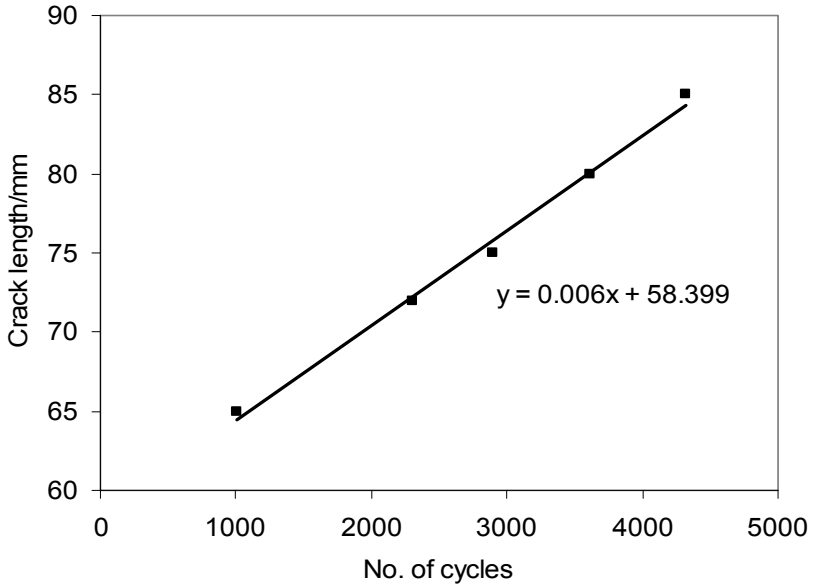

Figure 5.6(g) A plot of Crack length against No. of cycles for 11mm sinusoidal displacement amplitude at room temperature

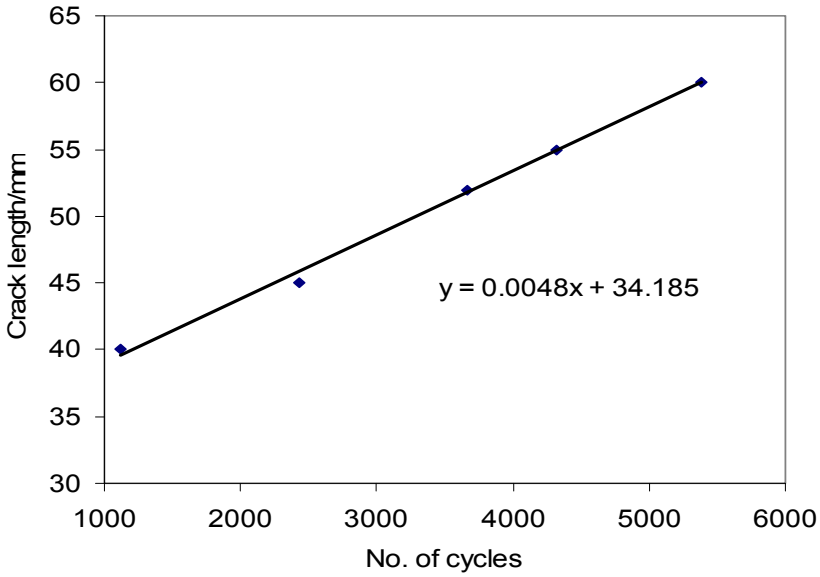

Figure 5.6(h) A plot of Crack length against No. of cycles for 12mm sinusoidal displacement amplitude at room temperature

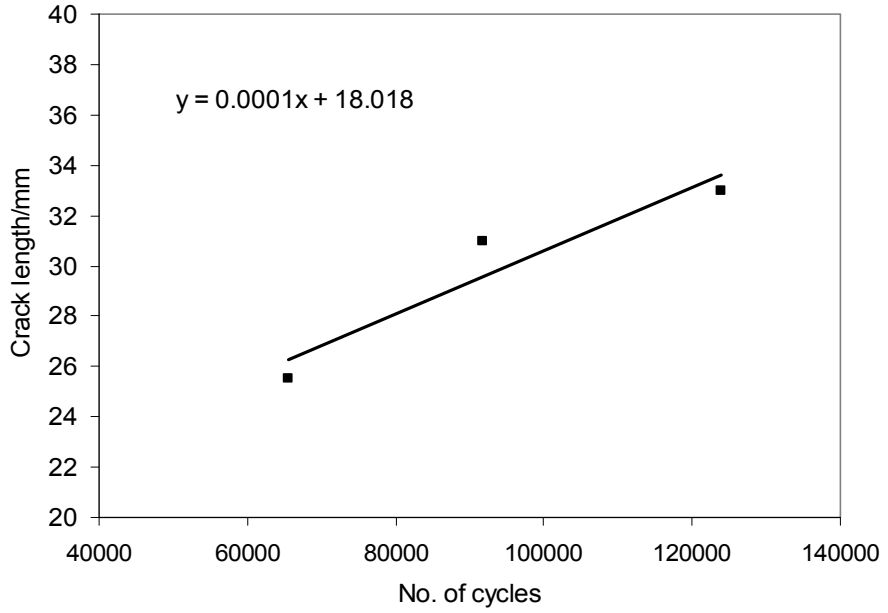

Figure 5.7(a) A plot of Crack length against No. of cycles for 3mm sinusoidal displacement amplitude at 70 ºC

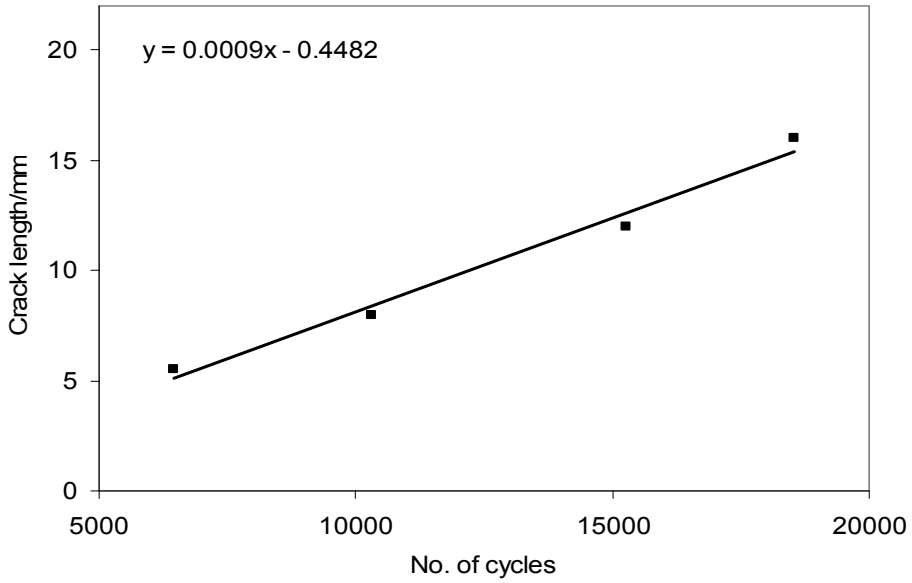

Figure 5.7(b) A plot of Crack length against No. of cycles for 4mm sinusoidal displacement amplitude at 70 ºC

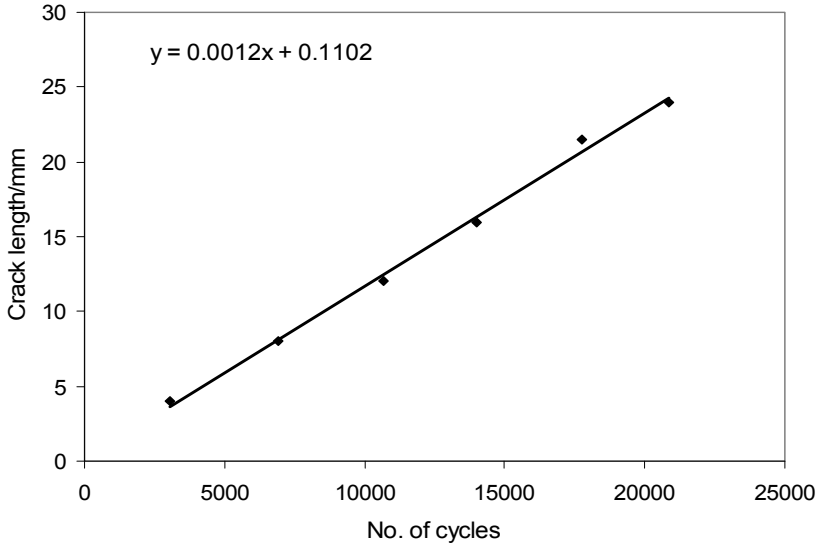

Figure 5.7(c) A plot of Crack length against No. of cycles for 5mm sinusoidal displacement amplitude at 70 ºC

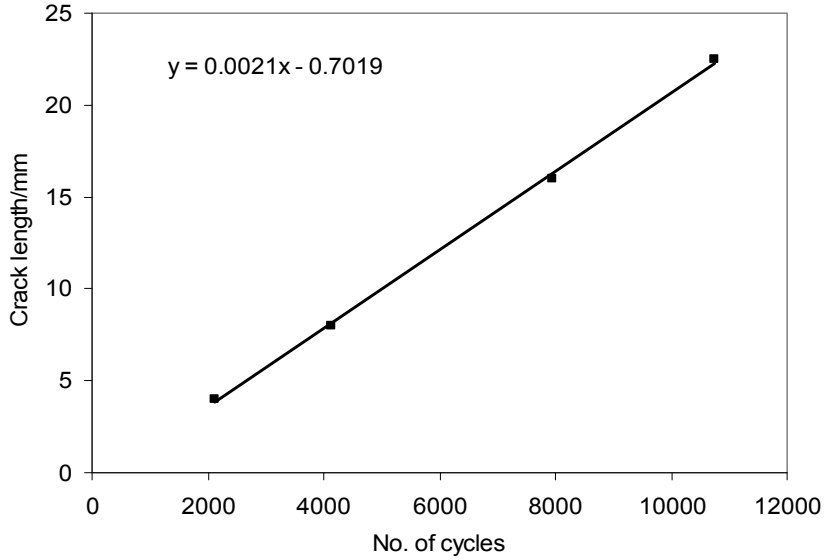

Figure 5.7(d) A plot of Crack length against No. of cycles for 6mm sinusoidal displacement amplitude at 70 ºC

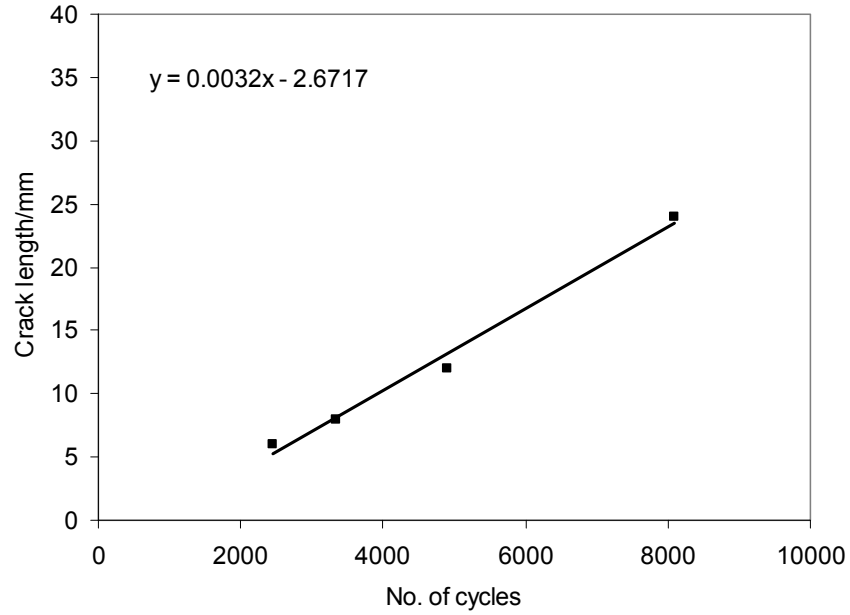

Figure 5.7(e) A plot of Crack length against No. of cycles for 7mm sinusoidal displacement amplitude at 70 ºC

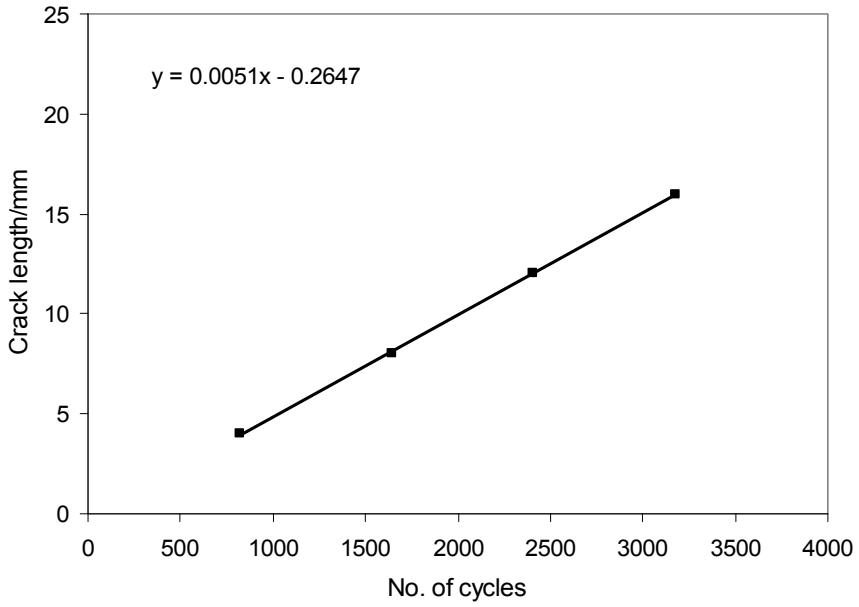

Figure 5.7(f) A plot of Crack length against No. of cycles for 8mm sinusoidal displacement amplitude at 70 ºC

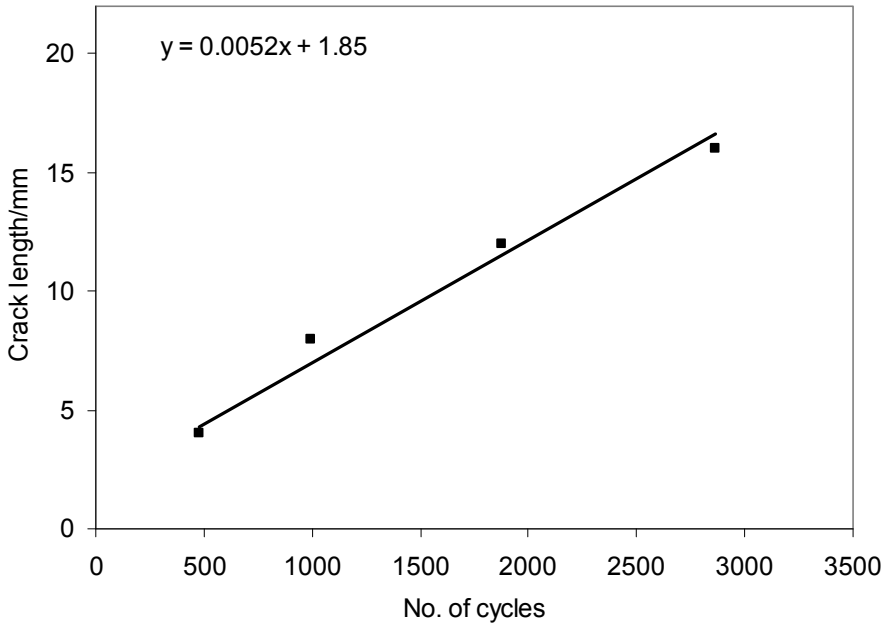

Figure 5.7(g) A plot of Crack length against No. of cycles for 9mm sinusoidal displacement amplitude at 70 ºC

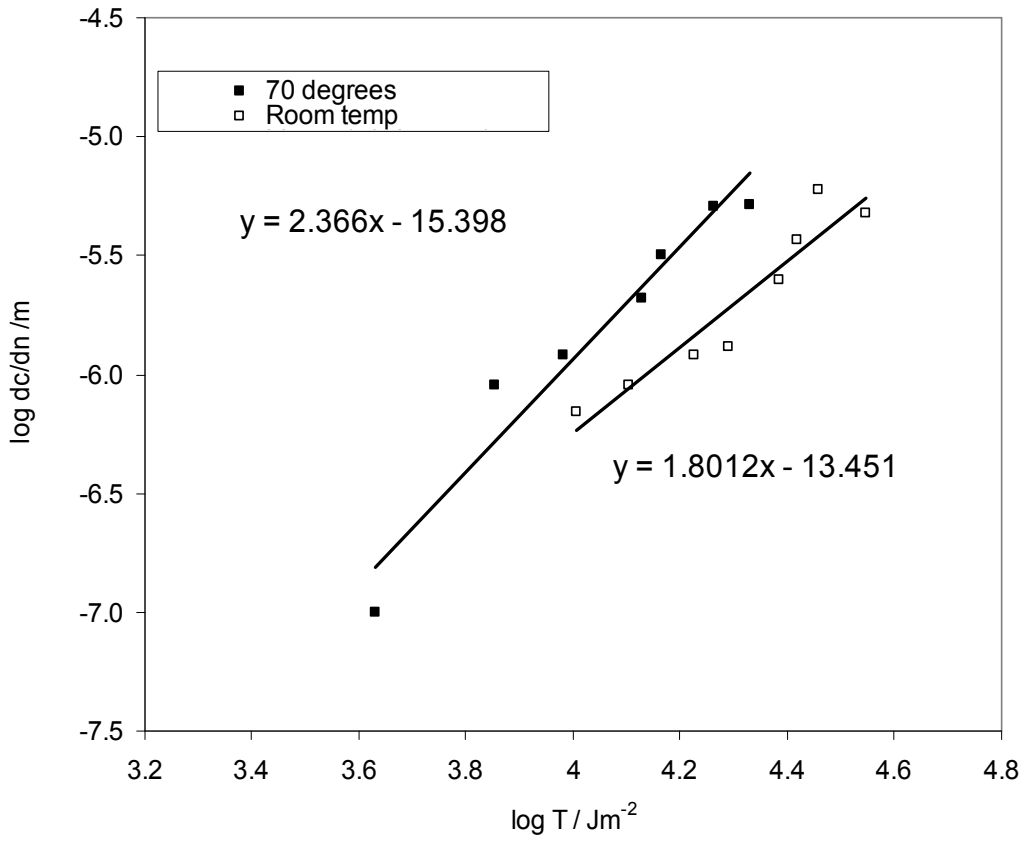

Figure 5.8 log dc/d*n* against log *T* for pure shear characterisation of NR 65 material at room temperature and 70 degrees Celsius.

5.2.4 **Experimental and predicted component force deflection behaviour in tension at room temperature and 70±1ºC**

Figures 5.9 and 5.10 show the results of experimental force deflection behaviour and FEA prediction of force deflection behaviour of the cylindrical component at room temperature and 70±1ºC respectively. The FEA prediction was determined using the Yeoh stored energy function characterised using the 1000th cycle test piece stress versus strain data obtained at room temperature (figure 5.2) and that at 70±1ºC (figure 5.4). In figure 5.9 there is good agreement between the experimental and predicted component force deflection behaviour until 25mm displacement above which the FEA prediction is somewhat greater than the experimentally measured force deflection curve. In figure 5.10, the agreement between the measured force deflection behaviour and the predicted force deflection behaviour is good until 20mm displacement, above which the predicted force deflection behaviour is again greater than the experimentally measured behaviour.

The observed discrepancies between the measured and FEA predicted component force deflection behaviour may be attributed, in part, to the slight difference in cross link density between the sheet material, from which the test piece stress strain curves were measured, and the bonded component material. In general, it is inherently difficult to achieve exactly the same amount of cross link density from batch to batch for cured elastomer materials. This picture is complicated by the fact that the experimental component force deflection response was determined after cyclically loading the component for 999 cycles at a maximum displacement at which the average strain energy density, in the component, was calculated to equal that obtained in the sheet test piece material stretched to 90% strain. The determination of maximum displacements, necessary in experiments, for softening of components and test pieces are at best estimates and not the exact required displacements, due to the use of average strain energy densities. The maximum average strain energy densities at which the bonded component and the sheet material stress strain test piece were softened are only of a similar order of magnitude. This difference in the maximum strain energy encountered in the component will also introduce a discrepancy between the measured and predicted component force deflection behaviour. The situation is further complicated at elevated temperatures; because the surrounding experimental temperature can be controlled reasonably well but the additional heat generated in the

bulk of the sample by the component during a test depends upon factors such as the rubber hysteresis and also the rate of heat lost during the test. Clearly this is going to be different between the bulky component and the much thinner test sheets. Considering these practical difficulties, it is evident from figures 5.9 and 5.10 that Yeoh stored energy function measured using the 1000th cycle at both temperatures give approximately the correct displacement and that it allows a sufficiently accurate measurement of the tearing energy to be made for this work.

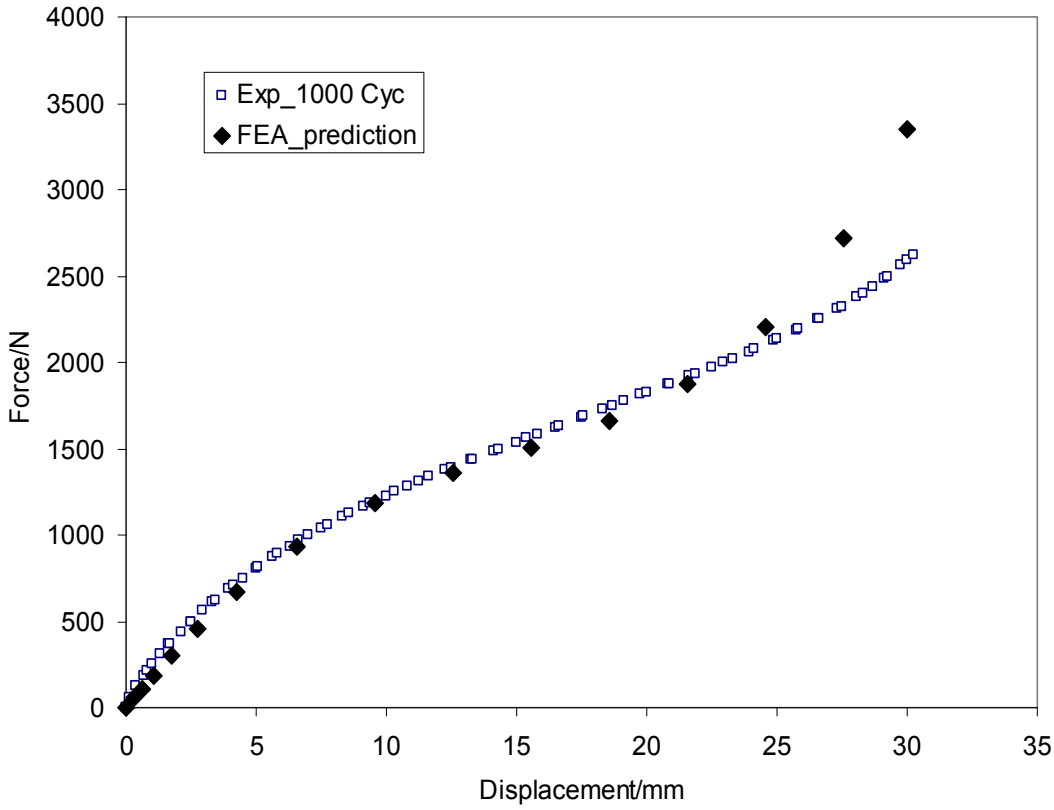

Figure 5.9 Experimental and predicted 1000th cycle force deflection behaviour of NR 65 phr elastomer material at room temperature

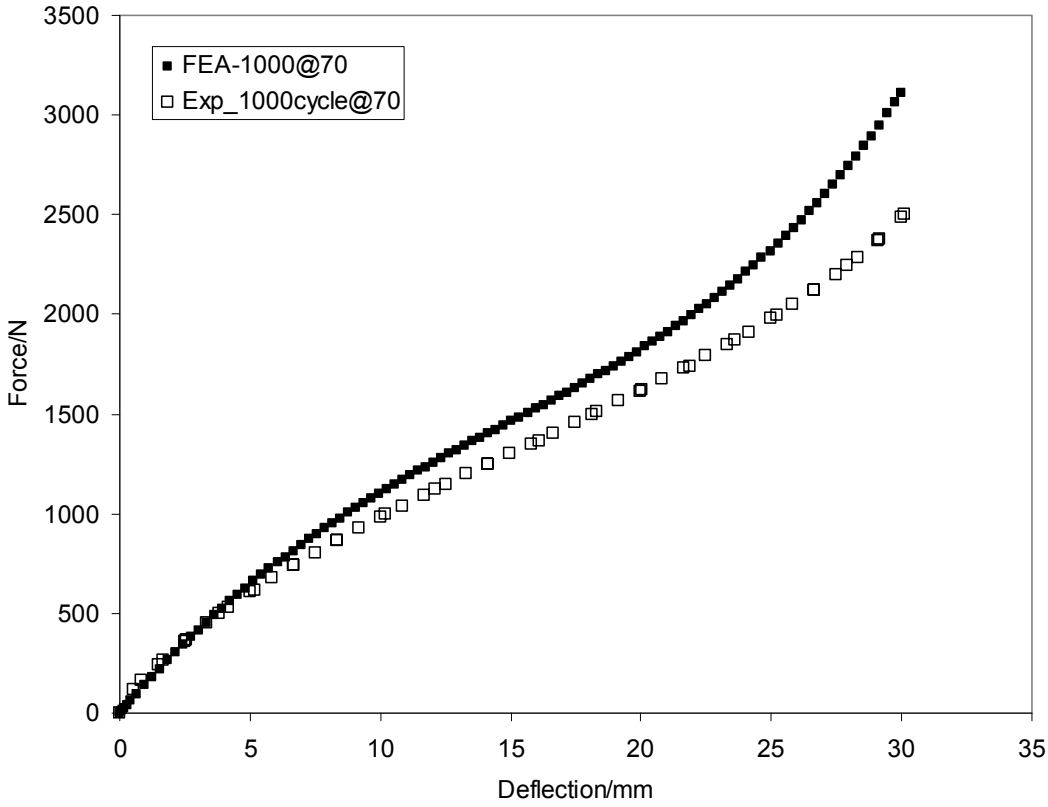

Figure 5.10 Experimental and predicted 1000th cycle force deflection behaviour of NR 65 phr elastomer material at 70 ºC

5.2.5 **Fatigue life prediction and experimental validation**

To predict the fatigue life of the bonded cylindrical component for a particular mode of loading and displacement amplitude, stored energy crack length relationship for that amplitude and mode of loading must first be determined using FEA techniques. To do this a series of models were made with a wide range of different crack lengths. The total stored energy in each model at a specific displacement was calculated using the finite element analysis techniques. A graph of the total energy in the model versus the crack length was created and the slope of the stored energy crack length curve at specific crack lengths determines the strain energy release rate crack length relationship for that displacement amplitude (Chapter 2, Eq.2-45). By combining the strain energy release rate crack length relationship with the respective power law relationship of figure 5.8 (Chapter 2, Eq.2-42), it is possible to derive a single functional relationship between the cyclic crack growth rate and the size of a crack in a component (Chapter 2,

Eq.2-46). This relationship can be inverted to form 1/(dc/dn) versus crack length. Integrating under 1/(dc/dn) versus crack length curve from an initial crack size c_0 to a final crack size c gives the number of cycles required to grow a crack between those limits and hence to predict the fatigue life if c is sufficiently large to cause a catastrophic failure.

In figures 5.11, 5.16, 5.22 and 5.27, stored energy crack length relationships for the bonded cylindrical component deformed in tension and shear at room temperature and 70±1ºC respectively are shown. FEA calculated strain energy release rate crack length relationship for tensile crack growth (figures 5.12 and 5.17) along the rubber-metal bond interface of the component show a general trend of increasing strain energy release rate with crack length for both room temperature crack growth and at 70±1ºC. This trend was also observed in the work of Busfield et al. (2005). Since an increasing strain energy release rate implies an increasing crack growth rate, the observed trend in tension suggests that the rate of crack growth at the rubber-metal bond interface increases with crack length in tension. On the contrary, the FEA calculated strain energy release rate crack length relationship for crack growth at the rubber-metal bond interface of the bonded component in shear (figures 5.23 and 5.28) initially increased through a maximum and then decreased. This suggests an initial increase in crack growth rate in shear to a peak value and a subsequent decrease in crack growth rate. This trend is observed for both room temperature and at 70±1ºC in shear. This phenomenon can be attributed to the cylindrical geometry of the bonded component studied in this work. In figures 5.13, 5.14, 5.15, 5.18, 5.19, 5.20, 5.21, 5.24, 5.25, 5.26, 5.29, 5.30 and 5.31 below plots of 1/(dc/dn) versus crack length for the respective test amplitudes and temperature conditions are presented.

Using the method discussed earlier, the number of cycles required to grow cracks at the rubber-metal bond edge of the elastomer component in tension and shear at both room temperature and 70±1ºC were calculated as N_p and compared with the experimentally measured number of fatigue cycles N_m in Table 5.1. It must be noted in table 5.1 that the value of c_0 in each calculation of N_p is an estimate of the initial average flaw size observed at the rubber-metal bond edge of the bonded component made as accurately as is practical using a careful visual inspection of the rubber-metal bond edge. The approach used here of estimating an initial average flaw size at the rubber-metal bond edge clearly does not take into consideration any local variations in the flaw size. The fatigue life predicted with the fracture mechanics approach generally

results in a fatigue life within a factor of 2 of the experimentally measured fatigue life cycles which is excellent especially when considering the extent that the predicted fatigue life depends on the initial size estimate of the flaw at the rubber-metal bond edge of the component. It is apparent in Table 5.1 that the method works well for the fatigue life predictions made at both room temperatures and 70ºC irrespective of the deformation mode.

5.2.6 **Predicted and measured component fatigue life in tension and shear at room temperature and 70 degrees Celsius**

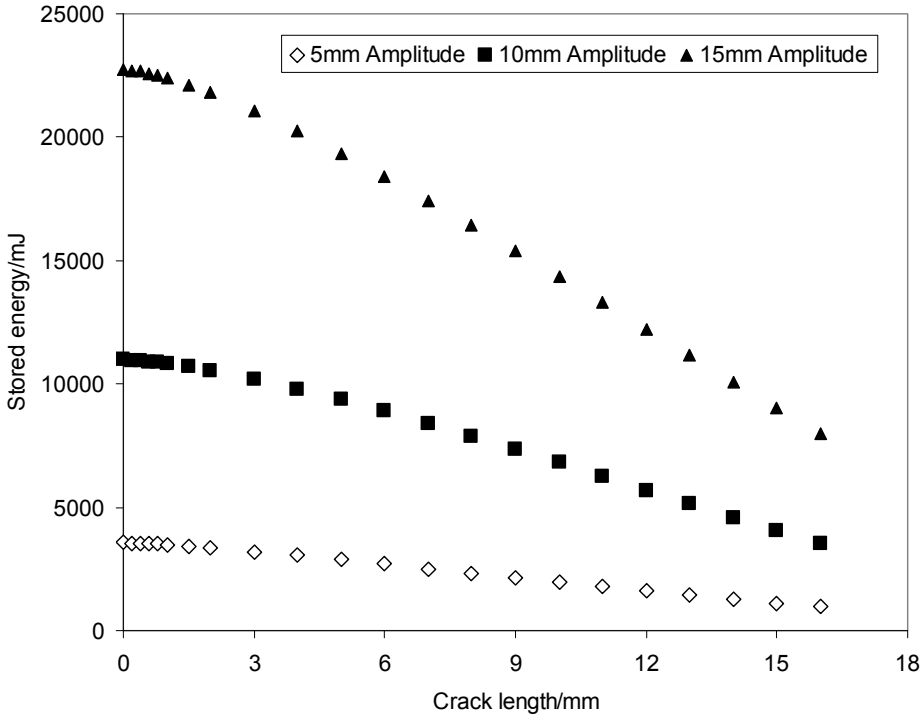

Figure 5.11 Stored energy against crack length for crack growth in tension at 5mm, 10mm and 15mm amplitudes respectively at room temperature

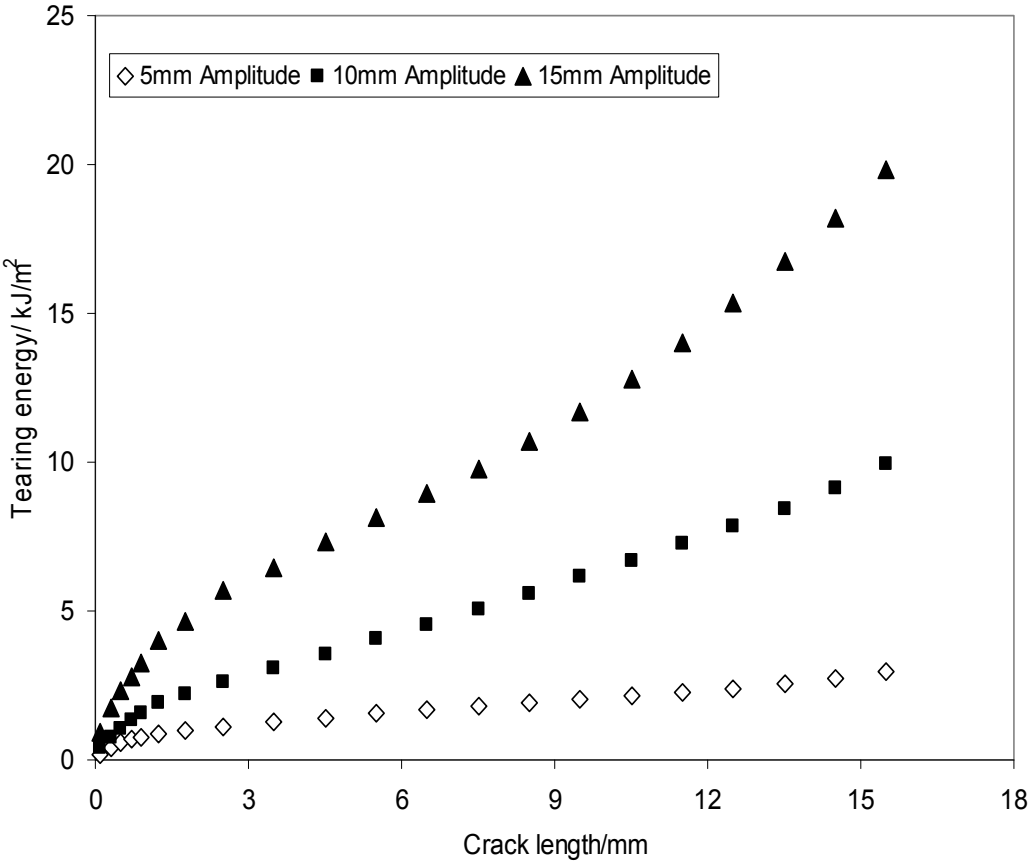

Figure 5.12 Tearing energy crack length relationship for crack growth in tension at 5mm, 10mm and 15mm amplitudes respectively at room temperature

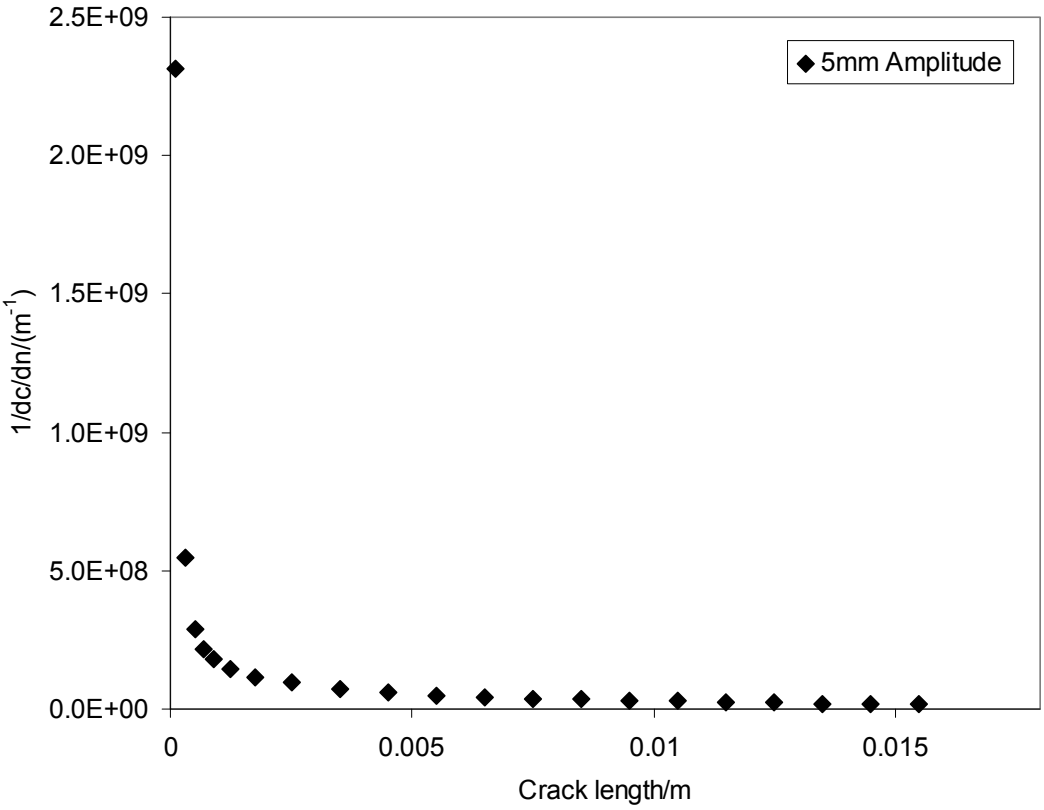

Figure 5.13 1/d*c*/d*n* versus crack length for crack growth in tension at 5mm amplitude at room temperature

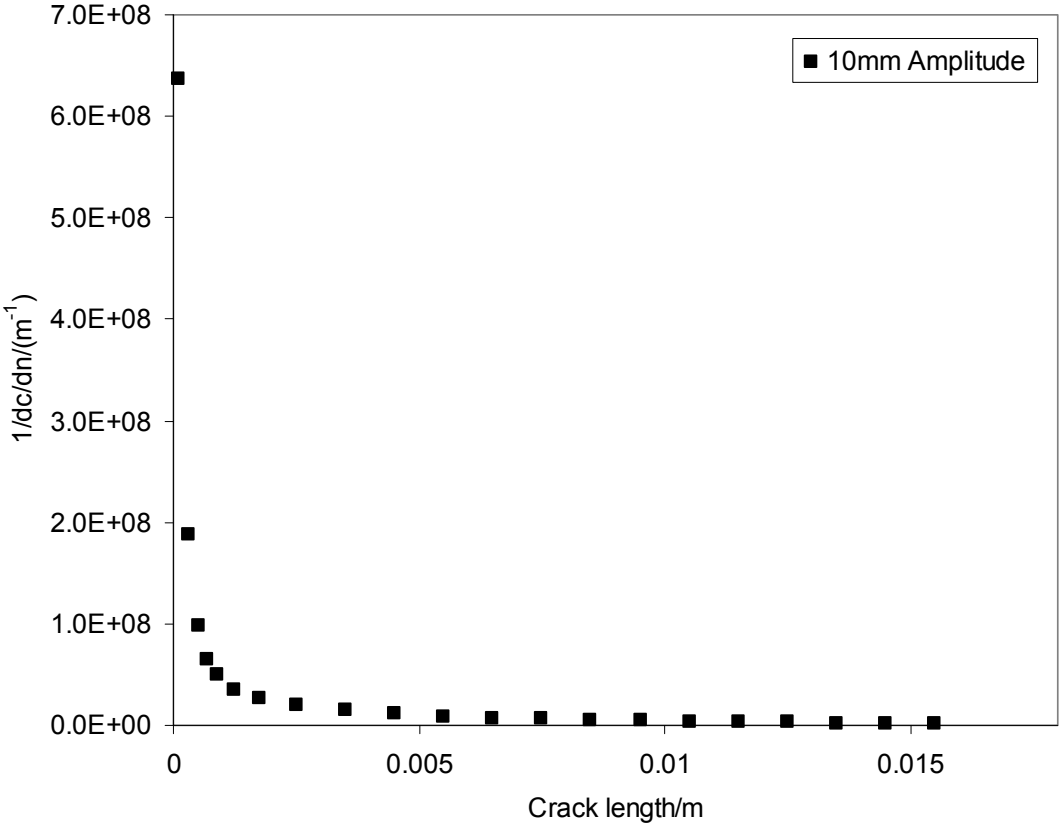

Figure 5.14 1/d*c*/d*n* vrs crack length for crack growth in tension at 10mm amplitude at room temperature

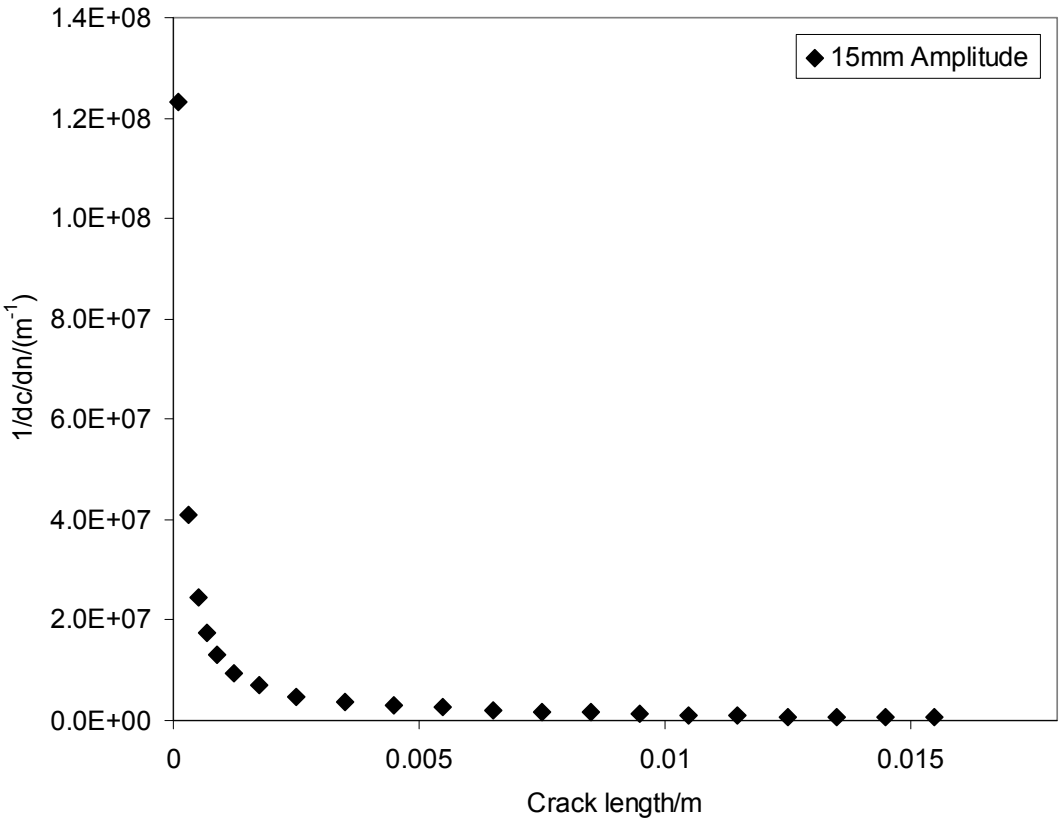

Figure 5.15 1/d*c*/d*n* vrs crack length for crack growth in tension at 15mm amplitude at room temperature

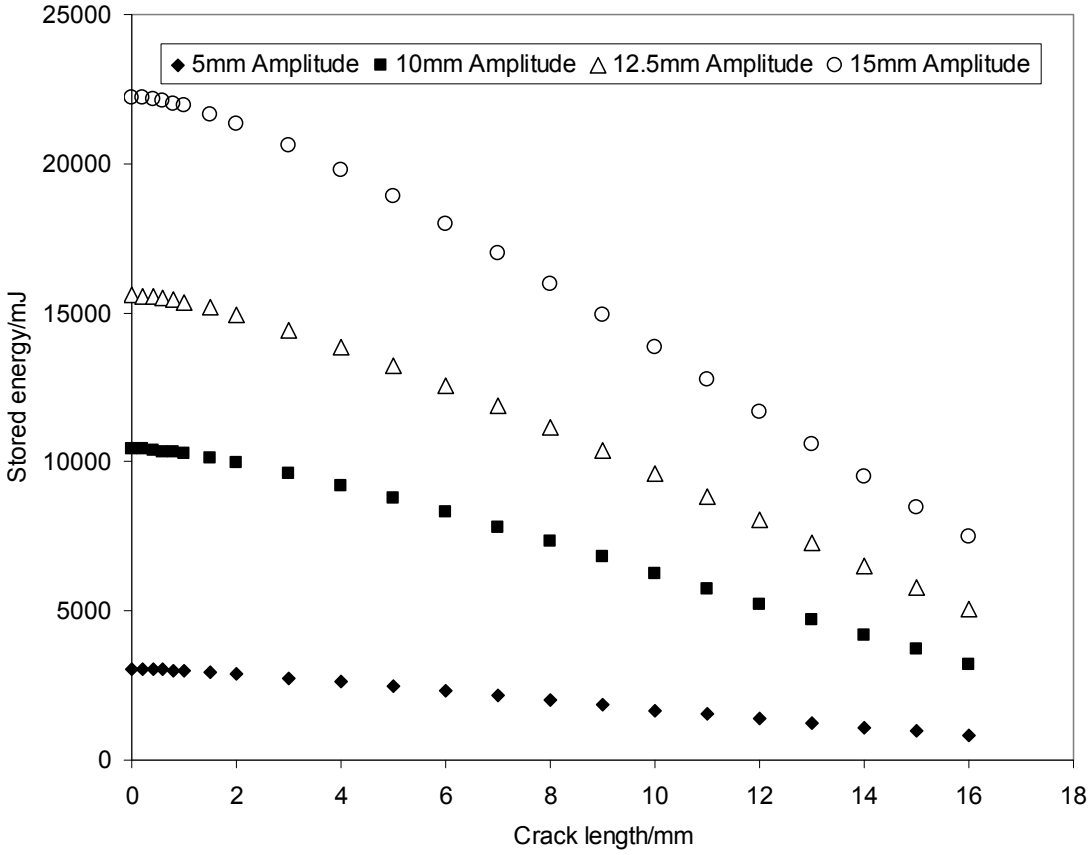

Figure 5.16 Stored energy against crack length for component crack growth in tension at 70 degrees Celsius

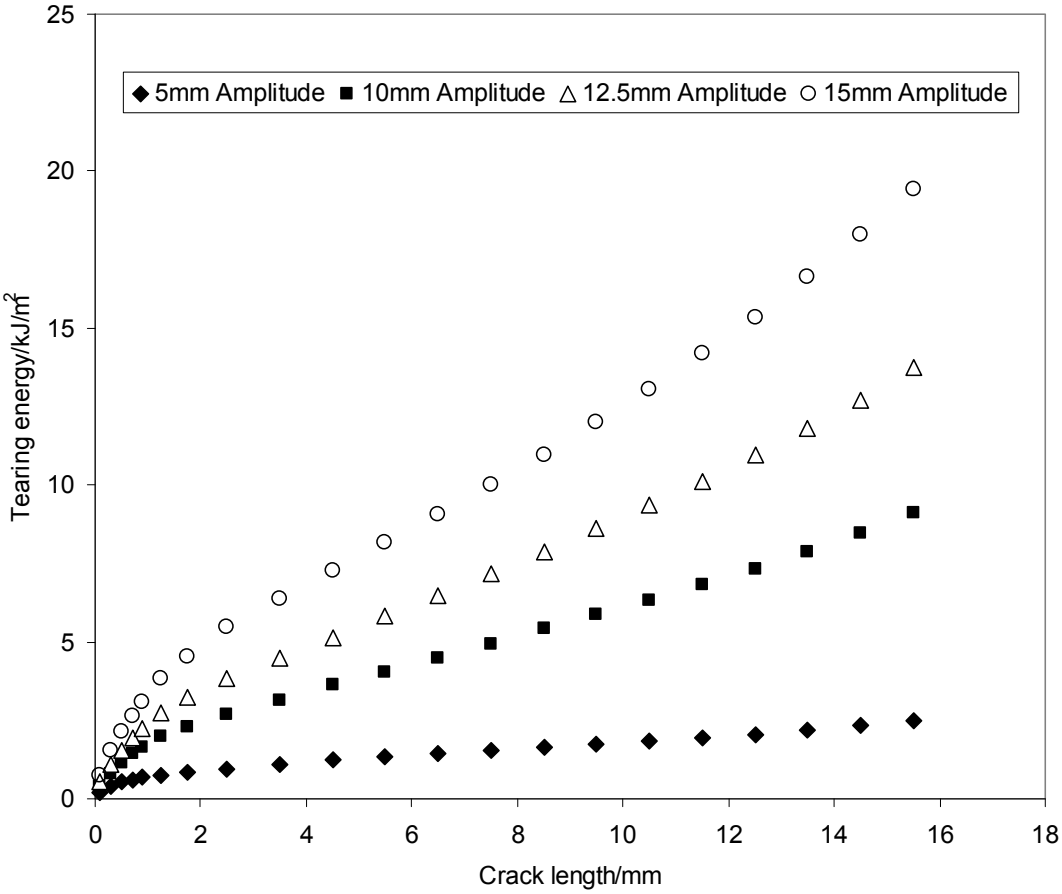

Figure 5.17 Tearing energy against crack length for component crack growth in tension and at 70 degrees Celsius

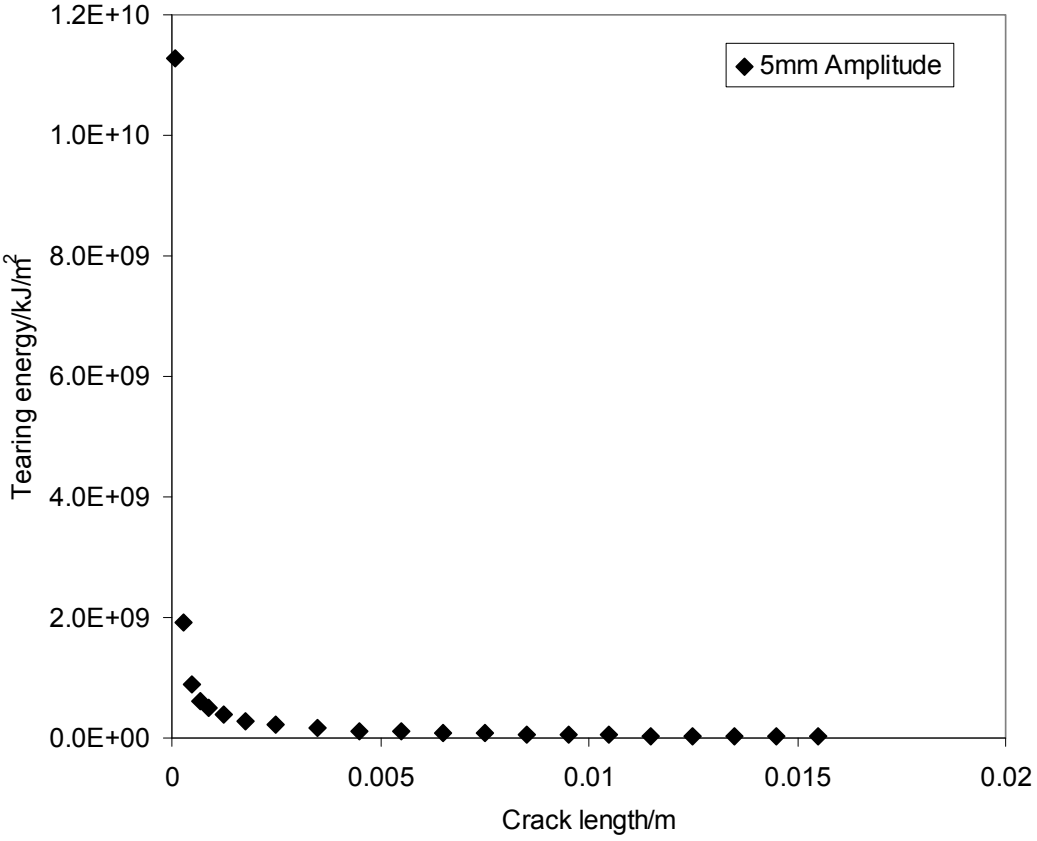

Figure 5.18 1/d*c*/d*n* vrs crack length for crack growth in tension at 5mm amplitude at 70ºC

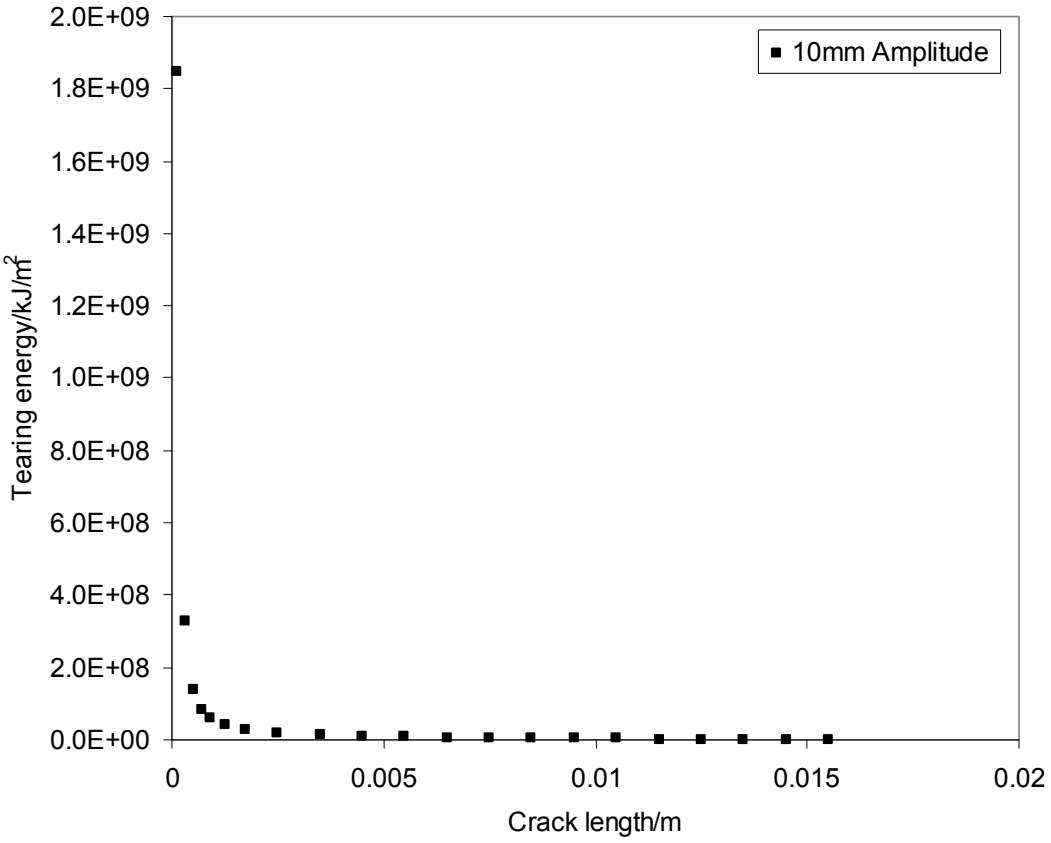

Figure 5.19 1/d*c*/d*n* vrs crack length for crack growth in tension at 10mm amplitude at 70ºC

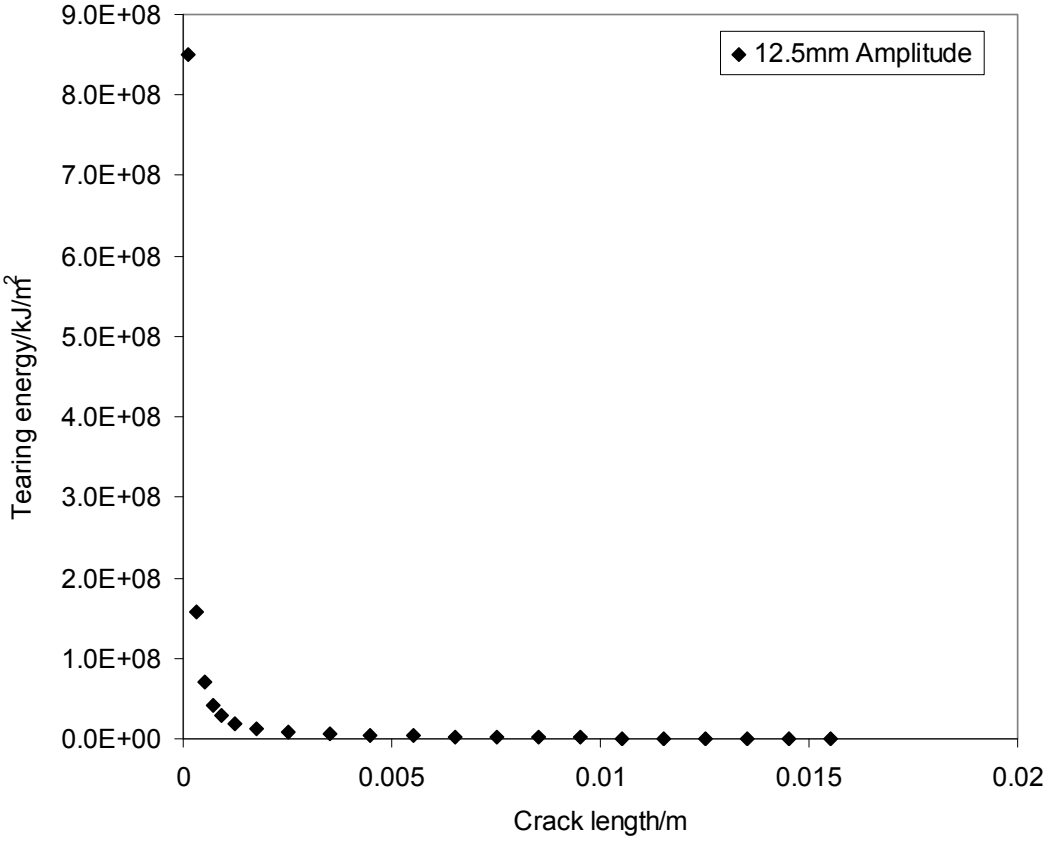

Figure 5.20 1/d*c*/d*n* vrs crack length for crack growth in tension at 12.5mm amplitude at 70ºC

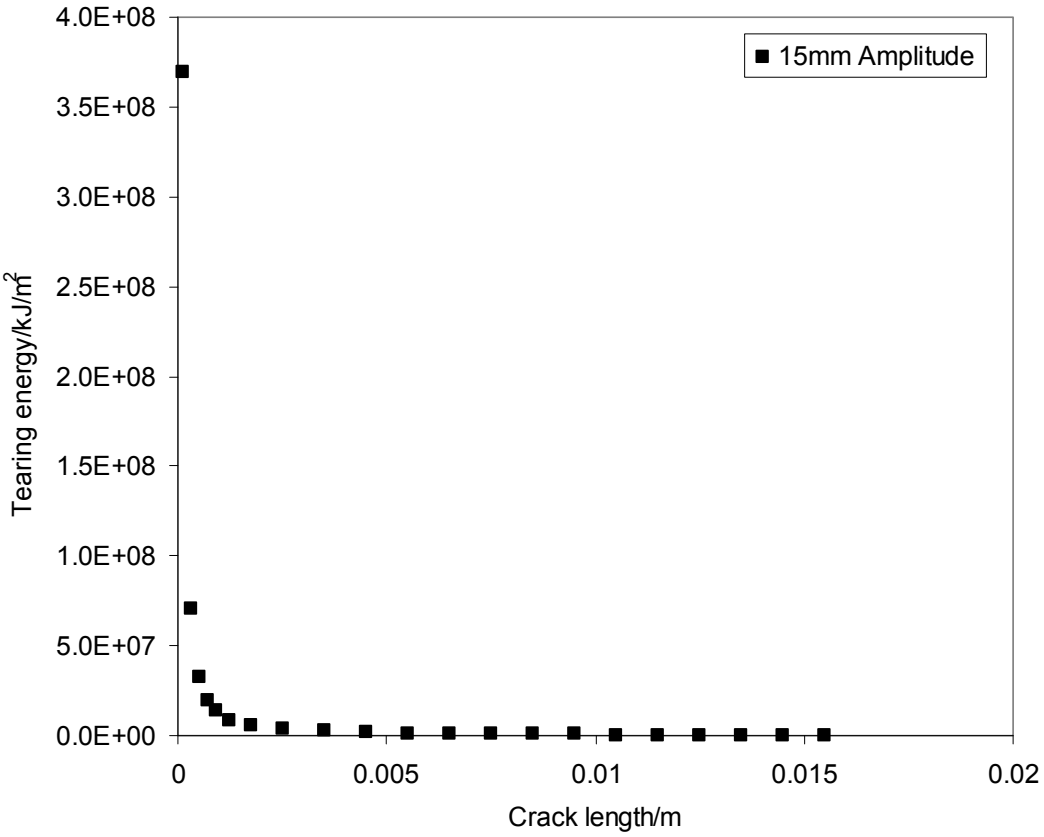

Figure 5.21 1/d*c*/d*n* vrs crack length for crack growth in tension at 15mm amplitude at 70ºC

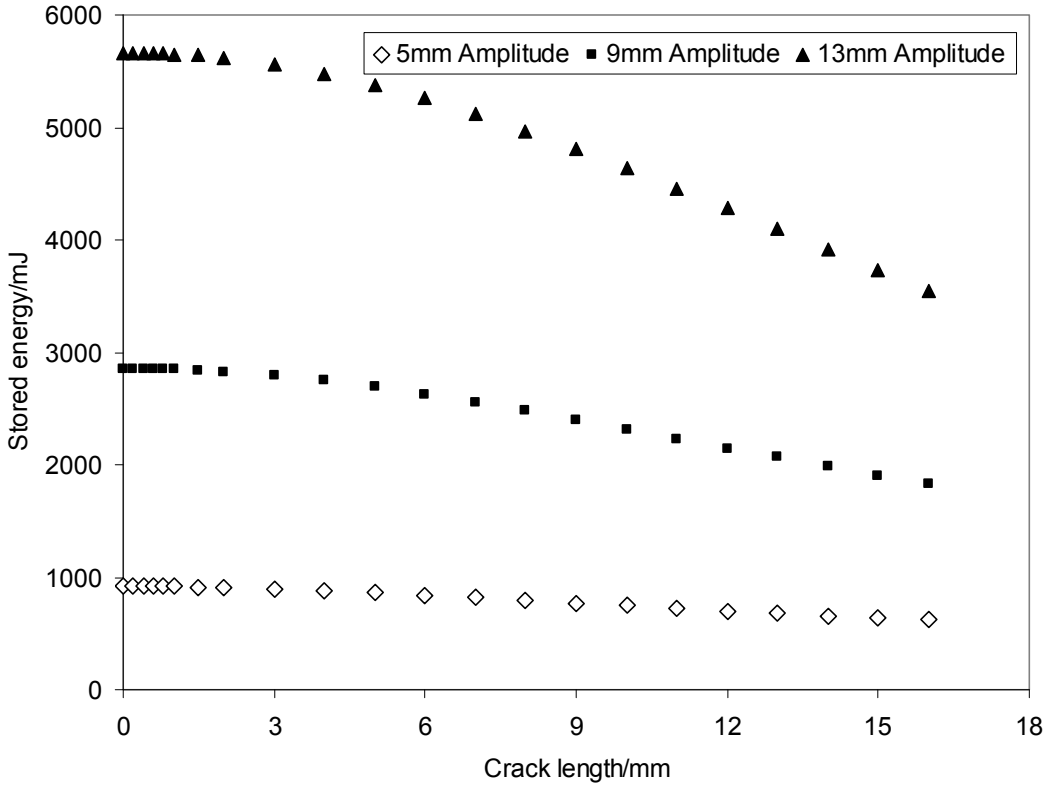

Figure 5.22 Stored energy crack length relationship for shear crack growth at 5mm, 9mm and 13mm amplitudes respectively at room temperature

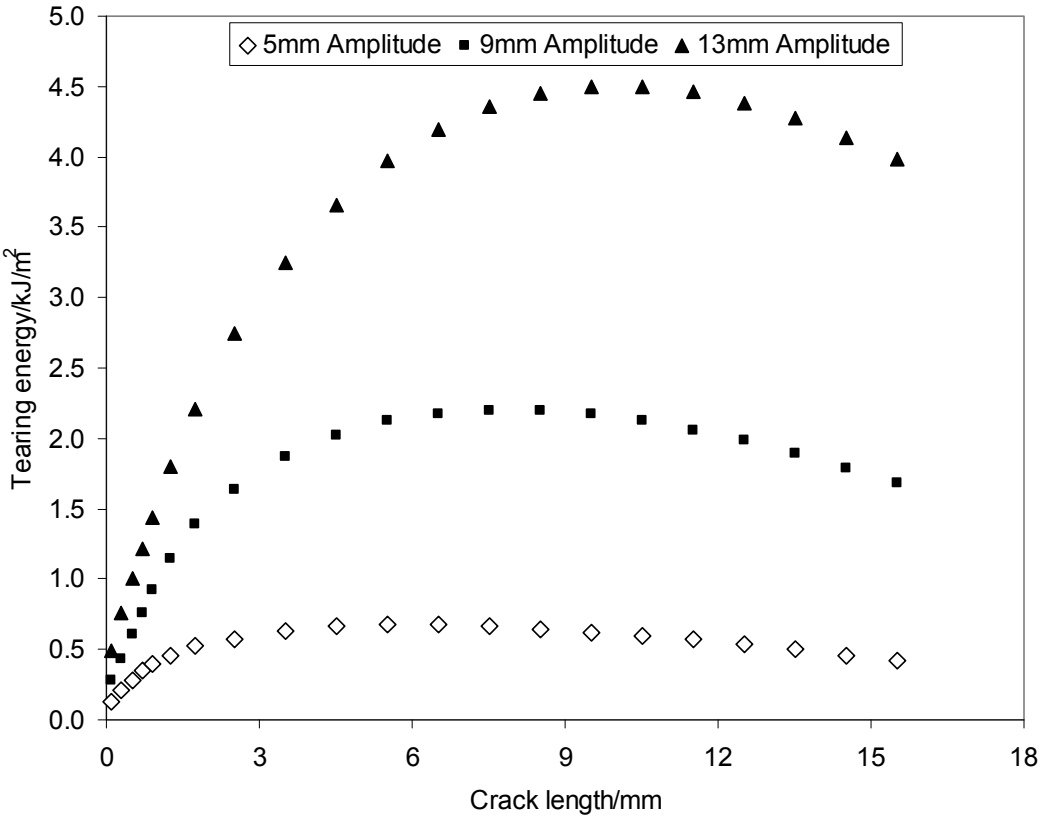

Figure 5.23 Tearing energy crack length relationship for shear crack growth at 5mm, 9mm and 13mm amplitudes respectively at room temperature

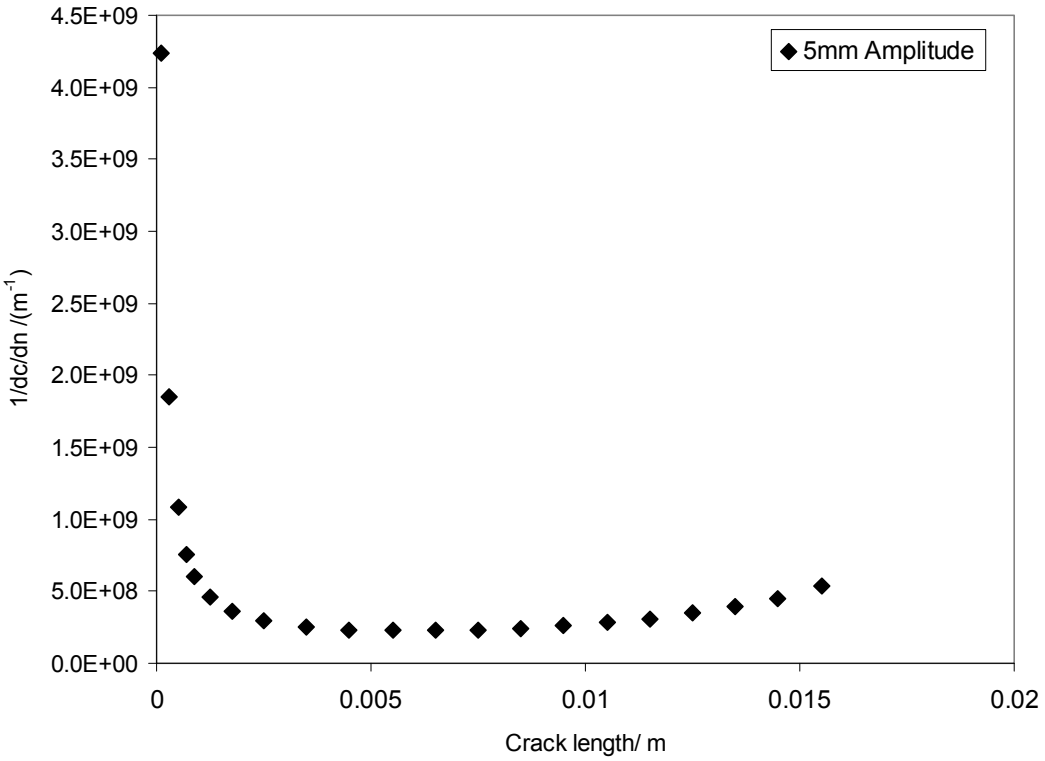

Figure 5.24 1/d*c*/d*n* against crack length for shear crack growth at 5mm amplitude at room temperature

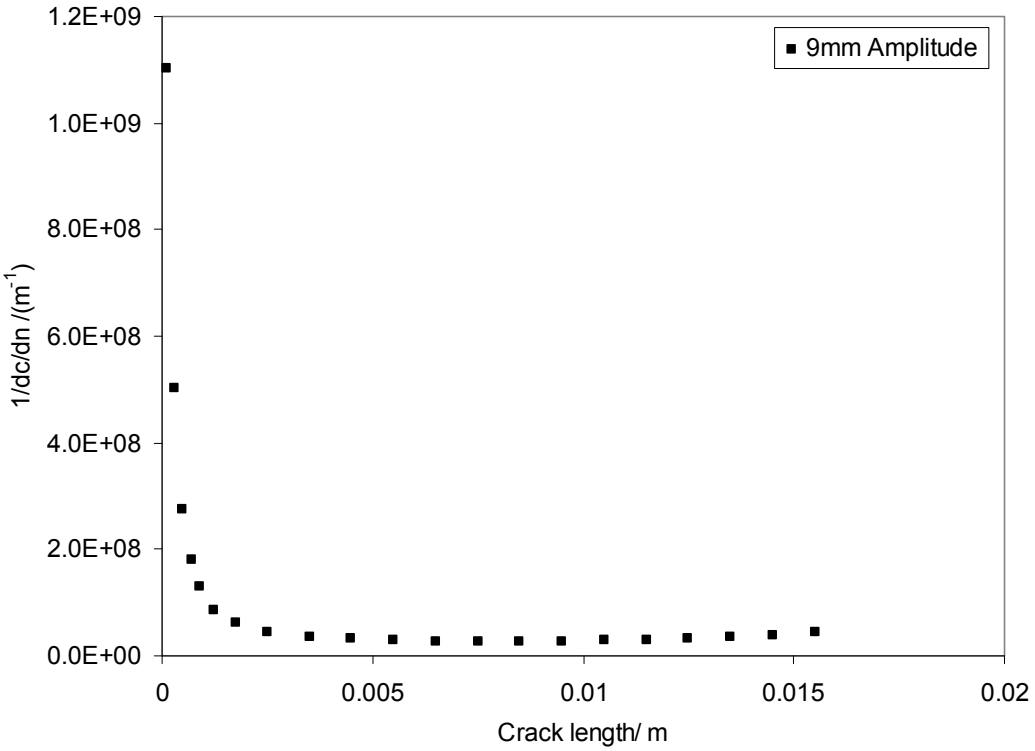

Figure 5.25 1/d*c*/d*n* against crack length for shear crack growth at 9mm amplitude at room temperature

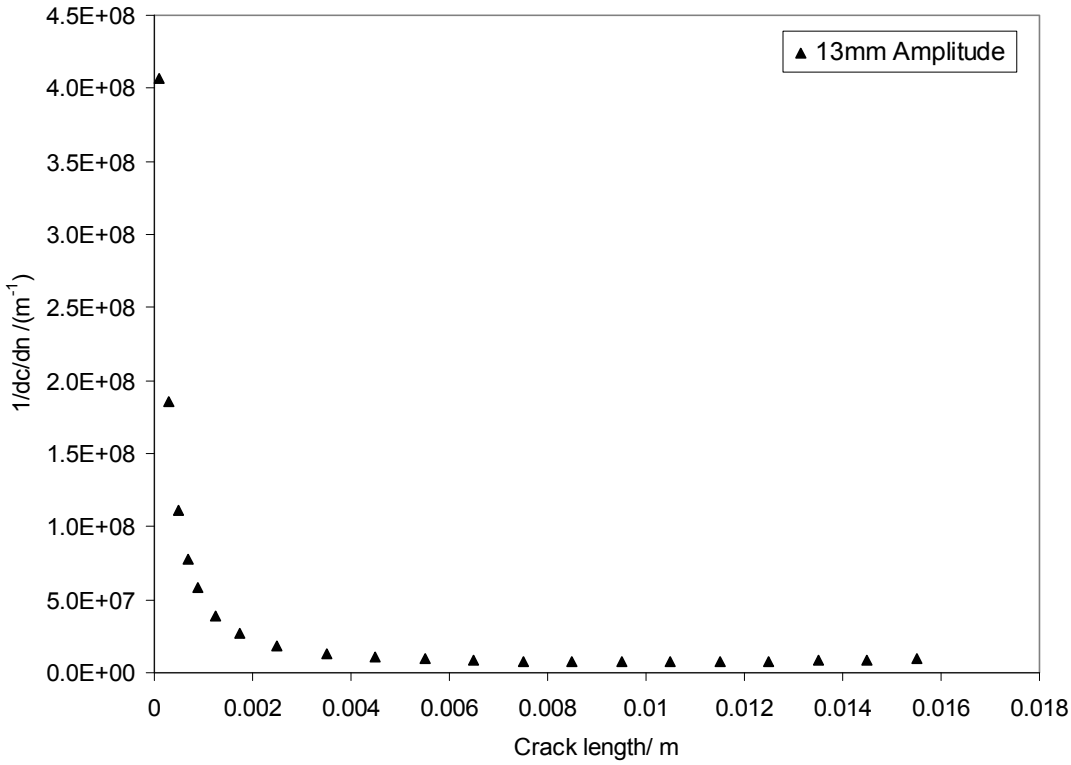

Figure 5.26 1/d*c*/d*n* against crack length for shear crack growth at 13mm amplitude at room temperature

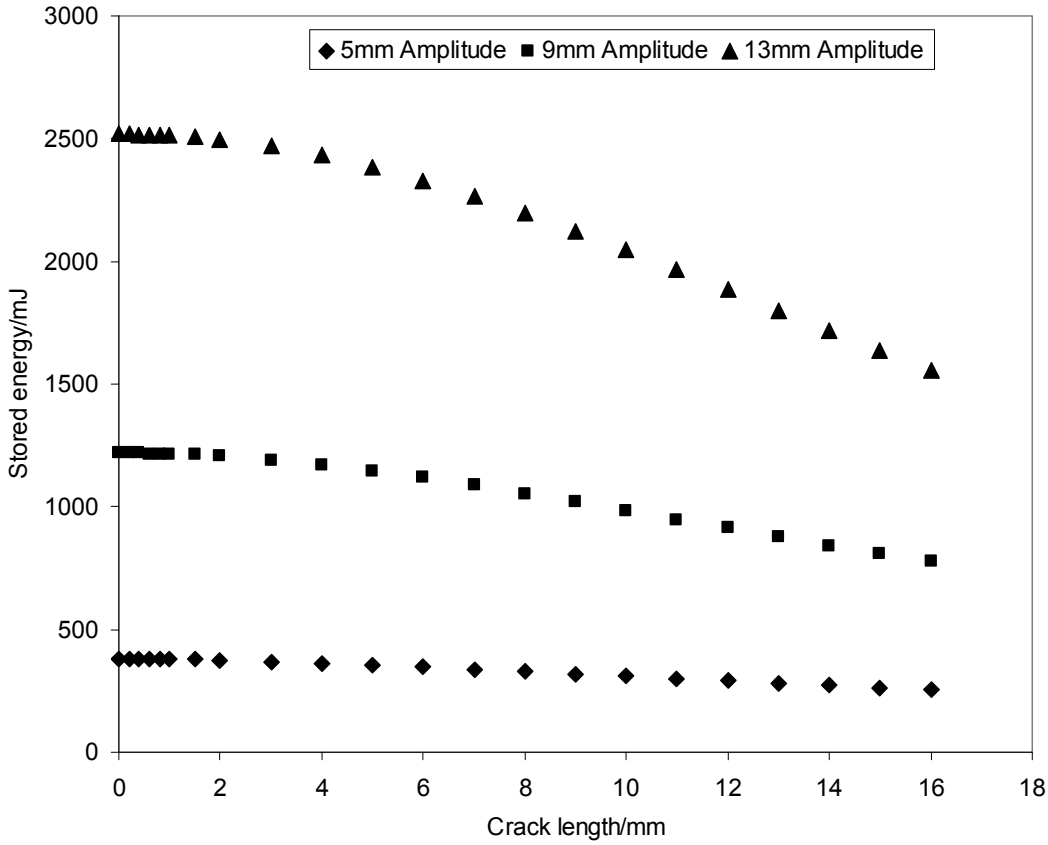

Figure 5.27 Stored energy crack length relationship for shear crack growth at 5mm, 9mm and 13mm amplitudes respectively at 70ºC

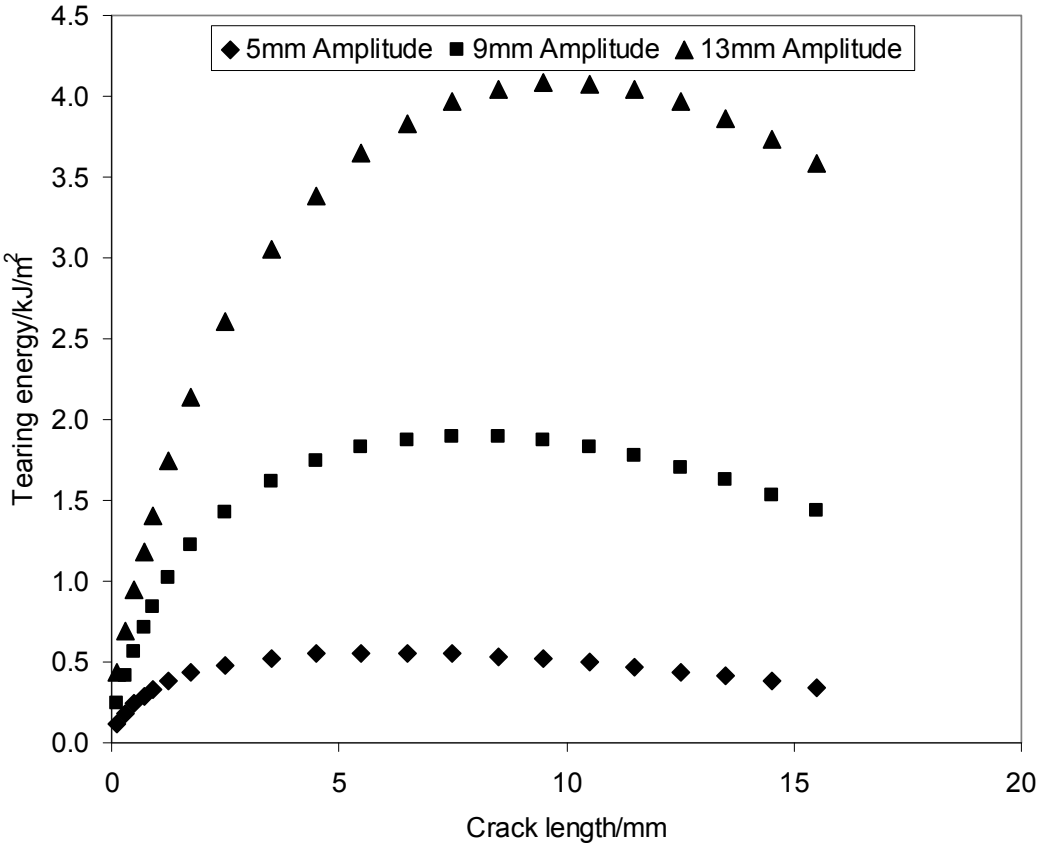

Figure 5.28 Tearing energy crack length relationship for shear crack growth at 5mm, 9mm and 13mm amplitudes respectively at 70ºC

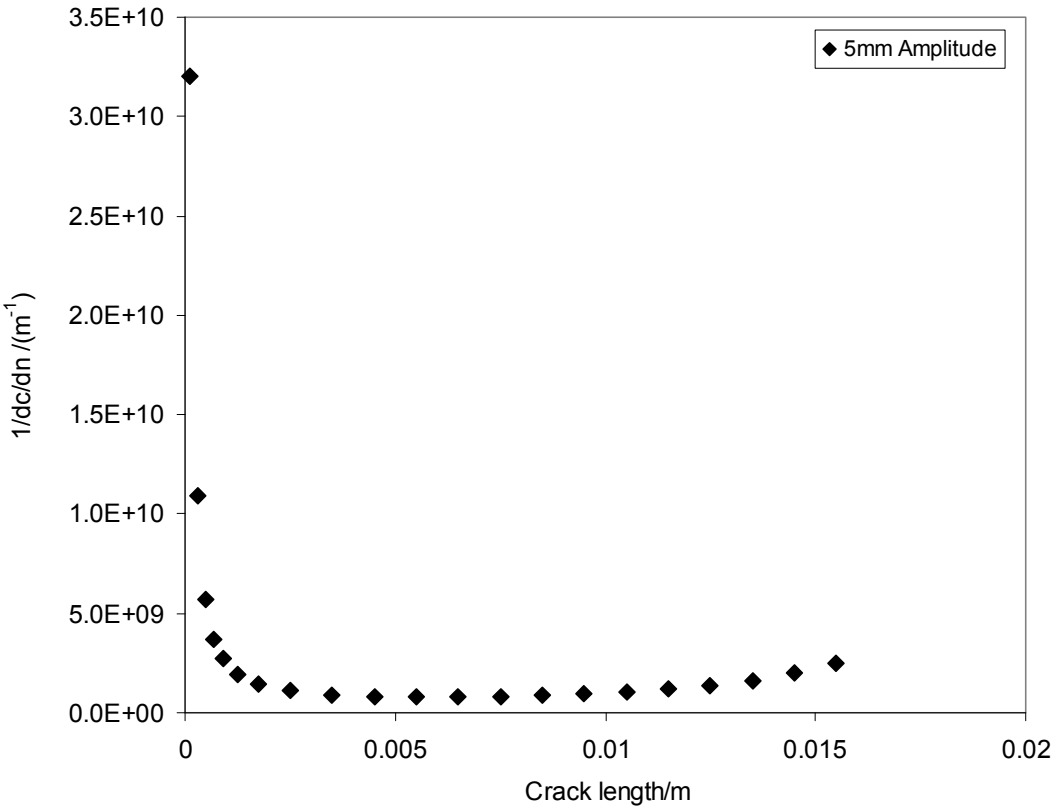

Figure 5.29 1/d*c*/d*n* against crack length for shear crack growth at 5mm amplitude at 70ºC

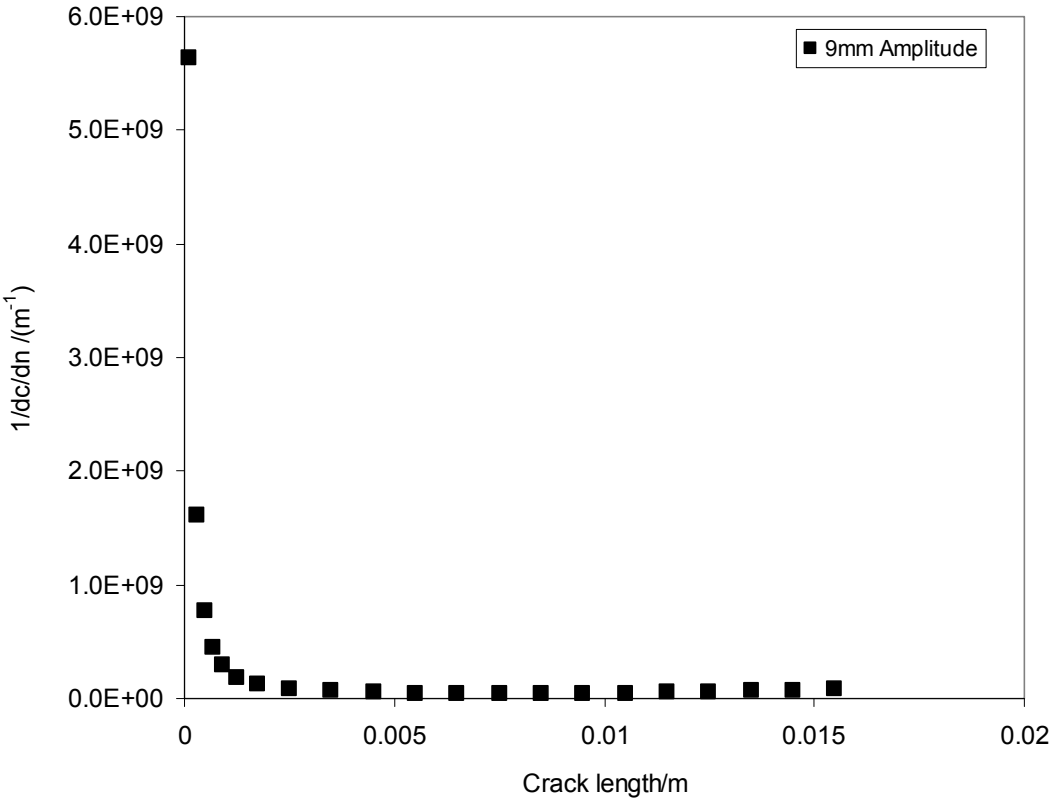

Figure 5.30 1/d*c*/d*n* against crack length for shear crack growth at 9mm amplitude at 70ºC

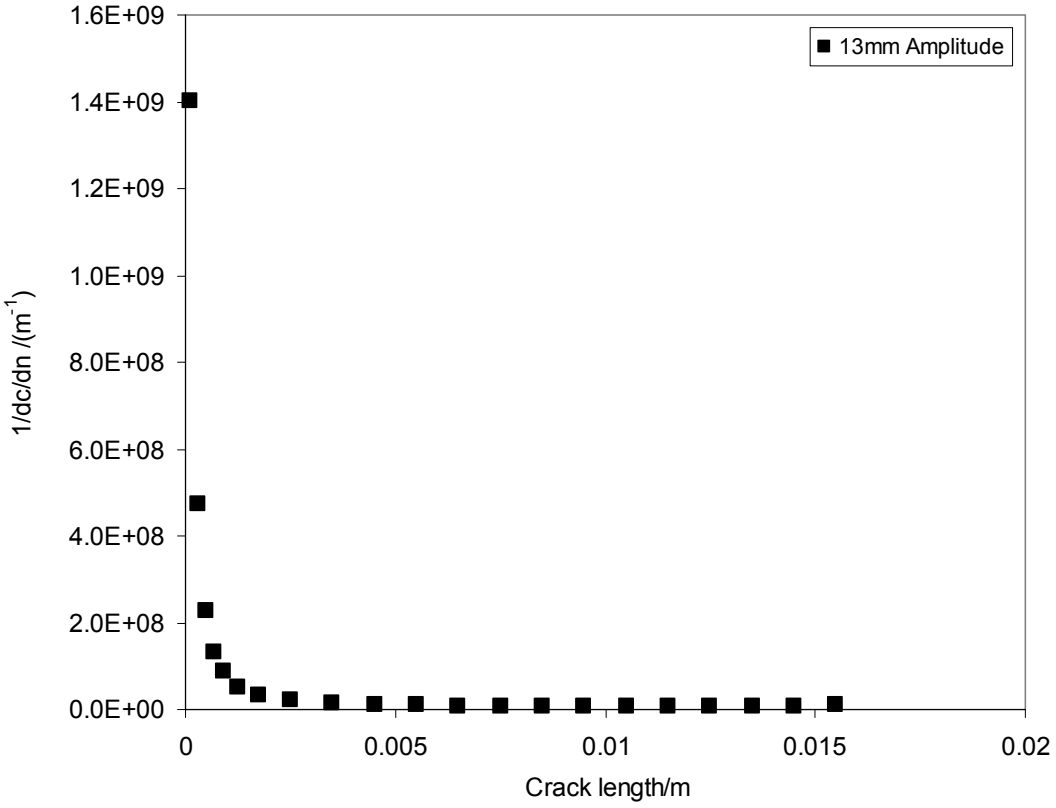

Figure 5.31 1/d*c*/d*n* against crack length for shear crack growth at 13mm amplitude at 70ºC

Table 5.1 Predicted and measured numbers of fatigue cycles required to grow cracks from estimated rubber–metal bond edge flaw size until specified crack size just before failure

Maximum Displacement/mm	Temperature/ºC	Tension Or Shear	Range of crack Lengths/mm	Measured No. of cycles N_m	Predicted No. of cycles N_p	N_p/ N_m
5.0	23	Tension	0.5-4	723 937	441 145	0.61
10.0	23	Tension	0.9-10	64 524	116 912	1.81
15.0	23	Tension	0.5-8	63 494	36 366	0.57
10.0	70	Tension	0.5-15	163 988	155 454	0.95
15.0	70	Tension	0.9-11	24 047	22 131	0.92
9.0	23	Shear	0.5-9	357 009	406 145	1.14
13.0	23	Shear	0.5-10	168 093	160 189	0.95
13.0	70	Shear	0.5-7	418 130	182 320	0.44

5.3 **Conclusion**

The fracture mechanics approach to fatigue life prediction of engineering components has been validated using a bonded cylindrical engineering elastomer component for fatigue crack growth within the 'power law' region of crack growth behaviour. The cylindrical geometry of the engineering elastomer component induced rubber-metal bond interface crack growth for both tensile and shear fatigue loading. The fatigue crack growth behaviour was successfully predicted for crack growth at both room temperature and 70±1ºC to within a factor of 2 for the bonded cylindrical component. For the first time, the cyclic stress softening associated with fatigue of filled elastomer materials was quantitatively accounted for by softening the dumbbell specimens for the stress strain characterisation and subsequent FEA strain energy calculations at a strain level deduced following the average strain energy density approach. The effect of temperature on the fatigue life of the cylindrical component was also well accounted for by the approach of characterising the material stress versus strain and the fatigue crack growth behaviour at the elevated test temperature. Considering the poor reproducibility of fatigue life predictions in previous work, the accuracy of the fracture mechanics approach method to predict the fatigue crack growth rate with an accuracy of 2 for the fatigue life at both room temperature and 70±1ºC is excellent.

CHAPTER SIX

6.0 Crack Bifurcation in a Pure Shear Test Piece

6.1 Introduction

The study of fatigue crack surfaces has been the subject of scientific research for many decades. In many cases fatigue crack surfaces have been observed to be rough. The roughness associated with fatigue crack surfaces is prominent when one considers the surface morphology of a sharp razor cut to that obtained after the crack has grown to steady state rate in an elastomer material. Papadopoulos (2008) reviews this phenomenon in a work which investigates rate transitions in fatigue crack growth in elastomers. The rough fatigue crack surface is, in part, thought to be the result of fatigue crack splitting during fatigue crack growth. Thomas (1958) in an explanation of the transition from sharp razor cut crack tip to a rough steady state crack tip suggested the rough crack tip to consist of multiple sharp crack tips. The study of fracture surfaces in elastomer materials is usually qualitative because no single technique can readily describe all the features present or can accurately describe the fracture surface structure. Fukahori and Andrews (1978) studied 2D fracture surface microscopic images by counting the number of steps crossing a reference line and weighted these according to their apparent depth. They differentiated the degrees of roughness by assuming that the broader the step lines, the deeper the steps, with the deeper steps casting a greater shadow. The technique gives an indication of the roughness at various parts of the fracture surfaces but; it would be challenging to differentiate small variations in depth. They observed fracture surface roughness in rubber at various values of strain energy release rate (tearing energy) under steady tearing and noted that there is a direct relation between the rate of propagation and the nature of the crack tip. They reported a general observation that increased crack growth rate due to an increase in the strain energy release rate results in smoother elastomer fracture surfaces. Gent and Pulford (1984) used a similar method to measure the distance between steps of the surface texture of 2D images. They attributed the variation in roughness to the joining of secondary cracks originating from flaws and filler particles. Furthermore, they observed that for the more tear resistant materials the height of the steps was greater. Quantitative analysis of fracture surface roughness is not a simple task since there is no

widely accepted parameter. Although there is general agreement that fatigue crack surfaces become rough with crack growth and that the extent of roughness is linked to the strain energy release rate associated with the crack growth, there is no agreement as yet on the mechanisms responsible for the creation of the rough fracture surfaces.

Gent et al. (2003), in a work to investigate why cracks turn sideways considered a rubber sheet with a small edge crack subjected to a far-field simple extension. They calculated the strain energy release rate for crack growth in both forwards and sideways directions. They observed that when the imposed extension is large, the strain energy release rate at which a small sideways crack will initiate is found to be about 60% of that for forwards crack growth for their specific material. It is clear therefore that for a crack to follow what appears at first sight to be a less energetically favourable pathway something else must be taking place. Cracks split or bifurcate due to extensive strain induced anisotropy particularly at the tip of the crack (Busfield et. al, 1997). This anisotropy results from the extensive local strain in the crack tip region and the potential for some materials such as NR to experience the onset of strain induced crystallisation. In effect it becomes easier for the crack to grow at right angles to the applied strain field as this still releases energy, albeit of a lesser amount than in the straight forward direction, because the material is much weaker in that direction. Cracks that form like this can now follow multiple pathways. Each individually shares some of the strain energy release rate from the initial single crack and so the crack growth rate slows down. The key concern now becomes which pathway is followed and how far apart do the two cracks have to grow apart for one to accelerate and become a dominant single crack tip.

It is beyond the scope of this thesis to consider the complications associated with modelling strain induced anisotropy. So the task of understanding why cracks deviate is not considered in detail. The somewhat simpler initial task is tackled which considers how far an already bifurcated crack has to grow, as clearly, understanding something about this distance helps understand the extent of the surface roughness of a fatigue fractured component. To do this, simple finite element analysis models that ignore any significant anisotropy in the strength at the crack tip were made. These models were used to model how the strain energy release rate associated with growth of split fatigue cracks compare, with the strain energy release rate of a single straight crack propagating along the central horizontal plane, in a typical filled Natural Rubber pure shear crack growth specimen, at the same strain. The objective of this study being

to investigate the effect of fatigue crack bifurcation on the generation of fatigue crack surface roughness by examining the behaviour of the characteristic strain energy release rates as cracks extend from an already split fatigue crack profile.

6.2 Results and discussion

In figure 6.1, a schematic of a pure shear specimen with a crack c splitting into two cracks c_1 and c_2 is shown. To model a crack into a finite element mesh, nodes along the direction of crack growth are released. Figure 6.2 shows typical finite element mesh for a pure shear crack growth specimen model with split cracks. The crack is modeled over a wide range of lengths by releasing the connection between nodes along a predetermined crack growth pathway. With each node release, provided the external boundaries do not move, the total stored energy in the model decreases.

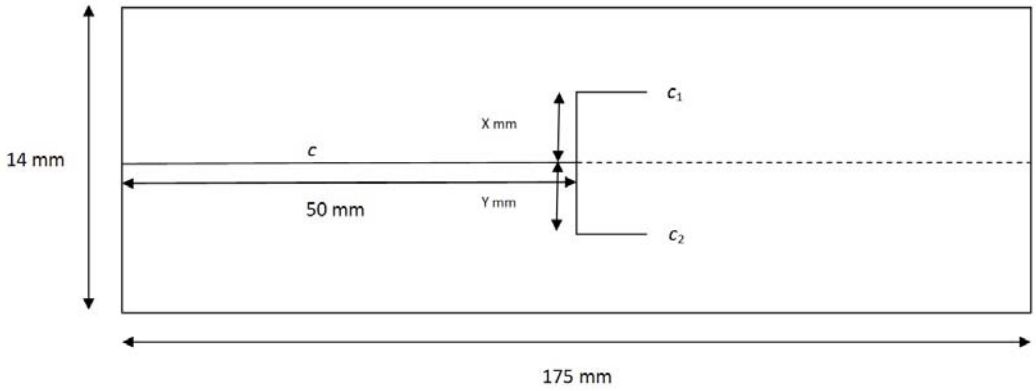

Figure 6.1 A schematic of a pure shear specimen with a crack (c) splitting into two cracks c_1 and c_2: Both c_1 and c_2 are parallel to the horizontal centre-line of the specimen

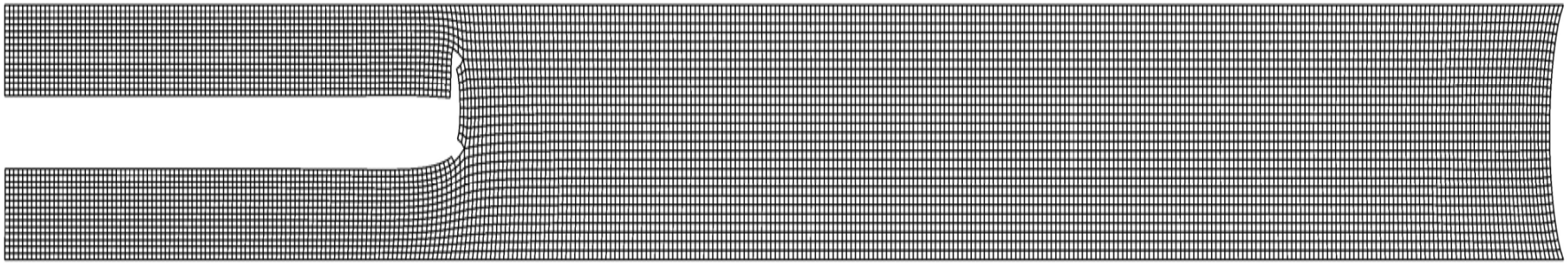

(a)

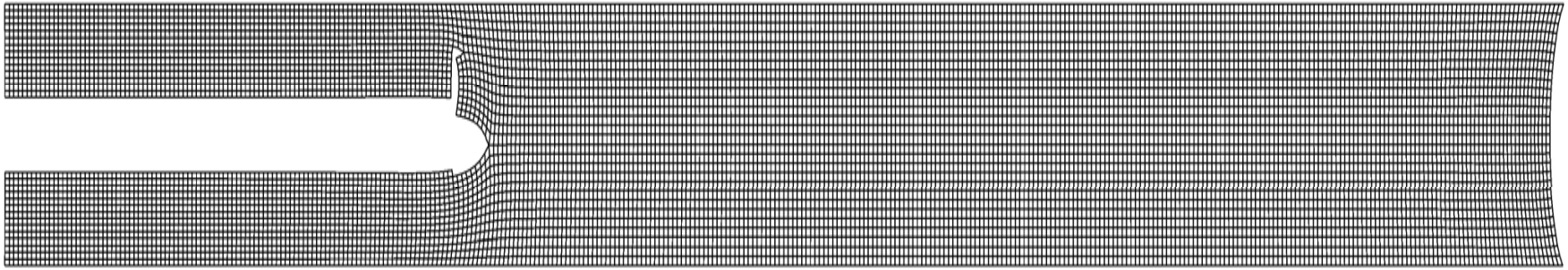

(b)

Figure 6.2 Deformed finite element meshes of a pure shear specimen showing split parallel cracks c_1 and c_2 with equal lengths (a) and, split crack c_2 extended keeping the initial length of split crack c_1 constant (b)

Figure 6.3 shows a typical curve of the total stored energy versus crack length relationship for a split crack (c_2) growing in a pure shear specimen at a global 20% strain.

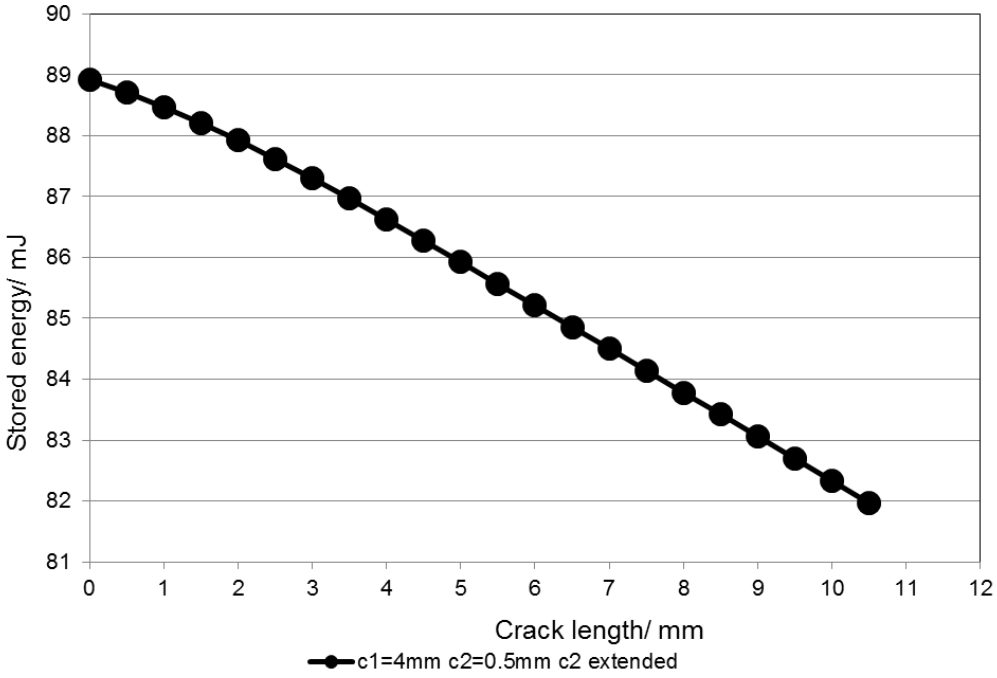

Figure 6.3 Stored energy crack length relationship for a split crack (c_2) growing in a pure shear specimen at 20% strain and, 0.5 mm measured vertical distance (y mm) from the horizontal centre-line of the specimen

Since all the finite element models in this work have 1 mm thickness dimension, and therefore one crack surface area has the same numerical value as the crack length, the negative of the slope (chapter 3, equation 3-4) at a specific crack length along the stored energy crack length curve gives the strain energy release rate at that crack length. In figure 6.4, the strain energy release rate of a single crack growing in a pure shear specimen at 20% strain and that of a split crack (c_2) growing at 20% strain are shown. Figure 6.4 shows that the strain energy release rate of a single crack growing in a pure shear specimen is constant. For the filled NR material used in this work, at 20% strain, the strain energy release rate for a single crack growing through the pure shear specimen was calculated to be 0.725 kJ/m^2.On the other hand, the strain energy release rate associated with growth of split crack c_2 whiles keeping c_1 constant, in figure 6.4,

varies. Initially the energy is uniformly distributed over the two cracks, as one of the cracks, c_2, is extended the strain energy release rate of 0.413 kJ/m^2 was calculated at a crack length of 0.25 mm.

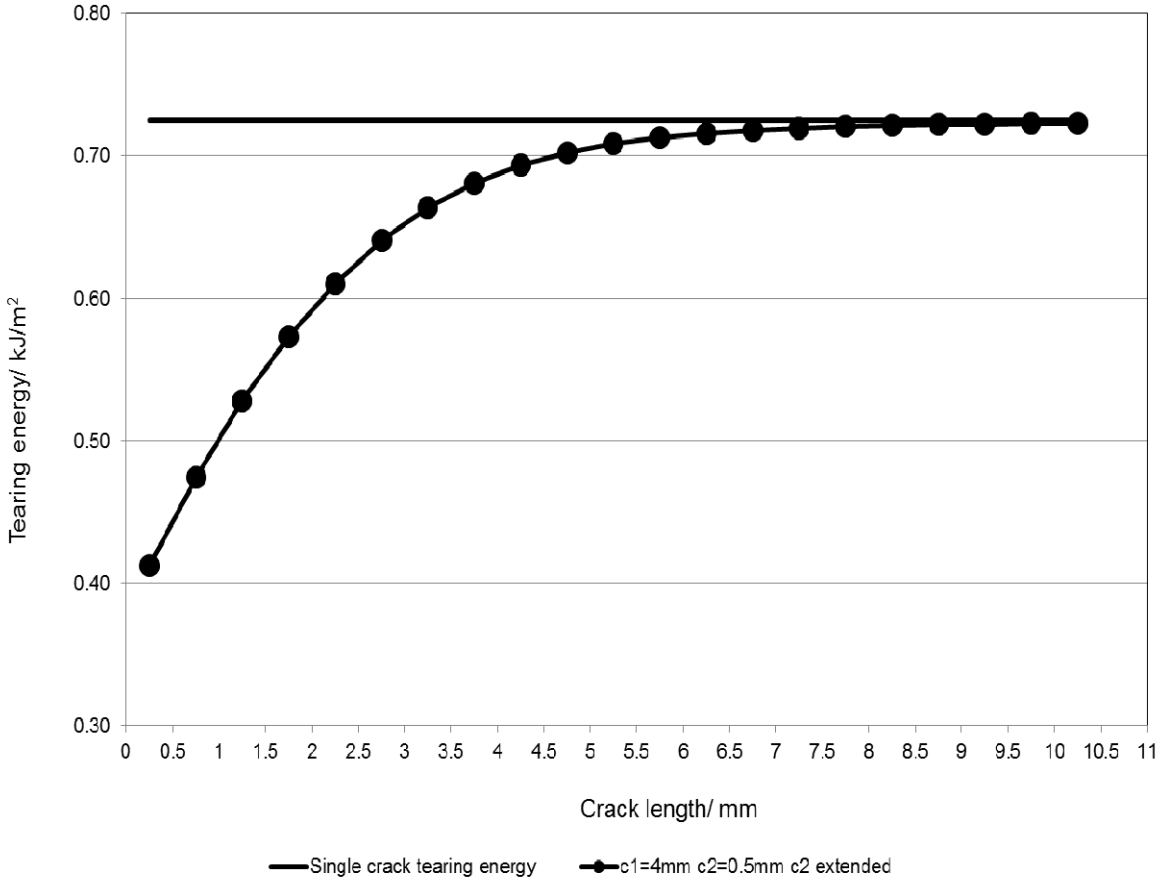

Figure 6.4 Tearing energy crack length relationships for a single and a split parallel crack (c_2) growing in a pure shear specimen at 20% strain

The strain energy release rate subsequently increases with extension through to a maximum of 0.723 kJ/m^2 at the final crack length of 10.25 mm by which point the initial split in the crack tip is no longer felt. The increase in strain energy release rate for a split crack c_2, upon extension of c_2 whilst keeping c_1 constant in figure 6.4, is due to simultaneous creation of new fracture surface as a result of split crack c_2 extending and transfer of energy from the split crack c_1 to c_2. At the limit of extension of split crack c_2, where the area around split crack c_1 is almost energy free, the strain energy release rate of split crack c_2 approaches that of a single crack c in a pure shear specimen

at 20% strain which is a constant. It is interesting to note that the strain energy release rate crack length curve of split crack c_2 in figure 6.4, does not extrapolate back to the origin of the graph but to an intercept strain energy release rate of approximately 0.374 kJ/m^2. This is a manifestation of the node release technique for measuring strain energy release rates, as the method requires the differences between two different models to be compared. Therefore the energy release rate is for a crack length somewhat between the two points where the total energy is being calculated. Since any point on the tearing energy axis in figure 6.4 corresponds to zero crack length extension, extrapolating the split crack c_2 curve to the vertical axis determines the strain energy release rate of split crack c_2 at zero extension. As a result of this slight inaccuracy the strain energy release rates calculated at an increase in 0.25 mm of a crack length is considered approximately the same as the initial strain energy release rates for a split crack.

In figure 6.5, the strain energy release rates for split crack c_1 in the five model instances described in chapter three are presented. It is important to note that in all of the model instances, split crack c_1 had a constant vertical distance of 4 mm from the horizontal centre-line plane of the pure shear specimen. The trend in the strain energy release rate versus crack length relationship is similar in all cases to that observed for the split crack in figure 6.4. In all the instances, the strain energy release rate increases with crack extension due to the combined processes of new fracture surface creation and transfer of energy from split crack c_2, which is kept at a constant length, to split crack c_1. It is interesting to note, however, that when extrapolation of the lines of fit through the strain energy release rate data set was made, all the lines converged approximately to a point on the tearing energy axis in figure 6.5, showing that at the outset all the models converge on a solution whereby the strain energy release rate is split evenly between both cracks. Strain energy release rates calculated for split crack c_1 for the different model instances at 0.25 mm crack extension had a mean of 0.356 kJ/m^2 and a standard deviation of 0.006 kJ/m^2. It can be inferred from figure 6.5 that at a constant vertical distance of 4 mm from the horizontal centre-line of the pure shear specimen, the initial energy of split crack c_1 in all the model instances is approximately constant. In figure 6.5, starting from the tearing energy axis, where split crack c_1 has zero extension, the strain energy release rate curves of the different model instances of split crack c_1 follow slightly different paths.

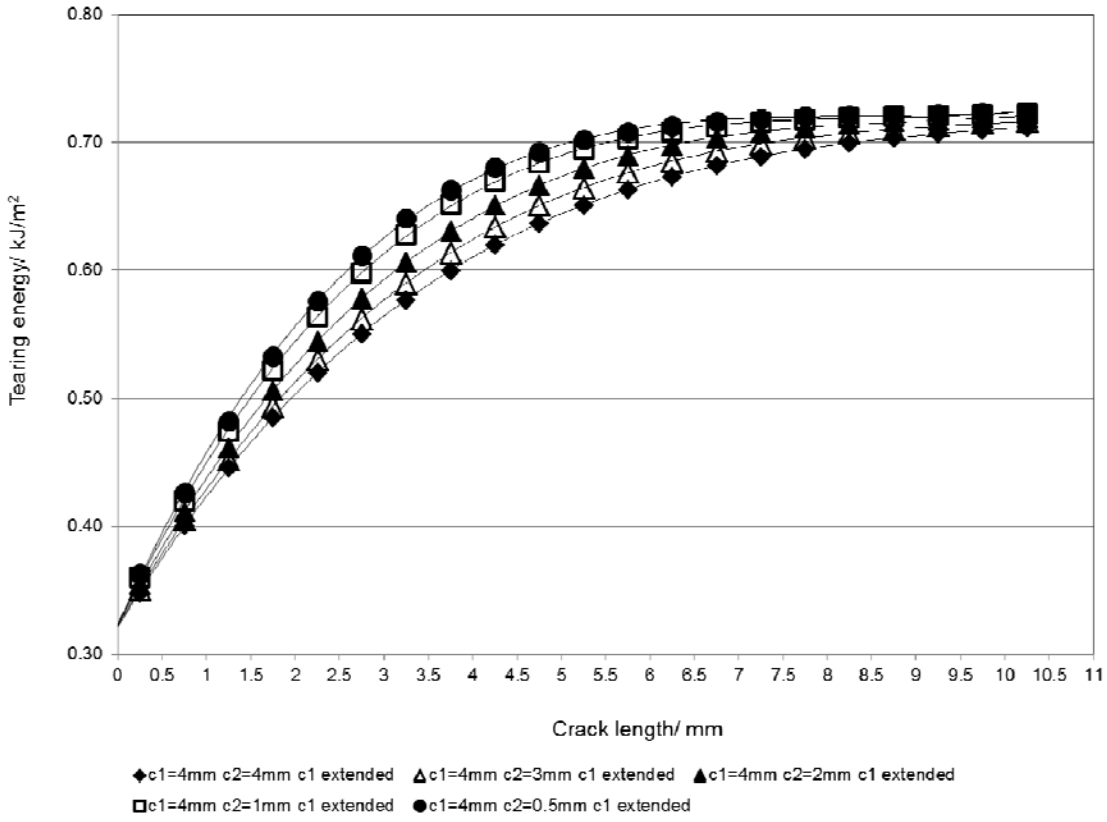

Figure 6.5 Tearing energy crack length relationships for split crack c_1 (where x = constant = 4 mm in all models) for the respective models

This trend can be attributed to a faster rate of energy transfer from split crack c_2, which is kept at a constant length when the cracks are closer together at the outset.

In figure 6.6, the strain energy release rate results for the different model instances of split crack c_2 are presented. The trends in the transfer of the strain energy release rate from being shared by both cracks to being dominated by a single crack are similar to that which has been observed and discussed in figures 6.4 and 6.5 but, unlike figure 6.5, strain energy release rate curves for split crack c_2 when extrapolated to the tearing energy axis does not converge to a single point. In this graph the vertical position of the extending split crack, c_2, was varied from the horizontal centre-line plane of the pure shear specimen. Figure 6.6 suggests that the initial strain energy release rates of split crack c_2 depend on its vertical distance from the horizontal centre-line plane of the pure shear specimen, or at least perhaps the proximity of the crack to the clamped boundary.

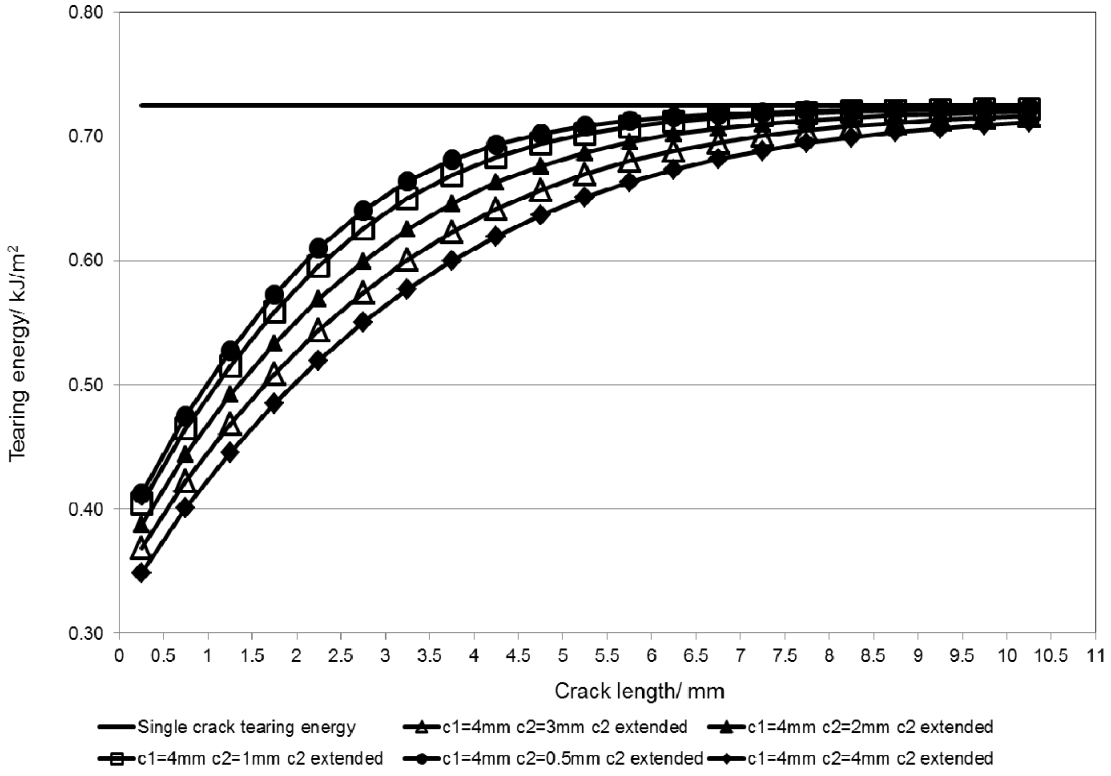

Figure 6.6 Tearing energy crack length relationships for split crack c_2 (where y varied and had values of 0.5 mm, 1 mm, 2 mm, 3 mm and 4 mm) for the respective models

A plot of the initial strain energy release rates for the split crack c_2 observed in figure 6.6 against the respective vertical distances from the central horizontal plane is shown in figure 6.7. The initial strain energy release rate of split crack c_2 is inversely proportional to the vertical distance of the split crack from the horizontal centre-line plane of the pure shear specimen. It is important to mention that in a separate analysis a single crack modeled in a pure shear specimen, and located 4 mm from the central horizontal plane of the specimen, there was no difference between the calculated values for the strain energy release rate and that derived for a single crack located in the middle of the specimen at the same strain.

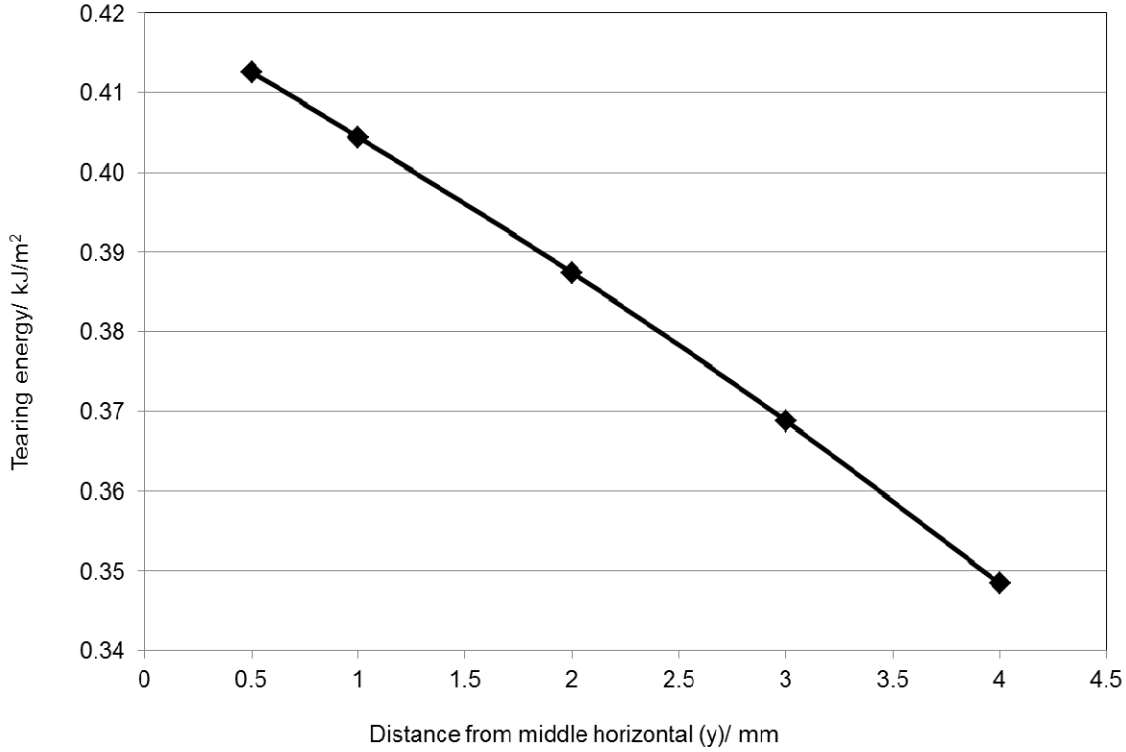

Figure 6.7 Initial tearing energies of split crack c_2, versus measured vertical distance (y mm) of the split crack from the pure shear specimen horizontal centre-line in the respective models at 20% strain

The trend in figure 6.7, therefore, is not caused by edge effects alone. The 16% difference in strain energy release rate observed for split crack c_2 located at 0.5 mm and 4 mm vertical distances respectively from the horizontal centre-line plane of the pure shear specimen was determined at 20% global strain to the specimen. It was of research interest to examine this difference in energy at higher strains. Therefore, split crack c_2 models where "c_1=4mm c_2=4mm c_2 extended" and "c_1=4mm c_2=0.5mm c_2 extended" were analyzed further at 40%, 60%, 80% and 100% strains. The difference in initial strain energy release rates for split crack c_2 at the different strains was calculated and has been presented in figure 6.8. The trend in figure 6.8 suggests that, the difference in initial strain energy release rate between split cracks with shorter vertical distance (y=0.5 mm in this work) from the horizontal centre-line and split cracks with longer vertical distance (y=4 mm in this work) from the horizontal centre-line of the pure shear specimen increases with strain.

As stated previously several physical processes are thought to be the causes of crack tip splitting; prominent among them being the interaction of advancing cracks with strain induced crystals or oriented aggregate filler particles in filled elastomers, which make the material around the crack tip region anisotropic. Strength anisotropy ahead of an advancing fatigue crack implies existence of weak local regions in the material around the crack tip. In figure 6.7, depending on the location of split crack c_2 in the pure shear specimen, it had initial strain energy release rates ranging from approximately 48 % to 57 % of the energy of a single crack growing through the horizontal centre-line of a pure shear specimen at 20 % strain. Figure 6.8 suggests that at higher strains split cracks located near the horizontal centre-line in a pure shear specimen have higher initial energy than that calculated for low strains. It can be inferred, therefore, that the existence of material anisotropy combined with the significant initial strain energy release rate available to split cracks, depending on their location and the global strain of the material, will cause split cracks to propagate under fatigue loading. In figure 6.6, apart from the initial strain energy release rates of split crack c_2 being a function of the location of the split crack from the horizontal centre-line plane of the pure shear specimen, at equivalent crack extensions split crack c_2 located nearer the horizontal centre-line released more energy than when farther from the horizontal centre-line. This trend suggests that the rate of propagation of split cracks at different locations from the horizontal centre-line of a pure shear specimen will not be uniform, rather split cracks with higher strain energy release rates will propagate faster. This phenomenon will induce energy transfer from split cracks with lower strain energy release rates to those with higher strain energy release rates subsequently resulting in “arrest” of low energy split cracks. It appears that advancing fatigue cracks, in an effort to overcome resistance caused by strain induced crystals and oriented aggregate filler particles, split at the tip. The split cracks, depending on their location and orientation, exploit the weak regions around the strain induced crystals and oriented aggregate filler particles and propagate. The most “energetic” and fast growing split crack subsequently gains the energy of the “weak” split cracks which eventually results in the “arrest” of the crack. The most energetic and fastest growing split cracks extend in length until conditions ahead of it (formation of strain induced crystals and presence of oriented aggregate particles) causes it to split and repeat the entire process. This cyclic process involving crack tip splitting, the growth of the most energetic split crack and the eventual “arrest” of lower energy split cracks, must in some part explain

the rough nature of fatigue crack surfaces compared with the smooth surfaces obtained from rapid catastrophic torn surfaces.

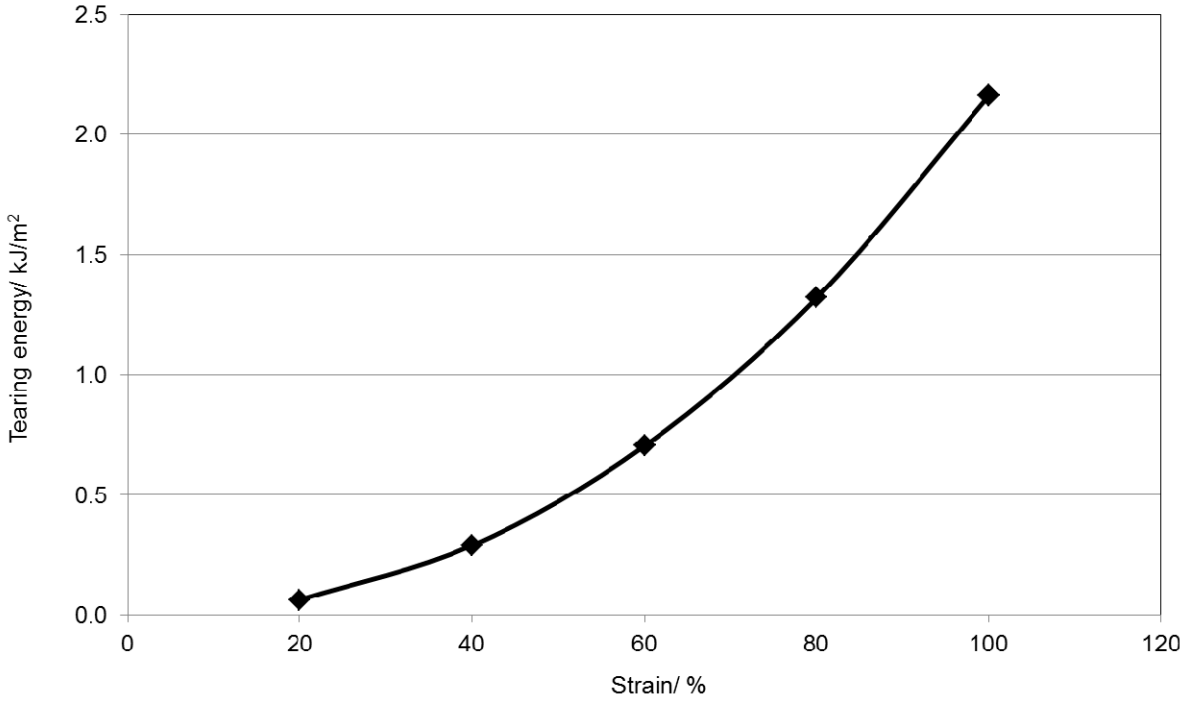

Figure 6.8 Dependence of the initial tearing energy of split cracks on strain

6.3 **Conclusion**

Following the suggestion of Thomas (1958), strain energy release rates due to growth of split fatigue cracks in a pure shear specimen have been calculated using finite element analysis. Upon extension of one split crack while keeping the second split crack at a constant length, all the split cracks studied in this work showed a general increase in strain energy release rate with extension; the strain energy release rate of the extending split crack approached that of a single crack through the horizontal centre-line of a pure shear specimen as the stain energy at the second split crack tip region approached zero. Using the method of extending one split crack whilst keeping the second split crack at a constant length, the initial strain energy release rate available to a split crack was successfully calculated. For a pure shear specimen fitted to the behaviour of a filled NR material used in this work, strain energy release rates of approximately 48% to 57% were calculated for split cracks at different vertical distances measured from the horizontal centre-line plane of the specimen. It was observed that the initial strain energy release rate of a split crack is a function of its location from the central horizontal plane of the pure shear specimen. Split cracks with shorter vertical distance measured from the horizontal centre-line plane had larger initial strain energy release rates and this trend is pronounced at higher strains. Considering the magnitude of the initial strain energy release rate available to split cracks and the general trend of increasing energy release rate with split crack extension, it can be concluded that, a cyclic process involving crack tip splits, growth of the most energetic split crack, and "arrest" of low energy split cracks may be the mechanism for crack advance in the presence of fatigue crack growth inhibitors such as strain induced crystals and aggregate filler particles. In conclusion, the observed and well reported rough nature of fatigue crack surfaces compared with the smooth surfaces obtained from rapid catastrophic torn surfaces in elastomer materials is, to a large extent, a byproduct of the cyclic crack split process studied in this work.

The next stage in this work would be to examine in much more detail exactly how the scale of the initial bifurcation of the crack tip plays an important role in the rate of crack growth of the advancing crack tip and again to investigate if it is possible to calculate for different sizes of splitting how far cracks have to advance from each other before the shortest crack is no longer felt. This can then be used to derive empirical measures of how crack surface roughness might develop.

CHAPTER SEVEN

7.0 Summary, conclusions and future work

7.1 Cyclic stress relaxation

This research has analysed fatigue in filled elastomer test pieces and bonded cylindrical engineering components. The research work was carried out in three stages. Firstly, cyclic stress relaxation was experimentally measured for carbon black filled natural rubber test pieces and bonded cylindrical elastomer engineering components. Cyclic stress relaxation is a manifestation of fatigue in filled elastomer materials. The result of cyclic stress relaxation of filled elastomer materials is significant reduction in stiffness of the material, over the first thousand fatigue cycles. This stiffness reduction which presents as a "downward" shift of the non-linear stress strain curve of filled elastomer materials, possess a design challenge. Neglecting cyclic stress relaxation in the design of elastomer components introduces inaccuracies in predicted component fatigue life.

Quantifying cyclic stress relaxation rate in percent per decade, it was observed that the relaxation rate is different for different modes of mechanical loading at the same extension ratio. Plotting the cyclic stress relaxation rate in terms of the maximum average strain energy density, however, correlates the results of both test piece and engineering components tested under different modes of loading into a single curve. This suggests a general dependence of the cyclic stress relaxation rate on only the maximum average strain energy density experienced in a loading cycle. In conclusion, the maximum average strain energy density approach allows the cyclic stress relaxation in a real component to be predicted from simple test piece results.

This research work was limited to carbon black filled natural rubber as the material of study. In order to validate the maximum average strain energy density approach for a wide range of elastomer material types, test temperatures, formulation and component geometries, future work is required. Cyclic stress relaxation measurements must be made using elastomer components made from different rubber types, other than carbon black filled natural rubber and of complex geometries other than a simple bonded cylinder. Cyclic stress relaxation measurements must also be made using test pieces made from the same compounds as those of the complexly

shaped elastomer components. The test piece and complex geometry component results, must then be correlated in terms of maximum average strain energy density, as has been done for carbon black filled natural rubber test pieces and bonded cylindrical elastomer component in this research, to establish the validity of the approach or otherwise to all elastomer materials and geometries.

7.2 Fatigue Life prediction of bonded rubber components

The fracture mechanics approach to fatigue life prediction of engineering components, was validated using a bonded cylindrical elastomer component for fatigue crack growth within the "power law" region of crack growth behaviour, in the second stage of this research work. The bonded cylindrical geometry of the elastomer component induced rubber-metal bond interface crack growth for both tensile and shear fatigue loadings. The fatigue crack growth behaviour was successfully predicted for crack growth at both room temperature and 70±1ºC to within a factor of 2 for the bonded cylindrical component. For the first time, the cyclic stress softening associated with fatigue of filled elastomer materials was quantitatively accounted for in the prediction by softening the dumbbell specimens for the stress strain characterisation and subsequent FEA strain energy calculations at a strain level deduced following the average strain energy density approach. The effect of temperature on the fatigue life of the bonded cylindrical component was also well accounted for by the approach of characterising the material stress strain and fatigue crack growth behaviour at the test temperature. Considering the irreproducibility of fatigue life predictions in previous work, the accuracy of the fracture mechanics approach to predict fatigue crack growth rate within a factor of 2 for the fatigue life at both room temperature and 70±1ºC is reasonable.

It is worth mentioning that, due to limited supply of bonded cylindrical engineering components in this research work, statistical validation of the accuracy of the fatigue life prediction could not be made. Future work is required in which larger numbers of engineering components, made from different rubber materials and compounds, are tested for fatigue crack growth, and subsequent fatigue failure, as well as a prediction of the fatigue life using fracture mechanics over a range of temperatures. The experimentally determined fatigue life, from large component samples, and the fracture mechanics predicted fatigue life can then be evaluated statistically, to establish the statistical significance of the factor of two accuracy observed in experiments in this

work which involved a relatively small number of components – a total of 65 components were altogether tested in this research work.

7.3 Finite element analysis of crack bifurcation in a pure shear specimen

The final part of this research work investigated the effect of fatigue crack tip splits on the evolution of fatigue crack surface roughness. The approach adopted for the investigation involved using finite element analysis to calculate the characteristic strain energy release rates associated with growth of bifurcated fatigue cracks in a pure shear specimen. As part of this approach, the trends in strain energy release rate versus crack extension obtained from growth of bifurcated cracks were examined in an effort to identify the mechanisms underlying fatigue crack surface roughness generation.

Finite element models were made of single fatigue cracks growing through the horizontal centre-line plane of a pure shear specimen. Models were also made of single fatigue cracks that initially grow along the horizontal centre-line of a pure shear specimen but subsequently split into two crack tips, with both split cracks having parallel orientation to the horizontal centre-line plane of the pure shear specimen and at known vertical distances from it. Strain energy release rates were then calculated for growth of the split fatigue cracks by extending one split crack tip whilst keeping the second split crack tip constant. Depending on the vertical distance of the split fatigue crack tip from the horizontal centre-line plane of the pure shear specimen, different strain energy release rate curves were obtained for the growth of the split crack. It was generally observed that, whilst keeping one split crack constant and extending a second split crack, strain energy release rate increased with extension. However, comparing the strain energy release rate curves at equivalent crack extension, split fatigue crack tips that had a shorter vertical separation from the central horizontal plane of the pure shear specimen released more energy, upon extension, than those with longer vertical distances from the horizontal centre-line plane. Physical phenomena such as strain induced crystalisation and crack tip filler particle interaction cause anisotropy and this is the source of the fatigue crack tip splitting. Observing the trends in strain energy release rates for growing split fatigue crack tips in this work, split crack tips with vertical distances nearest to the horizontal centre-line plane in a pure shear specimen will preferentially grow since they are the most energetic. This will lead to crack "arrest" of the tips with longer vertical distances from the horizontal centre-line plane in the pure shear specimen since they possess less energy. The rapid increase in the

strain energy release rate, of the split crack tip with shorter vertical distance from the central horizontal plane in the pure shear specimen, implies intensification of phenomenon such as strain induced crystalisation ahead of the growing tip. When the less energetic split crack tip becomes "arrested" the larger stress field developed around the advancing crack tip will produce more anisotropy which can repeat the whole cycle again. It appears, therefore, that advancing fatigue cracks, in an effort to overcome resistance caused by strain induced crystals and oriented aggregate filler particles, split at the tip. Examining the order of magnitude and trends in strain energy release rate versus crack extension for split fatigue cracks in a pure shear specimen; it appears that a cyclic process involving crack tip splits, growth of the most energetic split cracks, and "arrest" of low energy split cracks may be the mechanism for crack advance in the presence of fatigue crack growth inhibitors such as strain induced crystals and aggregate filler particles in elastomers.

In conclusion, the observed and well reported rough nature of fatigue crack surfaces compared with the smooth surfaces obtained from rapid catastrophic torn surfaces in elastomer materials is, to a large extent, a byproduct of the cyclic crack split process studied in this work.

Investigations into the characteristic strain energy release rate associated with growth of split fatigue cracks, in this work, was limited to two dimension plane stress models of a pure shear specimen and a single material type. Future work should be carried out to investigate the effect of material type on the trends in the characteristic strain energy release rate. The analysis may also be extended to complex three dimensional models of split fatigue cracks in elastomer components. It should also be extended to attempt to model the amount of anisotropy that is produced under different conditions to examine exactly which conditions create the split in the crack in the first place.

References

Abaqus, (1998). Abaqus/ Standard User's Manual, Version 5.8., Hibbit, Karlsson & Sorensen, Inc, Pawtucket, USA.

Abraham, F., (2002). "The Influence of Minimum Stress on the Fatigue Properties of Non Strain-Crystallising Elastomers", PhD thesis, Coventry University, Coventry, UK.

Allen, P.W. and Bloomfield, G.W., (1963), "Natural rubber hydrocarbon", in Bateman, L., (ed.), The Chemistry and Physics of Rubber-like Substances, Mclaren and Sons Ltd., Chapter 1, 3.

Andrews, E.H., (1961). "Stresses at a crack in an elastomer", Proceedings of the Physical Society, Vol. 77, p. 483.

Andrews, E.H., (1963). "Rupture propagation in hysteresial materials: stress at a notch", Journal of Mechanics and Physics of Solids, Vol. 11, p.231.

Andrews, E.H., (1964). "Crystalline morphology in thin films of natural rubber II. Crystallisation under strain", Proceedings of the Royal Society A, Vol. 277, p. 562.

Baker, C.S.L., (1988), "Non-sulphur vulcanisation", in Roberts, A.D., (ed.), Natural Rubber and Technology, Oxford University Press, Chapter 11, 457.

Barlow, F.W., (1988), Rubber Compounding: Principles, Materials and Techniques, Marcell Dekker Inc, 97.

Blow, C.M., (1971), Rubber Technology and Manufacture, Butterworths.

Bristow, G.M., (1970), "Improved compression set with peroxide-cured vulcanizates", NR Technology, I, 1.

British Standards: BS3558-1:1997

Brown, P.S, Porter, M. and Thomas, A.G. (1987). "The dependence of strength properties on crosslink structure in vulcanised polyisoprene", Kautschuk Gummi Kunst, Vol. 40, p. 17.

Brydson J.A. (1988), Rubbery Materials and their Compounds, Elsevier Applied Science.

Busfield J.J.C., Papadopoulos, I.C., Jha V., Liang H. and Thomas A.G. (2005). "Prediction of fatigue crack growth using finite element analysis techniques to three-dimensional elastomeric components", Plastics Rubber Composites, Vol.34, No. 8, p.349.

Busfield, J. J. C and Thomas A. G. (1999). "Indentation tests on elastomer blocks", Rubber Chemistry and Technology, Vol. 72, p. 876.

Busfield, J. J. C., Thomas, A. G. and Ngah, M. F., (1999)",Application of fracture mechanics for the fatigue life prediction of carbon black filled elastomers", Constitutive Models for Rubber. Edited by A. Dorfmann and A. Muhr. pp. 249-256.

Busfield, J. J. C., Tsunoda K., Davies, C. K. L., and Thomas A. G. (2002), "Contributions of time dependent and cyclic crack growth to the crack growth behaviour of non strain-crystallising elastomers",Rubber Chemistry and Technology, Vol. 75, p. 643.

Busfield, J.J.C. (2000). "The prediction of the mechanical performance of elastomeric components using finite element analysis", Ph.D. Thesis, Queen Mary, University of London.

Busfield, J.J.C., Ratsimba, C.H.H. and Thomas, A.G. (1997). "Crack growth and strain induced anisotropy in carbon black filled natural rubber", Journal of Natural Rubber Research, Vol. 12 p. 131.

Busfield, J.J.C., Ratsimba, C.H.H. and Thomas, A.G. (1999). "Crack growth and complex loading in filled elastomers", Finite Element Analysis of Elastomers, Professional Engineering Publishing Ltd., Bury St. Edmunds, p. 235.

Callister, W.D. (1994). An Introduction to Materials Science and Engineering - 3rd Edition. John Wiley and Sons, New York.

Chapman, A.V. and Porter, M., (1988), "Sulphur vulcanisation chemistry", in Roberts, A.D., (ed.), Natural Rubber and Technology, Oxford University Press, Chapter 12, 513.

Cunneen, J.I. and Higgins, G.M.C., (1963), "Cis-trans isomerism in natural polyisoprenes", in Bateman, L., (ed.), The Chemistry and Physics of Rubber-like Substances, Mclaren and Sons Ltd., Chapter 2, 19.

Davies, C.K.L., De, D.K. and Thomas, A.G. (1996). "Characterisation of the behaviour of rubber for engineering design purposes: (II) Stress relaxation under repeated stressing", Progress in Rubber and Plastics Technology, Vol.12, p. 208.

De, D.K. (1994). "The effect of particulate fillers on the strain energy function and the crack growth in rubbers", PhD Thesis: Queen Mary and Westfield College, London University.

Deeprasertkul, C. (2000). "Dynamic properties of carbon black filled elastomers containing liquids", PhD Thesis: Queen Mary and Westfield College, London University.

Derham, C. J., and Thomas, A. G. (1977), Rubber Chemistry and Technology, Vol. 50, p. 397.

Ellul, M.D. (1992). “Engineering with Rubber, how to design rubber components”, 2nd edition. Ed. by Gent A.N. Hanser, Munich.

Fagan, M.J. (1992). Finite Element Analysis - Theory and Practice, Longman Group, Harlow.

Fukahori, Y. and Andrews, E.H. (1978). “Fracture surface roughness in highly deformable polymers”, Journal of Materials Science Vol. 13, p.777.

Gent A.N. and Pulford C.T.R. (1984). “Mechanisms of rubber abrasion”, Journal of Polymer Science, Vol. 28, p. 943.

Gent, A. N. and Wang, C. (1993),Rubber Chemistry and Technology, Vol. 66, p. 712.

Gent, A.N. (1992). “Engineering with Rubber, how to design rubber components”, – 2nd edition. Hanser, Munich.

Gent, A.N. and Henry, A.W. (1967). “On the tear strength of rubbers”, Proceedings of the International Rubber Conference (Brighton), p.193.

Gent, A.N. and Tompkins, D.A. (1969). “Nucleation and growth of gas bubbles in elastomers”, Journal of Applied Physics, Vol. 40, p. 2520.

Gent, A.N., Lindley, P.B. and Thomas, A.G. (1964). “Cut growth and fatigue of rubbers. I. The relationship between cut growth and fatigue”, Journal of Applied Polymer Science Vol. 8, p. 455.

Gent, A.N., Razzaghi-Kashani, M. and Hamed, G.R. (2003). “Why do cracks turn sideways”, Rubber Chemistry and Technology, Vol. 76, p. 122.

Greensmith, H.W. and Thomas, A.G. (1955). “Rupture of rubber. Part III. Determination of tear properties”, Journal of Polymer Science, Vol. 18, p. 189.

Greensmith, H.W., Mullins, L. and Thomas, A.G. (1960). “Rupture of rubber”, Transactions of the Society of Rheology, Vol. 4, p. 179.

Griffith, A.A. (1920). “The phenomena of rupture and flow in solids”, Philosophical Transactions of the Royal Society A, Vol. 221, p. 163.

Gumbrell, S. M., Mullins, L. and Rivlin, R. S. (1953) Trans. Faraday Soc.,49,1495.

Hamed, G.R., (1992), “Materials and compounds”, in Gent, A.N., (ed.), Engineering Design with Elastomers, Hanser Verlag, Munich, Chapter 2, 33.

Huebner, K. H., Dewhirst, D. L., Smith, D. E., and Byrom T. G. (2001),”The Finite Element Method for Engineers”, John Wiley & Sons, Inc., 4th Edition.

James, A.G. and Guth, E. (1943). “Theory of elastic properties of rubber”, Journal of Chemical Physics, Vol. 11, p. 455.

Jerrams, S., Murphy, N., Hanley, J (2012).: “The Significance of Equi-biaxial Bubble Inflation in Determining Elastomeric Fatigue Properties”. Published in the book 'Elastomers' edited by Anna Boczkowska (ISBN 979-953-307-1019-5), InTech.

Kuhn, W., (1936), “Beziehungen zwischen molekülgröße, statischer molekülgestalt und elastichen eigenschaften hochpolymere stoffe”, Kolloid-Zeitschrift, 76, 258.

Kingston, J. Muhr, A. (2012), “Determination of effective flaw size for fatigue life prediction”, Constitutive models for Rubber VII, Editors Jerrams S and Murphy N, ISBN 978-0-415-68389-0, 337-342.

Lake G.J and Lindley P.B., Rubber J. (1964). “Ozone cracking, flex cracking and fatigue of rubber”, Vol.146, No.10, p.24.

Lake, G.J. (1970). “Application of fracture mechanics to rubber articles, with particular reference to tyres”, Proc. Int. Conference of Yield, Deformation and Fracture of Polymers, Cambridge UK.

Lake, G.J. (1983). “Aspects of fatigue and fracture of rubber”, Progress of Rubber Technology, Vol. 45, p. 89.

Lake, G.J. (1995). “Fatigue and fracture of elastomers”, Rubber Chemistry and Technology, Vol. 68, p. 435.

Lake, G.J. and Thomas, A.G. (1967). “The strength of highly elastic materials”, Proceedings of the Royal Society A, Vol. 300, p. 108.

Lake, G.J., Lindley, P.B. and Thomas, A.G. (1969). “Fracture mechanics of rubber”, Proceedings 2nd International Conference on Fracture (Brighton).

Lindley, P.B. (1974b) Engineering Design with Natural Rubber, 4th ed. The Malaysian Rubber Producers' Research Association, Hertford.

Lindley, P.B. and Thomas, A.G. (1962) “Fundamental study of the fatigue of rubbers”, The Fourth Rubber Technology Conference. ,London, UK, May 1962, Institute of Rubber Industries, p. 1-14.

Mars, W.V. and Fatemi, A. (2002). “A literature survey on fatigue analysis approaches for rubber”, International Journal of Fatigue, Vol. 24, p. 949.

Mars, W.V. and Fatemi, A. (2003). “Fatigue crack nucleation and growth in filled natural rubber”, Fatigue & Fracture of Engineering Materials & Structures, Vol. 26, p. 779.

McKenna, G. B., and Zapas, L. J. (1981), Rubber Chemistry and Technology, Vol. 54, 718 (1981).

Meyer, K.H. and Ferri, C., (1935), Helv. Chim. Acta., 18, 570.

Mooney, M. (1940). “A theory of large elastic deformation”, Journal of Applied Physics, Vol. 11, p. 582.

Morrell, S.H., (1987), “The chemistry and technology of vulcanisation”, in Blow, C.M. and Hepburn, C., (ed), Rubber Technology and Manufacture Plastic and Rubber Institute, Butterworths, 171.

Morton, M., (1987), Rubber Technology, Van Nonstrand Reinhold Co. New York.

Muhr, A.H., Tan, G.H. and Thomas, A.G., (1988) “A method of allowing for non-linearity of filled rubber in force-deflection calculations”, Journal of Natural Rubber Research, Vol. 3, p. 261-276.

Mullins, L. (1948) “Effect of stretching on the properties of rubber”, Rubber Chem. Technol., Vol. 21, p. 281-300.

Mullins, L. (1959). “Rupture of rubber. Part IX. Role of hysteresis in the tearing of rubbers”, Transactions of the Institute of Rubber Industries, Vol. 35, p. 213.

Mullins, L. and Tobin, N. R., (1965), Journal of Applied Polymer Science, Vol. 9 p. 2995.

Papadopoulos, I. C. (2006). “Predicting the fatigue life of elastomer components”, PhD Thesis: Queen Mary and Westfield College, University of London.

Papadopoulos, I. C., Thomas, A. G., and Busfield, J.J.C. (2008), ”Rate Transitions in Fatigue Crack Growth of Elastomers”, Journal of Applied Polymer Science, Vol. 109, pp. 1900-1910.

Payne, A.R. (1962) “The dynamic properties of carbon black loaded natural rubber vulcanisates”, Journal of Applied Polymer Science, Vol. 6, p. 57-63.

Payne, A.R. and Whittaker, R.E. (1972) “Influence of hysteresis on tensile and fatigue failure in rubbers”, Rubber Chemistry and Technology, Vol. 45, p. 1043-1050.

Pond, T. J., and Thomas, A. G. (1979),”Creep under repeated stressing”, Presented at AIRIEL International Rubber Conference, Venice, Italy, Oct 3-6, 1979, p. 810-817.

Porter, M., (1968), “The chemistry of the sulfur vulcanisation of natural rubber”, In Tobolsky, A.V., (ed), Chemistry of Sulphides, Interscience Publishers, New York, 165.

Porter, M., (1969), “Effect of reinforcing fillers on the chemical structure of sulfur vulcanizates of natural rubber”, Kautschuk Gummi Kunststoffe, 22, 80, 419.

Porter, M., (1973), “A new crosslinking system for natural rubber”, Kautschuk Gummi Kunststoffe, 26, 540.

Rice, J.R. (1968). “A path-independent integral and the approximate analysisof strain concentration by notches and cracks”, Journal ofApplied Mechanics, Trans ASME. Vol. 35. p.379.

Rivlin, R.S. (1956). “Large elastic deformations”, in Eirich, F.R. (ed.) Rheology Vol. 1, Academic Press, New York, p. 351.

Rivlin, R.S. and Saunders, D.W. (1951). “Large elastic deformations of isotropic materials VII. Experiments on the deformation of rubber”, Philosophical Transactions of the Royal Society A, Vol. 243, p. 251.

Rivlin, R.S. and Thomas, A.G. (1953). “Rupture of rubber. Part 1. Characteristic energy for tearing”, Journal of Polymer Science, Vol. 10, p. 291.

Skinner, T.D., and Watson, A.A., (1967), “EV systems for NR Part 1 and 2”, Rubber Age, 99, No 11&12, 76 & 69.

Sperling, L.H., (1986), Introduction to Physical Polymer Science, John Wiley & Sons, New York.

Sperling, L.H., (2001), Introduction to Physical Polymer Science, John Wiley & Sons, New York.

Thomas, A.G. (1955). “Rupture of rubber. Part II. The strain concentration at an incision”, Journal of Polymer Science, Vol. 18, p. 177.

Thomas, A.G. (1958). “Rupture of rubber. Part V. Cut growth in natural rubber vulcanizates”, Journal of Polymer Science, Vol. 31, p. 467.

Thomas, A.G. (1960). “Rupture of Rubber. Part VI. Further experiments on the tear criterion”, Journal of Applied Polymer Science, Vol. 3, p. 168.

Thomas, A.G. (1974). “Deformation and fracture of high polymers”, Ed. by H. Kausch, J.A. Hassel and R. Jaffe, Plenum Press, 1974.

Treloar, L.R.G. (1944) “Stress strain data for vulcanised rubber under various types of deformation”, Transactions of the Faraday Society, Vol. 40, p. 59-70.

Treloar, L.R.G. (1975). “The Physics of Rubber Elasticity”, 3rd Edition, Clarendon Press, Oxford.

Treloar, L.R.G., (1943), “The elasticity of a network of long chain molecules Part II”, Transactions Faraday Society, 39, 36, 241.

Tsunoda, K. (2001). “The role of visco-elasticity on the crack growth behaviour of rubber”, PhD Thesis: Queen Mary, University of London.

Wall, F.T., (1942), “Statistical thermodynamics of rubber: Part II”, Journal Chemical Physics, 10, 485.

Williams, M.L., Landel, R.F. and Ferry, J.D. (1955). “The temperature dependence of relaxation mechanisms in amorphous polymers and other glass forming liquids”, Journal of the American Chemical Society, Vol. 77, p 3701.

Wood, L.A. and Bekkedahl, N., (1946), “Crystallization of unvulcanized rubber at different temperatures”, Journal Applied Physics, 17, 362.

Yeoh, O.H. (1990). “Characterisation of elastic properties of carbon black filled rubber vulcanizates”, Rubber Chemistry and Technology, Vol. 63, p. 792.

Appendix – Refereed Journal papers published by the author as part of this research

CYCLIC STRESS RELAXATION (CSR) OF FILLED RUBBER AND RUBBER COMPONENTS

S. ASARE, A. G. THOMAS, J. J. C. BUSFIELD*

DEPARTMENT OF MATERIALS, QUEEN MARY UNIVERSITY OF LONDON, MILE END ROAD, LONDON, UK, E1 4NS

ABSTRACT

Under repeated stressing it is well known that rubber materials exhibit cyclic stress relaxation (CSR). Previous work has shown that the amount of relaxation observed from cycle to cycle is significantly greater than that expected from static relaxation measurements. The reduction in the stress attained on the second and successive loading cycles as compared to the stress attained on the first cycle in a stress strain cyclic test of fixed amplitude has been measured for elastomer test pieces and engineering components. It is seen that the peak force, under cyclic testing to a specific maximum displacement, plotted against the number of cycles on logarithmic scales produces a straight line graph, whose slope correlates to the rate of cyclic stress relaxation per decade. The rate of cyclic stress relaxation was found to increase with displacement amplitude in all modes of deformation. Plotting the rate of stress relaxation per decade against the maximum average strain energy attained in the cycle reduces the data measured in different deformation modes for both simple test pieces and components to a single curve. This approach allows the cyclic stress relaxation in a real component to be predicted from simple laboratory tests.

INTRODUCTION

Many engineering components undergo repeated stressing. Under specific conditions for many rubber components this results in fatigue failure such as that described by Busfield *et al.*,[1] Papadopoulos *et al.*[2] and Busfield *et al.*[3] Laboratory tests of vulcanized rubber also suggest that they may experience stress relaxation or creep which is substantially greater than might have been expected from static measurements. This cyclic stress relaxation (CSR) behavior is sometimes mistakenly referred to as the Mullins[4] effect. This is inappropriate, as the classical Mullins effect describes behavior where if the maximum strain experienced previously by the rubber is exceeded, the stress strain curve returns to the value measured in the virgin cycle. The relaxation phenomenon has been studied for simple extension by Derham and Thomas,[5] McKenna and Zappas,[6] Davies *et al.*[7] and Pond and Thomas,[8] but not for other deformation modes. It was found that the fractional relaxation or creep rate was strongly dependent on the maximum stress as well as the composition of the compound. In particular the filler content and the ability to strain crystallize appear to be important in enhancing the relaxation rate. A possible reason for this is that under large stresses the chemical bonds, particularly in the crosslinks, can fracture with the crystallites acting as stress raisers. A close correlation was found between the amount of creep and the molecular scission estimated from the measurements of set and changes in the equilibrium swelling by Pond and Thomas.[8] The sulphur-sulphur crosslinks are mechanically weaker than carbon-carbon crosslinks, this weakness is believed to promote greater strength[9] as they effectively introduce a yielding mechanism. Thus rubber compounds that are designed for maximum strength will probably show greater CSR. This picture is complicated by the presence of filler, which appears to increase the stress relaxation rate, making a contribution[8] even in a non-crystallizing rubber such as styrene butadiene rubber. The presence of the filler causes strain amplification[10] which will both stiffen the materials and will also most likely make these effects of CSR occur more readily at lower strains. The changes in the mechanical behavior have also been contrasted to changes in other properties such as electrical conductivity in filled elastomers by Busfield *et al.*[11]

In engineering applications the rubber experiences many modes of deformation and in this

* Corresponding author. Ph: +44 (0)20 78828886; Fax: +44 (0)20 7882 3390; email: j.busfield@qmul.ac.uk

paper we examine the relaxation in other modes, and also suggest how the various relaxation rates can be inter-related and how relaxation rates may be estimated for components of complex shape.

EXPERIMENTAL

The material used in this work was a commercially formulated 65 phr HAF 330 carbon black filled natural rubber compounds supplied by Trelleborg AVS. The formulation of the compound is presented in Table I. The rubber material was supplied as rubber sheets of approximately 2 mm thickness, from which pure shear samples of 175 mm length, 25 mm width and 2 mm thickness, were prepared. In addition, simple bonded suspension mounts were injection molded out of the same compound. Figure 1 shows a typical cylindrical bonded suspension component used in this study. It has dimensions of 42 mm in height (including bonded metal plates) and a diameter of approximately 47.5 mm. The two metal end plates were each 2 mm in thickness.

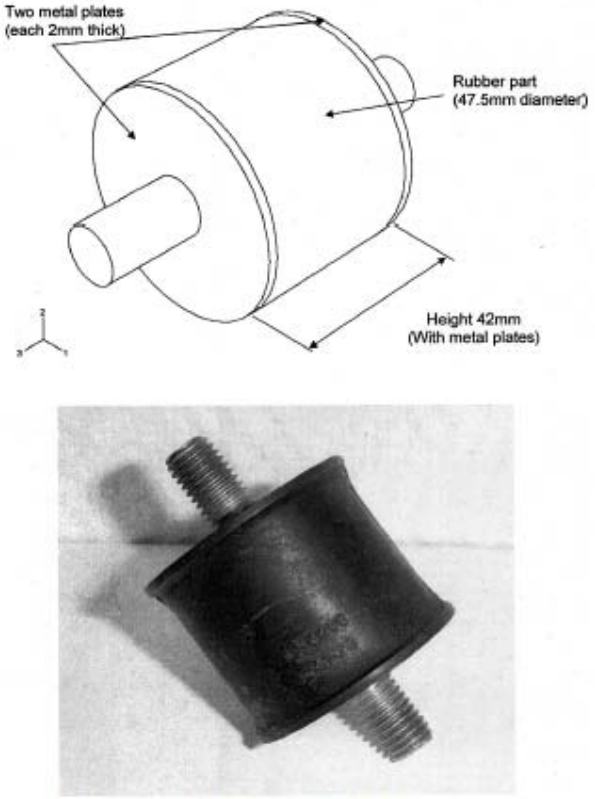

FIG. 1. — The 47.5mm diameter bonded cylindrical suspension component.

TABLE I
FORMULATION FOR THE MATERIALS USED IN THIS STUDY

Ingredients	Type	pphr
Rubber	SMR10CV	100
Carbon black	N330(HAF)	65
Stearic acid		2
Zinc oxide		5
Accelerator	TMTM-75	0.7
Accelerator	MBTS-80	1.5
Sulfur		1.5

An Instron 8872 Servo-hydraulic test machine was used to test both the test pieces and the cylindrical bonded components. Cyclic constant maximum displacement tests with sinusoidal wave form at 1 Hz frequency under fully relaxing conditions were carried out on all samples up to 3000 cycles. The pure shear samples were deformed over a range of maximum strains from 20% - 150%. The cylindrical mounts were deformed in tension, shear and compression by the following amounts, expressed as a percentage of the original rubber section height, 26% - 92%, 26% - 158% and 16% - 63% respectively. All measurements were carried out at 23 ± 2 °C. The maximum (peak) force attained at maximum displacement amplitude was monitored and recorded throughout each test with 1kN and 25kN load cells for test pieces and components respectively. The strains in the region of the bond are clearly inhomogeneous for the bonded test piece.

RESULTS AND DISCUSSION

CSR is known to occur in both filled and unfilled elastomer materials with the level of relaxation being greater in the case of filled elastomers. The amount of relaxation is known to be dependent on the filler content and also the level of maximum strain to which the material is subjected.

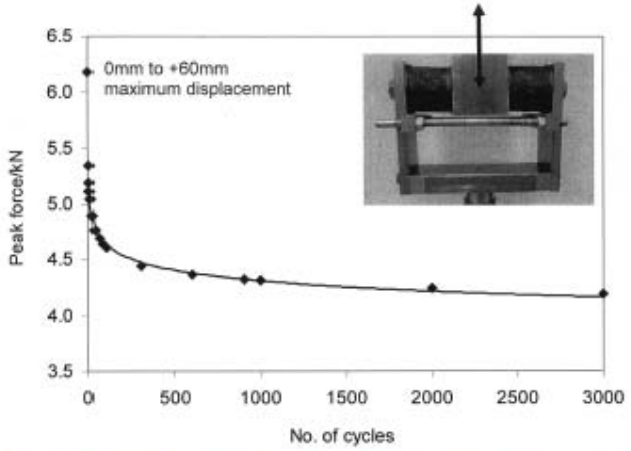

FIG. 2. — The maximum force plotted against the number of cycles for two bonded suspension mounts deformed in cyclic simple shear from 0 mm to 60 mm displacements.

Figure 2 shows the maximum force in each cycle plotted against the corresponding number of cycles for two rubber components deformed in simple shear from a fully relaxed condition to a maximum displacement of 60 mm. There is a rapid fall in the force required to deform the components in this test to the maximum displacement over the first few cycles. The reduction in the peak force, however, continues over the entire range but the rate of reduction diminishes as the test continues.

The CSR behavior, shown in Figure 2, when plotted in Figure 3 as the stress versus the log (number of cycles) gives a linear behavior except for the first few cycles as discussed by Davies *et al.*[7] and the slope can be taken as a measure of relaxation rate per decade. Figure 3 presents results of CSR measurements made on pure shear samples for a range of different maximum strains. Apart from the initial points, the data reduced well to straight lines. The causes of the less than perfect fit for the first point results from the first maximum displacement being attained before a whole loading and unloading cycle has been completed as discussed by Davies *et al.*.[7]

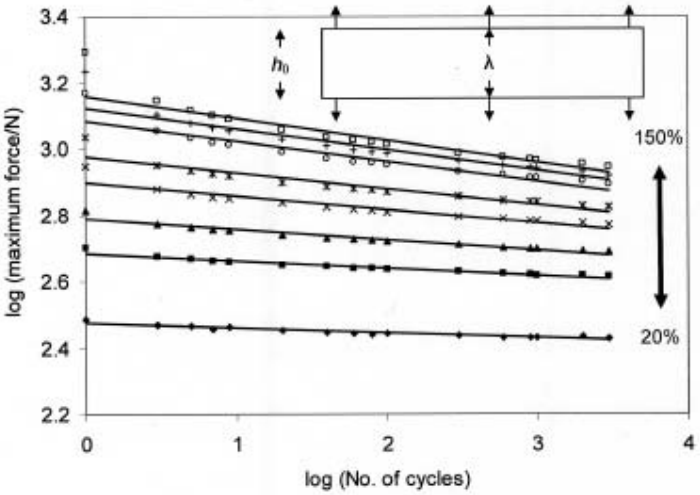

FIG. 3. — Plot of log (maximum force) against log (number of cycles) for pure shear samples tested at 20%, 40%, 60%, 80%, 100%, 120%, 140% and 150% maximum engineering strain.

Figure 4 shows how the slopes of the lines fitted to data in figure 3 change with the maximum strain in the test cycle. The CSR rate shows an increase of about a factor of 5 as the deformation is increased from 20% to 150% of the original component's height. The CSR measurements made on the bonded cylindrical engineering components in tensile, shear and compressive deformation directions are presented in figures 5, 6 and 7, respectively. In each deformation mode it is apparent that the rate of CSR increases with the extent of the deformation.

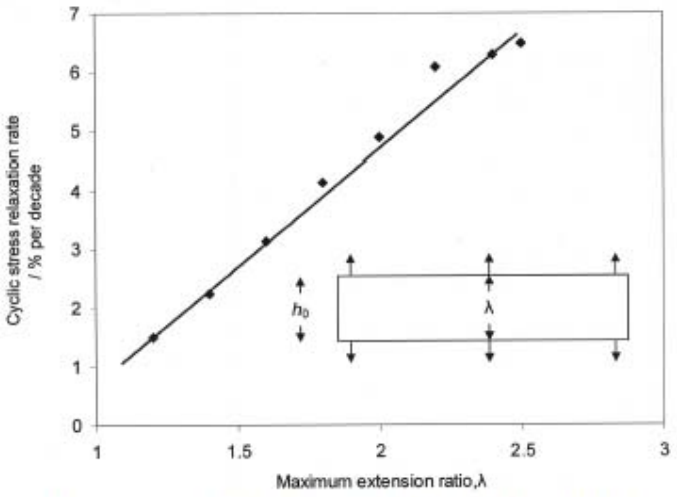

FIG. 4. — Cyclic stress relaxation rate against extension ratio for the pure shear test pieces.

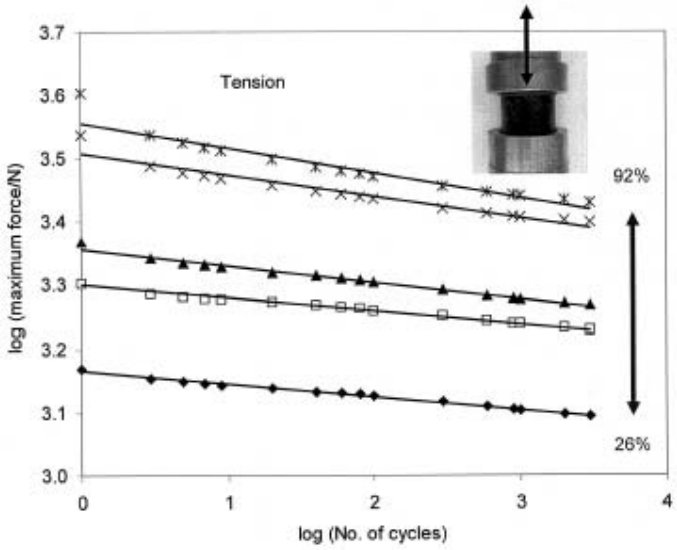

FIG. 5. — Plot of log peak force (maximum force) against log (number of cycles) for the bonded suspension mount at 26%, 40%, 53%, 79% and 92% maximum displacement expressed as a percentage of the rubber cylinder height in tension.

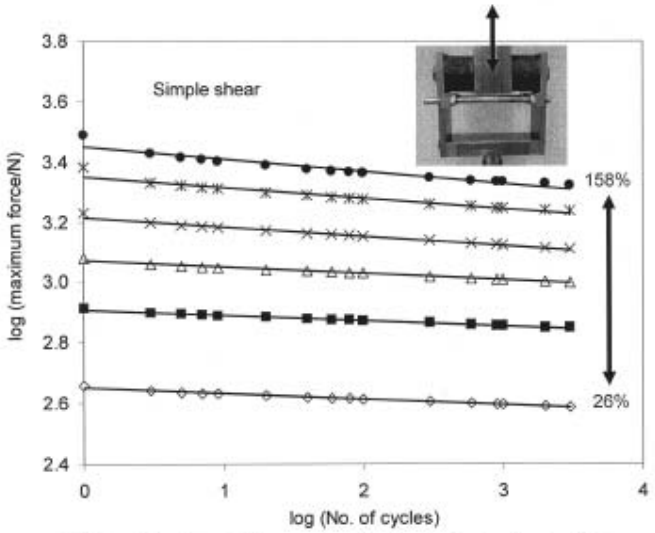

FIG. 6. — Plot of log peak force (maximum force) against log (number of cycles) for the bonded suspension mount at 26%, 53%, 79%, 105%, 132% and 158% maximum shear displacement expressed as a percentage of the rubber cylinder height.

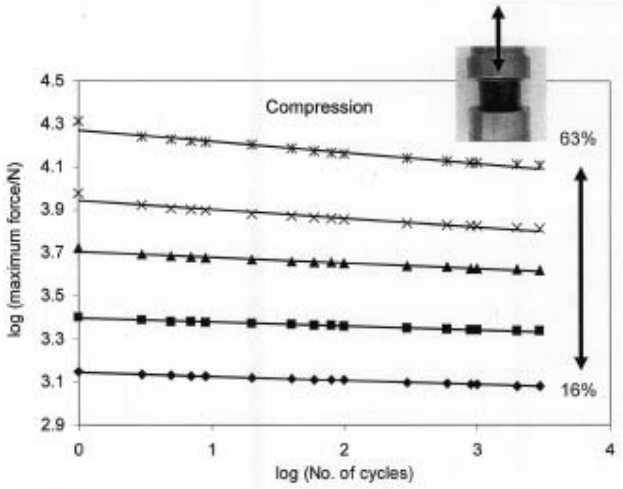

FIG. 7. — Plot of log peak force (maximum force) against log (number of cycles) for the bonded suspension mount at 16%, 26%, 42%, 53% and 63% maximum compression, expressed as a percentage of the cylinder rubber section height.

Figure 8 shows that the CSR rate for the various different modes of deformation when plotted against the maximum deformation, expressed as a percentage of the component's original rubber section height, are very different. One approach to the unification of these results is as follows. When a filled rubber is deformed, the elastic energy will be stored in the rubber phase only and will thus reflect the deformation of the rubber chains between the crosslinks. It is thought that the stress in a chain will be the factor which induces fracture in the chemical bonds in either the main chain or the crosslink or possibly slippage[12] of the rubber molecules over the surface of the filler, these being the two factors most commonly proposed to explain CSR. If so then the maximum average energy density as proposed by Muhr *et al.*[13] and adopted by Busfield and Thomas[14] may be an appropriate parameter with which to attempt correlation between the various deformation modes. The deformations applied to the bonded suspension mount are clearly inhomogeneous, particularly under simple extension or compression as a result of the constraints imposed by the bonded surfaces. This makes these geometries a more severe test of this approach. Thus the maximum average strain energy density, simply derived from the work done calculated by integrating the force deflection curve which is then divided by the rubber volume of the sample up to working strain, was adopted as the parameter to describe the CSR rate. This way of presenting the results are shown in Figure 9. This shows that this approach works well and that even for the inhomogeneous strains found in the component. Clearly the average strain energy density is a useful measure.

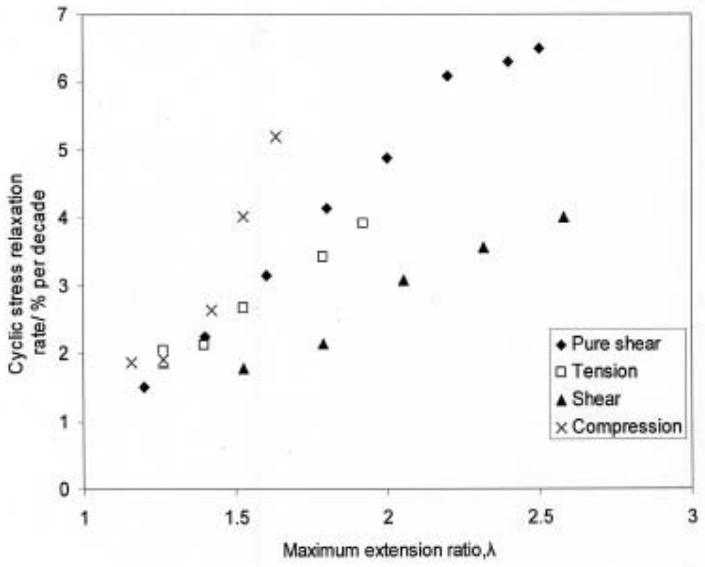

FIG. 8. — Cyclic stress relaxation rate plotted against the maximum engineering strain for the pure shear test pieces and maximum displacement divided by the rubber cylinder height for the suspension mount under different deformations.

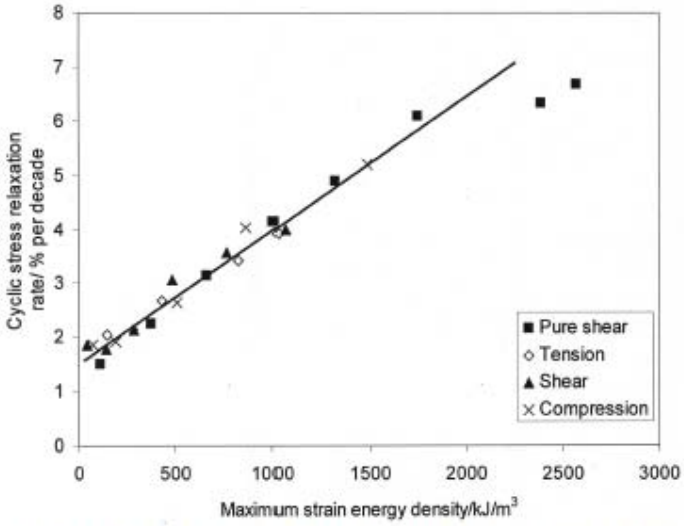

FIG. 9. — Cyclic stress relaxation rate plotted against the maximum average strain energy density for the pure shear test pieces and the suspension mount under different deformations.

This approach gives promise that it may be applied to more complex geometries and loading regimes encountered in engineering applications, so that the CSR for a component may be estimated from laboratory measurements to determine the behavior of the material itself.

CONCLUSIONS

CSR has been studied for engineering components and test pieces. The results of the studies confirm that the CSR rate increases with displacement amplitude (strain) for all directions of deformation in test pieces and components. Plotting the CSR rate in terms of average strain energy density reduces both test piece and component data to a single straight line. This suggests a general dependence of the CSR rate only on the average maximum strain energy density experienced in a loading cycle. The average strain energy density concept presents an approach for determining the amount of CSR of an elastomer component from a measure of the material's CSR behavior.

ACKNOWLEDGEMENTS

The authors would like to thank the Swedish Fatigue Network for the funding for the project, as well as Trelleborg AVS for the supply of the components and the rubber materials for this study. One of the authors, Samuel Asare, would also like to thank the Department of Materials at Queen Mary, University of London for his research scholarship.

REFERENCES

[1]J. J. C. Busfield, V. Jha, H. Liang, I. C. Papadopoulos, and A. G. Thomas, *Plast. Rubber Compos.* **34**, 349 (2005).

[2]I. C. Papadopoulos, A. G. Thomas, and J. J. C. Busfield, *J. Appl. Polym. Sci.* **109**, 1900 (2008).
[3]J. J. C. Busfield, K. Tsunoda, C. K. L. Davies, and A. G. Thomas, RUBBER CHEM. TECHNOL. **75**, 643 (2002).
[4]L. Mullins, RUBBER CHEM. TECHNOL. **21**, 281 (1948).
[5]C. J. Derham, and A. G. Thomas, RUBBER CHEM. TECHNOL. **50**, 397 (1977).
[6]G. B. McKenna, and L. J. Zapas, RUBBER CHEM. TECHNOL. **54**, 718 (1981).
[7]C. K. L. Davies, D. K. De, and A. G. Thomas, *Prog. Rubber Plast. Technol.* **12**, 208 (1996).
[8]T. J. Pond, and A. G. Thomas, "Creep Under Repeated Stressing," Presented at AIRIEL International Rubber Conference, Venice, Italy, Oct 3-6, 1979, p. 810-817.
[9]A. G. Thomas, *J. Appl. Polym. Sci.* **48**,145 (1974).
[10]L. Mullins, and N. R. Tobin, *J. Appl. Polym. Sci.* **9**, 2993 (1965).
[11]J. J. C. Busfield, A. G. Thomas, and K. Yamaguchi, *J. Polym. Sci., Part B: Polym. Phys.* **43**, 1649 (2005).
[12]V. Jha, A. A. Hon, A. G. Thomas, and J. J. C. Busfield, *J. Appl. Polym. Sci.* **107**, 2572 (2008).
[13]A. H. Muhr, G. H. Tan, and A. G. Thomas, *J. Nat. Rubber Res.* **3**, 261 (1988).
[14]J. J. C. Busfield, and A. G. Thomas, RUBBER CHEM. TECHNOL. **72**, 876 (1999).

[*Received June 2008, revised April 2009*]

Fatigue life prediction of bonded rubber components at elevated temperature

S. Asare and J. J. C. Busfield*

Earlier work has shown that a fracture mechanics approach can predict fatigue failure in rubber or elastomer components using a finite element analysis technique that calculates the strain energy release rate for cracks introduced into bonded rubber components. This paper extends this previous work to examine real fatigue measurements made at both room temperature and 70±1°C in both tension and shear using a cylindrical rubber to metal bonded component. This component generated fatigue failures not only in the bulk of the component but also at the rubber to metal bond interface. The fatigue crack growth characteristics were measured independently using a pure shear crack test piece. Using this independent crack growth data and an accurate estimate for the initial flaw size allowed the fatigue life to be calculated. This fracture mechanics approach predicted the crack growth rates well at both room temperature and 70±1°C.

Keywords: Polymer, Rubber, Elastomer, Fatigue, Fracture, Crack growth, Modelling, Finite element analysis

Introduction

The stress versus the number of cycles to failure approach, which has been adopted widely[1] to determine fatigue life of engineering components, has also historically been used[2] in the elastomer component industry. An alternative approach to predict the fatigue life of elastomer testpieces utilises fracture mechanics.[3] Lake[4] reviewed the fracture mechanics approach, whereby a crack under a particular loading configuration will have a strain energy release rate which will for a particular rubber correspond to a specific crack growth rate. The strain energy release rate, which is a measure of the energy required to create a unit area of new crack surface, is also referred to in the literature as the tearing energy T, as well as the toughness

$$T = -\frac{\partial U}{\partial A} \quad (1)$$

where A is the area of a single fracture surface of the crack and U is a measure of the internal energy stored in the component. The magnitude of T is determined by the viscous work that has to be carried out in the region of the crack tip.[5] Rivlin and Thomas[6] showed for the general case of the rupture of rubber that the relationship between the crack growth rate and the strain energy release rate was a material property, independent of the loading mode and specimen geometry. Similarly, Lindley and Thomas[7] showed that, under fully relaxing fatigue conditions, a characteristic relationship exists between the maximum strain energy release rate attained during the loading cycle and the crack growth rate per cycle. Busfield *et al.*[8] reported that the actual strain energy release rate against applied loading relationship was difficult to calculate accurately using simple empirical relationships for anything other than the simplest components. Therefore, for more complex types of component, investigators have resorted to approximate relationships for the strain energy release rate. For example, Lindley and Stevenson[9] used an approximate fracture mechanics approach to predict the fatigue behaviour of engineering mounts loaded in compression. This allowed an estimate for the fatigue life to be made of the correct order of magnitude. This technique for predicting fatigue failure has been dramatically extended by the advent of large deformation finite element analysis (FEA). It is now possible to calculate the strain energy release rate for specific loading configurations for cracks in any component geometry. Gent and Wang[10] adopted this type of FEA approach to investigate the crack growth behaviour of bonded elastomer suspension components subjected to a large shear. This technique was successfully used to predict the strain energy release rate and hence the mode of failure for these types of component. Busfield *et al.*[8,11] extended the FEA based fracture mechanics approach by calculating the relationships between the strain energy release rate and the crack size for testpieces and a gearbox mount at different amplitudes of cyclic fatigue loading and combined with the material crack growth rate versus strain energy release rate relationships to predict the crack growth rate in the gearbox mount under different modes of loading. This approach has also recently been used to predict other phenomena such as abrasion by Liang *et al.*[12,13] This approach is extended here by calculating the relationships between the strain energy release rate and the crack growth rate for a cylindrically shaped suspension component, fatigued in tension and simple shear deformation modes at both room temperature and 70±1°C. The strain energy release rate was calculated for very small cracks of the order of the size of existing defects (flaws) visually observed at the rubber–metal bond edge of the cylindrical component.

Department of Materials, Queen Mary University of London, Mile End Road, London E1 4NS, UK

*Corresponding author, email j.busfield@qmul.ac.uk

Received 22 November 2010; accepted 21 December 2010
DOI 10.1179/174328910Y.0000000004

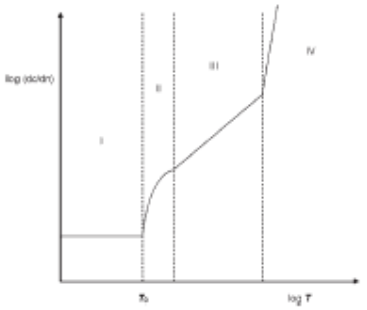

1 Typical double logarithmic plot of crack growth rate per cycle (dc/dn) against stored energy release rate T for filled NR elastomer: different regions highlight different types of tear behaviour

Figure 1 shows a typical double logarithmic plot of the crack growth rate per cycle (dc/dn) against the strain energy release rate T for a filled natural rubber (NR) elastomer. Lake[14] and Lake and Thomas[15] discuss the crack growth behaviour of rubber in the different regions. In this work, the crack growth behaviour of interest is described by region III which can easily described using a power law relationship

$$\frac{dc}{dn} = XT^{\Psi} \tag{2}$$

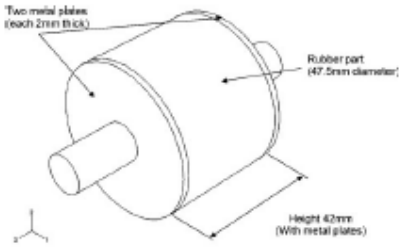

2 Cylindrical component used in this work

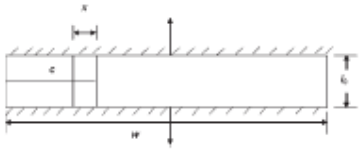

3 Schematic of pure shear crack growth test specimen

where X and Ψ are the characteristic fatigue crack growth parameters obtained from an independent measurement such as a pure shear cyclic crack growth test. For most rubber materials, the value of Ψ lies in the range of 1–6, with a typical value for NR being ~2 and for non-strain crystallising elastomers such as styrene butadiene rubber. For rubber components the deformations are large and the strains around the crack tip are complex. Therefore, a finite element approach is required to calculate the strain energy release rate for a crack of a specific size and orientation subjected to a particular cyclic deformation. The finite element method can be used to calculate a relationship between the crack length and the strain energy release rate, under specific loading conditions, in the form

$$T = \mathrm{F}(c) \tag{3}$$

Combining equations (2) and (3) to eliminate T, it is possible to derive a single functional relationship between the cyclic crack growth rate and the size of the flaw, and thus

$$\frac{dc}{dn} = \mathcal{J}(c) \tag{4}$$

This equation can be rearranged and integrated to predict the number of cycles to failure N_f, thus

$$\int_{c_0}^{c} \frac{dc}{\mathcal{J}(c)} = \int dn = N_f \tag{5}$$

where c_0 and c are the initial and final crack sizes respectively.

Experimental

The material used for this work was a commercially formulated 65 phr HAF 330 carbon black filled NR compound supplied by Trelleborg AVS (Sjöbo, Sweden). The rubber formulation is given in Table 1. The rubber materials were supplied as rubber sheets of ~2 mm thickness, from which pure shear samples of 175 mm width (w), 25 mm height (l_0=14 mm) and 2 mm thickness (t), were prepared as well as dumbbell testpieces using an ASTM D412 type C dumbbell die. In addition, simple bonded suspension mounts were

Table 1 Formulation for materials used in this study

Ingredient	Grade	phr
Rubber	SMR10CV	100
Carbon black	N330(HAF)	65
Stearic acid	...	2
Zinc oxide	...	5
Accelerator	TMTM-75	0·7
Accelerator	MBTS-80	1·5
Sulphur	...	1·5

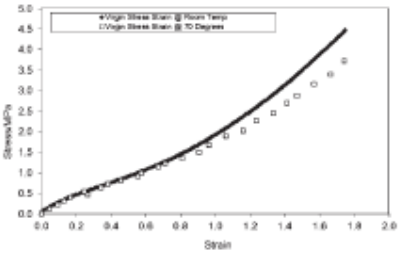

4 Stress strain behaviour for virgin dumbbell specimen in tension at room temperature and 70°C

injection moulded out of the same compound. Figure 2 shows a typical cylindrical bonded suspension component examined in this study. It has dimensions of 42 mm in height (including the bonded metal end plates) and a diameter of ~47·5 mm. The two metal end plates were each ~2 mm in thickness. Figure 3 shows a schematic for the pure shear crack growth rate test specimen used to characterise the cyclic crack growth rate versus tearing energy behaviour.

To determine the stress versus strain behaviour of the elastomer material, white marks were inserted on the reduced width section of the dumbbell specimen, equidistant from the centre and perpendicular to the longitudinal axis. The specimen was marked ungripped. The tensile test was carried out using an Instron 5567 universal test machine equipped with 1 kN load cell to measure the force and an optical extensometer to measure the displacement (strain) of the two white marks painted onto the surface of the testpiece. The tensile test was carried out at a strain rate of 50 mm min^{-1} for the room temperature (23 ± 2°C) characterisation. The stress versus strain behaviour at 70 ± 1°C was performed in an oven, which prevented the use of optical extensometer. Therefore, in this case the load was applied in a stepwise manner and the displacement was measured using a travelling microscope through a glass window in the oven. Figure 4 shows the virgin stress versus strain behaviour for the material at both temperatures.

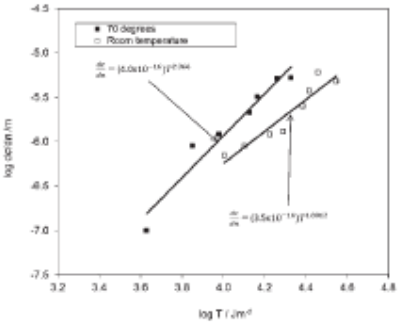

5 log dc/dn against log *T* from pure shear characterisation of NR65 material at room temperature and 70°C

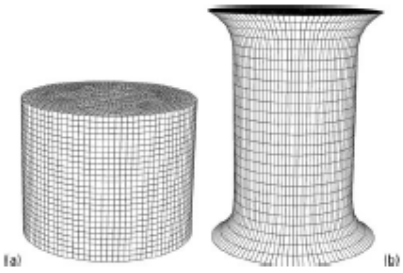

6 *a* meshed undeformed cylindrical component and *b* meshed cylindrical component deformed in tension

The stress strain behaviour was also measured on dumbbell testpieces that had been cyclically stress softened for 999 cycles at an appropriate prestrain at both room temperature and 70 ± 1°C. The one-thousandth cycle stress strain behaviour was used in the FEA to calculate the tearing energies associated with crack growth in the elastomer component. The one-thousandth cycle stress strain behaviour was used to account for the cyclic stress relaxation. Davies *et al.*[16] and more recently Asare *et al.*[17] have developed a strategy to correctly characterise the amount of cyclic stress softening present in a rubber component which depends upon the amount of the maximum average strain encountered in the testpiece. That is a materials characterisation on a testpiece that can be used to predict the behaviour in a component. To adopt this approach in this work, it was necessary to estimate the average strain in the elastomer component when stretched to the maximum cyclic displacement for a specific test. This then allows the specific maximum extension ratio at which to soften the testpiece for stress strain characterisation to be determined. Therefore, the appropriate strain to cycle the dumbbell test specimen is ~90% to characterise the stress softening that is encountered in the cylindrical components when stretched in tension to a maximum displacement of 30 mm. This approach ensured that the softening in the elastomer component under cyclic loading is accounted for in the testpiece stress strain characterisation rather than neglecting it as has been the practice in previous studies.

To characterise the fatigue crack growth behaviour, the pure shear testpieces were gripped along their long edges with a crack introduced as shown in Fig. 3 and fatigue tested with an Instron 8872 servohydraulic test machine equipped with a 25 kN load cell. The wave form of the test was sinusoidal with a frequency of 1 Hz. All testpieces had an initial razor cut of 30 mm inserted into them.

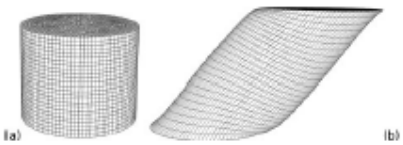

7 *a* meshed undeformed cylindrical component and *b* meshed cylindrical component deformed in simple shear

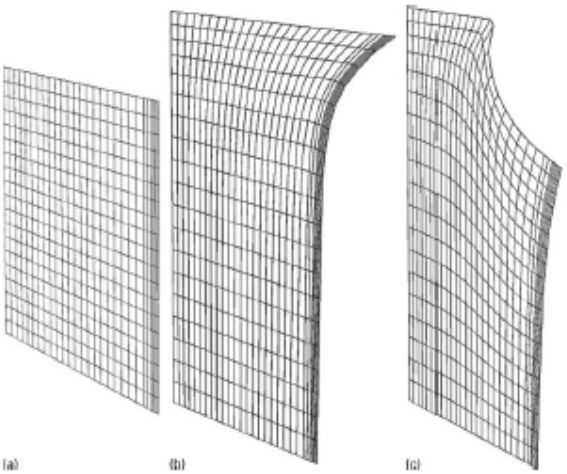

8 *a* undeformed axisymmetric mesh, *b* tension deformed axisymmetric mesh and *c* tension deformed axisymmetric mesh with crack

Papadopoulos *et al.*[18] have highlighted the risks of assuming that the initial crack growth behaviour from a razor cut is typical after the crack tip has roughened up. As a result, all the crack growth measurements were made after the initial razor induced high crack growth rate had reached a steady state condition. Crack lengths were measured at the corresponding number of cycles for tests at different displacement amplitudes. Plots of crack length against the number of cycles were then made to calculate the crack growth rate for specific displacement amplitudes. The fatigue crack growth behaviour was characterised at both room temperature (23±2°C) and 70±1°C in an oven.

Busfield *et al.*[19] showed that for a pure shear testpiece (Fig. 3) with unstrained height l_0, thickness t, width w and a crack of size c, the tearing energy T can be calculated using equation (6) below

$$T = \frac{U}{t(w-c+x)} \tag{6}$$

where x is a strip of material at the cracked part of the testpiece that is not energy free. x has been experimentally found to be ~28% of l_0. U is the strain energy density for a specific displacement in the uncut region far removed from the crack tip region. Equation (6) was used to calculate the tearing energies for each specific test amplitudes in the crack growth studies. The measured plot of log dc/dn against log T at both room temperature and 70±1°C is shown in Fig. 5. As expected the lower viscoelastic response at the elevated temperatures results in the crack growth rate being faster at a specific value of the tearing energy.

The force deflection behaviour of the cylindrical component was measured at room temperature (23±2°C) and 70±1°C (in an oven) using an Instron 8872 servohydraulic test machine run in a static mode and at a strain rate of 50 mm min^{-1}. The one-thousandth cycle force deflection behaviour (after cycling the component for 999 cycles at a maximum tensile displacement of 30 mm) was measured at room temperature and 70±1°C for the cylindrical component. The cylindrical component was also tested at different amplitudes and at a frequency of 1 Hz at room temperature and 70±1°C to determine the experimental number of cycles required to initiate and grow cracks to a measurable size. A sinusoidal wave form was used in all the tests. No initial razor cuts were inserted into the cylindrical component and the experiment was conducted under fully relaxing conditions. The fatigue tests were conducted in tension and shear deformation

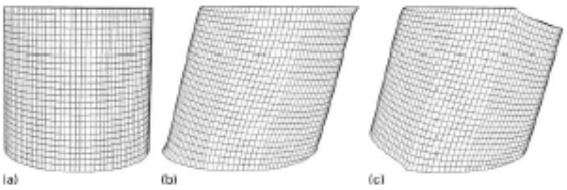

9 *a* undeformed half symmetry mesh, *b* simple shear deformed half symmetry mesh and *c* simple shear deformed half symmetry mesh with cracks

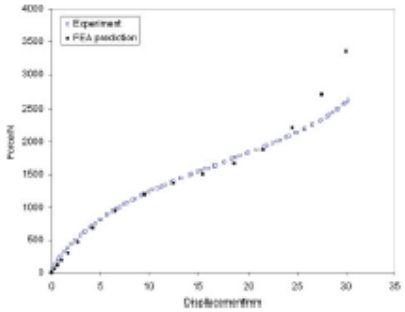

10 Experimental one-thousandth cycle force deflection behaviour and FEA prediction (using one-thousandth cycle dumbbell specimen stress strain data) of one-thousandth cycle force deflection behaviour of cylindrical component at room temperature

modes. The number of cycles required to initiate and grow cracks at the rubber/metal bond interface to a measurable size was recorded and the average crack length was measured using a Vernier calliper as a probe.

Finite element analysis

Finite element modelling has been used widely in the past to predict the stiffness of simple rubber components by, for example, Busfield and co-workers.[9,20] Here the method was initially used, to validate the model, to predict the stiffness of the cylindrical component using the approach suggested by Suphadon and Busfield.[21] This model also gives a good indication of any likely crack initiation sites. Subsequent models were used to calculate the tearing energies associated with cracks growing in specific locations in the component. The technique requires the definition of: the component geometry with a suitable finite element mesh; the material behaviour; the boundary conditions and the loading conditions. In this work, Abaqus (version 6·6–1) was used to model the component and display the results. The filled rubber in

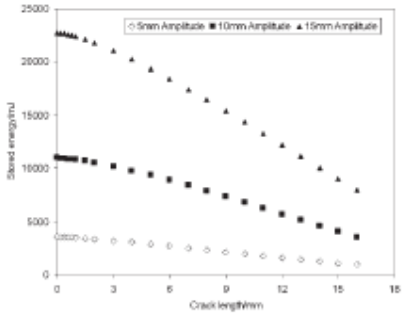

11 Stored energy against crack length for crack growing in cylindrical component under tension at 5, 10 and 15 mm peak displacement amplitude at room temperature

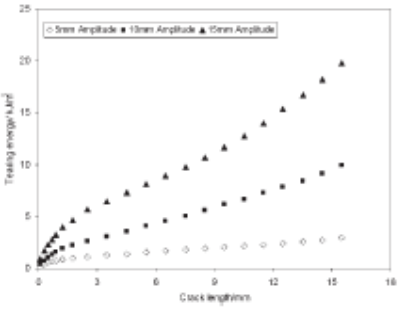

12 Tearing energy crack length relationship for crack growth in cylindrical component in tension at 5, 10 and 15 mm peak displacement amplitudes at room temperature

the model was described using a hyperelastic Yeoh[22] strain energy function as described by Liang *et al.*[12] The coefficients were derived from experimental stress strain data measured as described previously.

The energy balance technique was used to calculating the tearing energy associated with specific cracks being found in the component. This and other methods for calculating the tearing energy associated with crack growth in elastomer testpieces and components were evaluated by Busfield *et al.*[9,23] With this approach, the difference in the magnitude of the total internal strain energy dU is calculated between two models held at a fixed displacement where the crack tip area A is extended by a small area dA. The tearing energy is equal to dU/dA. This technique is also known as the node release or the virtual crack extension technique.

The component was unless otherwise specified modelled using eight-node linear brick, hybrid, constant pressure elements C3D8H. The first model was used to predict the force deflection behaviour in tension and to give an indication of regions of potential fatigue failure under tensile loading. The bottom surface nodes of the component were fully constrained and the top nodes

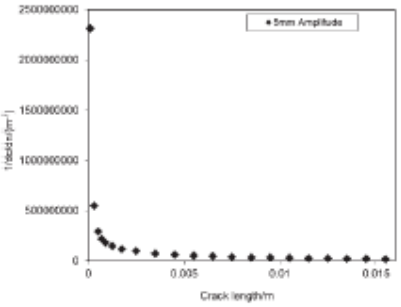

13 1/(dcld/n) versus crack length for crack growth in cylindrical component in tension at 5 mm amplitude at room temperature

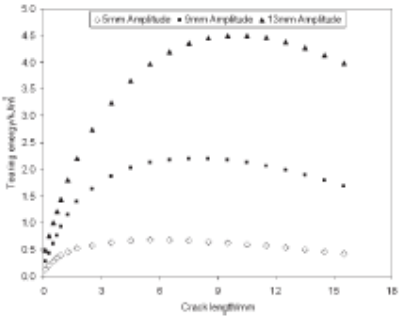

14 Tearing energy crack length relationship for crack growth in cylindrical component in shear at 5, 9 and 13 mm amplitudes respectively at room temperature

were all translated in the z direction. All top surface rotational degrees of freedom were constrained. All translational and rotational degrees of freedom of the bottom surface were constrained. The summation of all the reaction forces of the top surface nodes was recorded at different displacements to determine the component stiffness. The strain energy density distribution was also observed to indicate the regions of potential failure. Figures 6 and 7 show the displaced geometry under the tensile and shear loading respectively.

The crack growth was also modelled using finite element techniques. In tension it was apparent from the strain energy distributions observed in the crack free models that the parts would fail at the bond interface between the rubber and the metal plates as reflected in the actual fatigue behaviour. Owing to the symmetric nature of the component and the crack growth profile when loaded in tension, an axisymmetric model was developed to calculate the change in strain energy in the component with crack growth. The model was meshed with CAX4H axisymmetric elements. Figure 8*a* shows a meshed and undeformed axisymmetric model of the component. To account for small changes in the strain energy due to initial growth of defects (flaws) at the rubber–metal bond edge, the model was meshed with a high mesh density of 0·2 mm for the first part of the crack growth. The crack growth was modelled by releasing nodes at the rubber/metal bond interface. The virtual crack extension technique was used to calculate the tearing energy associated with crack growth along the rubber/metal bond interface. Figure 8*b* shows a meshed and deformed axisymmetric model of the cylindrical component in tension.

To model the component's fatigue crack growth in shearing a half symmetry three-dimensional model was used exploiting the symmetry found in the cylindrical component and the crack growth profile. Figure 9*a* presents a meshed and undeformed half symmetry model of the component. To account for small changes in the strain energy due to growth of defects (flaws) at the rubber–metal bond edge, the model was meshed with a mesh size of 0·2 mm for the first 1 mm of crack growth. The virtual crack extension technique was used to calculate the tearing energy associated with crack growth along the rubber/metal bond interface. Figure 9*c* presents a meshed and deformed half symmetry model of the cylindrical component in shear containing two cracks.

Results and discussion

Figure 10 compares the measured of the one-thousandth cycle force deflection behaviour at room temperature to the corresponding FEA prediction for the cylindrical component using the one-thousandth cycle stress strain data. The force deflection behaviour of the component is well predicted up to a maximum displacement of 25 mm after which the FEA model overestimates the force deflection behaviour. The modest discrepancy in the force deflection prediction after 25 mm maximum displacement can be attributed to the difference in maximum average strain energy density in the testpiece and the component during the stress softening. Also it is difficult to ensure identical cross-link densities in the compression moulded flat sheets and the injection moulded components studied in this work. This was checked using experiments that measure the equilibrium swelling in *n*-decane on the two samples. A cross-link density of $1{\cdot}452 \times 10^{-4}$ mol cm^{-3} was measured for the flat elastomer sheet material and a slightly higher value of $1{\cdot}609 \times 10^{-4}$ mol cm^{-3} was measured for the component material. It is evident from Fig. 10 that the average strain energy density approach for accounting for the cyclic stress relaxation in the strain energy calculations gives good results over a sufficiently wide range of displacement to be considered reliable for this work.

Figure 5 shows the crack growth characterisation results for the filled NR material. The slope determines Ψ to be 1·80 at room temperature and 2·37 at 70°C. As expected the filled NR material is weaker at elevated temperatures as less energy is required to grow a crack at a similar rate at 70°C. In practice components usually operate above the ambient temperature as a result of hysteresis. The need therefore arises to predict the fatigue life of components at

Table 2 Predicted and measured numbers of fatigue cycles required to grow cracks from estimated rubber–metal bond edge flaw size until specified crack size just before failure

Maximum displacement/mm	Temperature/°C	Tension or shear	Range of crack lengths/mm	Measured no. of cycles N_m	Predicted no. of cycles N_p	N_p/N_m
5·0	23	Tension	0·5–4	723 937	441 145	0·61
10·0	23	Tension	0·9–10	64 524	116 912	1·81
15·0	23	Tension	0·5–8	63 494	36 366	0·57
10·0	70	Tension	0·5–15	163 988	155 454	0·95
15·0	70	Tension	0·9–11	24 047	22 131	0·92
9·0	23	Shear	0·5–9	357 009	406 145	1·14
13·0	23	Shear	0·5–10	168 093	160 189	0·95
13·0	70	Shear	0·5–7	418 130	182 320	0·44

elevated temperatures. A rise in temperature reduces the fatigue crack resistance and therefore reduces the components fatigue life. As expected the stiffness was also seen to be reduced by an increase in temperature.

The methodology for predicting the fatigue life is illustrated in Figs. 11–13. Figure 11 shows the relationship between the FEA calculated total strain energy in the model versus crack length for a crack grown in tension in the cylindrical component at room temperature for different displacement amplitudes. By using equation (1), it is seen that the gradient along the curves of Fig. 11 gives the tearing energy relationship described by equation (3). This new relationship is plotted in Fig. 12, which shows that the tearing energy of the cracks at all the different amplitudes increases as the crack grows at the rubber/metal interface. Substituting this value for the tearing energy into equation (2) fitted to the data shown in Fig. 5 gives dc/dn given by equation (4). This relationship can be inverted as $1/(dc/dn)$ as shown in equation (5). Figure 13 shows $1/(dc/dn)$ versus crack length for crack growth in the cylindrical component in tension at 5 mm amplitude at room temperature. Integrating under the $1/(dc/dn)$ versus crack length curve from an initial crack size c_0 to a final crack size c gives the number of cycles required to grow a crack from c_0 to c (crack range c_0–c) and hence the fatigue life if c is large enough to cause a catastrophic failure. The method above was carried out for fatigue life prediction in tension and shear at room temperature as well as 70 ± 1°C. Figure 14 shows the tearing energy crack length relation of the component in shear and at room temperature. Unlike that in tension, the tearing energy increases at the beginning of the crack growth and then passes through a maximum. This trend can be attributed to the geometry of the component studied in this work. Using the method discussed above, the numbers of cycles required to grow cracks at the rubber–metal bond edge of the elastomer component in tension and shear at both room temperature and 70 ± 1°C were calculated as N_p and compared with the experimentally measured number of fatigue cycles N_m in Table 2.

The fatigue life predicted with the fracture mechanics approach generally results in a fatigue life within a factor of 2 to the experimentally measured fatigue life cycles which is excellent especially when considering the extent that the predicted fatigue life depends on the initial size estimate of the flaw at the rubber–metal bond edge of the component. The approach used here of estimating (after careful visual inspection of the rubber–metal bond edge) an initial average flaw size at the rubber–metal bond edge clearly does not take into consideration any small local variations in the flaw size. It is apparent from Table 2 that the method works well for the fatigue life predictions made at both room temperatures and 70 °C irrespective of the deformation mode.

Conclusions

The fracture mechanics approach to fatigue life prediction of engineering components has been validated using a cylindrical engineering elastomer component for fatigue crack growth within the 'power law' region of crack growth behaviour. The cylindrical geometry of the engineering elastomer component induced rubber/metal bond interface crack growth for both tensile and shear fatigue loading. The fatigue crack growth behaviour was successfully predicted for crack growth at both room temperature and 70 ± 1°C to within a factor of 2 for the cylindrical component. For the first time, the cyclic stress softening associated with fatigue of filled elastomer materials was quantitatively accounted for by softening the dumbbell specimens for the stress strain characterisation and subsequent FEA strain energy calculations at a strain level deduced following the average strain energy density approach. The effect of temperature on the fatigue life of the cylindrical component was also well accounted for by the approach of characterising the material stress strain and the fatigue crack growth behaviour at the test temperature. Considering the irreproducibility of fatigue life predictions in previous work, the accuracy of the fracture mechanics approach method to predict the fatigue crack growth rate with an accuracy of 2 for the fatigue life at both room temperature and 70 ± 1°C is excellent.

Acknowledgements

The authors would like to thank the Swedish Fatigue Network for funding the project, as well as Trelleborg AVS for the supply of the components and the rubber materials for this study. One of the authors, S. Asare, would also like to thank the Department of Materials at Queen Mary, University of London (London, UK) for his research scholarship.

References

1. W. D. Callister: 'An introduction to materials science and engineering', 7th edn; 2007, New York, John Wiley and Sons.
2. F. Abraham, T. Alshuth, and S. Jerrams: *Plast. Rubber Compos.*, 2001, **30**, 421–425.
3. C. M. Roland: *Plast. Rubber Compos.*, 2009, **38**, 349–354.
4. G. J. Lake: *Rubber Chem. Technol.*, 1995, **68**, 435–460.
5. K. Tsunoda, J. J. C. Busfield, C. K. L. Davies and A. G. Thomas: *J. Mater. Sci.*, 2000, **35**, 5187–5198.
6. R. S. Rivlin and A. G. Thomas: *J. Polym. Sci.*, 1953, **10**, 291–318.
7. P. B. Lindley and A. G. Thomas: Proc. 4th Rubber Technology Conf., London, UK, May 1962, Institute of Rubber Industries, 1–14.
8. J. J. C. Busfield, A. G. Thomas and M. F. Ngah: 'Constitutive models for rubber', (ed. A. Dorfmann and A. Muhr), 249–256; 1999, Rotterdam, Balkema.
9. P. B. Lindley and A. Stevenson: *Rubber Chem. Technol.*, 1982, **55**, 337–351.
10. A. N. Gent and C. Wang: *Rubber Chem. Technol.*, 1993, **66**, 712–732.
11. J. J. C. Busfield, V. Jha, H. Liang, I. C. Papadopoulos and A. G. Thomas: *Plast. Rubber Compos.*, 2005, **34**, 349–356.
12. H. Liang, Y. Fukahori, A. G. Thomas and J. J. C. Busfield: *Wear*, 2009, **266**, 288–296.
13. H. Liang, Y. Fukahori, A. G. Thomas and J. J. C. Busfield: *Wear*, 2010, **268**, 756–762.
14. G. J. Lake: *Prog. Rubber Technol.*, 1983, **45**, 89–143.
15. G. J. Lake and A. G. Thomas: *Proc. R. Soc. Lond. A*, 1967, **300A**, 108–119.
16. C. K. L. Davies, D. K. De and A. G. Thomas: *Prog. Rubber Plast. Technol.*, 1996, **12**, 208–220.
17. S. Asare, A. G. Thomas and J. J. C. Busfield: *Rubber Chem. Technol.*, 2009, **82**, 104–112.
18. I. C. Papadopoulos, A. G. Thomas and J. J. C. Busfield: *J. Appl. Polym. Sci.*, 2008, **109**, 1906–1910.
19. J. J. C. Busfield, K. Tsunoda, C. K. L. Davies and A. G. Thomas: *Rubber Chem. Technol.*, 2002, **75**, 643–656.
20. J. J. C. Busfield and C. K. L. Davies: *Plast. Rubber Compos.*, 2001, **30**, 243–257.
21. N. Siphaduon and J. J. C. Busfield: *Plast. Rubber Compos.*, 2009, **38**, 337–342.
22. O. H. Yeoh: *Rubber Chem. Technol.*, 1990, **63**, 792–805.
23. J. J. C. Busfield, C. K. L. Davies and A. G. Thomas: *Prog. Rubber Plast. Technol.*, 1996, **12**, 191–207.